The role of Nuclear Factor κB in the cellular response to different radiation qualities

Inaugural-Dissertation
zur
Erlangung des Doktorgrades
der Mathematisch-Naturwissenschaftlichen Fakultät
der Universität zu Köln

vorgelegt von

Kristina Koch
aus Ostfildern-Ruit

Köln, April 2013

Never stop wondering. Never stop wandering.

(unknown)

Contents

1   Introduction

Human spaceflight is a challenging field of research, as space travel has fascinated mankind for more than 50 years and space programs are heading towards further orbital and interplanetary exploration.

In 1961, Yuri Gagarin started manned space flight as the first human to travel into Earth orbit. Since then, human beings have been essential for the exploration of space. Not only ongoing projects like the habitable International Space Station (ISS; Fig. 1), but also future projects like a manned mission to Mars show the advantage of humans in space over robotic processes. Even though robotic space missions are necessary to prepare for manned operations, humans enable versatility and can react quickly when problems arise. Communication lags between Earth and a spacecraft travelling to Mars as it can take ∼ 20 minutes to send commands between the two, and another 20 minutes before a response is received (Nimon, 2013).

Fig. 1: *The International Space Station (ISS) from above.* The ISS is the largest human-made object ever to orbit the Earth and marked its 10th anniversary of continous human occupation on November 2nd, 2010. Since the first expedition, which was launched October 31st, 2000, the space station has been visited by 204 individuals up until November 2nd, 2012 (www.nasa.gov). It is located at an altitude of ∼ 400 km in low Earth orbit (LEO) (Credit: STS-114 Crew, NASA).

Main problems of manned space flight are several increased health risks, which humans face during long-term missions. This is due to several harmful environmental factors, including microgravity and radiation, which can cause major hazards to an astronaut (Thirsk *et al.*, 2009). Spending a long time in microgravity environment leads to severe bone and muscle mass loss, changes in cardiac performance and a fluid shift. Additionally, astronauts are exposed to a radiation environment that differs extremely from the radiation field on Earth. Humans in space are exposed to different kinds of radiation, as there is less or no protection from the Earth's atmosphere and magnetic field. They are constantly exposed to space radiation at a low dose rate over a long period of time. An increase in cancer risk is the main concern for astronaut exposure to space radiation, as it persists after landing (Durante and Cucinotta, 2008).

These risks have to be understood, for short-term trips into space but especially for long-term journeys. As radiation is one of the limiting factors, it has to be investigated, in which way the different radiation qualities influence future manned space missions, to alleviate given risks with appropriate countermeasures. In this work, the effect of space-relevant radiation on a molecular level is investigated.

1.1 Radiation

1.1.1 Radiation biology basics

Radiation biology is defined as the study of the biological effects of ionizing radiation on living systems. Ionizing radiation is radiation with enough energy so that during an interaction with an atom, it can remove tightly bound electrons from the orbit of an atom, causing the atom to become charged or ionized. In contrast, non-ionizing radiation, like electric and magnetic fields, radio waves or ultraviolet light is the part of the electromagnetic spectrum where there is insufficient energy to cause ionization.

The term ionizing radiation can be subdivided into the types of directly and indirectly ionizing radiation. Charged particles like electrons, protons, α-particles and heavy ions are directly ionizing. The likelihood of the effect hereby decreases with increasing velocity of the particle and increases with charge. With decreasing velocity, the chance of interaction between particle and matter increases, while the electric field gets stronger with increasing charge.

X-rays, γ-rays and neutrons are indirectly ionizing. They do not carry electrical charge and can transfer energy to charged particles during interactions with matter.

For a better understanding of radiation effects, a few basic terms are defined here.

Linear Energy Transfer (LET) is the average energy (ΔE) imparted to a medium by a charged particle per unit track length (ΔS). The corresponding unit is keV/μm. Low LET results in sparsely ionizing radiation, whereas high LET is densely ionizing (Pouget and Mather, 2001), resulting in different interactions with the target molecule. The diameter of a densely ionizing particle track ranges around several μm. During traversal of the cell, high atomic number and high-energy (HZE) particles loose energy which results in ionization of molecules. Particles with high LET cause a dense ionization along their track.

$$LET = \Delta E/\Delta S \qquad\qquad \textit{(Equation 1)}$$

Relative biological effectiveness (RBE) describes the effect size of a certain radiation quality in biological systems. It compares the effectiveness of a test ionizing radiation (D_{test}) to that of a reference radiation, e.g. X- or γ-rays (D_{ref}). RBE is dependent on dose, dose rate, biological endpoint of interest, LET, particle velocity and charge (Hall and Giaccia, 2012a).

$$RBE = D_{ref}/D_{test} \hspace{4cm} (Equation\ 2)$$

The **Bragg peak** describes the maximum of ionization density which a charged particle produces along its track. The number of ions that are created per unit of path length increases as the particle slows down. It reaches the Bragg peak close to the end of its trajectory. Here, residual energy is lost over a very short distance. The peak is followed by a rapid decrease of energy loss (Fig. 2).
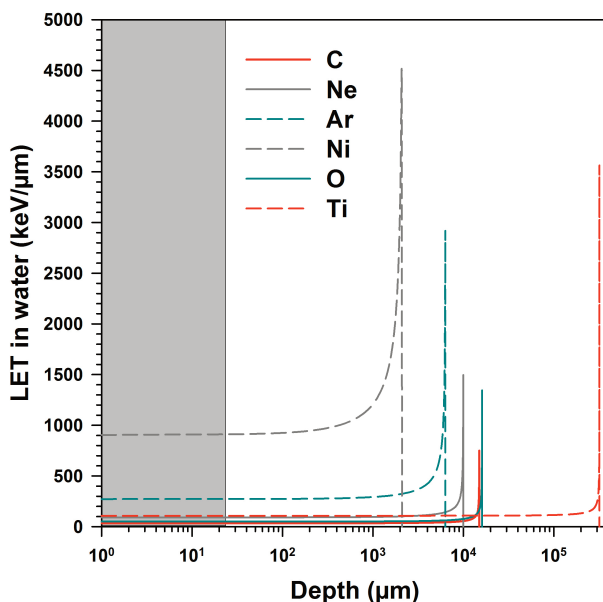
Fig. 2: *Bragg curves of all accelerated ions used in this work.* The Bragg curves show the energy loss while traversing through water of the following ions: ^{13}C (71 MeV/n, LET 34 keV/μm), ^{22}Ne (75 MeV/n, LET 92 keV/μm), ^{36}Ar (84 MeV/n, LET 272 keV/μm), ^{58}Ni (54 MeV/n, LET 906 keV/μm), ^{16}O (91 MeV/n, LET 51 keV/μm), and ^{48}Ti (997 MeV/n, LET 108 keV/μm). The energy on target and the average LET over the shaded area, which indicates the average thickness of a human cell, are given in brackets for each ion. Cells were irradiated in the consistent LET range before the Bragg peak (adapted from Hellweg, 2012).

1.1.2   Radiation environment in space

Radiation exposure in space severely differs from the natural radiation field humans are exposed to on Earth. Terrestrial radiation is largely characterized by low LET radiation (X-, β- or γ-rays) and partly high LET radiation in form of α-particles, e.g. from radon decay. Astronauts face a broad spectrum of radiation qualities, ranging from X-rays to high-energy particles such as electrons, neutrons, protons and heavy ions with high charges.

Most harmful factors which influence manned space missions are not only the cosmic ionizing radiation but also secondary radiation produced by interactions of cosmic radi-

ation with matter of the walls of the space ship. Protection from radiation by the Earth's magnetic field decreases as the distance from Earth increases.

The first indication of an effect of space radiation on the human body were events described by Apollo and Skylab astronauts as 'light flashes'. Nowadays it is known that these 'light flashes' are visual phenomena, caused by cosmic ray particles passing through the eye and directly interacting with the retina (Narici *et al.*, 2004).

On Earth, the average radiation dose reaches 2.4 mSv[1] per year. On the ISS, which is located at a height of ∼ 400 km, radiation doses of 0.5 mSv per day can be measured (Beaujean *et al.,* 2002; Reitz *et al.*, 2005). During extravehicular activities (EVAs), doses reach three times this amount (Berger and Reitz, 2006). During an interplanetary Mars mission, which is estimated to take up to three years (Grigoriev *et al.*, 1998), dependent on shielding and solar activity, equivalent doses of up to 1000 mSv at the blood-forming organs can be received (Horneck *et al.*, 2006). These values currently make space radiation a limiting factor for long-term missions in space (Durante and Cucinotta, 2008).
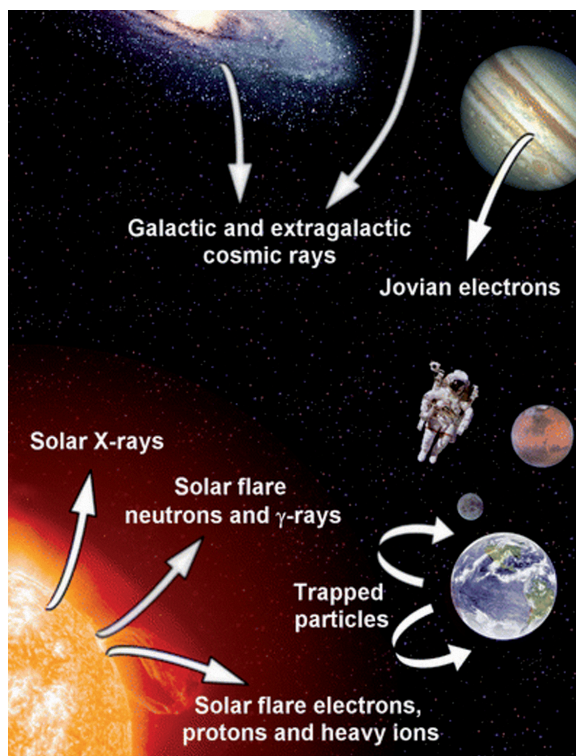
Fig. 3: *Radiation sources in space.* The space radiation environment in our Solar System is composed of different radiation qualities and sources. Primary components of the radiation field are galactic cosmic rays (GCR), which originate from outside our Solar System, and solar cosmic radiation (SCR), which constantly flows from the Sun. The radiation field is composed of a variety of radiation species, like electrons, protons, α-particles, X-rays, heavy ions, γ-rays and neutrons. Highly energetic ions are of main interest for long-term space missions, as these particles pose the most hazardous radiation risk for humans in space. (taken from Hellweg and Baumstark-Khan, 2007).

[1] **Sievert (Sv)** is the corresponding unit for the dose equivalent (H). H is the energy dose weighted by the biological effectiveness of a given radiation quality or radiation quality factor (Q). Q is a dimensionless radiation weighting factor and was derived from the measured RBE values. Q ranges from 1 at low LET (<10 keV/μm) to 30 at high LET (∼ 100 keV/μm). With very high LET Q decreases due to so-called over-kill or wasted energy (Durante and Cucinotta, 2008). 1 Sv = 1 J/kg.

H = radiation quality factor (Q) × absorbed dose (D) *(Equation 3)*

Primary components of the radiation field in space are galactic cosmic rays (GCR) and solar cosmic radiation (SCR, Fig. 3). GCR originate from outside our solar system. Main components are protons (87 %), α-particles (12 %) and heavy ions (1 %) covering the full range of elements, with some of them, like iron and carbon nuclei, being more abundant (George *et al.*, 2009).

In this work, heavy ions are of main interest, as they have a high RBE (Barendsen *et al.*, 1960; 1963; Skarsgard, 1998). For radiation effects on a molecular level, these high-energetic particles are several times more effective than X-rays. GCR fluxes vary with the solar cycle (Badhwar, 1997; Wilson *et al.*, 1989). During minimum solar activity, the GCR flux peaks, while it decreases during solar maximum. GCR can reach energies up to 10^{12} MeV.

Solar cosmic rays consist of 95 % protons and originate from the surface of the Sun. Further components are α-particles and heavy ions. During solar particle events (SPE), which originate from magnetically disturbed regions of the Sun, highly energetic charged particles are burst.

On a three-year mission to Mars, as described above, the exposure to GCR can accumulate to doses up to 1.0 Sv and thereby cause late effects to the astronauts' health. During solar flares, doses up to 4.2 Gy[2] can be reached (Horneck *et al.*, 2006), leading to severe acute effects in the human body. These values depend on the solar cycle and shielding condition.

Radiation protection is a complex issue as for high energy GCR passive shields are too massive to be practical and high-energy particles can penetrate thick shielding. Furthermore, they will likely produce showers of secondary radiation inside the spacecraft upon impact with the shielding material, which may be more harmful than the GCR themself (National Council on Radiation Protection and Measurements [NCRP], 2006).

1.1.3   Artificial radiation sources

To investigate its effects on human cells, space radiation has to be simulated as effectively as possible. Therefore, heavy ion accelerators are used to expose cells to highly energetic heavy particles, an important component of the space radiation field. About 26000 accelerators exist worldwide, with most of them used for medical applications like radiotherapy. Major research machines are only a tiny fraction of the total (Maciszewski and Scharf, 2004).

---

[2] **Gray (Gy)** is the corresponding unit for the absorbed dose (D), which is the energy deposited per mass unit. 1 Gy = 1 J/kg.

Beamtimes at two accelerators were available during this work, the *Grand Accélérateur National d'Ions Lourds (GANIL)* in Caen (France) and the heavy ion synchotron *(Schwerionen-Synchotron, SIS)* at the *Gesellschaft für Schwerionenforschung (GSI)* in Darmstadt (Germany).

The accelerator forms a beam of subatomic particles which are ionized, collected and directed into the particle accelerating facility. When an experiment is conducted, different beam variables like species and energy with its consequential LET are offered. As an example for a particle accelerator, Fig. 4 presents an overview of the GSI accelerator facility in Darmstadt, Germany.
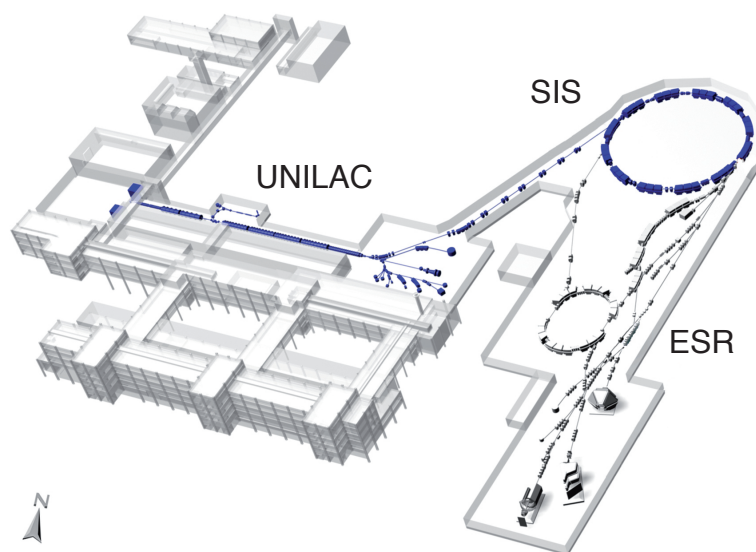
Fig. 4: *The GSI heavy-ion accelerator facility in Darmstadt, Germany.* The GSI was founded in 1969 as the Society for Heavy Ion Research (Gesellschaft für Schwerionenforschung). The accelerator allows to prepare ion beams of all the elements up to uranium in any state of electric charge. It accelerates these beams to nearly the speed of light. The linear accelerator (UNILAC) accelerates ions to 20 percent of the speed of light. In the heavy ion synchrotron (SIS) the ion beam is further accelerated up to 90 percent of the speed of light in the course of several hundred thousand revolutions. Previously accelerated ions can be stored in the experimental storage ring (ESR; Credit: GSI).

1.1.4 Effects of whole body radiation exposure in humans

Effects of ionizing radiation can be acute or delayed, depending on the time frame of radiation exposure as well as dose and dose rate. Furthermore, the quality of radiation is of importance, as the major hazard in manned spaceflight results from highly energetic particles. Acute effects, which are mostly due to exposure to high proton fluxes during solar flares, appear soon after irradiation (from minutes to a few days), while delayed effects like cancer can only occur after several years.

While the current estimates of cancer risks for adults aged 40 are between 0.001 and 0.01 for a chest X-ray, this increases up to more than 1 % for an ISS mission and reaches more than 10 % for a planned Mars mission (Durante and Cucinotta, 2008). The radiosensitivity of cells, tissues, organs or organisms depends on different circumstances. Cells are least sensitive in S phase, the part of the cell cycle in which DNA is replicated. They are most sensitive in G2/M phase, in which dublicated chromosomes are 'checked' for errors for subsequent cell divison. Furthermore, undifferentiated, quickly dividing and highly metabolically active cells are more sensitive compared to resting cells. Bone marrow, lymphoid organs and gastrointestinal stem cells for example are highly sensitive, whereas muscle, kidney and liver are fairly low radiosensitive (Bergonié and Tribondeau, 1906).

Table 1: *Radiation effects in humans after whole body irradiation (adapted from Hellweg and Baumstark-Khan, 2007).*

Chronic dose	Risk	
~ 0.4 Sv/year	First evidence of increased cancer risk as late effect from protracted radiation	
2-4 Sv/year	Chronic radiation syndrome with complex clinical symptoms	

Acute single dose	Effect	Outcome
0.1-0.03 Sv	First evidence of increased cancer risk as late effect (Pierce and Preston, 2000; Pierce *et al.*, 2012)	
< 0.25 Sv	No obvious direct clinical effect	
< 0.5 Sv	Nausea, vomiting	No early death anticipated
(> 0.7 Sv) 3-5 Sv	*Bone marrow syndrome*: Symptoms include internal bleeding, fatigue, bacterial infections and fever.	Death rate for this syndrome peaks at 30 days, but continues out to 60 days. Death occurs from sepsis
5-12 Sv	*Gastrointestinal tract syndrome*: Symptoms include nausea, vomiting, diarrhea, dehydration, electrolytic imbalance, loss of digestion ability, bleeding ulcers.	Deaths from this syndrome occur between 3 and 10 days post exposure. Death occurs from sepsis
> 20 Sv	*Central nervous system syndrome*: Symptoms include loss of coordination, confusion, coma, convulsion, shock, and the symptoms of the blood forming organ and gastrointestinal tract syndromes	No survivors expected

Table 1 lists radiation effects in humans after a whole body irradiation (Hellweg and Baumstark-Khan, 2007). The syndromes listed in this table depend on the sensitivity of the respective tissue and cells.

While the biological effects of protons are well investigated, the underlying mechanisms for damage caused by highly energetic particles are still largely unknown. One of the major uncertainties in risk prediction for space radiation are the poorly understood effects of extraordinary radiation qualities on cells, tissue and whole organisms. Also, the effect of dose rates in space on the biology of DNA repair, cell regulation and tissue response are of main interest (Durante and Cucinotta, 2008).

1.1.5 Biological consequences of radiation exposure on the cellular level

To understand the impact of radiation exposure on the human body, the radiation response processes on the molecular level have to be investigated. The most critical target within a cell is the cell nucleus, since it contains the genetic information in form of DNA and instructions required for the cell to perform its function.

DNA damage and repair. DNA can be damaged by ionizing radiation in a direct or in an indirect manner. Concerning indirect action, radiation interacts with other molecules within the cell, which might not be critical targets but may cause damage by producing free radicals. Due to the high amount of water in living matter, hydroxyl radicals generated by water radiolysis, are responsible for most damages to biomolecules, including DNA, causing single strand breaks (SSB), double strand breaks (DSB), oxidative base damages or base loss. In the direct action, radiation is directly interacting with the DNA molecule.

In case of a SSB, the undamaged second strand provides the template for DNA repair. DSB in mammalian cells can be repaired by non-homologous end-joining (NHEJ), single-strand annealing (SSA) and homologous recombination (HR) (Bennardo *et al.*, 2008).

DNA damage can be repaired in an error-free or in an error-prone way, which may lead to hazardous changes like genome rearrangement. Depending on the type and severity of the DNA damage, the cellular radiation response can have different outcomes. The progression of the cell cycle can be arrested so that the cell has the ability to repair its DNA and replace other damages biomolecules. Repair can either be error-free or error-prone, but in both cases the cell has the ability to survive in the end. While undergoing an error-prone repair, a mutation can occur, leading to a transformation with severe outcomes like tumor growth. The mutation can as well be too hazardous for the cell to

survive. Additionally, crosslinks in DNA can occur, either in the same strand or in the opposite strands of the DNA, leading to a block in DNA replication. The radiation damage can be so severe, that DNA repair is impossible. If that is the case, immediate or delayed cell death can occur (Dalinka and Mazzeo, 1985). Alternatively, the cell undergoes a permanent growth arrest, which can lead to premature differentiation or senescence.

Amount and type of damage are determined by the type and dose of radiation (Kraft, 1987; Baumstark-Khan *et al.,* 1993; Hada and Sutherland, 2006). Radiation with a low LET is sparsely ionizing, resulting in damages that are diffusely distributed (Fig. 5 A). High LET radiation thus causes clustered DNA damage with a high percentage of DSB (Fig. 5 B). Clusters caused by HZE particles are complex as they contain mixtures of various types of damages within a restricted DNA segment. These clusters are more difficult or even impossible to repair, compared to the diffuse and less severe DNA damage caused by sparsely ionizing radiation. Lesions caused by irradiation with densely ionizing radiation might be responsible for their high RBE for major biological endpoints (Fakir *et al.*, 2006; Hada and Sutherland, 2006). It was shown that HZE particles induce larger foci compared to X-rays (Costes *et al.*, 2006) with streaks of foci indicating the path of the particle track. Further, HZE nuclei produce lesions that persist longer (Desai *et al.*, 2005).
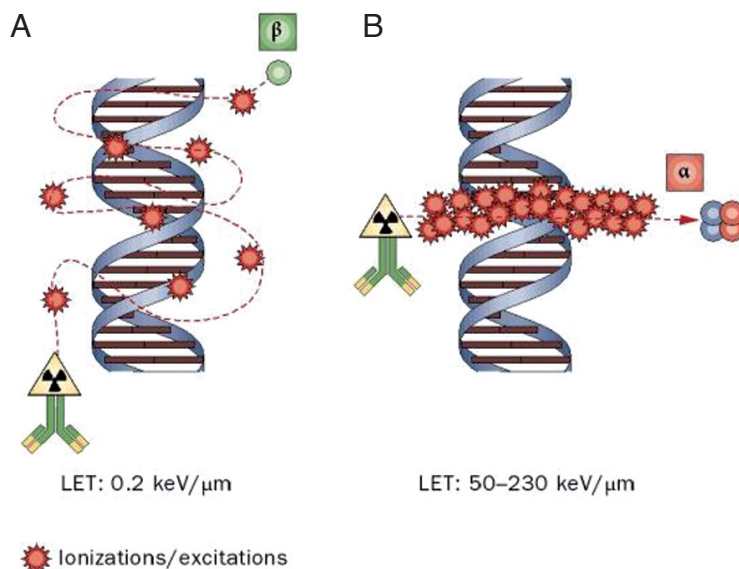
Fig. 5: *Different patterns of DNA damage depending on linear energy transfer (LET).* Low LET radiation produces diffuse DNA lesions that are easily repairable (A). α-particles with high LET are densely ionizing and produce clustered DNA damage along a linear track. These multiply damaged sites are poorly repairable (B) (modified from Pouget *et al.*, 2011).

The predominant cellular response to radiation is a **DNA damage response (DDR)** which starts with detection of DNA damage. It activates a cascade to signal the pres-

ence of lesions and to promote their repair (Jackson and Bartek, 2009). The signal transduction pathways activated by the DDR can lead to cell-protective and cell-altering but also destructive responses (Khanna *et al.*, 2001; Ohnishi *et al.*, 2002). One key factor to regulate cellular cascades initiated by genotoxic stress is *Ataxia telangiectasia-mutated* (ATM). ATM is a kinase that is activated upon DNA DSB and will be described in more detail in chapter 1.2.3. Depending on cell type, ATM can activate pathways that can either protect from or trigger apoptosis (Khanna *et al.*, 2001; Jackson and Bartek, 2009), including the Nuclear Factor κB (NF-κB) pathway.

Cell cycle arrest. As a consequence of DNA damage, DDR mechanisms regulate cell cycle progression (van Gent *et al.*, 2001; Jackson and Bartek, 2009). Cell cycle checkpoints are initiated to coordinate DNA repair processes (Krempler *et al.,* 2007; Pawlik and Keyomarsi, 2004). Checkpoints halt the cell cycle temporarily to avoid replication and segregation of damaged DNA, to provide time for the repair of DSBs or function to permanently remove damaged cells from the actively proliferating population. Upon DNA damage, the G1/S checkpoint can prevent replication of DNA, the S-phase checkpoint delays replicative DNA synthesis and the G2/M checkpoint is able to block entry into mitosis. Cell cycle checkpoints target Cyclin and Cyclin-dependent kinase (Cdk) complexes, that normally promote cell cycle progression.

Several studies investigate the interplay of DSB repair and cell cycle control mechanisms to reveal how cell cycle progression is regulated in the presence of DSBs, induced by ionizing radiation (Linke *et al.*, 1997; Cann and Hicks, 2006; Deckbar *et al.*, 2010). DNA damage initiates a chain of events, with ATM playing a critical role, as it targets downstream effectors like checkpoint kinases (ChK) and inhibits cell cycle progression in different phases of the cell cycle (Hall and Giaccia, 2012b).

Still, the underlying mechanism of the response to damage cluster caused by heavy ions is not well understood so far and has to be studied on a cellular and molecular level.

1.2 The transcription factor Nuclear Factor κB (NF-κB)

1.2.1 The NF-κB proteins

The Nuclear Factor κB (NF-κB)/Rel family is composed of inducible dimeric transcription factors which are involved in the regulation of more than 200 genes. Its members are DNA-binding proteins that recognize κB or κB-like DNA motifs (NF-κB-responsive elements, NREs).

NF-κB was originally identified as a protein that interacts with an 11-base pair sequence in the κ immunoglobulin light-chain enhancer in B-cells (Sen and Baltimore, 1986). This factor is involved in the cellular response to several stimuli and is essential for regulating immune response, inflammation, cell proliferation and cell death (Baldwin, 1996; Gómez *et al.,* 1997; Ghosh *et al.,* 1998; Li and Verma 2002; Karin and Lin, 2002; Bonizzi and Karin, 2004). Defects in the NF-κB pathway are related to tumor development as it gives the cells additional growth advantages.

The NF-κB/Rel family is composed of related proteins consisting of NF-κB1 (p50/p105), NF-κB2 (p52/p100), RelA (p65), c-rel and RelB (Moynagh, 2005; Hoffmann *et al.,* 2006). Fig. 6 gives an overview of all NF-κB/Rel and IκB proteins.
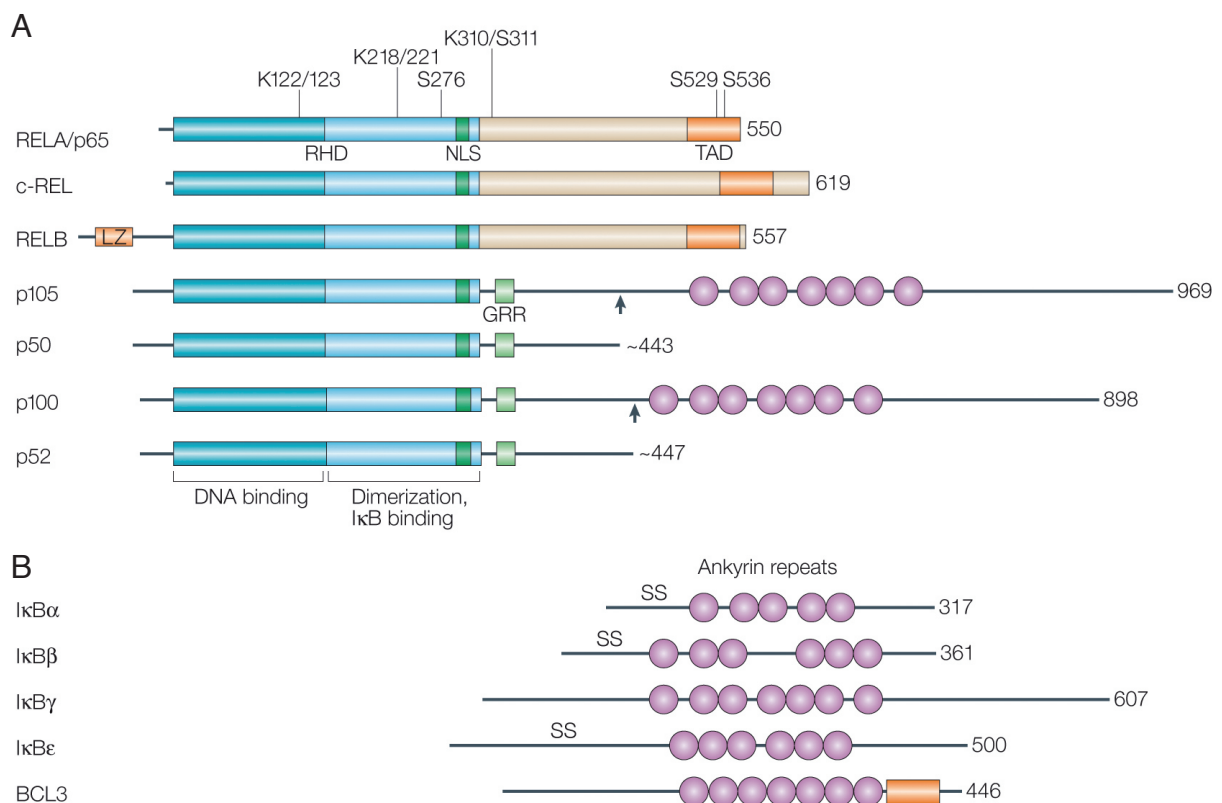
Fig. 6: *The family of mammalian NF-κB/Rel and IκB proteins.* (A) All NF-κB/Rel proteins with their respective number of amino acids indicated on the right. S276, S311, S529 an S536 indicate serine phosphorylation sites; lysines K122, K123, K218, K221 and K310 are sites of acetylation of RelA; (NLS) nuclear localization signal; (RHD) Rel-homology domain; (TAD) carboxy-terminal transactivation domain; (purple circles) ankyrin repeats; (GRR) glycine-rich region; (LZ) leucine zipper; (B) NF-κB regulating IκB inhibitory proteins; (SS) two serine residues, indicating sites of phosphorylation (taken from Chen and Greene, 2004).

All proteins share a ~ 300 amino acid N-terminal domain called the Rel homology domain (RHD) which contains sequences necessary for DNA binding, dimerization and nuclear localization. The RHD allows the formation of homo- and heterodimers, that bind to the κB-sites. These sites are located in the promoters and enhancer regions of genes. The c-rel, RelB and RelA proteins have a transactivation domain, which strongly activates transcription after binding to κB sites. p50 and p52 proteins lack this domain and therefore act as transcriptional repressors (May and Gosh, 1997).

Members of the NF-κB family, except for RelB, can form hetero- and homodimers with one another. The most common form is the p65 subunit associated with p50 or p52. In most cells, the cytosolic molecules IκBα, IκBβ or IκBε inhibit the release of NF-κB and thereby its activation. Additionally, the precursor proteins p100 and p105, which are processed to p52 and p50 respectively, are able to function as IκB-like proteins. They are characterized by IκB-typical ankyrin repeats, a 33-amino-acid motif that mediates protein-protein interaction (Hayden and Gosh, 2004). IκB proteins mask the nuclear-localization sequences (NLS) on the NF-κB subunits and retain them in the cytosol.

1.2.2   The classical and non-canonical NF-κB pathway

Three major types of signaling to activate NF-κB have been identified; the classical (canonical), the alternative (non-canonical) and the genotoxic stress-induced (s. 1.2.3) pathway. In the classical and the non-canonical pathway the signal is transmitted via receptors into the cell (Fig. 7). In the classical pathway, NF-κB is activated by a variety of different stimuli like pro-inflammatory cytokines, e.g. tumor necrosis factor α (TNF-α) or Interleukin 1 (IL-1), growth factors like c-Myc, Ras and p53 or by microbial and viral infections via Toll-like receptors (TLR). Activation of NF-κB involves phosphorylation of two serine residues in IκB proteins. This modification triggers their ubiquitination and degradation by the proteasome. The classical pathway is defined as being mediated by a NF-κB essential modulator (NEMO)-dependent IκB kinase (IKK). Ubiquitination of IκB depends on activation of the upstream IKK complex, formed by the homologous kinases IKKα and IKKβ, the non-enzymatic proteins IKKχ or NEMO and the protein ELKS, rich in glutamine (E), leucine (L), lysine (K) and serine (S) (Madonna *et al.*, 2012). After degradation of IκB, free NF-κB translocates into the nucleus and activates its target genes involved in innate immune and inflammatory responses, developmental processes, cellular growth and inhibition of apoptosis (Karin and Ben-Neriah, 2000, Karin and Delhase, 2000). This classical pathway mostly involves p50/RelA or p50/c-Rel dimers.
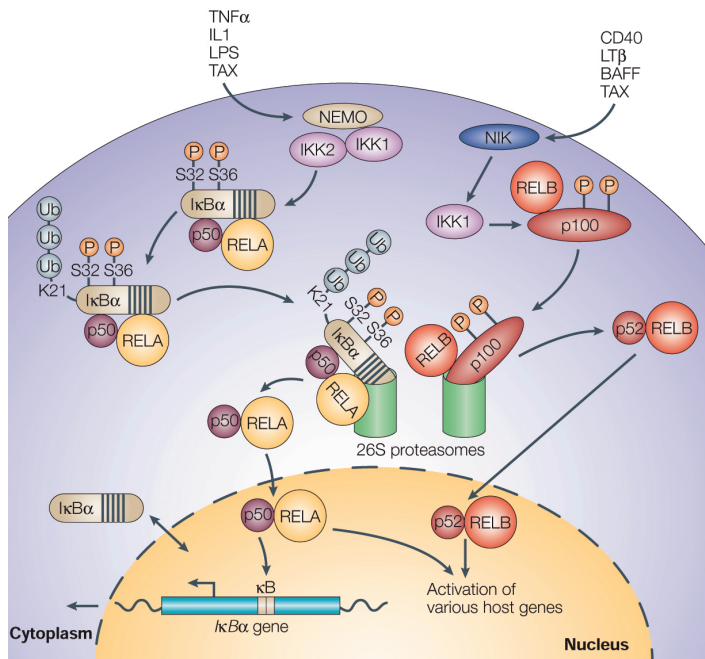
Fig. 7: *Activation of the classical and the non-canonical NF-κB pathway.* The classical NF-κB pathway is triggered by various signals, including those mediated by innate and adaptive immune receptors. It involves activation of the IKK complex (IKK1, also known as IKKα, and IKK2, also known as IKKβ), IκBα phosphorylation and subsequent degradation. In the non-canonical pathway, phosphorylated p100 is processed to p52, depending on NIK and IKKα (IKK1), but not on the trimeric IKK complex (taken from Chen and Greene, 2004).

The non-canonical pathway does not involve NEMO (Shih *et al.*, 2011) and depends on the specific activation of a homodimer of IKKα, which is activated via the NF-κB inducing kinase (NIK). The pathway starts at membrane receptors of the tumor necrosis factor receptor (TNF-R) superfamily. Factors binding to these receptors are e.g. B-cell activation factor (BAFF), lymphotoxin β (LTβ) or CD40 ligand (CD40L). The mechanism of the non-canonical pathway relies on the inducible processing of p100 instead of degradation of IκB. Finally, a heterodimer with RelB is formed and translocated into the nucleus to activate genes involved in cell survival (Senftleben *et al.*, 2001). The non-canonical pathway regulates biological functions such as lymphoid organogenesis, B-cell survival and maturation, dendritic cell activation and bone metabolism (Dejardin, 2006).

1.2.3   The genotoxic stress-induced NF-κB pathway

The third pathway which activates NF-κB is induced by genotoxic stress, especially by DSB (Fig. 8). Several pathways have been environmentally developed by the cell to detect and repair DNA damage (Wood, 1996; Karagiannis and El-Osta, 2004; Reddy and Vasquez, 2005). As a response to genotoxic stress, the kinase ATM is one key factor to regulate cellular cascades, activated when DSB are present in the cell nucleus. In resting conditions, ATM is kept inactive in a dimeric form in the nucleus. Its activation is regulated by the heterotrimer Mre11/Rad50/NBS (Falck *et al.*, 2005; Uziel *et al.*, 2003) which binds to DSB extremities and leads to ATM autophosphorylation. Upon

DSB induction, the ATM dimers dissociate and one molecule phosphorylates the adjacent one. ATM can respond to alterations in chromatin formation (Bakkenist and Kastan, 2003) and is known to initiate the nuclear cascade which leads to NF-κB activation. It was shown that the response to the genotoxic agent camptothecin (CPT) (He *et al.*, 2007) and to low LET ionizing radiation (Lee *et al.*, 1998) are ATM-dependent. The activated NF-κB is a p50/p65 heterodimer.

DNA damage further results in an increased nuclear translocation of the proteins p53-inducible death domain-containing protein (PIDD) (Lin *et al.*, 2000) and NEMO (IKKγ). Upon genotoxic stress, PIDD, together with receptor-interacting protein 1 (RIP1) and NEMO, forms a complex, which accumulates in the nucleus (Janssens *et al.*, 2005). The PIDD/RIP/NEMO complex enhances sumoylation of NEMO.
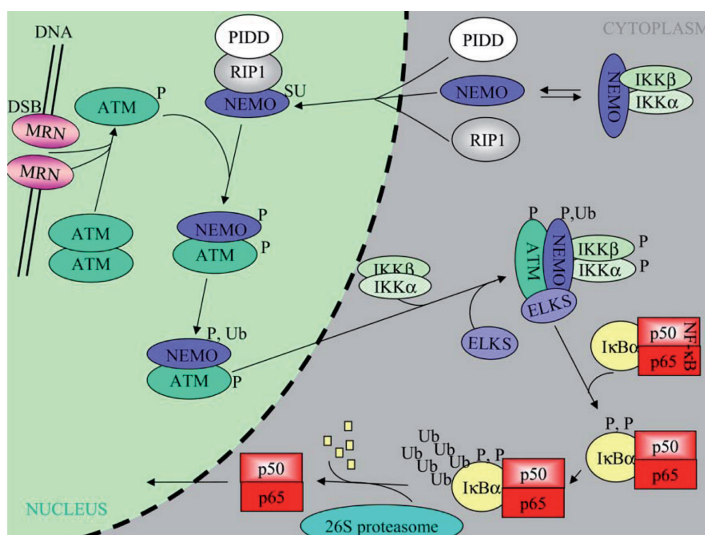
Fig. 8: *Activation of the genotoxic stress-induced NF-κB pathway.* NF-κB activation triggered by DSB results in two independent cascades. ATM is activated and additionally PIDD translocates into the nucleus. Both cascades converge when ATM phosphorylates NEMO. Modified NEMO leaves the nucleus and associates with IKKα and IKKβ. The activated IKK complex phosphorylates IκBα. From here, signalling resembles the classical NF-κB pathway (adapted from Habraken and Piette, 2006).

The two distinct cascades, involving ATM and PIDD respectively, converge, when ATM binds to and phosphorylates NEMO. Subsequently, NEMO is further mono-ubiquitinited. The NEMO/ATM complex leaves the nucleus and associates with IKKα and IKKβ. Together with ELKS, IKK phosphorylates IκB and allows its poly-ubiquitination, leading to proteasomal degradation. Here, the pathway triggered by DNA damage merges with the canonical pathway, involving p65/p50 heterodimers and IκB.

1.2.4 Activation of NF-κB in response to ionizing radiation

The molecular mechanisms, leading to different cellular outcomes after irradiation with heavy ions are still under investigation. Though, it has been shown, that NF-κB is not only involved in regulating gene expression after treatment with inflammatory stimuli,

carcinogens, stress and growth factors but also ionizing radiation, which promotes binding of NF-κB to DNA (Brach *et al.*, 1991; Sahijdak *et al.*, 1994; Ahn *et al.*, 2007). Further, different radiation qualities such as heavy ions with a medium LET (~ 270 keV/µm) were shown to activate NF-κB in human embryonic kidney cells (Baumstark-Khan *et al.*, 2005; Hellweg *et al.*, 2007).

NF-κB is involved in pro-survival signalling (Rashi-Elkeles *et al.*, 2006) and regulates apoptosis by inducing the expression of anti-apoptotic proteins in many cell types (Baichwal and Baeuerle, 1997; Chen and Greene, 2003; Kucharczak *et al.*, 2003). NF-κB gives cells a growth and survival advantage and its activation therefore contributes to the radioresistance of tumor cells (Li and Sethi, 2010; Baldwin, 2001). At the same time, defects in this pathway are related to tumor development as NF-κB activation can result in survival of mutation-prone cells. Further, the NF-κB pathway is involved in inflammation processes (Chastel *et al.*, 2004) as its activation results in production of pro-inflammatory cytokines.

Heavy ion experiments have revealed a strong dependency of RBE for different biological endpoints on LET, ion species, energy and charge (Bird and Burki, 1975; Stoll *et al.*, 1995; Wulf *et al.*, 1985; Yatagai, 2004). Exposure to accelerated heavy ions results in stronger activation of NF-κB in human cells than X-rays (Baumstark-Khan *et al.*, 2005). It was shown that activation of NF-κB differs depending on the heavy ion species and its LET in human embryonic kidney cells (HEK; Hellweg *et al.*, 2011a). Additionally, the potential to activate NF-κB by energetic carbon ions with an LET below 80 keV/µm was comparable to the effect induced by X-rays (Hellweg *et al.*, 2011b). The maximal NF-κB activation was observed in a LET range of 80-300 keV/µm (Hellweg *et al.*, 2011a).

As previously described, the LET also influences the type of DNA damage, as densely ionizing radiation causes DSB containing and non-DSB clustered DNA damage. So far, the role of NF-κB in DNA repair is not fully understood.

The central role of NF-κB in cellular survival and inflammatory responses of the tissue after exposure to ionizing radiation makes it an important pharmacological target for modulating the cellular radiation response. In cancer therapy using heavy ions such as carbon ions, understanding the role of NF-κB will be of importance for revealing the underlying mechanisms of the cellular radiation response. Inhibiting NF-κB might promote the killing effect of radiation therapy by suppressing survival signals. Radiation therapy acts through the induction of DSBs resulting in elimination of cancerous cells via different death mechanisms including apoptosis (Li *et al.*, 2001). Further, investigating the role of NF-κB in the cellular radiation response will not only be of interest for

astronauts, who are exposed to a potentially life-threatening radiation environment during long-term space missions, but also relevant for cancer therapy. For risk assessment, more detailed knowledge concerning NF-κB and the involvment in cellular outcomes after irradiation with different radiation qualities is needed.

1.2.5   Biological endpoints in NF-κB investigation

To investigate NF-κB and its involvement in the cellular outcome after irradiation, different biological endpoints are of interest. In this work, growth, cell cycle progression, survival and expression of its target genes were investigated.

1.2.5.1 NF-κB in growth and survival

The importance of NF-κB in survival was revealed by mice lacking the RelA gene, which had embryonic lethal consequences, due to an increased sensitivity of hepatocytes to the apoptotic action of TNF-α (Beg *et al.*, 1995). Further evidence for these findings was shown by different cellular models, in which inactivation of NF-κB lead to increased apoptotic sensitivity of cells after exposure to various stimuli or stress conditions (Bottero *et al.*, 2001; Busuttil *et al.,* 2002; Van Antwerp *et al.,* 1996; Wang *et al.,* 1996).

Active NF-κB induces transcription of a set of genes, coding for anti-apoptotic proteins. Defects in NF-κB result in increased susceptibility to apoptosis leading to increased cell death. A number of anti-apoptotic genes like TNF receptor-associated factors 1 and 2 (TRAF1 and TRAF2; Sheikh and Huang, 2003), cellular inhibitor of apoptosis proteins 1 and 2 (c-IAP1 and c-IAP2; Deveraux and Reed, 1998) or caspase 8-FAS-associated death domain (FADD)-like IL-1β-converting enzyme inhibitory protein (c-FLIP; Kreuz *et al.*, 2001) are induced by NF-κB. NF-κB further regulates activities of the caspase family, which is central to most apoptotic processes (Sheikh and Huang, 2003).

One major signalling pathway involving anti-apoptotic functions of NF-κB is the TNF receptor 1 (TNF-R1) signalling pathway, which is induced after irradiation (Luce *et al.*, 2009). Further common genes known to be involved in regulation of apoptosis are X chromosome-linked inhibitor of apoptosis protein (XIAP), B-cell lymphoma 2 (BCL-2) and B-cell lymphoma-extra large (BCL-X$_L$).

Under certain circumstances, NF-κB has pro-apoptotic functions and amplifies cell death. This is due to the induction of genes coding for the death receptor Fas or its ligand FasL (Ravi *et al.*, 1998a).

Defects in the NF-κB pathway are related to tumor growth and proliferation and over-expression of NF-κB target genes gives cells additional growth advantages (Baichwal and Baeuerle, 1997; Sonenshein, 1997). Therefore, anti-tumor therapies seek to block NF-κB activity to inhibit proliferation or to sensitize tumor cells to conventional therapies, such as chemotherapy.

1.2.5.2 NF-κB and cell cycle regulation

NF-κB might be involved in cell cycle arrest in order to allow DNA repair (Li *et al.*, 1994; Russell *et al.*, 2002; Zhou *et al.*, 1999). It was shown to be involved in the induction of cyclin D1, which is an essential element of the transition of G1 to S phase (Guttridge *et al.,* 1999). Additionally, NF-κB was shown to regulate the cell cycle through actions on the cyclin-dependent kinase (CDK)/cyclin-dependent kinase inhibitor (CKI) system (Joyce *et al.,* 2001). Activators of CDKs are, amongst others, the cell cycle regulating growth arrest and DNA damage-inducible gene 45 (GADD45) genes. GADD45 genes are activated by ionizing radiation, with GADD45β being regulated by NF-κB (Liebermann and Hoffmann, 2008). *Ataxia-telangiectasia*-patients lacking ATM, which induces NF-κB activation via the genotoxic stress-induced pathway, suffer from extreme radiosensitivity and cell cycle anomalies (Lavin and Shiloh, 1996). Further, it was found that NF-κB is involved in the regulation of different cell cycle phases following treatment with DNA-damaging agents and TNF-α. Besides, cells, which were unable to activate NF-κB, underwent transient G2-M arrest and extensive cell death (Wuerzberger-Davis *et al.*, 2005).

In response to radiation, the progression of the cell cycle is arrested to allow more time for DNA repair. Depending on the severity of DNA damage, the cell can repair the damage or is not able to repair and undergoes cell death.

The outcome of the cell depends on radiation quality, dose, cell type, dose rate and the cell cycle phase at the time of radiation exposure. The role of NF-κB in cell cycle regulation after irradiation with HZE particles is not fully understood.

1.2.5.3 NF-κB and its target genes

To obtain an overview on NF-κB-dependent gene expression after irradiation with different radiation qualities, a variety of genes was analysed in this work. Common genes, which are expected to be involved in the radiation response were investigated, as gene expression after radiation exposure and the role of NF-κB within is not completely understood. To obtain a primary overview, genes involved in cell cycle, p53 signalling, stress response, apoptosis, DNA damage, the NF-κB pathway and oxidative stress were investigated initially.

As this work focusses on NF-κB as a central element in the cellular radiation response, the expression of NF-κB target genes was of special interest. Table 2, taken from Nishikori (2005), shows only a small selection of the various processes in which NF-κB target genes are involved.

Table 2: *Selection of NF-κB target genes (taken from Nishikori, 2005).* All of the genes shown are related to tumor progression. (VEGF) vascular endothelial growth factor; (IL-8) Interleukin 8; (IL-6) Interleukin 6; (COX2) cyclooxygenase 2; (iNOS) inducible nitric oxide synthase; (MMP-9) metalloproteinase-9; (uPA) urokinase plasminogen activator; (ICAM-1) intracellular adhesion molecule-1; (VCAM-1) vascular cell adhesion molecule-1; (ELAM-1) endothelial-leukocyte adhesion molecule-1.

Activity	Genes
Inflammation	TNF, IL-1, chemokines
Cellular immortality	Telomerase
Cell survival	BCL-X$_L$, c-IAP, XIAP, c-FLIP
Angiogenesis	VEGF, TNF, IL-1, IL-8
Proliferation	TNF, IL-1, IL-6, cyclin D1, c-MYC
Tumor progression	COX2, iNOS, MMP-9, uPA
Metastasis	ICAM-1, VCAM-1, ELAM-1

Amongst the large number of genes regulated by NF-κB, gene expression analysis focussed on genes involved in the regulation of the inflammatory response, tumorigenesis and apoptosis. Expression of NF-κB-dependent genes coding for cytokines, ligands and receptors, inflammatory response genes etc. was analysed to get an insight into the underlying mechanism of different cellular outcomes after exposure to space-relevant radiation.

1.2.6 Inhibiting the NF-κB pathway by chemicals and by RNAi

Targeted inhibition of the NF-κB pathway helps to reveal molecular mechanisms and its role in the cellular radiation response. Further, it might induce and increase the killing effect in cancer therapy, when combined with chemo- or radiotherapy.

In this work, the chemical inhibitors MG-132 and KU-55933 were used to suppress the NF-κB pathway and to investigate its impact on the radiation response. MG-132 inhibits the proteasome, which is essential for degradation of the ubiquitinated IκB-inhibitor. Zanotto-Filho *et al.* (2009) showed, that MG-132 presented an increased apoptotic effect compared to other inhibitors in leukemia cells. Further, MG-132 arrested cells in

G2/M phase of the cell cycle and blocked doxorubicin-induced NF-κB activation. MG-132 was shown to be an effective inducer of apoptosis in tumor cells and may be a potent anticancer agent (Banerjee and Liefshitz, 2001).

KU-55933 interferes with the DNA damage induced pathway by inhibiting ATM and showed that it acts as a radiosensitizing agent in preclinical studies (Kuroda *et al.*, 2012). Cell cycle arrest in the G2 phase after irradiation with ionizing radiation could be effectively abrogated by inhibiting ATM with KU-55933 (Landsverk *et al.*, 2011).

Fig. 9 shows the targets of MG-132 and KU-55933 in a schematic view of the classical and the genotoxic induced NF-κB pathway.
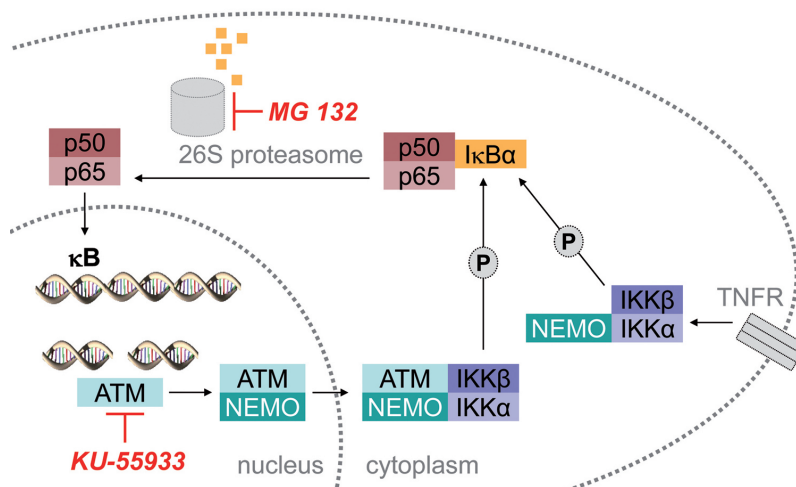
Fig. 9: *Chemical inhibition of the NF-κB pathway.* KU-55933 targets ATM, which is activated by DNA DSB in the genotoxic stress-induced NF-κB pathway. In the classical and the genotoxic stress-induced pathway, MG-132 inhibits the proteasome from degrading IκBα.

In addition to chemically inhibiting elements of the NF-κB pathway, a stable transfection using RNA interference (RNAi) to knockdown RelA expression was performed. The mechanism of RNAi was discovered in the nematode worm *Caenorhabditis elegans* as a response to double-stranded RNA (dsRNA) which resulted in sequence-specific gene silencing (Fire *et al.*, 1998). RNAi was discovered as a system within living cells that helps to control which genes are active and how active they are. As a consequence, antisense RNA was used as an approach to inhibit gene expression (Hannon, 2002). The RNAi pathway results in degradation of targeted mRNA by the RNAi induced silencing complex (RISC; Fig. 10). Different methods can be chosen to achieve mRNA cleavage. DsRNA can be introduced into the cell, which is subsequently cleaved by dicer into small interfering RNAs (siRNA). SiRNAs are 21-23 nucleotides in length and can also directly be introduced into the cell. They associate with RISC and are directed to the target mRNA. SiRNA does not allow stable transfection and only works under transient transfection conditions.

Alternatively, vectors expressing short hairpin RNA (shRNA) can be stably transfected into the cell. The vector is transported into the nucleus, where shRNA is expressed by RNA polymerase III (Pol III). ShRNA is translocated into the cytoplasm where is is cleaved into siRNAs, which associate with RISC. Here, the different pathways converge. In order to stably transfect cells, a DNA vector expressing shRNA was used in this work.
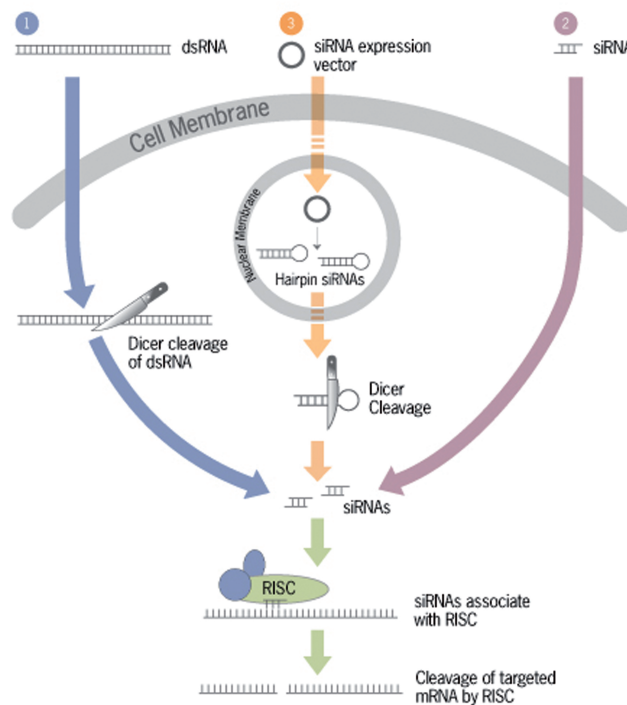
Fig. 10: *The RNAi pathway.* Three distinct approaches lead to cleavage of the target mRNA by the RNA-induced silencing complex (RISC). In non-mammalian cells, dsRNA is introduced into the cell and further cleaved into siRNA by cytoplasmatic nucleases (Dicer) (1). In mammalian cells, RNAi can be triggered by transiently transfecting siRNA (2) or stably transfecting cells with DNA vectors expressing shRNA (3). In all cases, shRNA is further processed into siRNA. All three pathways converge at the association of siRNA with RISC (Credit: Invitrogen).

1.3 Aim of this thesis

Amongst all space environmental factors, microgravity and cosmic radiation are two of the main limiting factors for long-term orbital and interplanetary space missions, causing severe health risks for the astronaut. In order to provide a better basis for risk assessment and countermeasure development, the effects of space-relevant radiation on the cellular level have to be investigated.

It was shown that the transcription factor NF-κB is strongly activated by fluences and ion species with high LET that are of relevance in space radiation environment. It is hypothesised that the NF-κB pathway is a potential pharmacological target for mitigation of the radiation response as it might enhance survival of cells exposed to heavy ions. Even though the NF-κB pathway has been investigated extensively throughout

the last years, not much is known about its role in the cellular response to space-relevant radiation. More detailed knowledge in this field is necessary to improve risk estimation and assess the questions of how to prevent acute effects like cell death after high dose irradiation as well as late effects like cell transformation during chronic low-dose exposure.

Specifically, the following tasks were accomplished:

1. Investigate NF-κB activation after exposure to different radiation qualities and quantities.
2. Chemical inhibition of key elements of different NF-κB subpathways to analyze their role in NF-κB activation induced by low and high LET ionizing radiation.
3. Knockdown of an important NF-κB subunit to assess its role in the cellular response to space-relevant radiation.
   3.1 Characterization of the stably transfected knockdown cell line concerning cellular proliferation, cell cycle progression and gene expression.
   3.2 Effects of NF-κB subunit knockdown on cell cycle progression, cellular survival and gene expression after exposure to low and high LET radiation.

2 Material and Methods

2.1 Material

2.1.1 Chemicals

Chemicals were purchased at Sigma Aldrich (Steinheim, Germany), if not otherwise stated.

2.1.2 Vectors

SureSilencing™ shRNA Plasmids (SABiosciences, Frederick, MD, USA) were designed to specifically knockdown the expression of RelA using the pGene Clip™ Hygromycin Vecor (Promega, Mannheim, Germany) as the backbone. Pre-designed shRNA plasmids were delivered in a set of four individual vectors specific for the same gene (Clone ID 1 to 4) plus one negative control (NC) shRNA vector. All vectors contain the Hygromycin-resistance marker (Fig. 11).
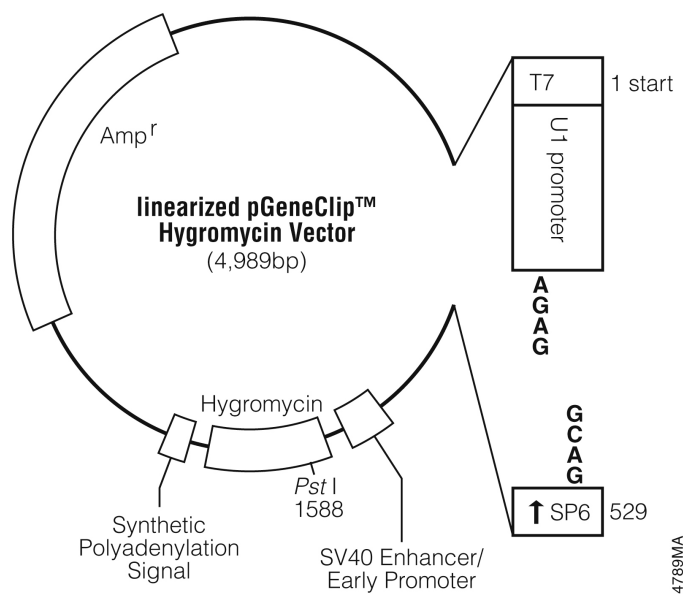
Fig. 11: *pGene Clip™ Hygromycin Vector circle map (Promega, Mannheim, Germany).* The vector contains amongst others a transcription site for the T7 bacteriophage RNA polymerase, a human U1 promoter and termination site, a promoter for the SP6 RNA polymerase, an Simian virus 40 (SV40) enhancer and early promoter as well as coding regions for Hygromycin phosphotransferase and β-lactamase (Amp^r).

Representative sequences used to design the enclosed shRNA refer to the RefSeq Accession # NM_021975 and are listed below:

Clone ID	Insert sequence
1	CCTGAGCACCATCAACTATGA
2	GACCTTCAAGAGCATCATGAA
3	GCTCAAGATCTGCCGAGTGAA
4	GCGCATCCAGACCAACAACAA
NC	ggaatctcattcgatgcatac

2.1.3 Oligonucleotides

Restriction enzymes and PCR primers were purchased from Promega, New England Biolabs (Beverly, MA, USA) or SABiosciences.

2.1.4 Antibodies

Immunofluorescence was conducted using an anti-NF-kappaB p65 rabbit monoclonal antibody (Epitomics, Burlingame, CA, USA; Catalog# 1546-1) with a working dilution of 1:250. For detection of the primary antibody, a TRITC-coupled swine anti-rabbit antibody (Dako; Agilent Technologies, Karlsbrunn, Germany; Catalog# R0156), diluted 1:250, was used.

2.1.5 Cell lines

The starting cell line for further stable transfection was HEK-pNF-κB-d2EGFP/Neo L2. For generating this cell line, HEK-293 cells, generated from human embryonic kidney cells (Graham *et al.*, 1977), were stably transfected with the plasmid pNF-κB-d2EGFP/Neo (Fig. 12), a reporter system to monitor NF-κB activation. The subclone L2 was selected (Hellweg *et al.*, 2003). In this cell line, d2EGFP, the destabilized variant of EGFP, is used to report NF-κB activity in human cells. Therefore d2EGFP is under the control of a synthetic promoter, which consists of four NF-κB binding sites (5'-GGGAATTTCC-3') and the RNA polymerase binding site from the thymidin kinase promoter. For selection purposes the vector further contains a kanamycin/neomycin resistance gene under the control of a bacterial promoter and the SV40 enhancer. HEK-pNF-κB-d2EGFP/Neo L2 cells were transfected with a SureSilencing™ shRNA Plasmid (Fig. 11) targeting RelA. The selected clone was named 'HEK shRNA RelA' and is characterized by a RelA knockdown (KD) level of 83.1 % and a resistance against Hygromycin.
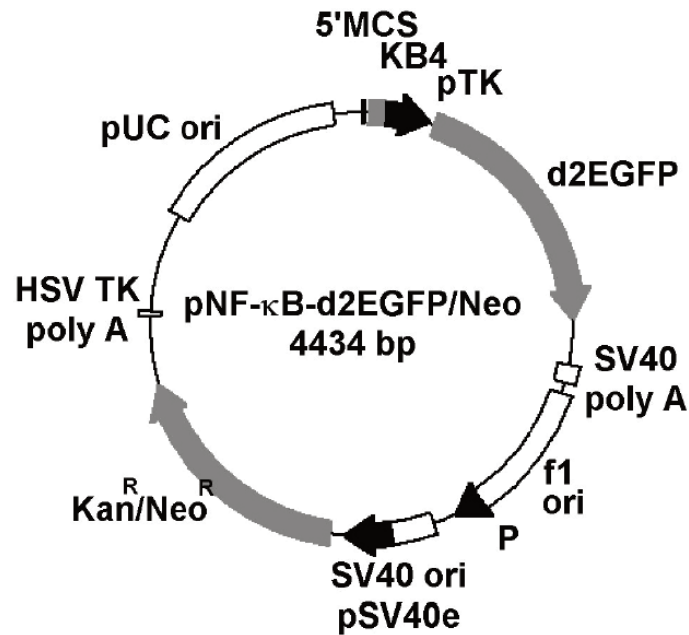
Fig. 12: *pNF-κB-d2EGFP/Neo vector circle map.* The pNF-κB-d2EGFP/Neo plasmid was used for stable transfection of HEK-293 cells (Hellweg *et al.*, 2003). Here, the d2EGFP gene is under control of an NF-κB-dependent promoter to report NF-κB activation. (f1 ori) f1 single strand DNA origin; (HSV TK poly A) Herpes simplex virusthymidine kinase polyadenylation signal; (Kan^R/Neo^R) kanamycin/neomycin resistance gene; (KB4) 4x NF-κB response element; (5´MCS) 5´ multiple cloning site; (P) bacterial promoter for expression of Kan^R/Neo^R gene; (pSV40e) SV40 early enhancer; (pUC ori) pUC plasmid replication origin; (SV40 ori) SV40 origin of replication; (SV40 poly A) SV40 late mRNA polyadenylation signal, (pTK) thymidine kinase minimal promoter.

2.2   Molecular biological methods

2.2.1   Plasmid ampification and verification

The shRNA plasmid was propagated by bacterial transformation and extraction of DNA, and its identity was checked by restriction analysis.

2.2.1.1 Transformation

100 µl of competent *E. coli* DH5α-cells (Stratagene; Agilent Technologies, Karlsbrunn, Germany) were thawed on ice for 5-10 min. 2 µl of each SureSilencing™ shRNA Plasmid (30 - 50 ng/µl) was added to the cells and mixed well before incubating for 10-15 min on ice. Cells were heat-shocked at 42 ˚C for 45 s and placed back on ice for additional 2-3 min. 1 ml of antibiotic free Luria Bertani (LB)-medium (20 g/l, in ddH$_2$O, autoclaved) was added and cells were shaken for 30-45 min at 37 ˚C. Cells were centrifuged for 3 min at 2500 x g. The supernatant was removed, leaving ∼ 100 µl liquid

including the pellet in the tube. The pellet was resuspended and plated on selective LB-agar (35 g/l, in dd$_H$2O, autoclaved) plates containing ampicillin (Biochrom GmbH, Berlin, Germany) with a final concentration of 50 µg/ml for selection and incubated at 37 °C over night (o/n).

2.2.1.2 Preparation of plasmid DNA

One colony from an agar plate was added to 100 ml of LB-medium containing 50 µg/ml ampicillin and cultured o/n under permanent shaking. For preparation of plasmid DNA the Plasmid Maxi Kit (Qiagen, Hilden, Germany) was used. Bacteria were harvested by centrifugation at 4 °C for 15 min at 4000 x g. The supernatant was discarded and the cell pellet was resuspended in 10 ml P1 resuspension buffer. 10 ml P2 lysis buffer were added, the solution was gently mixed and cells were lysed for 5 min at room temperature. 10 ml of P3 neutralisation buffer were added and the solution was mixed. After incubating the solution for 20 min on ice, it was centrifuged at 4 °C for 30 min at 13000 x g. Columns were equilibrated by applying 10 ml of QBT equilibration buffer. The supernatant was applied to the column, which was then washed twice with 30 ml of washing buffer QC. The DNA was eluted with 15 ml of elution buffer QF and collected in a 50 ml falcon tube. It was precipitated by adding 0.7 volumes of 100 % isopropanol and centrifugation at 4 °C for 30 min at 4000 x g. The supernatant was removed and the pellet was washed with 10 ml 70 % EtOH. After centrifuging again at 4 °C for 10 min at 4000 x g, the supernatant was removed and the DNA pellet was dried at room temperature. Afterwards, the pellet was resuspended in 100 µl TE storage buffer (10 mM Tris, 1 mM EDTA, pH 8.0).

2.2.1.3 Analytical cleavage of DNA

To verify the correct size of all plasmids, an analytical cleavage with the restriction enzyme *ScaI* was performed. Digestion of the shRNA plasmid with *ScaI* resulted in fragments sized 3346 and 1643 bp indicating the presence of shRNA insert of 20 bp. For the reaction mix, 2 µl RE 10x buffer, 2 µl template DNA (10 ng), 1 µl *ScaI* (10 u/µl) and 15 µl ddH$_2$O were mixed in a 0.5 ml tube. Restriction digestion was run at 37 °C for 1 h in the thermoblock TRIO (Biometra, Göttingen, Germany).

2.2.1.4 Electrophoretic separation of DNA fragments

Separation of DNA fragments was performed by agarose gel electrophoresis. Agarose (Serva Electrophoresis, Heidelberg, Germany) was added to 1x TAE buffer (50x TAE buffer: 242 g Tris base, 57.1 ml glacial acetic acid, 100 ml 0.5 mol/l EDTA pH 8.0, ad 1 l

ddH$_2$O) to the final concentration of 1 % and solubilized by boiling. DNA was visualised by adding 1:10000 diluted SYBR® Safe DNA Gel Stain (Invitrogen, Karlsruhe, Germany) to the DNA samples. After cooling to less than 65 °C DNA samples were mixed with 6x DNA Loading Dye (Fermentas; Thermo Scientific, Schwerte, Germany) and loaded onto the gel. In order to define the size of the separated fragments, a DNA size maker (GeneRuler™ 1kb DNA Ladder; Fermentas) was also loaded onto the gel.

2.2.2   Gene expression analysis

mRNA expression levels were determined by reverse transcriptase quantitative real-time polymerase chain reaction (real-time RT-qPCR). Therefore, RNA was isolated according to 2.2.2.1 and reverse transcribed into cDNA (s. 2.2.2.3). Gene expression analysis, as described hereafter, was conducted to determine knockdown levels of RelA with the RT^2 qPCR Primer Assay (s. 2.2.2.4), to investigate the kinetics of expression levels of selected NF-κB target genes by real-time qPCR (s. 2.2.2.5) and to finally examine whole sets of target genes with the RT^2 Profiler™ PCR Array (s. 2.2.2.6).

2.2.2.1 RNA isolation

RNA was isolated for subsequent determination of mRNA levels by real-time RT-qPCR. For statistically significant results in the knockdown verification, each sample was prepared in triplicates. At a density of ∼ 50 % cells were lysed with RLT buffer containing 10 % 14.3 mol/l β-Mercaptoethanol and transferred into an RNase-free Eppendorf tube with an iced syringe. RNA was isolated using the RNeasy® Mini Kit (Qiagen) according to the manufacturers protocol. To avoid overloading of the columns, not more than 700 µl of buffer containing lysed cells were used for RNA isolation. As RNA was used for cDNA synthesis and subsequent RT-qPCR, the additional DNase treatment step was included to eliminate residual genomic DNA. For preparing the DNase I stock solution, DNase I (1500 Kunitz units; Qiagen) was diluted in 550 µl RNase-free H$_2$O. The DNase I stock solution was further diluted 1:8 in RDD buffer (Qiagen). Subsequently, 80 µl of the DNase I incubation mix were added to the columns and incubated for 15 min at room temperature. RNA was eluted in 50 µl RNase-free H$_2$O.

2.2.2.2 Integrity of RNA

RNA concentration and purity were measured photometrically (A$_{260/280}$) with the Nano-Drop 2000c Spectrometer (Thermo Scientific). Additionally, RNA concentration, RNA integrity (RNA Integrity Number; RIN) and rRNA ratio (28S/18S) were measured by

micro-electrophoresis using the RNA 6000 Nano Assay in the Agilent 2100 Bioanalyzer (Agilent Technologies).

For gene expression analysis with the RT^2 Profiler™ PCR Arrays (SABiosciences), further RNA quality control with RT^2 RNA QC PCR array (SABiosciences) was performed, as described in 2.2.2.6.

2.2.2.3 cDNA synthesis

Quality, integrity and quantity of isolated RNA were analyzed according to 2.2.2.2. Subsequently, RNA was reverse transcribed into cDNA using the RT^2 First Strand Kit (SABiosciences). A preliminary genomic DNA (gDNA) elimination step was conducted, as recommended in the protocol:

Reaction Mix:

Total RNA	1000 ng
5X gDNA Eimination Buffer (GE)	2 µl
ddH$_2$O	ad 10 µl

To detect genomic DNA contamination in isolated RNA samples, one sample lacking reverse transcriptase was used as a negative control. The reaction mix was incubated at 42 °C for 5 min.

The RT reaction mix for one sample contained

5X RT Buffer (BC 3)	4 µl
Primer & External Control Mix 3 (PC2)	1 µl
RT Enzyme Mix 3 (RE3)	2 µl
ddH$_2$O	3 µl

The RT reaction mix was added to the gDNA Elimination Mixture and incubated at 42 °C for 15 min. The reaction was stopped by heating at 95 °C for 5 min. CDNA concentration at this stage was 50 ng/µl. Finally 91 µl of H$_2$O were added to each 20 µl cDNA synthesis reaction to obtain a final cDNA concentration of 9 ng/µl. CDNA samples were stored at -20 °C.

For real-time qPCR experiments as described in 2.2.2.5, cDNA synthesis was performed using the iScript cDNA Synthesis Kit (BioRad). Therefore, 1000 ng RNA was transcribed in 4 µl iScript reaction mix with 1 µl iScript reverse transcriptase. CDNA was diluted to 5 ng/µl with DNase-free water.

2.2.2.4 Determination of knockdown-level by real-time qPCR

Knockdown levels of RelA mRNA were determined using the RT^2 qPCR Primer Assay (SABiosciences). The primer pairs *SYBR® Green Human RELA* and *SYBR® Green Human HPRT 1* were used for targeting the gene of interest (GOI) V-rel reticuloendo-theliosis viral oncogene homolog A (RELA) and the housekeeping gene (HKG) Hypoxanthine phosphoribosyltransferase (HPRT; Tab. 3).

Table 3: *qPCR primer pairs as described in the RT² qPCR Primer Assay (SABiosciences).* All genes listed are human genes. (HPRT) Hypoxanthine phosphoribosyltransferase 1; (RELA) V-rel reticuloen-dotheliosis viral oncogene homolog A.

Gene symbol	RefSeq Accession #	Amplicon size	Melting temperature
RELA	NM_021975.3	65 bp	80 °C
HPRT1	NM_000194.2	89 bp	76.5 °C

Every single sample of the seeded triplicates was analysed by three real-time qPCR reactions to characterize the expression levels of the GOI and the HKG. The HKG was used to normalize the results. The qPCR experiment was set up in a 96-well PCR plate (4titude, Surrey, UK) as depicted in Fig. 13.

	1 2 3	4 5 6	7 8 9	10 11 12
A	Clone #1 Seeding #1 P1 P2 P3	Clone #3 Seeding #3 P1 P2 P3	Clone #1 Seeding #1 P1 P2 P3	Clone #3 Seeding #3 P1 P2 P3
B	Clone #1 Seeding #2 P1 P2 P3	Clone #4 Seeding #1 P1 P2 P3	Clone #1 Seeding #2 P1 P2 P3	Clone #4 Seeding #1 P1 P2 P3
C	Clone #1 Seeding #3 P1 P2 P3	Clone #4 Seeding #2 P1 P2 P3	Clone #1 Seeding #3 P1 P2 P3	Clone #4 Seeding #2 P1 P2 P3
D	Clone #2 Seeding #1 P1 P2 P3	Clone #4 Seeding #3 P1 P2 P3	Clone #2 Seeding #1 P1 P2 P3	Clone #4 Seeding #3 P1 P2 P3
E	Clone #2 Seeding #2 P1 P2 P3	Clone #5 Seeding #1 P1 P2 P3	Clone #2 Seeding #2 P1 P2 P3	Clone #5 Seeding #1 P1 P2 P3
F	Clone #2 Seeding #3 P1 P2 P3	Clone #5 Seeding #2 P1 P2 P3	Clone #2 Seeding #3 P1 P2 P3	Clone #5 Seeding #2 P1 P2 P3
G	Clone #3 Seeding #1 P1 P2 P3	Clone #5 Seeding #3 P1 P2 P3	Clone #3 Seeding #1 P1 P2 P3	Clone #5 Seeding #3 P1 P2 P3
H	Clone #3 Seeding #2 P1 P2 P3	NTC	Clone #3 Seeding #2 P1 P2 P3	NTC
	PCR primers specific for RELA		PCR primers specific for HPRT	

Fig. 13: *Setting up real-time PCR validation of knockdown.* The figure represents a 96-well plate. The reactions in the first set of six numbered columns characterizes the knockdown-level of RELA in the in-dicated RNA samples, while columns 7 to 12 depict the expression of HPRT in the corresponding RNA samples. (NTC) no template control; (P1)-(P3) triplicate PCR reaction.

The real-time qPCR reaction mix for one PCR tube was composed referring to the RT^2 qPCR Primer Assays protocol as follows:

RT^2 SYBR Green qPCR Master Mix	12.5 µl
ddH_2O	8.5 µl
Template cDNA (27 ng)	3 µl
10 µM PCR primer pair stock	1 µl

As a negative control DNA was replaced by H_2O.

Real-time qPCR analysis was performed in the Opticon2 thermocycler (BioRad, Munich, Germany) according to the protocol in Table 4.

The quality of the qPCR was controlled (s. 2.2.2.5) and data were analysed as described hereafter.

Table 4: *Real-time qPCR protocol for validation of RELA knockdown levels.* The cycling conditions are taken from the RT^2 qPCR Primer Assay protocol (SABiosciences).

	Cycles	Time	Temperatures
Initial denaturation	1	10 min	95 °C
Denaturation		15 s	95 °C
Annealing	40	35 s	55 °C
Plate Read			
Elongation		30 s	72 °C
Melting curve		read every 0.2 °C	60-95 °C
Final	1	1 min	29 °C

To determine the percentage of knockdown measured by real-time qPCR, an Excel-based data analysis template provided by SABiosciences was used. The detailed algorithm, which is used in this sheet for calculations is described in detail in the Sure-Silencing™shRNA Plasmids protocol (SABiosciences). It includes determination of the arithmetical average of the technical triplicate PCR C_t values and standard deviations for both genes (RELA and HPRT1) and individual ΔC_t values for each biological replicate transfection of each design and the negative control. It calculates average ΔC_t and its standard deviation across the biolological replicates and the average $\Delta \Delta C_t$ and its standard deviation for each design based on the $\Delta \Delta C_t$ method:

$\Delta C_t = C_t \text{ (GOI) - } C_t \text{ (HKG)}$ *(Equation 4)*

$\Delta \Delta C_t = \Delta C_t \text{ (KD) - } \Delta C_t \text{ (NC)}$ *(Equation 5)*

Finally, the average knockdown and its 95 % confidence interval (C.I.) is calculated. The interpretation of the design is defined as follows:

Successful design: Observed KD ≥ 70 % and an upper 95 % C.I. boundary ≥ 55.5 %
Failed design: Observed KD < 33.3 % and a lower 95 % C.I. boundary < 55.5 %

2.2.2.5 Real-time qPCR for selected NF-κB target genes

To investigate the dose-effect relationship and the kinetics of NF-κB-dependent gene expression, the expression of two NF-κB target genes, NFKBIA and GADD45beta, was analysed by real-time RT-qPCR. GAPDH was used as housekeeping gene.

For real-time RT-qPCR experiments investigating NFKBIA and GADD45beta, reverse transcription of purified RNA into cDNA was performed using the iScript cDNA Synthesis Kit (s. 2.2.2.3). To investigate the qPCR efficiency for each gene of interest, a dilution series of standards (25 - 0.008 ng/well cDNA) was prepared additionally. Therefore, 3 µl cDNA of each sample were pooled. Standards were measured in triplicates and samples and negative controls in duplicates.

Primers used for gene expression analysis have previously been established in the Cellular Biodiagnostics working group and are listed below:

Gene	Primer sequence	Amplicon size
GAPDH	fwd CAATGACCCCTTCATTGACC	146 bp
	rev GATCTCGCTCCTGGAAGATG	
GADD45beta	fwd ACAGTGGGGGTGTACGAGTC	155 bp
	rev TTGATGTCGTTGTCACAGCA	
NFKBIA	fwd AACCTGCAGCAGACTCCAC	137 bp
	rev TGCTCACAGGCAAGGTGTAG	

The reaction mix was composed as follows:

SYBR Green Mix (Invitrogen)	12.5 µl
forward (fwd) primer (0.2 µmol/l)	0.5 µl
reverse (rev) primer (0.2 µmol/l)	0.5 µl
Template cDNA (5 ng/µl)	2 µl
ddH$_2$O	ad 25 µl

For NFKBIA, betaine (N,N,N-trimethylglycine, Sigma) was added to the reaction mixture to a final concentration of 1 mol/l to facililate amplification due to the high GC content of the target sequences. Quantitative real-time analysis was performed in the Opticon2 thermocycler in 96-well plates according to Table 5:

Table 5: *qPCR protocol for investigations of the dose-effect relationship and the kinetics of NF-κB-dependent gene expression.* NFKBIA and GADD45beta were NF-κB target genes of interest. GAPDH was used as housekeeping gene.

	Cycles	Time	Temperatures
Initial denaturation	1	2 min	50 °C
	1	2 min	95 °C
Denaturation		15 s	95 °C
Annealing	44	30 s	61 °C (NFKBIA)
			61.9 °C (GADD45beta)
			60 °C (GAPDH)
Elongation		30 s	72 °C
Plate Read			
		20 s	78 °C
Plate Read			
Melting curve		read every 0.2 °C	60-95 °C
Final	1	1 min	29 °C

Quality of RT-qPCR was controlled as described hereafter. Subsequently, the PCR efficiency (E) was determined by means of the dilution series of cDNA standards. Therefore, a linear regression analysis was applied, resulting in a slope, which enables calculation of the PCR efficiency according to the equation

$$E = 10^{(-1/slope)}$$ *(Equation 6)*

An optimal PCR results in an efficiency (E) of 2, which indicates the exact doubling of the PCR product in each cycle. The threshold for determining the threshold cycle (C_t) was set manually in the exponential part of the amplification plots in the logarithmic diagram of the standard curve (Fig. 14). For comparison of all samples and genes, the threshold was kept constant throughout all PCR runs. Gene expression results of the housekeeping gene were used to measure background variation in gene expression. The software REST© (Relative Expression Software Tool; W. Pfaffl & G.P. Horgan, TU Munich, Germany) was used for statistical evaluation of the expression of target genes

relative to the reference gene GAPDH. Expression levels were related to each other according the following equation:

$$\text{Relative gene expression} = \frac{(E_{\text{Target gene}})^{\Delta C_t \, \text{Target gene (control - sample)}}}{(E_{\text{Reference gene}})^{\Delta C_t \, \text{Reference gene (control - sample)}}} \qquad \textit{(Equation 7)}$$
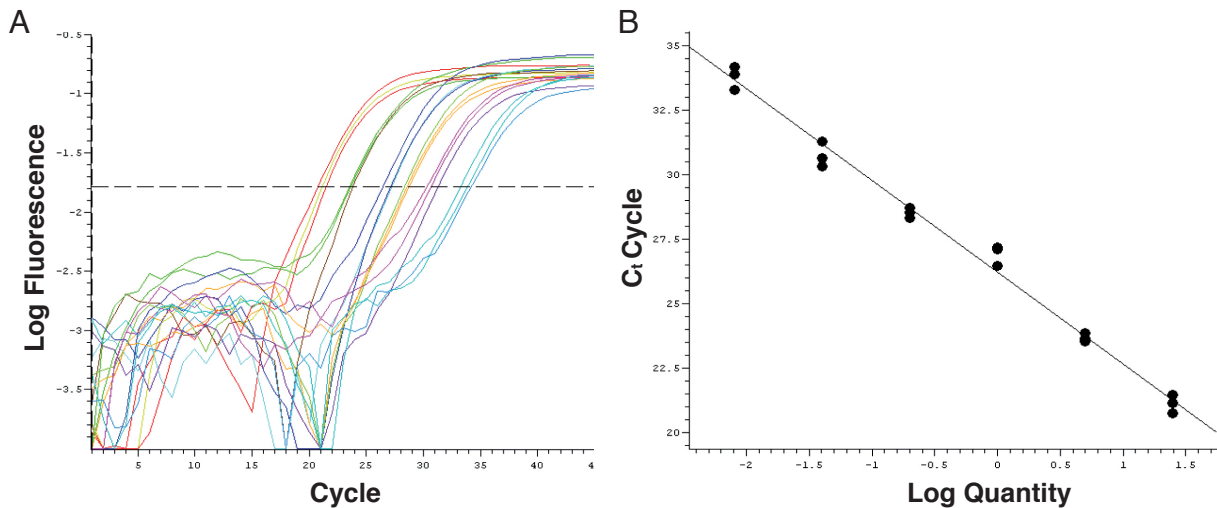
Fig. 14: *Real-time qPCR amplification plots and standard curve.* (A) The amplification plot shows the increasing fluorescence with increasing cycle number. The dotted line indicated the manually set threshold, which is located in the exponential part of the curve. (B) The respective standards curve is shown on the right, indicating a slope resulting in a PCR efficiency of ∼ 2.

To control the quality of the qPCR, a dissociation (melting) curve was run immediately after each cycling program. The settings for the melting curve are listed in the above-mentioned real-time qPCR protocol. Additionally, the quality of selected PCR products was further tested by loading the PCR product on an agarose gel as described in 2.2.1.4.

2.2.2.6 Real-time qPCR array

To assess RNA quality and to rule out genomic DNA contamination for subsequent gene expression analysis with RT² Profiler™ PCR Arrays, the RT² RNA QC PCR array (SABiosciences) was used. The detailed setup of the quality control plate and its functions is described in the RT² RNA QC PCR Array protocol. The array detects inhibition of reverse transcription or of PCR amplification, genomic DNA contamination, false positive signals and multi-peak dissociation curves. In detail, it includes analysis of high (HK1, ACTB) and low (HK2, HPRT1) housekeeping gene expression levels as well as

reverse transcription (RTC), positive PCR (PPC), genomic DNA (GDC), no reverse transcription (NRT) and no template (NTC) controls (s. 3.4.2, Table 11). Data analysis of this array is based on a Excel-based template provided by SABiosciences. After entering C_t values, interpretations are performed according to the algorithm which is described in detail in the RT² RNA QC PCR Array protocol. For genomic DNA contamination, e.g., C_t values must be greater than 35 in order to interpret the results as genomic DNA contamination not affecting the gene expression profiling results. If C_t values are less than 35, genomic DNA contamination is evident.

Human RT² Profiler™ PCR Arrays (SABiosciences) were used for expression profiling of 89 genes per sample. Two different arrays were available, with one being customized, individually composed of genes of interest of several singalling pathways and one array focussing on genes targeted by NF-κB. An overview of all genes included in these arrays is listed in Table 17 (s. Appendix). Each well of these arrays contains primers for the respective gene. Only cDNA samples, which had been approved by the RT² RNA QC PCR Array to prevent false positive signals by genomic DNA contamination, were used for further analysis. The RT-qPCR master mix for one 96-well plate was was set up according to the RT² Profiler™ PCR Array protocol:

RT² SYBR Green qPCR Master Mix	1350 µl
ddH₂O	1248 µl
Template cDNA (9 ng/µl)	102 µl

Quantitative real-time analysis was performed in the Opticon2 thermocycler according to Table 6. Results were analysed according to the algorithm decribed in the RT² RNA QC PCR Array protocol. It is based on the $\Delta\Delta C_t$ method:

$\Delta C_t = C_t \text{ (target gene) - } C_t \text{ (reference gene)}$ *(Equation 8)*

$\Delta\Delta C_t = \Delta C_t \text{ (sample) - } \Delta C_t \text{ (control)}$ *(Equation 9)*

The relative expression of treated sample versus control was calculated by means of equation 10. As efficiency curves for the 89 genes were not available, a PCR efficiency of 2 was assumed:

Relative gene expression $= 2^{-\Delta\Delta C_t}$ *(Equation 10)*

Table 6: *Cycling conditions for real-time PCR according to the RT² Profiler™ PCR array protocol*.

	Cycles	Time	Temperatures
Initial denaturation	1	10 min	95 °C
Denaturation		15 s	95 °C
Annealing	40	35 s	55 °C
Elongation		30 s	72 °C
Plate Read			
Elongation		20 s	78 °C
Plate Read			
Final	1	1 min	95 °C
		2 min	65 °C
Melting curve		read every 0.2 °C	65-95 °C

2.3 Cell culture

2.3.1 Culture conditions

Cell culture work was conducted using a sterile tissue culture hood (Hera safe, Kendro, Berlin, Deutschland). HEK-pNF-κB-d2EGFP/Neo L2 cells were grown under standard conditions in 75 cm² flasks (Nunc, Wiesbaden, Germany) in selection-medium (S-medium), consisting of α-medium (ALPHA MEM-medium; Biochrom) with addition of the following agents:

Fetal bovine serum (FBS)	10 %
L-glutamine	2 mmol/l
Glucose	0.34 %
Penicillin/Streptomycin	10,000 IE / 10,000 µg/ml
Neomycin/Bacitracin	1 mg / 50 U/ml
Amphotericin B	250 µg/ml
G418	0.6 mg/ml

For culturing HEK shRNA RelA cells, 200 µg/ml Hygromycin (US Biological, Massachusetts, USA) was added to the S-medium. For some experiments, cells were grown in α-medium, which does not contain G418 and Hygromycin.

Cells were grown at 37 °C, saturated humidity and in a 5 % CO_2 / 95 % air atmosphere. To ensure that the newly established cell line HEK shRNA RelA is free from *Myco-*

plasma contamination, it was screened at the Leibnitz-Institut DSMZ-Deutsche Samm-lung von Mikroorganismen und Zellkulturen GmbH (Braunschweig, Germany) by Dr. Uphoff (s. 7.5).

2.3.2 Coating of cell culture vessels with Poly-D-Lysine

For transporting cells or handling them for longer terms at room temperature, tissue culture plates or wells were coated with Poly-D-Lysine (final concentration: 0.01 mg/ml) to allow a stronger binding of cells to the substrate, as they would easily detach other-wise. Therefore, the culture vessels were coated with Poly-D-Lysine for 15 min at room temperature and subsequenty washed three times with PBS.

2.3.3 Cultivation of cells

Passaging of cell lines was accomplished once a week by using standard detachment procedures using phosphate buffered saline (137 mM NaCl, 2.3 mM KCl, 4.3 mM $Na_2HPO_4*7H_2O$, 1.4 mM KH_2PO_4, pH set to 7.4, autoclaved) and 0.05 % trypsin con-taining 0.02 % EDTA (PAN-Biotech, Aidenbach, Germany) solution. For counting cells, a Fuchs-Rosenthal counting chamber (W. Schreck, Hofheim, Germany) was used. Cells were seeded to a density of 1.5 - 3 x 10^4 cells/cm^2. Medium was changed as required every few days.

2.3.4 Freezing and thawing of cells

For preservation in liquid nitrogen, confluent cells were trypsinized and centrifuged for 5 min at 80 x g at room temperature. The pellet was resuspended in the required volume (2 x 10^6 cells/ml) of freezing medium (10 % Dimethylsulfoxid in α-medium) and pipetted into cryotubes (Nunc). Tubes were stored at -80 °C for at least 24 hours and subsequently transferred to liquid nitrogen for long-term storage.

Cryotubes were thawed in a 37 °C water bath (Lauda, Königshofen, Germany). Cells were added to 20 ml of prewarmed α-medium and plated in 75 cm^2 cell culture flasks. After 24 hours medium was exchanged to remove residual DMSO.

2.3.5 Cytotoxicity of chemical inhibitors

Cytotoxicity of the chemical inhibitors KU-55933 and MG-132 was measured by means of the MTT assay. Here, reduction of MTT (3-(4,5-dimethylthiazole-2-yl)-2,5-diphenyltetrazolium bromide) to formazan can be correlated to the activity of cellular enzymes and measured colorimetrically. HEK-pNF-κB-d2EGFP/Neo L2 cells were see-ded in 96-well plates (BD Biosciences, Heidelberg, Germany; area per well: 0.3 cm^2)

and preincubated with each inhibitor for 20 and 72 hours. NF-κB was activated by adding tumor necrosis factor α (TNF-α). After removing medium, cells were incubated for 1 h at 37 °C with serumfree α-medium containing 0.1 mg/ml MTT. Subsequently, cells were lysed with DMSO/SDS solution (99.4 % (v/v) DMSO, 0.6 % (v/v) acetic acid, 10 % (w/v) SDS) while shaking them for 20 min with 30 rpm.

100 % DMSO was used to measure the background signal of a dead cell layer. As a negative control, cells were not treated with TNF-α. Finally, absorbance of formazan was measured with the fluorescence/luminescence/absorption microplate reader LAMBDA Fluoro 320 (MWG Biotech AG, Penzberg, Deutschland) at 562 nm. Cell survival was calculated as a ratio of formazan-absorbance of treated vs. untreated samples.

2.3.6 RNA interference (RNAi)

2.3.6.1 Determination of cytotoxic Hygromycin B concentration

For selection of cells which were successfully stably transfected with the SureSilencing™ shRNA plasmid, the appropriate concentration of the antibiotic Hygromycin B had to be determined. HEK-pNF-κB-d2EGFP/Neo L2 cells were seeded in S-medium in a 96-well plate. At a cell density of ∼ 80 %, Hygromycin B (50 mg/ml) was added to the medium to final concentrations ranging from 0 to 400 µg/ml. As a positive control of the cytotoxic effect, 10 % EtOH was added to the medium. One well served as a blank-control and was therefore left empty.

After 10 days, medium was removed, cells were washed with PBS and finally stained with 200 µl of formaldehyde/cristal violet solution per well. After 30 min, the staining solution was removed and cells were washed with PBS. Cell growth was determined by measuring absorbtion at a wavelength of 410 and 592 nm in the LAMBDA Fluoro 320 and calculated as a ratio of absorbance values of treated vs. untreated sample.

Formaldehyde/crystal violet solution:

Crystal violet (Merck, Darmstadt, Germany)	0.1 g
Formaldehyde	3.7 %
H_2O	ad 100 ml

2.3.6.2 Stable transfection

HEK-pNF-κB-d2EGFP/Neo L2 cells were seeded in Poly-D-Lysine-coated 6-well-plates (Nunc). Each single one of the 6 wells was allocated for transfection with one of the five SureSilencing™ shRNA Plasmids. Four of these plasmids were coding for different tar-

geting sequences of RelA mRNA, while the fifth plasmid was a negative control vector containing a scrambeled artificial sequence which did not match any human, mouse or rat gene. Cells in the sixth well served as a negative control and were mock transfected. Each transfection was performed three times.

Transfection was conducted at a cell density of ∼ 50 %. Therefore, DNA concentration of each vector was measured and DNA was mixed with serumfree α-medium as well as 6 µl of transfection reagent according to the FuGENE 6® (Roche, Mannheim, Germany) protocol. Cells in each well were transfected with 2 µg of DNA.

After three days of incubation, cells were transfered into Ø 6 cm cell culture dishes (Nunc) containing selective medium containing 400 µg/ml Hygromycin. Medium was changed regularly. After approximately 10 days, cells were seeded for RNA isolation (s. 2.2.2.1) to measure the knockdown level of RelA in the mixed population of Hygromycin-resistant cells.

2.3.6.3 Clone selection

Two cell lines showing the highest knockdown level were chosen for further clone selection. Therefore, cells had to be singularized by seeding 50 cells in a 96-well-plate containing Hygromycin-medium. Cells were incubated for 2-3 weeks until they grew colonies. Single colonies were washed with PBS, trypsinised and transfered to a 25 cm^2 cell culture flask (Nunc) containing 5 ml of Hygromycin-medium. When cells had reached a density of 80-100 %, their knockdown level was determined by seeding them in triplicates and proceeding according to 2.2.2.1- 2.2.2.4.

2.3.7 Growth kinetics

To characterize differences in growth behaviour between HEK-pNF-κB-d2EGFP/Neo L2 and HEK shRNA RelA, both cell lines were seeded with the same cell number (1 x 10^4 cells/cm^2) in Poly-D-Lysine-coated 6-well plates. To ensure identical growth conditions, both cell lines were seeded in S-medium. Twice a day the cell number of one well was determined until cells have reached the stationary growth phase.

The doubling times for the cell lines were calculated based on the slope of the growth curve (m) during exponential growth:

Doubling time = ln 2/m   *(Equation 11)*

2.3.8 Colony forming ability test (CFA test)

A cell survival curve describes the relationship between the radiation dose and the proportion of cells that survive (Fig. 15). The fraction of cells surviving is plotted on a logarithmic scale against a dose on a linear scale. A cell which is apparently intact as it is synthesizing protein and DNA, but has lost the capacity to divide indefinitely is by the definition of the colony forming ability test dead. A survivor that has retained its reproductive integrity and is able to proliferate indefinitely to produce a colony is said to be clonogenic. The colony forming assay (Puck and Marcus, 1956) determines the ability of one cell to form a colony after exposure to ionizing radiation. One colony is defined to consist of at least 50 cells, resulting from six doublings. A dose of 100 Gy is necessary to destroy cell function in nonproliferating systems. By contrast, the mean lethal dose for loss of proliferative capacity is usually less than 2 Gy (Hall and Giaccia, 2012c).

The multitarget model describes the survival curve in terms of its initial slope (D_1) resulting from single-event killing; the final slope (D_0) resulting from multiple-event killing; and either n or D_q to represent the size or width of the shoulder of the curve. The parameters are correlated according to equation 12:

$$D_q = D_0 + \ln n \qquad\qquad\qquad \textit{(Equation 12)}$$

D_1 is the dose required to reduce the fraction of surviving cells to 0.37. D_0 is reciprocal of the slope in the exponential part of the curve. The extrapolation number n and the quasi-threshold dose D_q measure the width of the shoulder. The larger the value n, the larger is the shoulder of the survival curve.
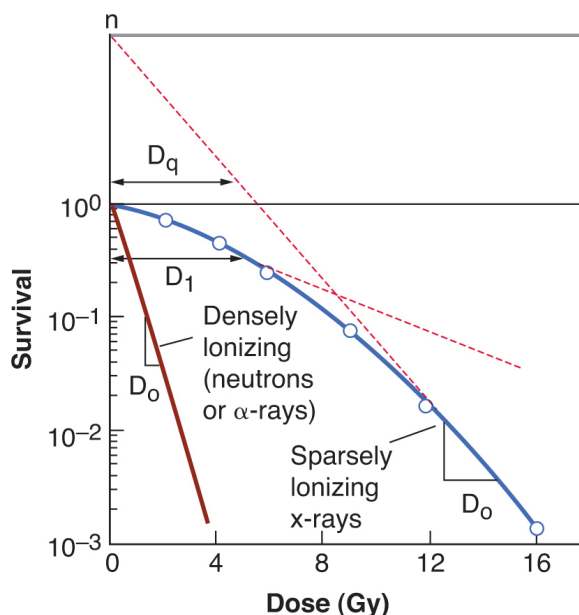
Fig. 15: *Clonogenic survival of mammalian cells exposed to radiation.* The graph illustrates the multitarget model. The curve is described by the initial slope (D_1), the final slope (D_0), and a parameter that represents the width of the shoulder, either n or D_q. Densely ionizing radiation results in a dose-response curve which is a straight line from the origin. For sparsely ionizing radiation, the curve displays a shoulder, while at higher doses it becomes straight again (taken from Hall and Giaccia, 2012c).

Cells were seeded in Ø 6 cm cell culture dishes or 25 cm² cell culture flasks and irradiatied with different doses of either X-rays or heavy ions according to 2.4. Subsequently, each irradiated sample was trypsinized, counted and seeded in Ø 6 cm cell culture dishes or 25 cm² cell culture flasks with a defined cell number. The cell number was determined according to the plating efficiency (PE) and the anticipated lethal effect of irradiation. Six experiments were performed with six dishes/flasks per dose. After irradiation cells grew for 14 to 21 days without medium change and were fixed afterwards with formaldehyde/crystal violet solution (s. 2.3.6.1). Colonies were counted and data were analysed according to 2.3.8.1. Only colonies containing more than 50 cells were scored as survivors.

2.3.8.1 Data analysis of CFA

To analyse clonogenic survival, plating efficiency (PE) and surviving fraction (SF) were calculated as follows using the software tool DOSE (by Dr. Christa Baumstark-Khan, DLR, Germany):

PE = colonies observed / number of cells plated   *(Equation 13)*

SF = colonies counted / cells seeded x (PE/100)   *(Equation 14)*

The probability that all targets will not be hit is defined as survival S. DOSE calculates S by dividing the PE of irradiated samples (PE_D) by the PE of unirradiated control ($PE_{D=0}$):

$S = PE_D / PE_{D=0}$ *(Equation 15)*

The relative survival of non-irradiated cells equals 1. DOSE calculates S and its natural logarithm (ln S) from the PE for each colony count, resulting in a semilogarithmic survival curve. The underlying algorithm, derived from the multitarget model (Kellerer and Hug, 1968), is defined as follows:

$S = 1 - (1 - e^{D/D_0})^n$ *(Equation 16)*

For higher doses, the equation can be simplified to the following regression line equation:

ln S = constant of proportionality (v) × dose (D) + ln n   *(Equation 17)*

ln S is defined by a regression line with the slope v and the axis intercept ln n.

$v = -1 / D_0$ *(Equation 18)*

2.3.9 Detection of NF-κB-dependent d2EGFP expression by flow cytometry

NF-κB can be induced by a variety of stimuli, including irradiation with X-rays or heavy ions (s. 2.4) and the cytokine TNF-α. TNF-α was used as a positive control in irradiation experiments. Therefore, TNF-α (stock solution: 10 ng/µl) was added to the growth medium to a final concentration of 10 ng/ml at a cell density of ∼ 50 %. At several time-points cells were washed with PBS, trypsinized and fixed with cold 3.5 % formaldehyde in PBS. After storing the samples at 4 °C for 30 min, PBS was added to dilute formal-dehyde to less than 1 %. NF-κB activation was determined by measuring GFP expression in a flow cytometer.

The Fluorescent Activated Cell Scanner (FACScan, BD Biosciences) is equipped with an argon laser (488 nm) for excitation and three fluorescent emission detection channels (FL1 515-545 nm, FL2 564-606 nm, FL3 > 670 nm). EGFP is characterized by an emission maximum (λ_{max}) of 509 nm and an excitation spectrum peaking at 470 nm and was therefore measured in the FL1 channel. Data were collected by the CellQuest software. For each sample, the forward (FSC) and side scatter (SSC) as well as the fluorescence of 20,000 cells were detected and afterwards displayed in WinMDI V2.8 (Windows Multiple Document Interface for Flow Cytometry; J. Trotter, Scripps Institute, La Jolla, CA, USA).

2.3.9.1 Evaluation of flow cytometry data from d2GFP analysis

The cell population was displayed in a dot plot using the WinMDI V2.8 software. FSC and SSC were used to define a region of intact cells which were further evaluated. From the gated population, a histogram showing the frequency of cells with a defined fluorescence intensity was plotted. Markers for d2EGFP[-] and d2EGFP^{+} cells were set by means of untreated and TNF-α treated cells (Fig. 16).
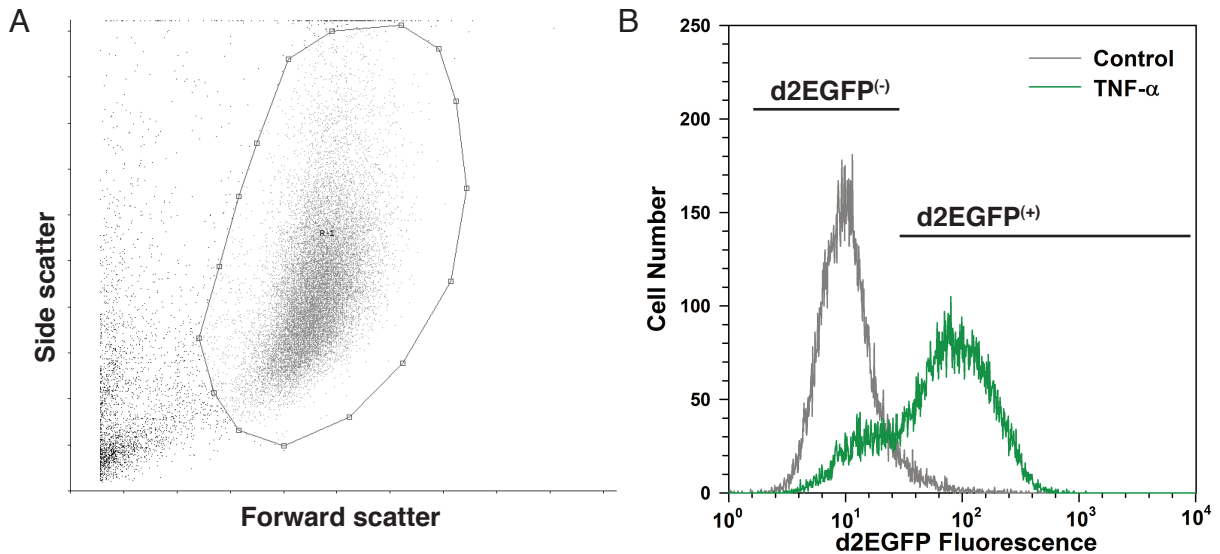
Fig. 16: *Flow cytometry data analysis of NF-κB activation.* The dot plot (A) of a cell population allows to manually define a region in respect to cell size (forward scatter) and granularity (side scatter). Events outside this region are not taken into acount for further analysis. A threshold for the forward scatter was set in order to eliminate the debris. The histogram (B) shows the d2EGFP fluorescence of the gated cell population. In the control sample, markers for d2EGFP[(-)] and d2EGFP[(+)] cells are set. The percentage of d2EGFP[(+)] cells was used as a value for measuring NF-κB activation. The green graph represents a typical histogram of HEK-pNF-κB-d2EGFP/Neo L2 cells 18 hours after treatment with 10 ng/ml TNF-α.

2.3.10   Cell cycle analysis by flow cytometry

To analyse distribution of cells in the cell cycle after irradiation, DNA was stained with propidium iodide (PI). Cells were seeded in Ø 3 cm culture dishes and irradiated with different doses. After several timepoints, cells were detached with 1.5 ml trypsin which was subsequently added into a 15 ml falcon containing 4.5 ml of iced 100 % EtOH. Samples were stored at -20 °C for at least 24 hours.

For analysis, 12 ml of PBS was added, and cells were centrifuged for 5 min at 1000 x g at room temperature. The supernatant was discarded and 1 ml of PI staining solution, containing RNase A to digest residual RNA, was added. Samples were incubated at 37 °C for 1 hour. Afterwards, red fluorescence was measured by flow cytometry.

PI staining solution:

RNase A (1 mg/ml)	50 µl (50 µg/ml)
100 % Triton X-100	1 µl (0.1 %)
PI (2.5 mg/ml)	8 µl (20 µg/ml)
PBS	ad 1000 µl

2.3.10.1 Evaluation of flow cytometry data from cell cycle analysis

PI produces a fluorescent DNA adduct that can be excited at 488 nm with a broad emission centred around 600 nm. It was detected with the FL2 channel of the FACScan. Fluorescence of 20,000 stained cells was measured and histograms were set up using the CellQuest software. Analysis was accomplished with WinMDI V2.8, Cylchred (Cardiff University, UK) and Flowing Software 2. As already described for evaluation of flow cytometry data from EGFP analysis, intact cells were selected by defining a region in the SSC versus FSC dot plot. Additionally, a FL2-width (FL2-W)/FL2-area (FL2-A) density plot was displayed to exclude doublets and cell debris from analysis. The PI fluorescence of gated cells was shown in a histogram, quantifying cells throughout the scale of fluorescence intensity, which is directly proportional to the amount of the DNA content (Fig. 17).

Cylchred or Flowing Software 2 were used to determine the relative distribution of the cell cycle phases by automatically or manually defining G1, S or G2 phase. In G2, the DNA content was the double of that observed in G1, and the DNA content during S-phase ranges between the ones of G1 and G2.
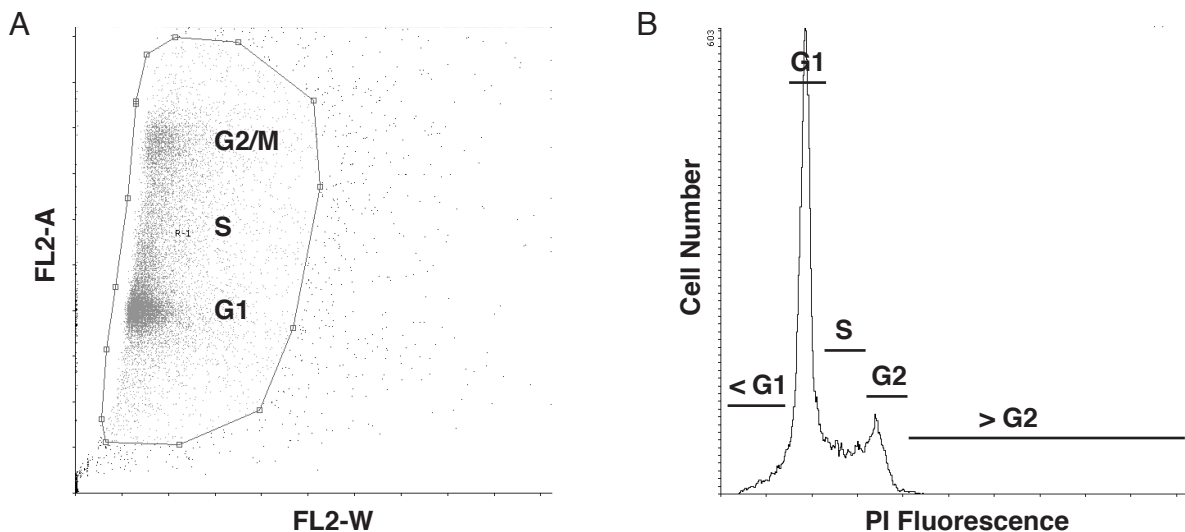
Fig. 17: *Flow cytometry data of cell cycle analysis.* The dot plot (A) of a cell population allows to manually define a region in respect to width (FL2-W) and area (FL2-A) of the fluorescence signal and thereby excluding cell doublets. Events outside this region are not taken into acount for further analysis. The histogram (B) shows the PI fluorescence of the gated cell population. PI fluorescence intensity is directly proportional to the DNA content and can therefore be used to draw conclusions regarding the cell cycle phases.

2.3.11 Visualisation of RelA by immunofluorescence

Cells were plated on Poly-D-Lysine coated 16-well (8.6 cm^2/well) glass chamber slides (Lab-Tec®; Thermo Scientific). At a density of ∼ 50 %, cells were irradiated. At time-points between 0 to 2 hrs cells were fixed with 3.5 % formaldehyde in PBS for 30 min and washed with PBS afterwards. Cell membranes were permeabilized on ice by adding 0.5 % Triton X-100/1 % bovine serum albumin (BSA) in PBS for 15 min and sub-sequently washed again with 1 % BSA in PBS. Unspecific binding of the antibodies was prevented by blocking with 50 % FCS in PBS for 1 h at room temperature. Cells were incubated with the primary anti-RelA antibody (Epitomics) diluted in PBS at room temperature for 1 h in a humidified chamber. Before adding the secondary antibody (Dako), cells were washed with 1 % BSA in PBS. Cells were incubated light-protected for 1 hour with the red-fluorescent secondary antibody, diluted in PBS. After washing with PBS, the nucleus was visualized by incubation with blue-fluorescent DAPI solution (4´,6-Dia-midino-2-phenylindole; Sigma Aldrich; 0.1 µg/ml in PBS) for 15 min. Subsequently cells were washed again with PBS. Finally, the wells were removed from the slide and cover slips were fixed with mounting medium (ProLong® Gold; Invitrogen). Pictures were taken using a laser scanning microscope (Nikon Eclipse 80i) with the scanning system 'Nikon D-Eclipse D1', analysing cells with laser wavelengths 405 and 543 nm.

2.4 Irradiation of cells

2.4.1 Irradiation with X-rays

X-irradiation was performed at DLR in Cologne using a Gulmay RS225 X-ray source (Xstrahl, Surrey, United Kingdom). Cells were irradiated at room temperature with 200 kV and 15 mA at a dose rate of ∼ 1 Gy/min at room temperature. To eliminate soft X-rays, a copper (0.5 mm) filter was used. Cells were irradiated in petri dishes (Ø 3 or 6 cm). Doses up to 16 Gy were used, with an LET of 0.3 to 3 keV/µm. Control flasks were sham-irradiated.

2.4.2 Irradiation with heavy ions

Irradiation with heavy ions was performed at the heavy ion accelerator *Grand Accéléra-teur National d'Ions Lourds* (GANIL) in Caen, France, or at the *Gesellschaft für Schwerionenforschung* (GSI) in Darmstadt, Germany. Cells were incubated for at least two days before heavy ion exposure. They were irradiated at room temperature in Poly-

D-Lysine coated 25 cm^2 cell culture flasks. Prior to irradiation, flasks were completely filled with serum-free α-medium to avoid desiccation during irradiation, closed and fixed in an upright position in front of the ion beam (Fig. 18). Control flasks were sham-irradiated. Dosimetry was performed by determining the fluence[3] (F) in particles/cm^2 (P/cm^2) by Isabelle Testard (GANIL) or Michael Scholz (GSI). To convert fluence to energy dose, the following formula (Wulf *et al.*, 1985) was applied:

Dose (Gy) = 1.6 x 10^{-9} x LET (keV/µm) x F (P/cm^2)   *(Equation 19)*

Table 7 shows the characteristics of the accelerated ions that were used for heavy ion beam experiments in this work. After irradiation, serum-free α-medium was discarded and cells were either directly fixed for analysis or further cultivated under standard conditions.
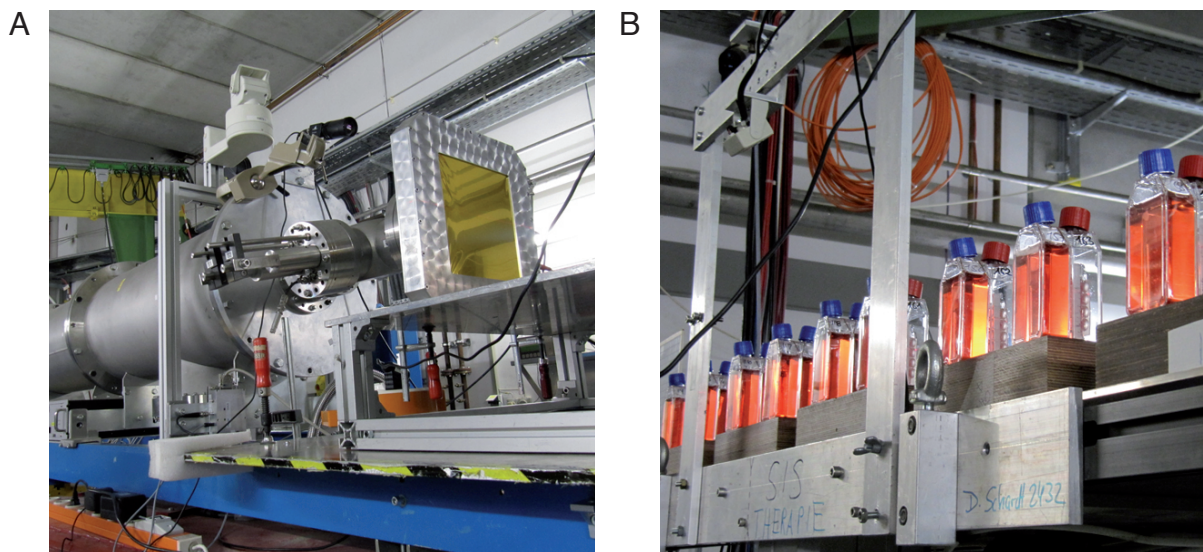
Fig. 18: *Heavy ion experiment at the Gesellschaft für Schwerionenforschung (GSI) in Darmstadt.* (A) Beam exit window at the heavy ion synchrotron SIS. (B) For ion exposure, cells were grown in 25 cm^2 cell culture flasks. Flasks were placed in an upright position in front of the ion beam exit (Pictures were taken during beam time in August 2012).

---

[3] **Fluence (F)** is the number of particles (ΔN) per unit area (ΔA).
F = ΔN/ΔA   *(Equation 20)*

Table 7: *Characteristics of heavy ions used in this work.*

Ion	Energy (MeV/n)	Energy on target [4] (MeV/n)	LET in H_2O (keV/µm)	Penetration depth in H_2O (µm)	Accelerator
^{13}C	75	71.4	34.2	15120	GANIL
^{22}Ne	80	74.5	91.8	10000	GANIL
^{36}Ar	95	83.8	271.5	6336	GANIL
^{58}Ni	75	54.1	905.9	2092	GANIL
^{64}Ni	1000	996.9	174.5	263600	GSI
^{16}O	95	90.8	50.5	16149	GANIL
^{48}Ti	1000	996.9	107.7	319900	GSI

[4] Effective irradiation energy at the cell monolayer after the energy losses in detectors, exit window, air and bottom of the cell culture vessel (1200 µm polystyrene).

3 Results

The aim of this project was to assess the role of NF-κB in the cellular response to different ionizing radiation qualities that are relevant for human spaceflight in order to contribute to risk assessment and to understand basic principles for the development of appropriate countermeasures. Therefore, methods to inhibit the NF-κB pathway at different levels were established. The classical and the genotoxic stress-induced NF-κB pathways were investigated and inhibition was performed by chemicals as well as by RNAi. Finally, this work demonstrates the outcome of cells with and without an intact NF-κB pathway after exposure to space-relevant radiation qualities. Biological endpoints under investigation were cell growth and progression through the cell cycle, cellular survival and expression of NF-κB target genes after radiation exposure.

The original cell line, which was used in this work, was HEK-pNF-κB-d2EGFP/Neo L2. These cells were generated by stable transfection of human embryonic kidney cells (Graham *et al.,* 1977) with the plasmid pNF-κB-d2EGFP/Neo, a reporter vector to monitor NF-κB activation (Hellweg *et al.,* 2003). In these cells, activation of NF-κB leads to the expression of the reporter destabilized enhanced green fluorescent protein (d2EGFP) by binding to the synthetic promoter (κB4-TK) of the integrated plasmid. The NF-κB pathway in this cell line was characterized by visualizing RelA translocation to the cell nucleus, determining the kinetics of NF-κB activation after radiation exposure as well as the extent of NF-κB activation and the cellular survival after exposure to several energetic heavy ions.

3.1 Activation of NF-κB

NF-κB activation in HEK-pNF-κB-d2EGFP/Neo L2 cells by TNF-α and by different radiation qualities was shown by immunofluorescence and by flow cytometry of NF-κB dependent d2EGFP expression, respectively.

3.1.1 Translocation of NF-κB into the nucleus

The NF-κB subunits RelA (p65) and p50 (NFKB1) have been described to translocate into the nucleus (Whiteside and Israel, 1997) after degradation of their inhibitor IκBα (encoded by the NKBIA gene) as a result of exposure to different agents such as pro-inflammatory cytokines, e.g. TNF-α.

To show the intracellular location of NF-κB with and without activation of this pathway by TNF-α, HEK-pNF-κB-d2EGFP/Neo L2 cells were treated with 10 ng/ml TNF-α for

30 min and fixed with 70 % Ethanol. Immunofluorescence staining was performed using a RelA antibody and a TRITC-coupled polyclonal swine anti-rabbit antibody was used for its detection. Cells were counterstained with DAPI to visualize the nuclei. Without TNF-α treatment, the red fluorescence signal indicating RelA is uniformly distributed in the cytoplasm (Fig. 19 A, B). 15 and 30 min after treatment with the known NF-κB activator TNF-α, the predominant part of RelA is localized in the nucleus, with no or only very low fluorescence in the cytoplasm (Fig. 19 C, D).
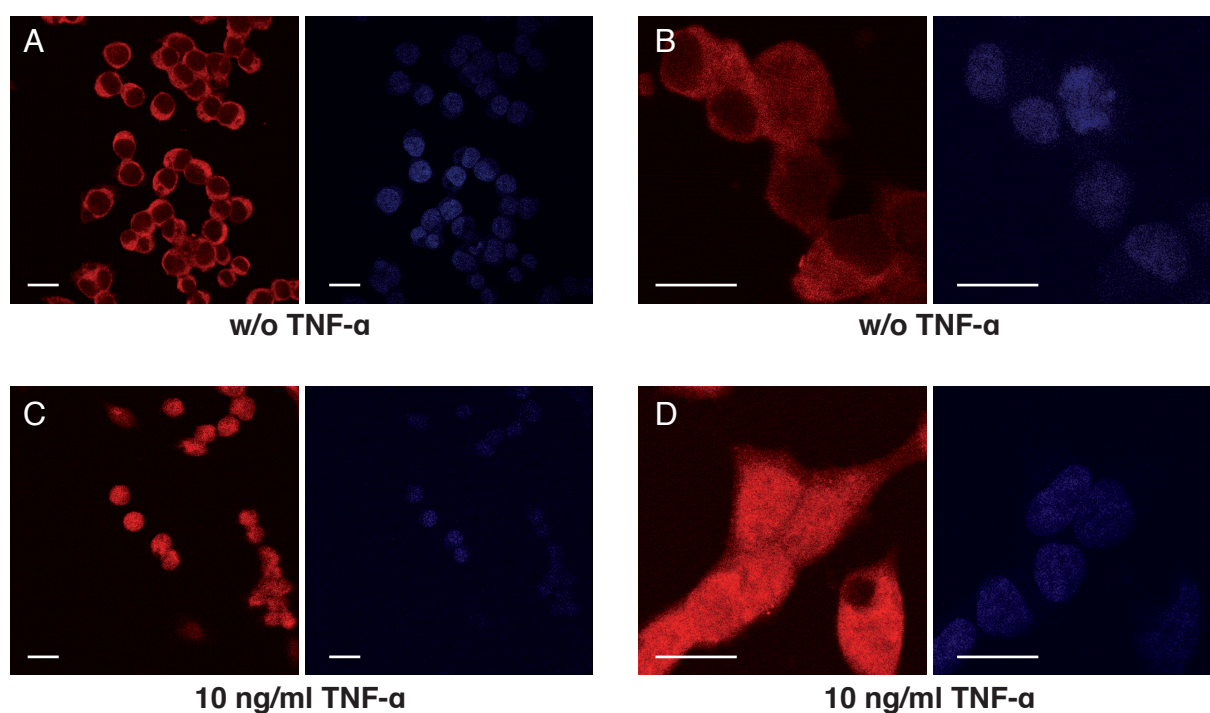
Fig. 19: *RelA is translocated into the nucleus after treatment with TNF-α.* Immunofluorescence staining of RelA in HEK-pNF-κB-d2EGFP/Neo L2 cells using a monoclonal rabbit anti-p65 antibody (Epitomics; red). (A, B) mock treatment: medium change; (C) 15 min after treatment with 10 ng/ml TNF-α; (D) 30 min after treatment with 10 ng/ml TNF-α. Nuclei were counterstained with DAPI (blue). The length of the scale bars is 20 μm.

3.1.2 Kinetics of NF-κB activation by different agents

To investigate NF-κB activation after exposure to different radiation qualities by quantifying d2EGFP[(+)] cells, the time point of maximum d2EGFP expression after induction had to be determined. Kinetics of NF-κB activation was investigated after exposing HEK-pNF-κB-d2EGFP/Neo L2 cells to different radiation qualities and doses or treating them with TNF-α. Cells were fixed at different time points and NF-κB activation was analyzed by flow cytometry.

Fig. 20 A shows the kinetics of NF-κB-dependent d2EGFP expression after irradiation with X-rays and after treatment with 10 ng/ml TNF-α. The percentage of d2EGFP[(+)] cells, indicating NF-κB activation, reaches its maximum at 16 to 18 hours after treatment and decreases thereafter. TNF-α induces NF-κB activation in more than 50 % of the cells and is thereby a significantly stronger inducer of NF-κB activation in comparison to X-rays.

Fig. 20 B shows the resulting kinetics of NF-κB activation after exposure to ^{13}C ions (75 MeV/n, LET 34 keV/µm). The percentage of d2EGFP expressing cells again reaches its maximum after 16 to 18 hours and subsequently decreases. Further, the activation of NF-κB by both X-rays and ^{13}C ions increases with higher doses. [13]C ions are a much stronger inducer of NF-κB activation than X-rays.
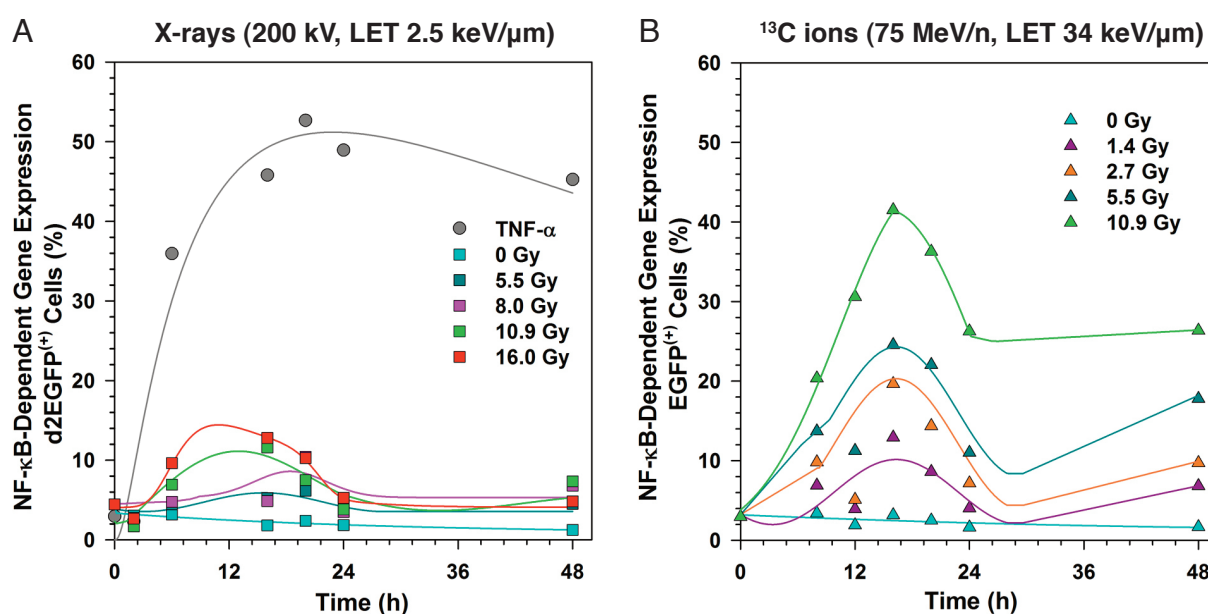
Fig. 20: *Kinetics of NF-κB-dependent d2EGFP expression in HEK-pNF-κB-d2EGFP/Neo L2 cells after radiation exposure.* Cells were irradiated with different doses of X-rays (A) and ^{13}C ions (B). 10 ng/ml TNF-α was used as a positive control (A). At different time points after induction cells were fixed with 3.7 % formaldehyde and d2EGFP expression was analysed by flow cytometry.

3.1.3 NF-κB activation and cellular survival depend on the level of Linear Energy Transfer (LET)

It has been shown that heavy ions of different Linear Energy Transfer (LET) have a varyingly strong impact on the amount of NF-κB-dependent d2EGFP expression and cellular survival (Hellweg, 2011). Here, the results for NF-κB activation (Fig. 21 A) and colony forming ability (Fig. 21 B) in HEK-pNF-κB-d2EGFP/Neo L2 cells after irradiation

with four different energetic heavy ions are shown, mainly complementing the already published results in the LET range below 100 keV/μm. Cells were irradiated with [13]C (75 MeV/n, LET 34 keV/μm), [16]O (95 MeV/n, LET 51 keV/μm), [22]Ne (80 MeV/n, LET 92 keV/μm) and [58]Ni (75 MeV/n, LET 906 keV/μm) ions. After 18 hours, cells were fixed and the percentage of d2EGFP[(+)] cells was analysed by flow cytometry. Additionally, cells were seeded directly after irradiation to determine their clonogenic survival ability. The potential to activate NF-κB increases with higher doses and is higher for ions with an LET below 100 keV/μm compared to [58]Ni ions with an extremely high LET of 906 keV/μm. For these ions, the ability to activate NF-κB decreases.

The colony forming ability decreases with increasing doses and further depends on the LET. Heavy ions with an LET of 34 to 92 keV/μm have the most severe killing effect. In extremely high LET ranges, the killing potential is lower. The parameters describing the survival curves are listed in Table 8.
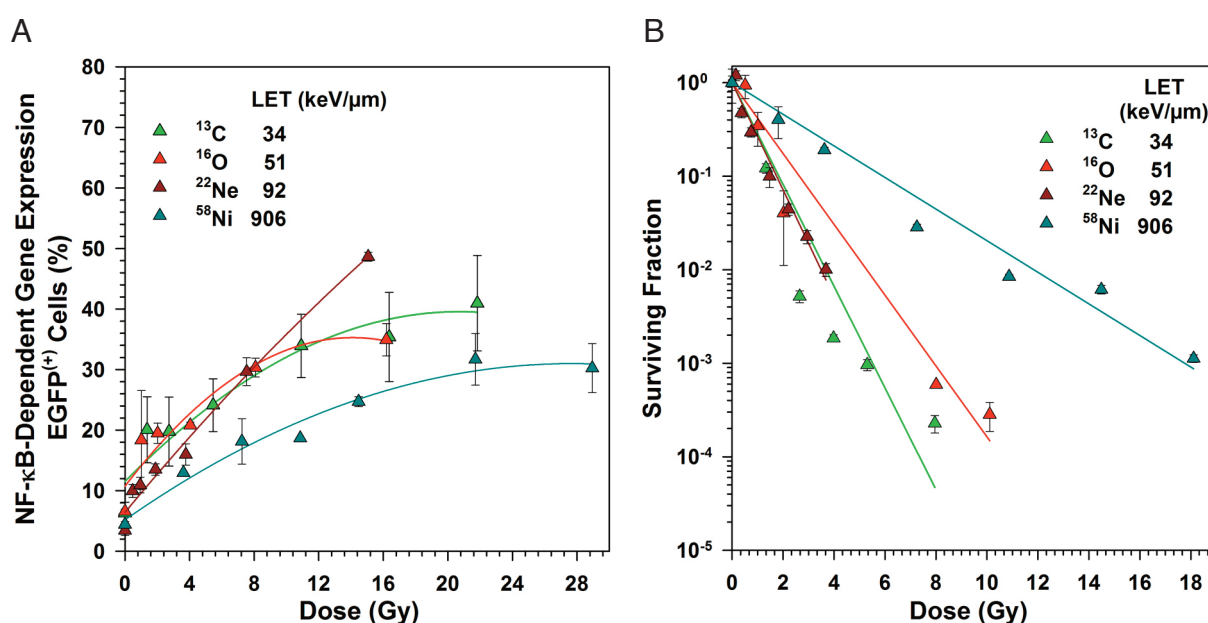
Fig. 21: *Activation of NF-κB-dependent d2EGFP expression and clonogenic survival after exposure to different energetic heavy ions.* HEK-pNF-κB-d2EGFP/Neo L2 cells were irradiated with ions of different energy and LET ([13]C: 75 MeV/n, LET 34 keV/μm; [16]O: 95 MeV/n, LET 51 keV/μm; [22]Ne: 80 MeV/n, LET 92 keV/μm and [58]Ni: 75 MeV/n, LET 906 keV/μm). 18 hours after irradiation, cells were fixed with 3.7 % formaldehyde and d2EGFP expression was analysed by flow cytometry (A). For investigating clonogenic survival, cells were seeded in Petri dishes immediately after irradiation and colonies were fixed and stained after 14 to 21 days (B). For the colony forming ability (CFA) test, standard error (SE) from six replicates per dose is shown. Doses (Gy) were calculated from fluences (P/cm^{2}) according to Equation 19 (s. 2.4.2). (MeV/n) MeV/nucleon; (LET) linear energy transfer.

Table 8: *Parameters of the survival curves (single-hit-multi-target model).*

Ion	Energy (MeV/n)	LET in H_2O (keV/μm)	D_0 (Gy)	n	D_q (Gy)	r^2
^{13}C	75	34	0.88 ± 0.04	0.51 ± 0.08	-0.59 ± 0.11	0.92
^{16}O	95	51	1.44 ± 0.07	0.59 ± 0.01	-0.77 ± 0.20	0.93
^{22}Ne	80	92	0.78 ± 0.02	0.90 ± 0.04	-0.08 ± 0.04	0.97
^{58}Ni	75	906	2.96 ± 0.17	0.51 ± 0.09	-2.01 ± 0.38	0.91

3.2   Inhibition of the NF-κB pathway by chemical inhibitors

The classical and the genotoxic stress induced NF-κB pathway might contribute to the cellular radiation response. To study its role in cell death, survival and other biological endpoints, a system to inhibit NF-κB in HEK-pNF-κB-d2EGFP/Neo L2 cells had to be developed. The first aim was to test chemical inhibitors for their ability to suppress NF-κB activaton by targeting different elements of its pathway. The ATM inhibitor KU-55933 and the proteasome inhibitor MG-132 were both tested for their cytotoxicity and efficacy to suppress NF-κB activation after treatment with different agents.

3.2.1   Cytotoxicity of ATM inhibitor KU-55933 and proteasome inhibitor MG-132

To determine the appropriate concentration of inhibitors, first, the concentration at which cytotoxic effects of KU-55933 and MG-132 appear had to be determined. Inhibitors were added to the cells in increasing concentrations. After 100 hours, growth of the cells was analysed by the MTT test.
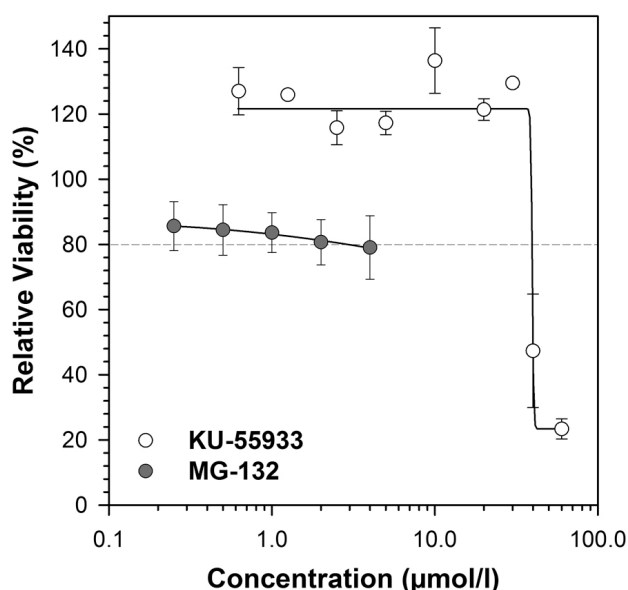
Fig. 22: *Growth of HEK-pNF-κB-d2EGFP/Neo L2 cells after treatment with increasing concentrations of the ATM inhibitor KU-55933 and the proteasome inhibitor MG-132.* 100 hours after adding the inhibitor, the number of viable cells was analysed by means of the MTT test. Means and standard error of two independent experiments with three replicates each are shown. The dotted reference line indicates 80 % relative viability.

Fig. 22 shows the relative viability of HEK-pNF-κB-d2EGFP/Neo L2 cells after adding KU-55933 and MG-132. MG-132 is not cytotoxic within the tested range of concentration. For KU-55933, viability of the cells decreases suddenly at a concentration of 30 µmol/l.

3.2.2 Chemical inhibition of TNF-α-induced activation of the NF-κB pathway

The ability of KU-55933 and MG-132 to suppress NF-κB signaling was initially tested by activating NF-κB with TNF-α in presence of each inhibitor, respectively. Thus, the appropriate concentration for suppressing NF-κB signaling in the classical pathway could be determined. The inhibitor concentration was added to cells in varying concentrations and NF-κB activation was measured by detecting the reporter protein d2EGFP by flow cytometry. Fig. 23 A depicts NF-κB suppression by MG-132. It was shown that a non-cytotoxic concentration of 2 µmol/l was sufficient to abolish NF-κB activation almost completely. KU-55933 was not able to suppress classical NF-κB signaling within its non-cytotoxic range (Fig. 23 B).
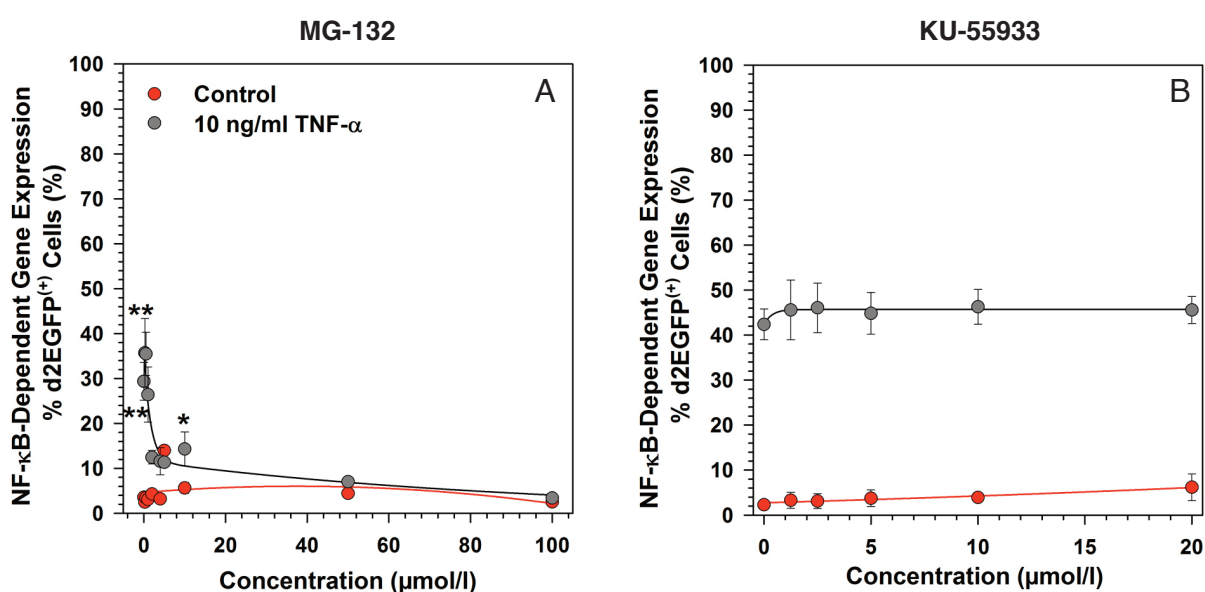
Fig. 23: *Effect of the proteasome inhibitor MG-132 (A) and the ATM inhibitor KU-55933 (B) on TNF-α induced activation of the NF-κB pathway.* Cells were preincubated with the inhibitor for 1 hour. Subsequently, 10 ng/ml TNF-α was added. Cells were detached and fixed with 3.7 % formaldehyde after 18 hours. NF-κB-dependent d2EGFP expression was measured by flow cytometry. Mean and SE of three independent experiments are shown. $p \leq 0.05$ *, $p \leq 0.01$ **, showing a significant difference of TNF-α treated cells versus TNF-α and MG-132 treated cells.

3.2.3 Chemical inhibition of radiation-induced activation of the NF-κB pathway

Both inhibitors were finally tested for their ability to suppress radiation induced NF-κB activation. In presence of each of the inhibitors, cells were irradiated with different doses of X-rays and ^{36}Ar ions. Both, MG-132 and KU-55933 were able to completely suppress radiation-induced NF-κB activation (Fig. 24). While a concentration of 2 µmol/l of MG-132 was used, 10 µmol/l had been shown to be the appropriate, non-cytotoxic concentration for KU-55933, as described in the literature (Hickson *et al.*, 2004).
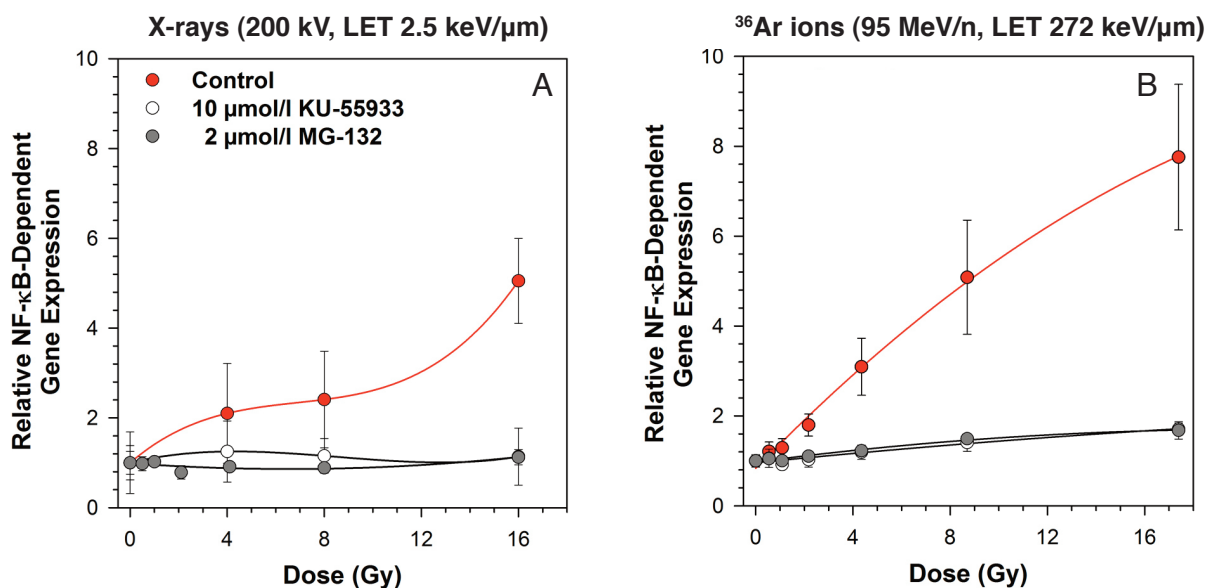
Fig. 24: *Suppression of radiation-induced activation of the NF-κB pathway by KU-55933 and MG-132.* Cells were preincubated with the inhibitor for 1 hour and subsequently irradiated with X-rays (200 kV, LET 2.5 keV/µm, A) or ^{36}Ar ions (95 MeV/n, LET 272 keV/µm, B). After 18 hours, NF-κB-dependent d2EGFP expression was measured by flow cytometry. The percentage of d2EGFP$^{(+)}$ cells was normalized to the mock-irradiated control. For ^{36}Ar ions, doses (Gy) were calculated from fluences (P/cm^2) according to Equation 19 (s. 2.4.2). Mean and SE of three independent experiments are shown.

3.3 Inhibition of the NF-κB pathway by RNA interference (RNAi)

As the tested chemicals are not NF-κB-specific, they are not adequate to investigate the role of NF-κB in different biological endpoints, as observed cellular responses cannot be ascribed to this pathway. Further, the tested chemicals Parthenolide, Capsaicin, Isohelenin and caffeic acid phenethyl ester (CAPE) were either cytotoxic or insufficient in suppressing NF-κB-dependent d2EGFP expression and therefore, results are not shown in this work.

To investigate NF-κB more specifically, RNA interference (RNAi) was chosen as an additional method. The NF-κB subunit RelA (p65) was chosen as the target for mRNA degradation and subsequent decrease of RelA protein levels.

3.3.1 Stable transfection of HEK-pNF-κB-d2EGFP/Neo L2 cells with shRNA vectors

To establish a cell line with a permanent RelA knockdown, a stable transfection was performed using shRNA vectors, containing a Hygromycin resistance marker for selection of transfected cells (s. 2.1.2). The shRNA plasmids were propagated in *E. coli*. The quality of the plasmid preparation from transformed *E. coli* was controlled by restriction digestion and visualized on an agarose gel (Fig. 25).
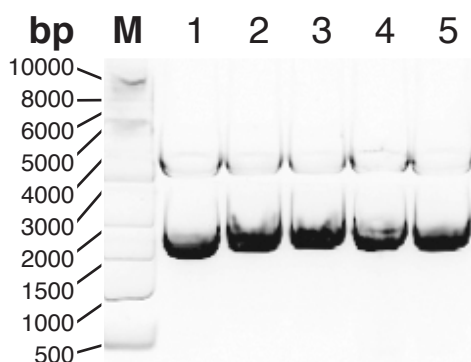
Fig. 25: *Control digestion of the pGene Clip™ Hygromycin Vector.* Digestion with ScaI. Expected fragments: 1643 bp, 3346 bp; (1-5) RELA-1-RELA-5; (M) GeneRuler 1 kb DNA ladder.

To determine the appropriate cytotoxic concentration of Hygromycin, it was added to HEK-pNF-κB-d2EGFP/Neo L2 cells in varying concentrations. It was shown that the minimum concentration needed to kill shRNA untransfected HEK-pNF-κB-d2EGFP/Neo L2 cells was 400 µg/ml (Fig. 26). Once the stably transfected cell population was available, a maintenance concentration of 200 µg/ml was chosen for continued cell growth.
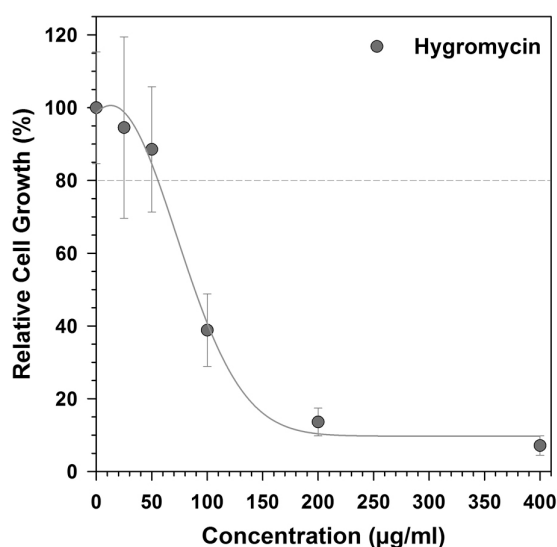
Fig. 26: *Viability of HEK-pNF-κB-d2EGFP/Neo L2 cells after being cultivated in culture medium containing varying concentrations of Hygromycin.* Medium was changed after 4 and 7 days. After 11 days, cells were fixed and stained with a formaldehyde/crystal violet solution. Cell growth was determined by measuring crystal violet absorbance at a wavelength of 592 nm. The dotted reference line indicates 80 % relative viability.

HEK-pNF-κB-d2EGFP/Neo L2 cells were transfected with four individual shRNA plasmids specific for RelA. A fifth transfection using a negative control shRNA plasmid was performed. Hygromycin resistant cells were harvested 11 days after it had been added

to the medium and RNA of each of the five transfected cell populations was isolated (s. 2.2.5). RNA was controlled according to the parameters RNA concentration, RNA integrity (RIN), rRNA ratio (28S/18S) and purity (A260/280; s. 2.2.2.2). For an adequate quality control and a subsequent cDNA synthesis, the samples had to exhibit a RIN of at least 9. Samples showing a RIN of less than 9 were not reliable. In most cases, the RIN was 10, the highest possible value. Additionally, samples had to exhibit a rRNA ratio and a A260/280-value of ~ 2. Due to the high number of RNA samples tested in this work, Fig. 27 representatively depicts one example of an appropriate RNA sample that was used for further cDNA synthesis.
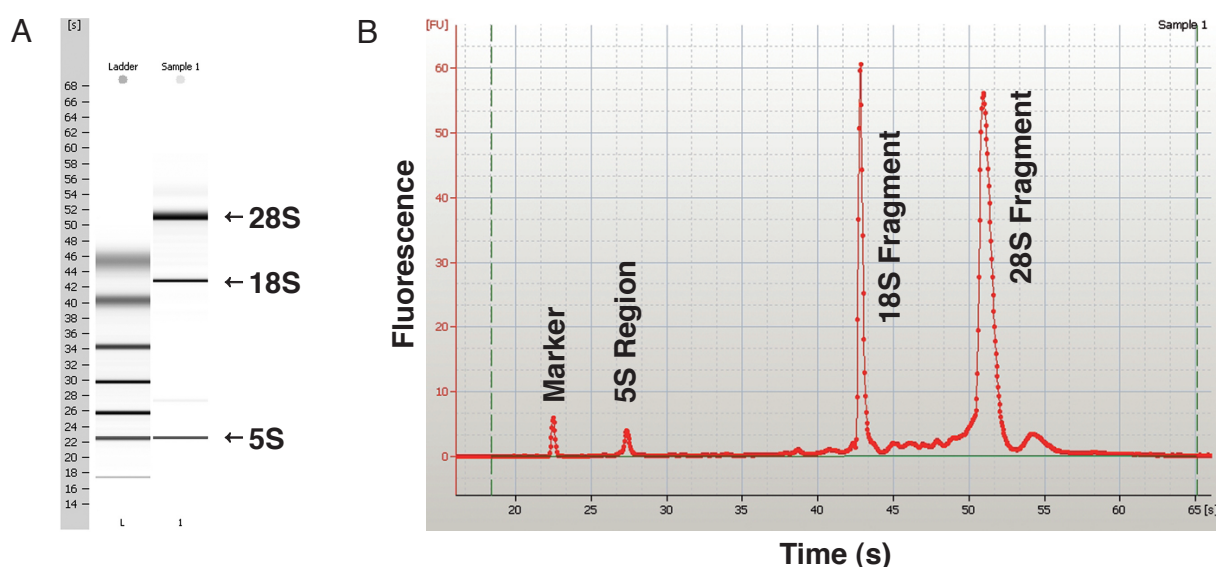
Fig. 27: *RNA quality control using the Eukaryote Total RNA Nano Assay (Thermo Scientific).* Intact 18S and 28S rRNA subunits are visualised on a gel-like image (A) and by electropherogram (B). This example shows the electrophoresis results of RNA extracted from untreated HEK-pNF-κB-d2EGFP/Neo L2 cells, displaying a RIN of 9.8, an rRNA ratio of 2.0 and a concentration of 154 ng/µl.

3.3.2   Verification of RelA-knockdown on mRNA level

After RNA quality control, cDNA was synthesised by reverse transcription, with 1000 ng RNA being used for each sample, and analysed by qPCR (s. 2.2.2.4). To control the quality of the qPCR, a melting curve program was run immediately after completion of the PCR program. Results showed the expected melting temperatures of 80 °C for the RELA PCR product and 76.5 °C for HPRT1 (Fig. 28 A). Controlling the PCR quality by performing a dissociation curve was conducted with every real-time RT-qPCR in this work. The quality of the PCR product and the primer was further tested by loading the PCR product on an agarose gel. Bands were visible at the expected sizes of 65 bp (RELA) and 89 bp (HPRT1; Fig. 28 B).

A

B
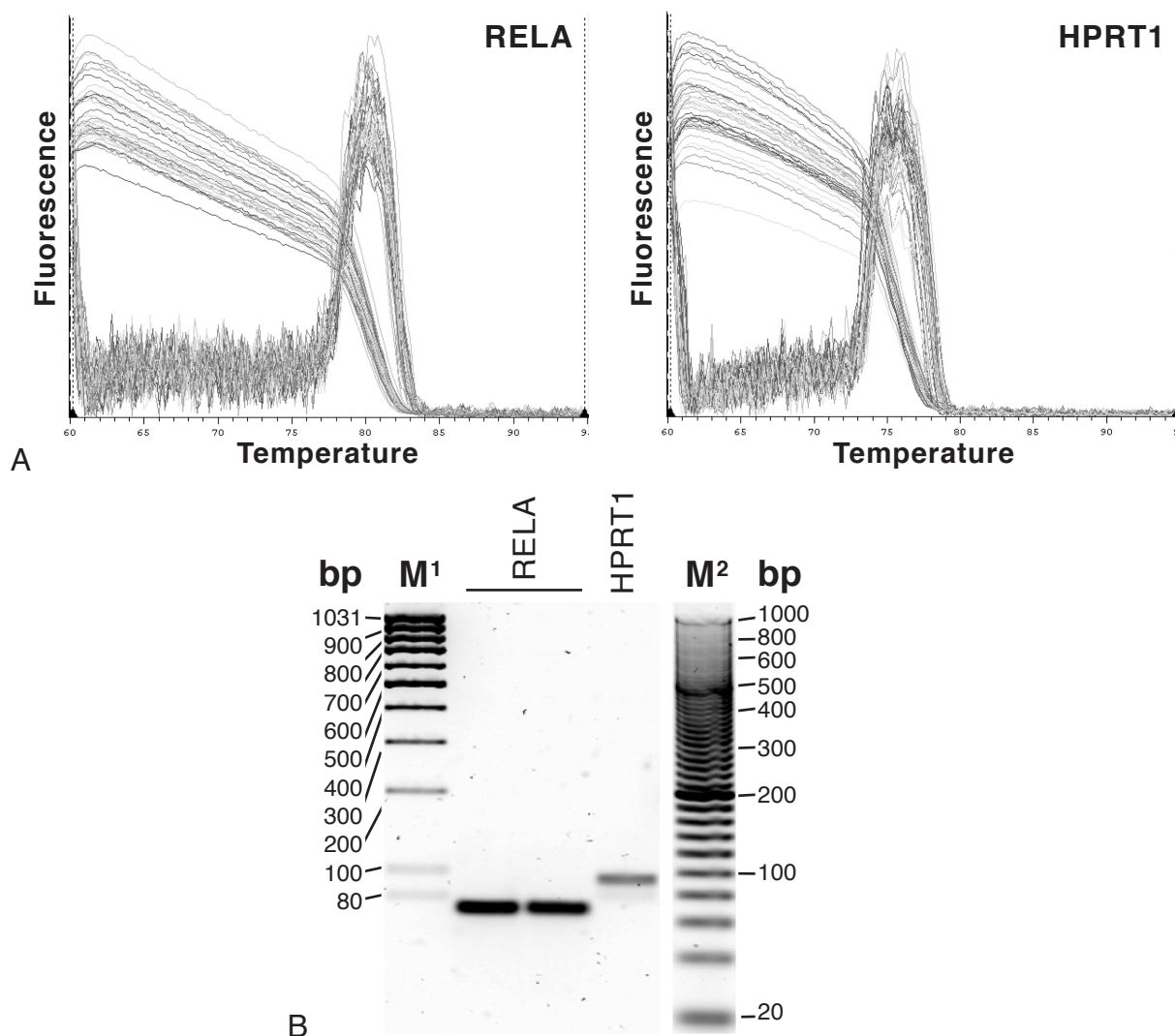
Fig. 28: *Quality control of real-time RT-qPCR.* (A) dissociation curve showing the expected melting temperatures of 80 °C for RELA and 76.5 °C for HPRT1; (B) agarose gel showing the PCR products of SA Biosciences primer for RELA (65 bp) and HPRT1 (89 bp); (M1) low range DNA ladder (Fermentas); (M2) 20 bp low ladder (SIGMA).

To determine the efficiency of each shRNA plasmid in down-regulating RelA expression, the percentage of RelA-knockdown of each stably transfected cell population had to be assessed. The knockdown level of each shRNA plasmid after stable transfection into HEK-pNF-κB-d2EGFP/Neo L2 cells was calculated from the C_t values of RelA expression in transfected cells, using a validation sheet (SABiosciences; Table 9). This Excel-based data analysis template performs the calculation as described in 2.2.2.4. Calculations displayed the highest knockdown level in cells that had been stably transfected with plasmids RELA-1, showing a knockdown level of 52.7 %, and RELA-4 with a knockdown level of 47.6 % (Fig. 29).

Table 9: *RelA knock-down[5] in Hygromycin-resistent cells after stable transfection with the shRNA plasmids RELA-1 to RELA-4.*

DATE	Real-Time PCR Result for RELA shRNA														
09.09.2010	RELA-1			RELA-2			RELA-3			RELA-4			Negative Control		
Transfection	1	2	3	1	2	3	1	2	3	1	2	3	1	2	3
RELA PCR 1	20.93	21.35	21.58	20.46	21.25	21.31	21.6	21.12	20.97	21.75	21.62	21.51	20.79	20.86	20.8
RELA PCR 2	21.52	21.64	21.71	21.05	21.21	21.51	21.75	20.87	20.96	21.41	21.54	21.45	20.95	20.88	20.6
RELA PCR 3	21.48	21.66	21.83	20.88	21.25	21.4	21.54	21.1	21.05	21.65	21.66	21.73	20.77	20.84	20.89
Average C_t	21.31	21.55	21.71	20.80	21.24	21.41	21.63	21.03	20.99	21.60	21.61	21.56	20.84	20.86	20.76
SD C_t	0.33	0.17	0.13	0.30	0.02	0.10	0.11	0.14	0.05	0.17	0.06	0.15	0.10	0.02	0.15
QC 1	!	OK	OK	!	OK	OK	OK	OK	OK	OK	OK	OK	OK	OK	OK
HPRT PCR 1	19.03	19.48	19.87	19.45	19.74	19.43	19.86	19.12	20.11	19.53	19.99	20.39	20.06	20.22	20.02
HPRT PCR 2	19.89	19.73	19.78	19.66	19.77	19.8	19.78	19.2	19.83	19.71	19.95	20.1	20.21	20.32	20.08
HPRT PCR 3	19.55	20.07	19.93	19.97	20.21	19.97	19.97	19.7	20.42	19.71	19.78	20.12	19.54	20.36	19.92
Average C_t	19.49	19.76	19.86	19.69	19.91	19.73	19.87	19.34	20.12	19.65	19.91	20.20	19.94	20.30	20.01
SD C_t	0.43	0.30	0.08	0.26	0.26	0.28	0.10	0.31	0.30	0.10	0.11	0.16	0.35	0.07	0.08
QC 2	!	OK	OK	OK	OK	OK	OK	!	OK	OK	OK	OK	!	OK	OK
ΔC_t	1.82	1.79	1.85	1.10	1.33	1.67	1.76	1.69	0.87	1.95	1.70	1.36	0.90	0.56	0.76
SD ΔC_t	0.54	0.34	0.15	0.40	0.26	0.29	0.14	0.34	0.30	0.20	0.13	0.22	0.37	0.07	0.17
Average ΔC_t	1.82			1.37			1.44			1.67			0.74		
SD ΔC_t BIO	0.03			0.29			0.49			0.30			0.17		
Overall Mean SD ΔC_t	0.22			0.34			0.52			0.32			0.22		
$\Delta\Delta C_t$	1.08			0.63			0.70			0.93					
Overall SD $\Delta\Delta C_t$	0.31			0.41			0.56			0.38					
QC 3	OK			OK			!			OK					
Percent of Control	0.47			0.65			0.61			0.52					
Percent Knock Down	52.70			35.38			38.54			47.59					
+ SD	9.18			15.87			19.84			12.27					
- SD	11.39			21.04			29.29			16.02					

Report:	Percent Knock Down	95 % Confidence Interval		Design
RELA-1	52.70	(39.61	62.95)	Mediocre
RELA-2	35.38	(11.11	53.03)	Mediocre
RELA-3	38.54	(4.47	60.46)	Mediocre
RELA-4	47.59	(29.13	61.25)	Mediocre

SuperArray
Bioscience Corporation

[5] Real-time RT-qPCR results for shRNA plasmids RELA-1 to RELA-4. The table shows the validation sheet (supplied by SABiosciences, formerly SuperArray) for determining the knockdown-level of RNAi plasmids. This Excel-based data analysis template calculates the percentage of knockdown, interpreting a successful design as an observed knockdown-level of ≥ 70 % and an upper 95 % confidence interval boundary of ≥ 55.5 %. Each set of three columns represents a shRNA construct (RELA-1 to RELA-4) and the negative control (NC). Each column within a set represents one replicate transfection. Each row represents a technical replicate. For both, RelA and the reference gene HPRT1, the average and standard deviation (SD) of the C_t values of each transfection were calculated. The internal quality control (QC) reports 'OK' if the SD of the replicates' C_t is below 0.3, indicating sufficient reproducibility. For each transfection, the ΔC_t is calculated by substraction of the C_t of HPRT from the C_t of RelA. For all replicates of each plasmid (triplicate PCR reactions and biological replicates), the average and SD of ΔC_t were determined. The expression difference between cells transfected with shRNA plasmid and the negative control plasmid where then computed by subtracting the respective ΔC_t values ($\Delta\Delta C_t$). The SD of $\Delta\Delta C_t$ had to be smaller than 0.55 to pass QC. The relative expression was calculated according to equation 10 (s. 2.2.2.6) and expressed as percent of control. The percent knockdown was determined by subtracting the relative expression from 100 %. The confidence interval for knockdown was determined using the same formulas on +SD and -SD.
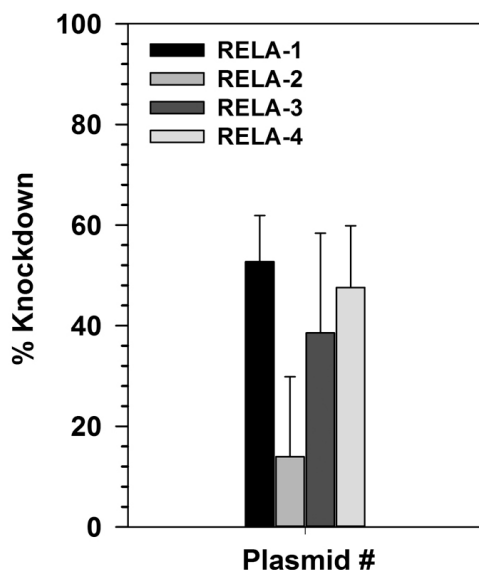
Fig. 29: *Selection of the most effective shRNA plasmid by comparing the knockdown level.* Total RNA of the Hygromycin-resistant polyclonal populations was isolated two weeks after transfection with the five plasmids (RELA-1 to -4). RelA knockdown was verified by RT-qPCR after transfection of HEK-pNF-κB-d2EGFP/Neo L2 cells with shRNA. Means and SD of three individual experiments with three replicates each are shown.

By reason of their high knockdown-level, cell populations that were transfected with plasmids RELA-1 or RELA-4 were chosen to further processing to achieve a greater and more consistent level of knock-down. Colonies grown from single cells were isolated from the polyclonal population. In each clone the plasmid was integrated randomly into genomic DNA, resulting in possible position effects on shRNA expression.
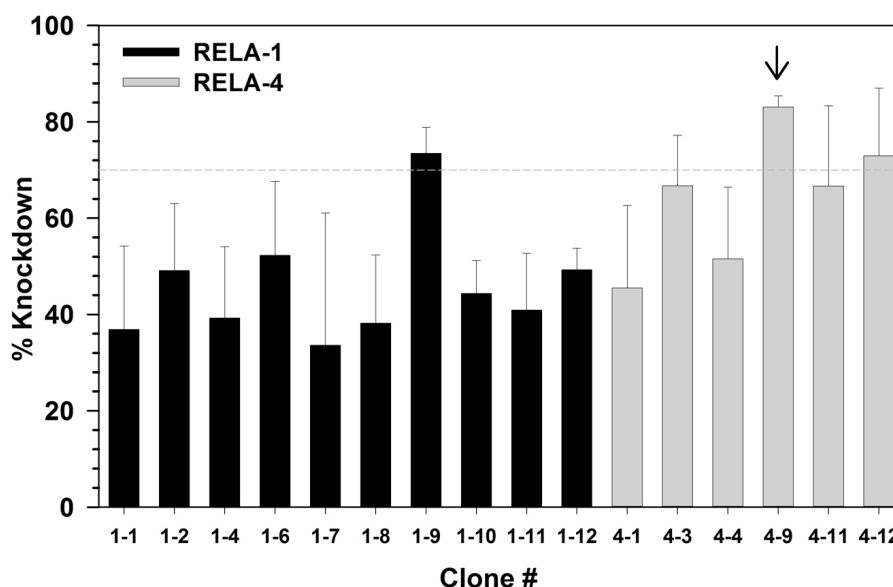
Fig. 30: *RelA knockdown level of different HEK-pNF-κB-d2EGFP/Neo L2 clones isolated from polyclonal populations transfected with the plasmids RELA-1 or RELA-4.* The arrow depicts clone #9 ('HEK shRNA RelA'), which had been transfected with the plasmid RELA-4 and shows the highest knockdown level of more than 80 %. All knockdown-levels were calculated with the SABiosciences validation sheet (Table 9 and 10). Means and SD of triplicate PCR reactions and three biological replicates are shown. The dotted line indicates the threshold of 70 %, from which the knockdown is defined as 'successful'.

After RNA isolation and quality control of monoclonal cell populations according to 2.2.2.1 and 2.2.2.2, the RelA knockdown of each clone was determined by RT-qPCR, similar to the procedure described to investigate the knockdown level of the polyclonal populations. A selection of clones and their respective knock-down level is depicted in Fig. 30. Table 10 shows the real-time RT-qPCR results displayed in the SABiosciences' validation sheet for the selected clone, which was named 'HEK shRNA RelA' and is characterized by a RelA knock-down level of 83.1 % (mean of three individual experiments) and a resistance against Hygromycin.

Table 10: *RelA knock-down[6] in clone #9 that resulted from stable transfection of HEK-pNF-κB-d2EGFP/Neo L2 cells with the shRNA plasmid RELA-4.*

DATE	Real-Time PCR Result for RelA shRNA						
05.08.2011	RelA-1				Negative Control		
Transfection	1	2	3		1	2	3
RelA PCR 1	22.04	22.67	22.65		20.63	20.72	20.94
RelA PCR 2	22.46	22.85	22.81		20.55	20.98	21.08
RelA PCR 3	22.57	23.05	22.7		21.02	20.85	21.24
Average C_t	22.36	22.86	22.72		20.73	20.85	21.09
SD C_t	0.28	0.19	0.08		0.25	0.13	0.15
QC 1	OK	OK	OK		OK	OK	OK
HPRT PCR 1	18.03	18.7	18.42		19.64	19.95	19.77
HPRT PCR 2	18.31	18.77	18.81		19.6	20.08	19.76
HPRT PCR 3	18.43	18.84	18.81		19.73	19.64	19.75
Average C_t	18.26	18.77	18.68		19.66	19.89	19.76
SD C_t	0.21	0.07	0.23		0.07	0.23	0.01
QC 2	OK	OK	OK		OK	OK	OK
ΔC_t	4.10	4.09	4.04		1.08	0.96	1.33
SD ΔC_t	0.35	0.20	0.24		0.26	0.26	0.15
Average ΔC_t	4.08				1.12		
SD ΔC_t BIO	0.03				0.19		
Overall Mean SD ΔC_t	0.16				0.23		
$\Delta\Delta C_t$	2.95						
Overall SD $\Delta\Delta C_t$	0.28						
QC 3	OK						
Percent of Control	0.13						
Percent Knock Down	87.10						
+ SD	2.27						
- SD	2.76						

Report:	Percent Knock Down	95 % Confidence Interval	Design
RelA-1	87.10	(83.94 89.64)	Successful

♪ SuperArray
Bioscience Corporation

[6] Example of real-time RT-qPCR result for clone #9 ('HEK shRNA RelA'), isolated from the polyclonal population which had been stably transfected with plasmid RELA-4. The table shows the validation sheet (supplied by SABiosciences) that was also used for determining the highest knockdown-level of the polyclonal cell populations after transfection with the four different shRNA plasmids (Table 9). A set of three columns represents one clone. This validation sheet was modified so that only clone #9 and the negative control (NC) are shown. Each column within a set represents one biological replicate with three technical replicates during qPCR. Each row represents one technical replicate and three independent seedings.

3.3.3 Verification of RelA-knockdown on protein level

Knockdown efficiency was further determined by comparing the fluorescence intensity of the untreated original and the knockdown-cell line after immunofluorescence staining using the RelA antibody. Images of both cell lines were acquired using a laser scanning microscope (Nikon Eclipse 80i) with the scanning system 'Nikon D-Eclipse D1' set to the same illumination time. Fig. 31 depicts RelA-staining of HEK-pNF-κB-d2EGFP/Neo L2 (Fig. 31 A) and HEK shRNA RelA (Fig. 31 B) cells. Comparing the fluorescence signal of both cell lines, the observed intensity is strongly reduced in the knockdown cell line. Still the tendency of the RelA signal to be restricted to the cytoplasm occurs in both cell lines in the uninduced state.
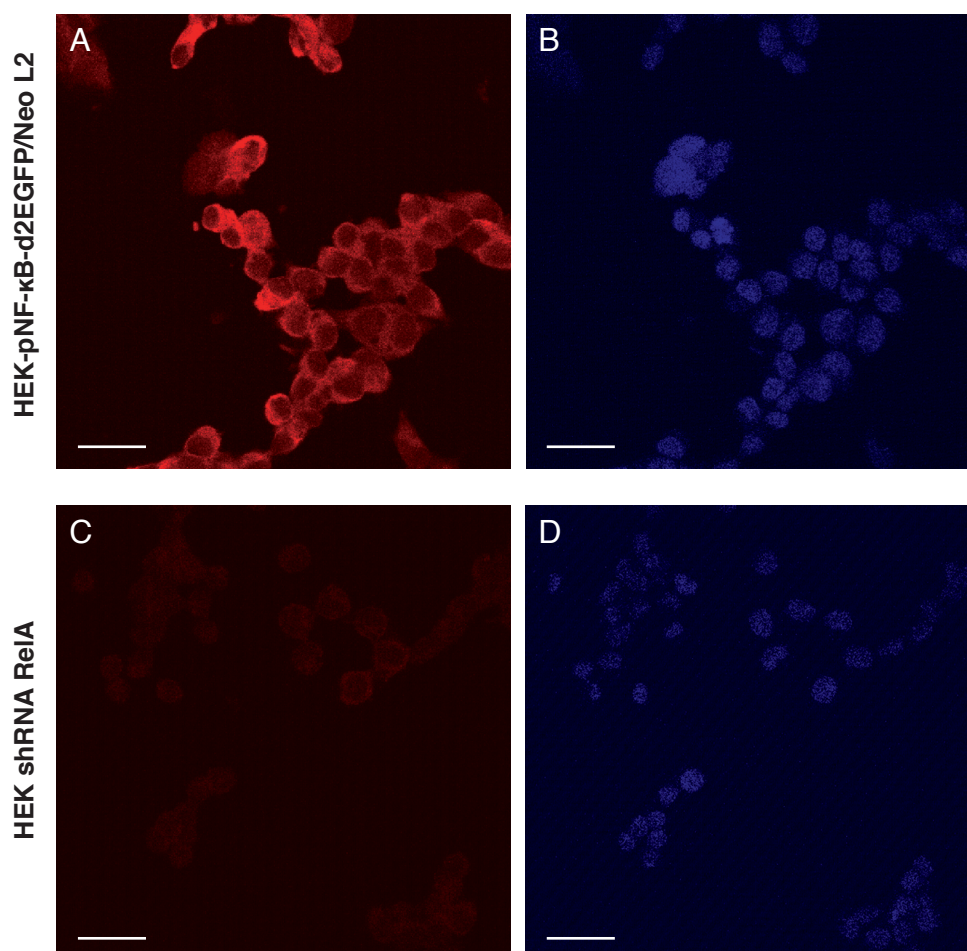
Fig. 31: *Visualisation of RelA after RelA knockdown.* Immunofluorescence staining was performed with fixed cells using a monoclonal rabbit anti-p65 antibody (Epitomics). Without activation of NF-κB, the RelA signal is restricted to the cytoplasm. In the knockdown cell line the intensity of red fluorescence is reduced. (A) HEK-pNF-κB-d2EGFP/Neo L2 cells; (B) HEK shRNA RelA cells. The length of the scale bar is 20 μm.

3.3.4 Verification of RelA-knockdown on reporter protein level

To visualize the RelA-knockdown of the selected clone on reporter protein level, the original HEK-pNF-κB-d2EGFP/Neo L2 cell line, as well as the knockdown (HEK shRNA RelA) and the control cell line, which was transfected with a negative control shRNA vector, were treated with different radiation qualities or with TNF-α. d2EGFP fluorescence was measured 18 hours after treatment by flow cytometry. Fig. 32 A-C depict histograms obtained by flow cytometry.
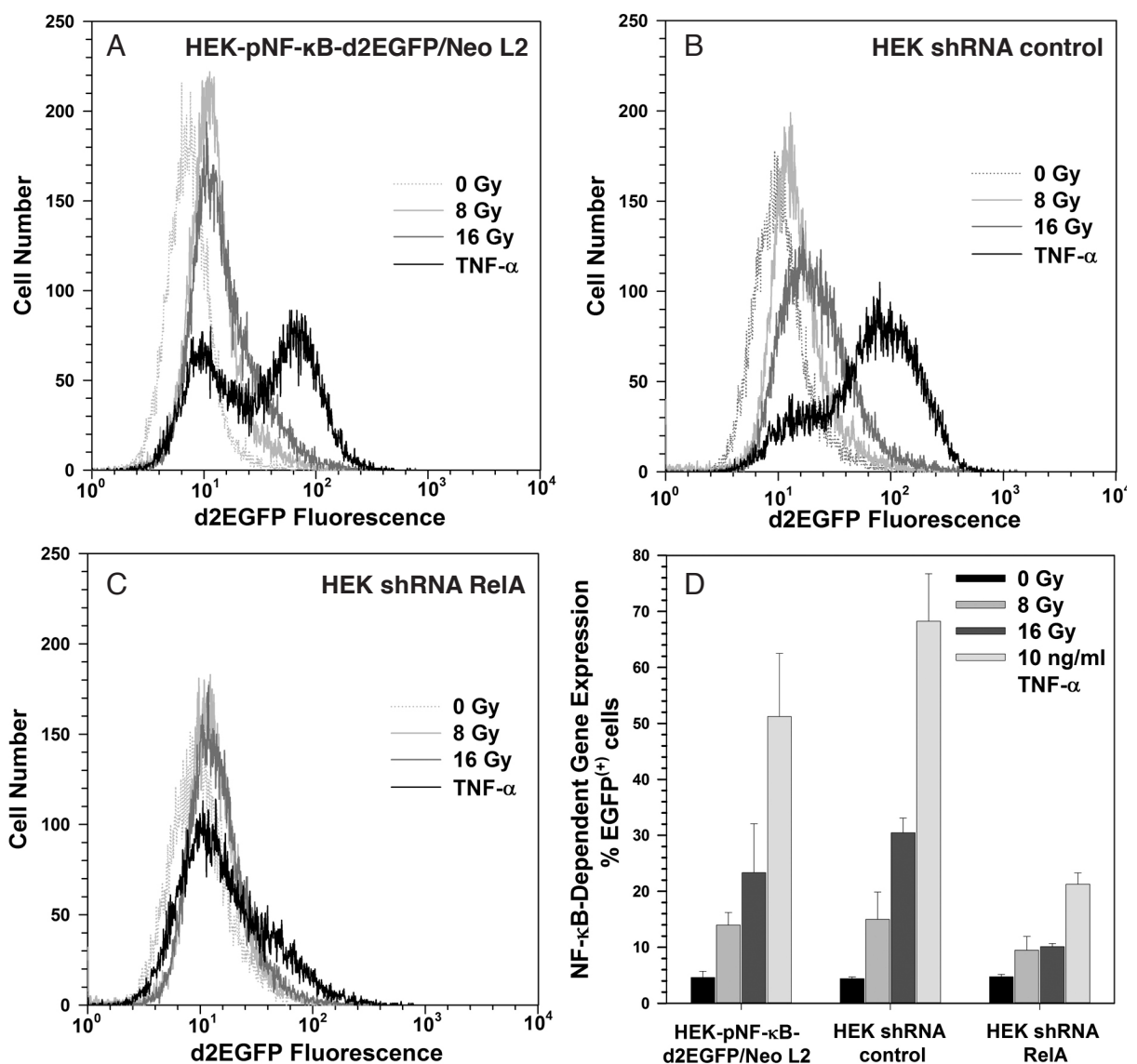
Fig. 32: *Activation of NF-κB dependent d2EGFP expression in different cell lines by TNF-α and X-rays.* Cells were harvested and fixed for flow cytometry 18 hours after treatment. Histogram overlays of representative flow cytometric analysis are shown in A, B and C. (A) HEK-pNF-κB-d2EGFP/Neo L2; (B) HEK shRNA control; (C) HEK shRNA RelA; (D) summarizes the results of two individual experiments, showing mean and standard error.

The original HEK-pNF-κB-d2EGFP/Neo L2 cell line as well as the control transfected cell line exhibit a strong increase in d2EGFP[(+)] cells after treatment with X-rays and TNF-α. Fluorescence intensifies with increasing doses and reaches ∼ 50-70 % after TNF-α-treatment. HEK shRNA RelA cells show a very low increase in fluorescence intensity after treatment with a maximum in d2EGFP[(+)] cells of only ∼ 20 % (Fig. 32 C and D). A similar effect was shown for ^{13}C ions. After irradiation with increasing dose, fluorescence intensity reaches up to 20 % in the original and the control cell line, whereas d2EGFP was not inducible in the knockdown-cell line (Fig. 33).
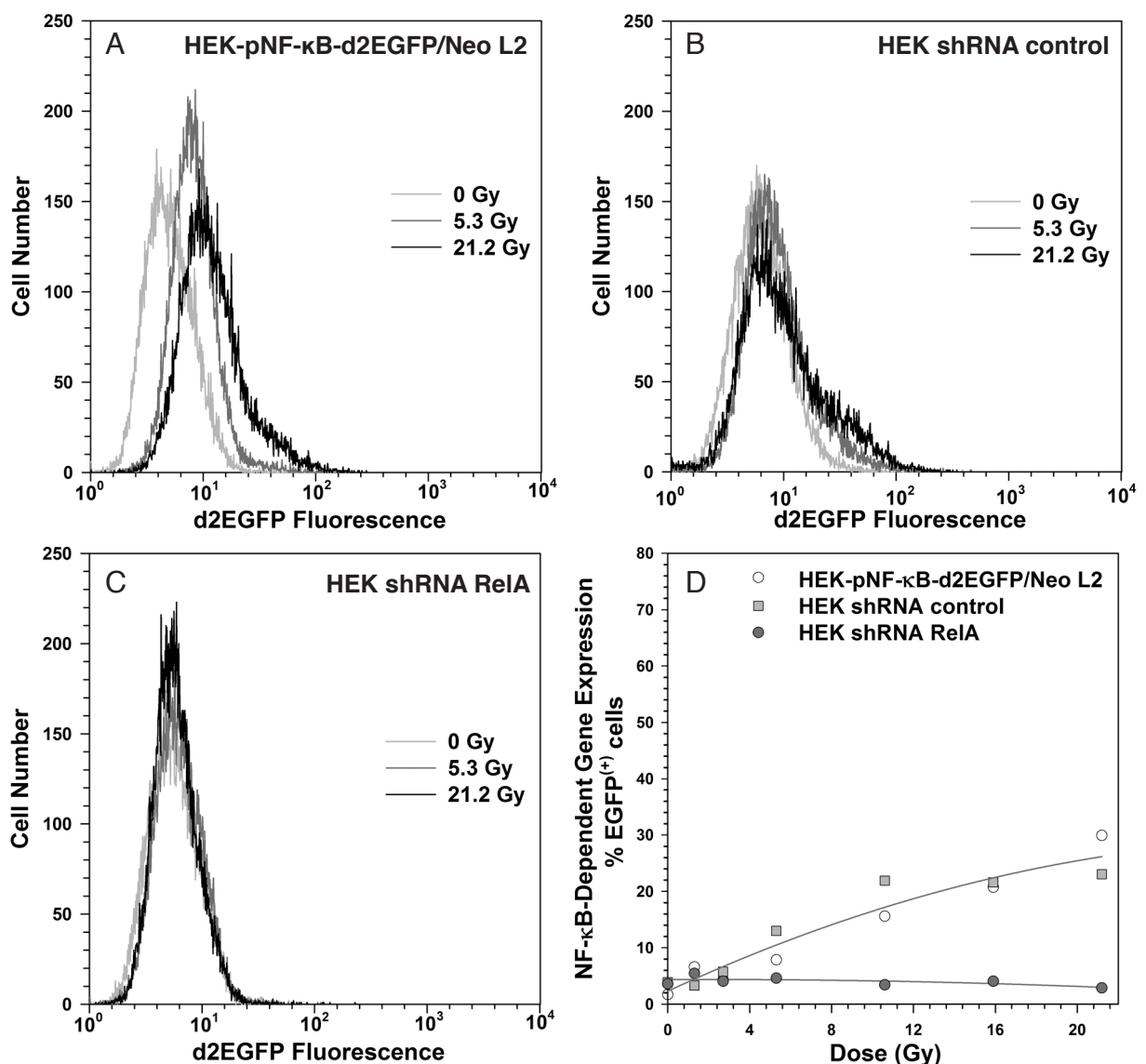
Fig. 33: *Activation of NF-κB dependent d2EGFP expression in different cell lines by ^{13}C ions (75 MeV/n, LET 34 keV/µm).* Cells were harvested and fixed for flow cytometry 18 hours after irradiation. Doses (Gy) were calculated from fluences (P/cm²) according to Equation 19 (s. 2.4.2). Histogram overlays of flow cytometric analysis are shown in A, B and C. (A) HEK-pNF-κB-d2EGFP/Neo L2; (B) HEK shRNA control; (C) HEK shRNA RelA; (D) dose effect curve with a combined regression curve for HEK-pNF-κB-d2EGFP/Neo L2 and HEK shRNA control cells.

3.4 Characterization of the RelA-knockdown cell line

3.4.1 HEK shRNA RelA cells exhibit a prolonged lag-phase in growth experiments

To investigate the effect of NF-κB on the growth rate, both cell lines were seeded with the same starting cell number and counted twice a day up to a time point of ∼ 260 hours, when cells had reached confluence. Compared to the original cell line, HEK shRNA RelA cells show a prolonged lag phase with an initial decrease in cell number (Fig. 34). While HEK-pNF-κB-d2EGFP/Neo L2 cells transfer to the exponential growth phase (logarithmic, log) after 24 to 48 hours, the knockdown cell line enters this phase only after 48 to 72 hours. Once the cells have reached the log phase, there is no significant difference in the growth velocity. During this phase, the doubling time is 28.2 hours for both cell lines. In the final plateau phase, the knockdown cells seem to grow slightly less confluent than the original cell line, which was also observed during cultivation of the cells.
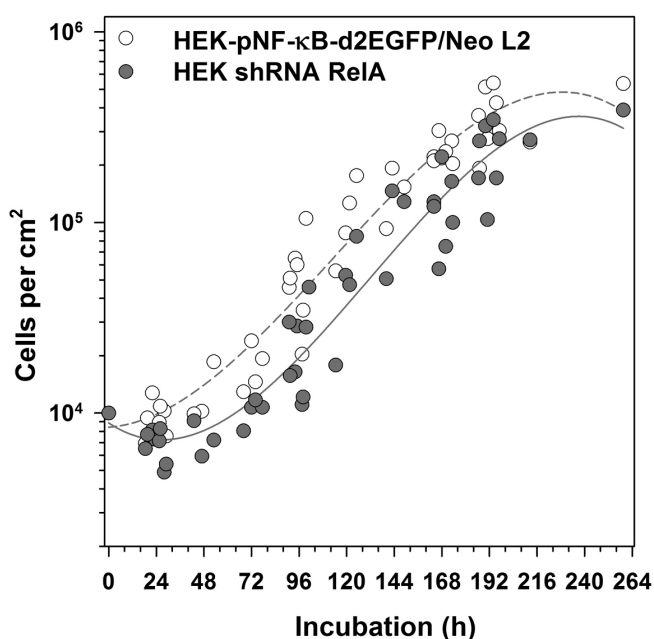
Fig. 34: *Growth kinetics of HEK shRNA RelA cells compared to the original cell line.* 1×10^4 cells/cm^2 cells were seeded in 6-well plates and cultivated in S-medium. Twice a day the cell number of one well was counted after detaching cell by trypsination. The graph shows a summary of four independent experiments.

3.4.2 Changes in gene expression in absence of RelA

To compare gene expression in both cell lines, two different RT^2 Profiler™ PCR Arrays (SABioscience) were used. The first array was customized and contained a set of 89 genes, involved in the NF-κB signaling pathway, cell cycle, apoptosis, p53 signaling, stress and toxicity pathways, DNA damage etc. This customized array was designed to analyse the expression of selected genes which might be of relevance to the cellular radiation response. The second array was commercially available and restricted to 89 NF-κB target genes (RT^2 Profiler™ PCR Array: Human NF-κB Signaling Targets).

To assure a consistent RNA quality in advance, the concentration and purity of all RNA samples was determined and all samples were tested for ribosomal RNA band integrity as described in 2.2.2.2. After cDNA synthesis (s. 2.2.2.3), samples were additionally investigated with an RT^2 RNA QC PCR array (SABiosciences) to assure proper RNA and cDNA quality and to rule out genomic DNA contamination. This array includes the RNA quality control parameters housekeeping gene expression levels, reverse transcription and polymerase chain reaction efficiency as well as genomic and general DNA contamination (s. 2.2.2.6). Table 11 shows an example of the cDNA quality plate. The results showed that no RNA sample impurities were affecting reverse transcription or PCR, no genomic DNA contamination was detectable or affecting the results and that the PCR system was clean. Samples were only used for further analysis, when the given quality control parameters were assessed as correct.

Table 11: *Quality control[7] of cDNA for further gene expression analysis with the RT^2 Profiler™ PCR array (SABiosciences), using the analysis template of the RT^2 RNA QC PCR array.*

	Sample Name	S1	S2	S3	S4	S5	S6	S7	S8	S9	S10	S11	S12
Row	Control Name						Ave Ct						
A	ACTB	18.44	18.82	18.85	19.09	18.70	19.52	18.48	22.61	18.27	18.12	18.56	18.21
B	HPRT1	23.54	23.99	23.31	23.64	23.35	23.84	22.86	23.29	22.62	22.94	22.96	22.48
C	RTC	24.60	24.95	24.62	24.88	24.52	24.74	24.22	24.80	24.18	24.62	24.29	23.08
D	PPC	20.68	20.93	20.83	20.88	20.54	20.43	20.07	20.28	20.12	20.07	20.17	20.42
E	GDC	35.00	35.00	35.00	35.00	35.00	35.00	35.00	35.00	35.00	34.68	35.00	35.00
F	NRT	35.00	35.00	35.00	35.00	35.00	35.00	35.00	35.00	35.00	35.00	35.00	35.00
G	PPC - H$_2$O	20.66	21.21	21.33	20.89	20.87	20.85	20.44	20.35	20.36	20.49	20.29	20.48
H	NTC	35.00	35.00	35.00	35.00	35.00	35.00	35.00	35.00	35.00	35.00	35.00	35.00

Housekeeping Genes Expression Levels

Reverse Trascription Control (RTC): Are RNA sample impurities affecting reverse transcription?													
$C_t^C - C_t^G$		3.94	3.74	3.29	3.99	3.65	3.89	3.78	4.45	3.82	4.13	4.00	2.60
Cut-off	5	NO	NO	NO	NO	NO	NO	NO	NO	NO	NO	NO	NO
Positive PCR Control (PPC): Are RNA sample impurities affecting PCR?													
$C_t^D - C_t^G$		0.02	-0.28	-0.50	-0.01	-0.33	-0.42	-0.37	-0.07	-0.24	-0.42	-0.12	-0.06
Cut-off	3	NO	NO	NO	NO	NO	NO	NO	NO	NO	NO	NO	NO
No Reverse Transcription (NRT) control: Is genomic DNA contamination detectable?													
C_t^F		35.00	35.00	35.00	35.00	35.00	35.00	35.00	35.00	35.00	35.00	35.00	35.00
Cut-off	35	NO	NO	NO	NO	NO	NO	NO	NO	NO	NO	NO	NO
Genomic DNA Contamination (GDC) control: Will it affect the results?													
C_t^E		35.00	35.00	35.00	35.00	35.00	35.00	35.00	35.00	35.00	34.68	35.00	35.00
Cut-off	35	NO	NO	NO	NO	NO	NO	NO	NO	NO	YES	NO	NO
No Template Control (NTC): Is the PCR system clean?													
C_t^H		35	35	35	35	35	35	35	35	35	35	35	35
Cut-off	34	YES	YES	YES	YES	YES	YES	YES	YES	YES	YES	YES	YES

[7] This example displays the results of a real-time RT-qPCR plate investigating the quality of 12 cDNA samples of both, the original and the knockdown cell line, after irradiation with different doses of X-rays. For each sample, the validation sheet (supplied by SABiosciences) reports the average C_t value and further contains a number of PCR controls that test for RNA integrity, the presence of inhibitors of reverse transcription and PCR amplification and genomic and general DNA contamination.

After assuring a proper quality of all samples, the samples were further characterized with the RT² Profiler™ PCR Arrays. The results of both arrays were combined. In the following results, the standard error (SE) is shown for only those genes which were present in both arrays or in case that experiments had been repeated. A list of all genes is shown in Table 17 (s. Appendix). Table 12 shows genes that are more than threefold up- or downreglated in the knockdown cell line compared to the original cell line. All investigated genes and their respective values of up- or downregulation are listed in Table 18 (s. Appendix).

Table 12: *Gene expression in HEK shRNA RelA cells compared to the original cell line HEK-pNF-κB-d2EGFP/Neo L2 using the RT² Profiler™ PCR array [8] (SABiosciences).*

Gene symbol	Description	Relative gene expression $\mu \pm SE$
CCND1	Cycin D1	-3.69 ± 1.15
IL8	Interleukin 8	-8.12 ± 5.20
JUN	Jun oncogene	4.25 ± 2.48
RELA	V-rel reticuloendotheliosis viral oncogene homolog A	-6.18 ± 1.47
TNF	Tumor necrosis factor	-3.37 ± 1.54

[8] The table shows all genes from both, the customized and the NF-κB signaling array, that are more than threefold up- or downregulated in HEK sRNA RelA cells compared to HEK-pNF-κB-d2EGFP/Neo L2 cells. 162 genes were investigated. Mean and standard error of the expression level were calculated from up to five individual experiments with untreated cells. Prior to investigating gene expression with the RT² Profiler™ PCR arrays, a proper RNA and cDNA quality was confirmed.

3.4.3 Differences in gene expression of both cell lines after TNF-α-treatment

TNF-α, which is known to be a strong NF-κB activator, was added to the cells for 6 hours, which was shown to be an appropriate time point to investigate NF-κB target gene expression (Fig. 40). Subsequently RNA was isolated and tested for its integrity as described in 2.2.2.1 and 2.2.2.2. After cDNA synthesis, the RT² RNA QC PCR Array was performed for quality control and gene expression was investigated using the RT² Profiler™ PCR Arrays as described in 2.2.2.6. Table 13 shows the expression profile for each cell line respectively. C_t values of TNF-α treated cells were compared to the C_t values of the untreated sample of the respective cell line. Only genes more than

threefold up- or downregulated are shown. A list of all genes and the corresponding amount of regulation is shown in Tables 19 and 20 (see Appendix).

In the original cell line, a set of CXCL genes and TNF itself are strongly upregulated by TNF-α treatment. The NF-κB inhibitor NFKBIA shows an 6.3-fold upregulation.

In the knockdown cell line, the gene expression profile reveals five downregulated NF-κB target genes. None of the genes activated by TNF-α in HEK-pNF-κB-d2EGFP/Neo L2 cells is notably regulated in the knockdown cell line.

Table 13: *Gene expression in HEK-pNF-κB-d2EGFP/Neo L2 (green) and HEK shRNA RelA (red) cells 6 hours after treatment with TNF-α (10 ng/ml) using the RT² Profiler™ PCR array[9] (SABiosciences).* (L2) HEK-pNF-κB-d2EGFP/Neo L2; (SH) HEK shRNA RelA.

Gene symbol	Description	Relative gene expression μ ± SE	
		L2	**SH**
CXCL1	Chemokine (C-X-C motif) ligand 1	**11.73**	-1.28
CXCL10	Chemokine (C-X-C motif) ligand 10	**5.14**	-1.42
CXCL2	Chemokine (C-X-C motif) ligand 2	**6.51**	-1.01
IL8	Interleukin 8	**5.35 ± 0.31**	2.77 ± 1.65
NFKBIA	Nuclear factor of kappa light poly peptide gene enhancer in B-cells inhibitor, alpha	**6.31 ± 0.52**	1.84 ± 0.11
TNF	Tumor necrosis factor	**13.91 ± 0.53**	2.49 ± 0.21
CCR5	Chemokine (C-C motif) receptor 5	1.58	**-4.59**
EXO1	Exonuclease 1	1.02	**-4.92**
IL10	Interleukin 10	1.04	**-3.11**
MT3	Metallothionein 3	1.04	**-3.11**
SOD3	Superoxide dismutase 3, extra cellular	1.04	**-3.11**

[9] The table shows all genes from both, the customized and the NF-κB signaling array that are more than threefold up- or downregulated (bold). 162 genes were investigated. The standard error of the expression level is shown for genes occurring in both arrays.

3.4.4 The RelA-knockdown cell line does not show significant changes in cell cycle progression

It was shown that NF-κB is involved in cell cycle regulation by inducing cyclin D1, which is involved in the G1/S transition (Guttridge *et al.*, 1999). Further, results of gene expression studies (Table 12) showed a nearly four-fold downregulation of CCND1 (cyclin D1) in the knockdown cell line compared to the original cell line. Therefore, the distribution of cells in the different phases of the cell cycle was investigated for both cell lines during 48 hours (Fig. 35). In HEK shRNA RelA cells, there was a tendency towards a decreased percentage of cells in S-phase, but the amount of cells in different cell cycle phases did not differ significantly in both cell lines.
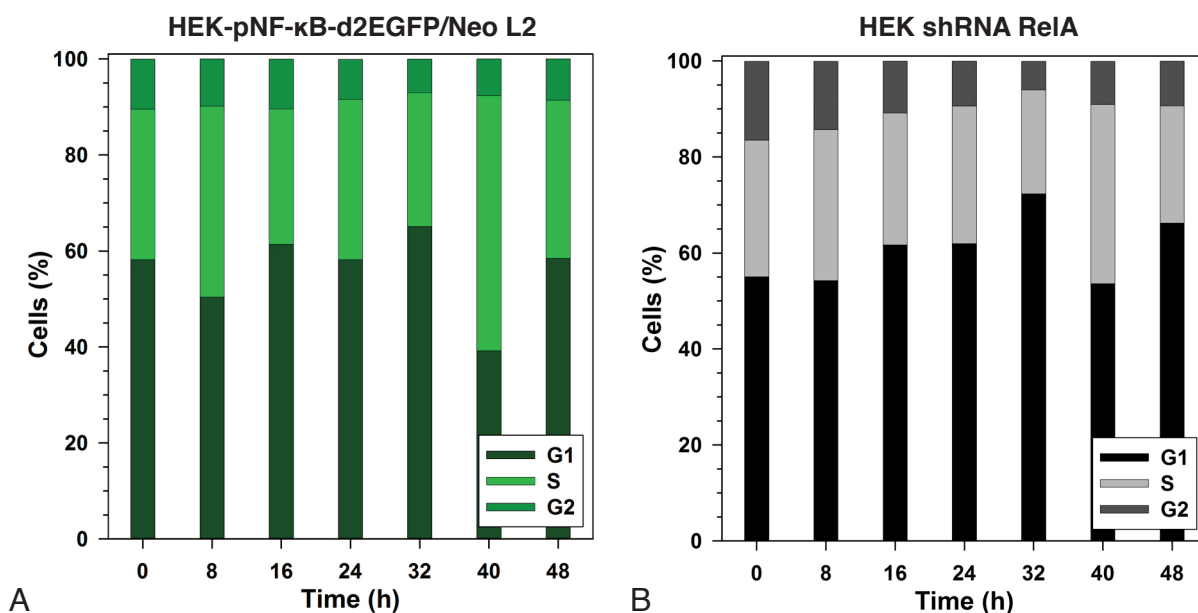
Fig. 35: *Comparison of cell cycle progression within 48 hours in the original (A) and the knockdown cell line (B).* Distribution of the cell cycle phases G1, S and G2 was investigated by fixing cells in 70 % ethanol at different time points and analysing PI stained cells by flow cytometry. Data from up to four individual experiments was combined. Percentages were calculated by the Flowing Software 2 (by Perttu Terho).

3.5 Effects of RelA-knockdown on the cellular radiation response

After characterising both cell lines regarding different biological endpoints, the effect of the RelA knockdown on the radiation response was investigated. Cells were irradiated with different radiation qualities to subsequently study differences in their survival ability, cell cycle progression and gene expression.

3.5.1 HEK cells are more sensitive to X-irradiation in absence of RelA

The effect of the RelA-knockdown on radiosensitivity was investigated by irradiating cells with X-rays and subsequently determining their clonogenic survival ability. Colonies were counted after 14 to 21 days. HEK shRNA RelA cells showed a significantly heightened radiosensitivity with p-values ≤ 0.001 for 2, 6 and 8 Gy and p-values ≤ 0.01 for 4 Gy (Fig. 36). The parameters describing the survival curves of both cell lines are listed in Table 14.
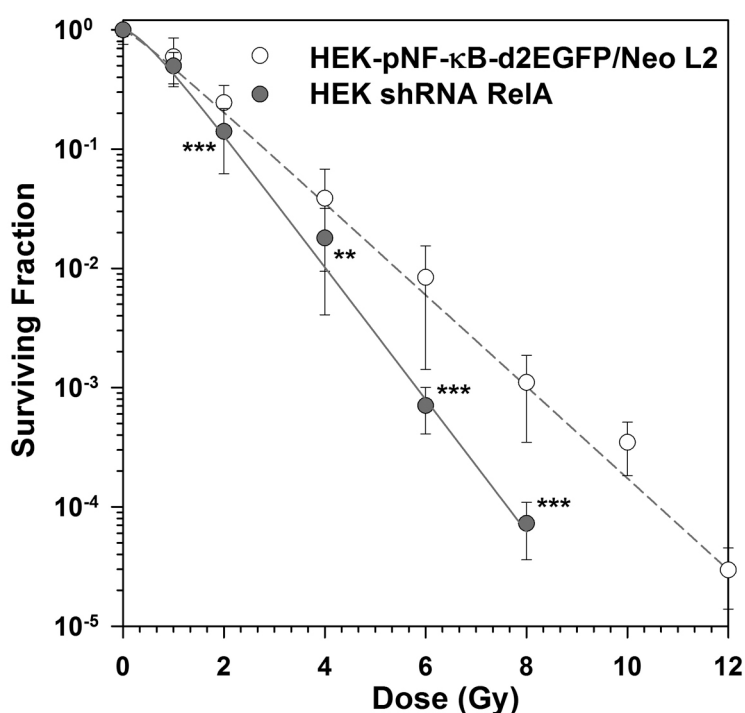
Fig. 36: *Clonogenic survival after exposure of HEK shRNA RelA and HEK-pNF-κB-d2EGFP/Neo L2 cells to 200 kV X-rays.* Survival was determined by the colony forming ability test. Colonies were fixed and stained 14 to 21 days after irradiation. Data from four individual experiments with each six replicates were combined. p ≤ 0.05 *, p ≤ 0.01 **, p ≤ 0.001 ***.

Table 14: *Parameters describing the survival curves (single-hit-multi-target model) after X-irradiation.*

Cell line	D_0	n	D_q	r^2
HEK-pNF-κB-d2EGFP/Neo L2	1.13 ± 0.02 Gy	1.21 ± 0.12	0.22 ± 0.11 Gy	0.94
HEK shRNA RelA	0.78 ± 0.02 Gy	1.69 ± 0.18	0.41 ± 0.09 Gy	0.95

3.5.2 The RelA-knockdown cell line does not show changes in colony forming ability after exposure to heavy ions

As it was shown that the colony forming ability depends on the LET, survival curves after irradiation with heavy ions were performed (Fig. 37). To investigate the effect of the RelA knockdown on the cellular response to accelerated heavy ions, the colony forming ability of both cell lines was investigated. Cells were irradiated with ^{64}Ni ions (1000

MeV/n, LET 175 keV/µm) and seeded 4 hours after irradiation. Colonies were counted after 14 to 28 days. In comparison to X-rays, exposure to high-LET radiation revealed a more efficient killing effect. However, no differences in radiosensitivity between both cell lines could be observed. The parameters describing the survival curves of both cell lines are listed in Table 15.
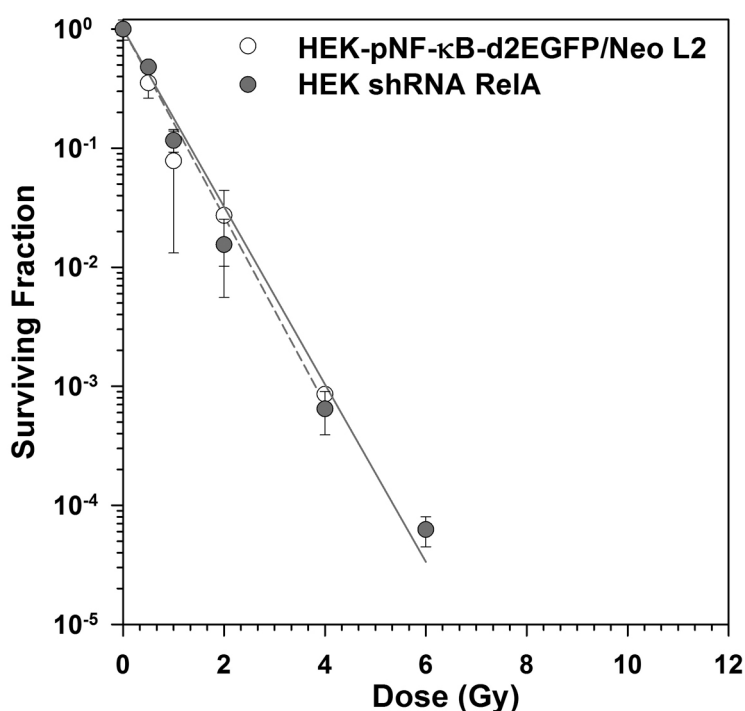
Fig. 37: *Clonogenic survival after exposure of HEK shRNA RelA and HEK-pNF-κB-d2EGFP/Neo L2 cells to ^{64}Ni ions (1000 MeV/n, LET 175 keV/µm). Survival was determined by the colony-forming ability test (CFA). For investigating clonogenic survival, cells were seeded in Petri dishes 4 hours after irradiation. Colonies were fixed and stained after 14 to 28 days. Mean and SD from six replicates per dose is shown. Doses (Gy) were calculated from fluences (P/cm^2) according to Equation 19 (s. 2.4.2).*

Table 15: *Parameters descrining the survival curves (single-hit-multi-target model) after irradiation with ^{64}Ni ions.*

Cell line	D_0	n	D_q	r^2
HEK-pNF-κB-d2EGFP/Neo L2	0.55 ± 0.05 Gy	0.72 ± 0.11	0.18 ± 0.07 Gy	0.87
HEK shRNA RelA	0.57 ± 0.02 Gy	0.76 ± 0.10	0.16 ± 0.07 Gy	0.95

3.5.3 Cell cycle progression after irradiation with X-rays and heavy ions

The effect of radiation on cell cycle progression and changes in the knockdown cell line were investigated by irradiating cells with different radiation qualities and doses and determining cell cycle distribution at different time points after irradiation. Cell cycle distribution was analysed by flow cytometry as described in 2.3.10.

After irradiating cells with 2 Gy of X-rays, a shifting of the amount of HEK-pNF-κB-

d2EGFP/Neo L2 cells in each cell cycle phase can be observed. After 8 to 16 hours, the number of cells being in G1 phase starts to decrease and to increase in the G2 phase (Fig. 38). From 16 to 24 hours after X-irradiation, cells in G2-phase significantly increase compared to the untreated control. At ∽ 40 hours after irradiation, the distribution in the cell cycle is normalized. Comparing these results to the knockdown cell line, no significant changes can be seen.
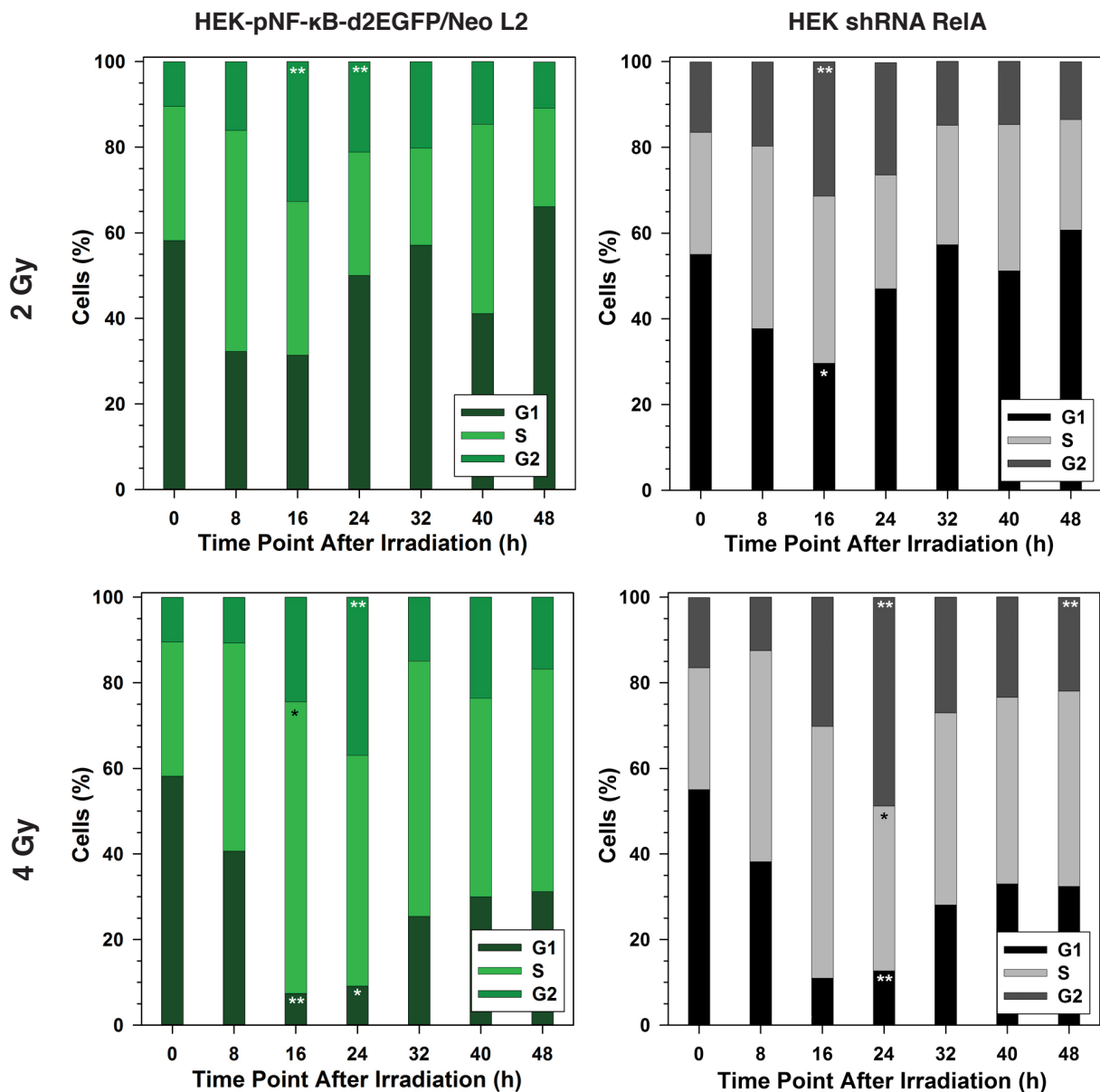
Fig. 38: *Comparison of cell cycle progression within 48 hours in the original (A) and the knockdown cell line (B) after X-irradiation.* Cells were irradiated with 200 kV X-rays and fixed in 70 % Ethanol at different time points after irradiation. Distribution of the cells in the cell cycle phases G1, S and G2 was investigated by flow cytometric analysis of PI stained cells. Data from up to four individual experiments were combined. Percentages were calculated by the Flowing Software 2 (by Perttu Terho). p ≤ 0.05 *, p ≤ 0.01 **, showing a significant difference of irradiated versus non-irradiated cells (Fig. 35) for each time point.

Similar effects were shown for an X-ray dose of 4 Gy. After exposure to this dose, the redistribution of cell cycle phases was more severe, with significant decreases in G1-phase 16 and 24 hours after irradiation (Fig. 38). As already observed in the untreated control (Fig. 35), the S-phase generally seemed to be less prominent compared to G1 and G2 phase in HEK shRNA RelA cells. However, these results are only a tendency and differences between original and knockdown cell line are not significant.

It was then investigated, whether irradiation with heavy ions reveals clearer differences in cell cycle progression between both cell lines, as heavy ions have an higher impact on NF-κB activation. Therefore, cells were irradiated with 2 Gy of ^{48}Ti ions (1000 MeV/n, LET 108 keV/μm) and fixed at different time points after irradiation (Fig. 39).
As already observed in the cell cycle experiment using X-rays, the distribution of cells shifts towards the G2 phase 16 to 24 hours after irradiation. In contrast to X-rays, a longer time is required after irradiation with ^{48}Ti ions for the return of the cell cycle distribution to the initial situation. Even after 48 hours, both cell lines are arrested in the G2 phase. The heavy ion experiment was conducted only once due to the limited availability of beam time, therefore the significance could not be determined. Cell cycle progression was analysed by comparing histograms and calculating the amount of cells in each cell cycle phase by the Flowing Software 2. From these results, no noticeable differences of the HEK shRNA RelA cells compared to HEK-pNF-κB-d2EGFP/Neo L2 cells could be observed.

Fig. 39: *Cell cycle distribution at different time points after heavy ion exposure in the original and the knockdown cell line.* (0 Gy) Mock irradiated controls of HEK-pNF-κB-d2EGFP/Neo L2 and HEK shRNA RelA cells; (2 Gy) irradiation with ^{48}Ti ions (1000 MeV/n, LET 108 keV/μm) of HEK-pNF-κB-d2EGFP/Neo L2 and HEK shRNA RelA cells. Cell cycle profiles after analysing PI-stained cells by flow cytometry are indicated. In each histogram, the x-axis denotes the number of cells, while the y axis shows the emitted fluorescent light and therefore the DNA content. (TP) timepoint after irradiation. Percentages were calculated by the Flowing Software 2 (by Perttu Terho).

3.5.4 Time course of NF-κB-dependent gene expression after ⁴⁸Ti irradiation

For the subsequent NF-κB target gene array, an appropriate time point for analysis of NF-κB dependent gene expression as a response to radiation exposure had to be determined (Fig. 40).
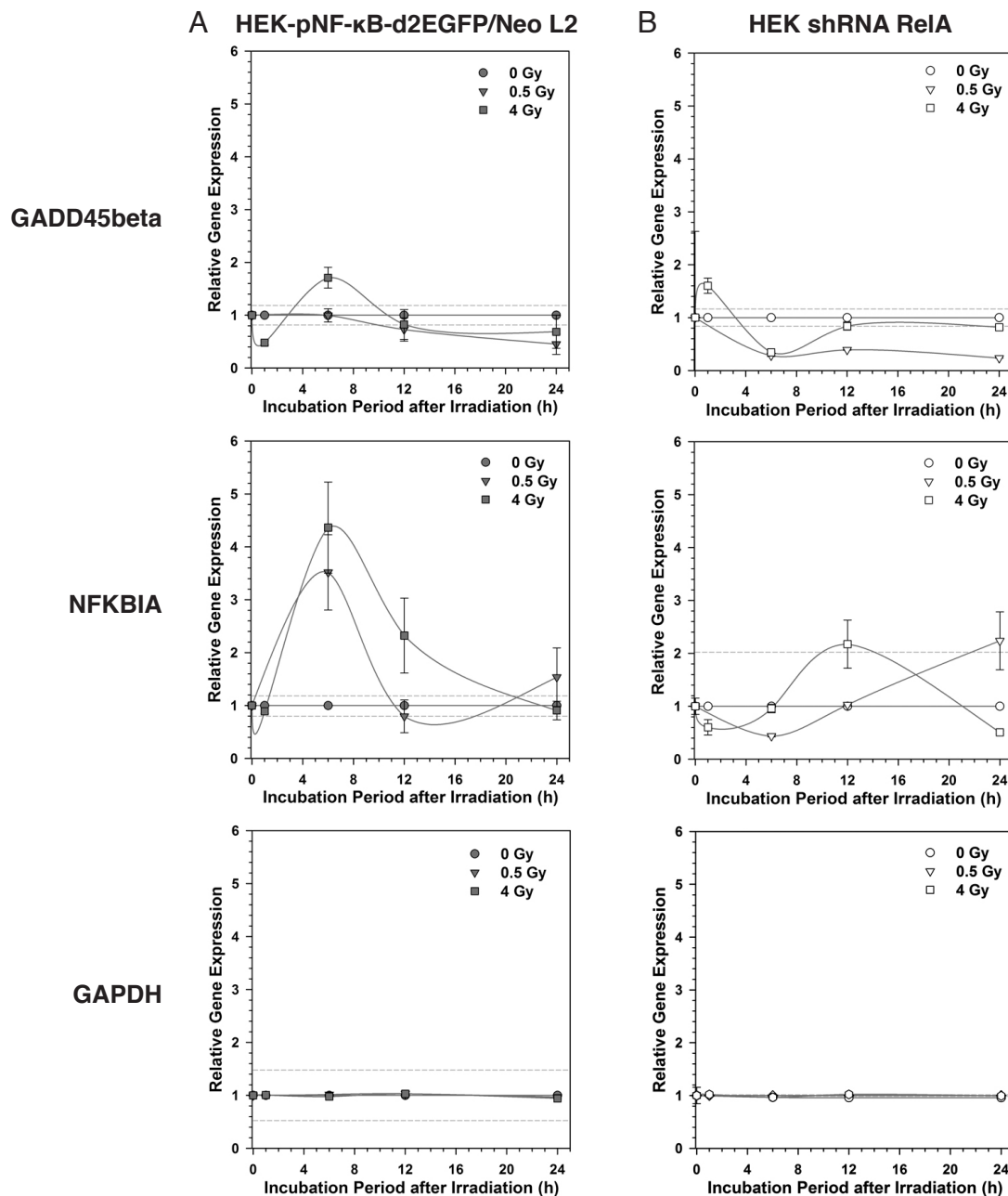
Fig. 40: *Relative gene expression of the NF-κB target genes GADD45beta and NFKBIA in HEK-pNF-κB-d2EGFP/Neo L2 (A) and HEK shRNA RelA (B) cells after irradiation with different doses of ⁴⁸Ti ions (1000 MeV/n, LET 108 keV/μm).* Gene expression was assessed by RT-qPCR, using GAPDH as a reference gene to normalize the results. The dotted line indicates the normal variation of expression. Mean and standard deviation of relative gene expression are shown for three replicates.

Therefore, cells were irradiated with two different doses of ^{48}Ti ions (1000 MeV/n, LET 108 keV/µm). GADD45beta and NFKBIA are known to be expressed NF-κB dependently, thus these genes were used to investigate the time course of NF-κB dependent gene expression by real-time RT-qPCR. GAPDH was used to normalize the results. RNA was tested for all quality control parameters as described in 2.2.2.2. In the HEK-pNF-κB-d2EGFP/Neo L2 cell line, expression of both genes peaks after 6 hours. The extent of relative gene expression increases with rising doses. In the knockdown cell line, NFKBIA regulation does not exceed the normal variation of the expression after 24 hours and GADD45beta is slightly downregulated 6 hours after irradiation. The extent of gene regulation in HEK shRNA RelA cells cannot be related to the radiation dose.

3.5.5 Gene expression after X- and heavy ion irradiation in the original and in the RelA knockdown cell line

The aim of this experiment was to investigate the regulation of gene expression in HEK-pNF-κB-d2EGFP/Neo L2 and in HEK shRNA RelA cells after irradiation with different radiation qualities and doses. Therefore, cells were irradiated with X-rays and ^{48}Ti ions (1000 MeV/n, LET 108 keV/µm). After 6 hours, RNA was isolated and tested for integrity, as described in 2.2.2.1 and 2.2.2.2. Additionally, a RT^2 RNA QC PCR Array was run for quality control (s. 2.2.2.6). Gene expression was analysed, using the already described target gene arrays. For samples being irradiated with X-rays, only the array including genes from the NF-κB signaling pathway was used. For ^{48}Ti ions, also the customized array was applied. This was due to the fact that the X-ray experiment was the last of all target gene array experiments. At that time it was already decided to focus in detail on NF-κB regulated genes only.

Samples being irradiated with X-rays were exposed to the doses 0.5, 4 and 8 Gy. From previous experiments and from results of other working groups, a higher biological effectiveness for titanium ions was assumed, and therefore, lower doses were applied. Doses for ^{48}Ti ions were 0.5 and 4 Gy.

Expression profiles for both cell lines with genes more than threefold up- or downregulated are shown in Table 16. A list of the results for all genes is shown in Tables 21 to 26 (s. Appendix).

In HEK-pNF-κB-d2EGFP/Neo L2 cells, the amount of upregulated genes as well as the intensity of upregulation increases with increasing doses of X-rays. A similar effect can be observed when regulated genes after irradiation with 4 Gy of both, X-rays and ^{48}Ti ions, are compared. After irradiation with ^{48}Ti ions, the amount of upregulated genes

increases, as well as the intensity of regulation for genes that are regulated by both radiation qualities. Highly upregulated are genes from the group of CXCL chemokines and TNF. The same effect had already been observed after TNF-α-treatment.

In HEK shRNA RelA cells, almost none of the genes from the expression profile of HEK-pNF-κB-d2EGFP/Neo L2 cells were regulated after exposure to low- and high LET radiation. The only gene that appeared to be regulated in both cell lines after irradiation with ^{48}Ti ions was JUN. JUN expression after exposure to X-rays and ^{48}Ti ions cannot be compared, as JUN was only present in the customised target gene array, which had not been applied to X-irradiated samples. No correlation between the amount of genes and the intensity of regulation to dose or radiation quality can be observed in the knockdown cell line.

[10] Cells were irradiated with X-rays (200 kV, 0.5, 4 and 8 Gy) and ^{48}Ti ions (1000 MeV/n, LET 108 keV/µm, 0.5 and 4 Gy). RNA was isolated 6 hours after treatment. Differences in gene expression were analysed using the RT^2 Profiler™ PCR array (SABiosciences). The table shows all genes from both, the customized and the NF-κB signaling array, that are more than threefold up- or downregulated (bold). 162 genes were investigated. The standard error of the expression level is shown for genes occurring in both arrays.

Table 16: *Gene expression in HEK-pNF-κB-d2EGFP/Neo L2 (green) and HEK shRNA RelA (red) cells after treatment with ionizing radiation[10]. (L2) HEK-pNF-κB-d2EGFP/Neo L2; (SH) HEK shRNA RelA.*

Relative gene expression (μ ± SE)

Gene symbol	X-rays 0.5 Gy L2	X-rays 0.5 Gy SH	X-rays 4 Gy L2	X-rays 4 Gy SH	X-rays 8 Gy L2	X-rays 8 Gy SH	^{48}Ti 0.5 Gy L2	^{48}Ti 0.5 Gy SH	^{48}Ti 4 Gy L2	^{48}Ti 4 Gy SH
BIRC3	1.10	-1.22	1.58	1.50	**3.16**	1.26	1.09	1.17	1.35	-1.28
CD83	-1.11	1.03	2.39	1.53	**3.81**	2.08	1.22	1.22	**4.26**	1.60
CXCL1	1.56	1.08	**4.22**	1.54	**8.94**	2.05	1.23	-1.27	**9.27**	1.41
CXCL10	1.03	1.08	**5.53**	2.29	**21.86**	2.10	1.15	-1.14	**9.72**	-1.01
CXCL2	1.02	1.34	2.55	2.15	**4.72**	1.80	1.65	1.14	**4.41**	1.04
IL8	1.21	1.21	**3.27**	1.39	**7.26**	1.02	1.24 ± 0.10	-0.10 ± 1.16	**5.71 ± 0.64**	1.72 ± 0.20
JUN							1.28	1.11	**7.93**	**3.30**
LTA	1.99	1.20	2.26	2.90	**3.23**	1.56	1.04	1.14	-2.10	-1.56
NFKB2	1.22	1.35	2.80	1.85	**3.94**	2.01	-1.02 ± 0.01	1.09 ± 0.03	2.16 ± 0.90	1.15 ± 0.05
NFKBIA	1.16	1.07	2.25	1.79	**4.23**	2.05	0.08 ± 1.15	1.13 ± 0.04	**3.57 ± 0.12**	1.63 ± 0.09
RELB	1.22	1.20	1.47	1.48	**3.05**	1.38	-1.18	1.08	1.09	-0.12
TNF	1.03	1.08	2.69	1.16	**9.32**	1.14	1.53 ± 0.15	0.26 ± 1.40	**8.40 ± 0.19**	0.84 ± 1.86
CCL11	1.27	**3.22**	2.14	**3.26**	2.58	2.11	-1.42	1.26	-2.55	1.45
CD80	1.16	1.35	1.74	**4.37**	2.39	1.34	-1.05	1.41	-1.60	-2.21
EGR2	1.21	-1.02	2.05	**3.17**	2.75	1.59	-1.08	1.29	-2.11	-1.86
JUN							1.28	1.11	**7.93**	**3.30**
LTB	1.22	1.16	1.80	**4.78**	2.55	2.33	-1.11	1.31	-2.80	-2.17
TNFRSF1B	1.07	1.10	1.56	**9.69**	2.22	**5.65**	-1.05	1.07	-2.28	**-7.09**
TNFSF10	1.26	1.19	1.70	**5.37**	1.72	**3.13**	-1.07	1.06	-1.88	**-3.26**

4 Discussion

The aim of the project was to study the role of the NF-κB pathway in the cellular response after exposure to high LET radiation as it occurs in space. For this purpose, different approaches to inhibit or knockdown key components of this pathway were taken. Motivation for this work was the hypothesis, that activation of NF-κB enhances survival of cells exposed to space relevant radiation qualities as NF-κB is known to be activated by fluences of accelerated heavy ions that can be reached during long-term missions (Baumstark-Khan *et al.*, 2005; Hellweg *et al.*, 2011). Therefore, the NF-κB pathway is a potential pharmacological target for mitigation of the radiation response. Inhibition or knockdown of this pathway might reduce cellular survival after exposure to different radiation qualities. These findings eventually facilitate risk estimation and support the development of appropriate countermeasures.

The cell line HEK-pNF-κB-d2EGFP/Neo L2 was used as an essential tool for all experiments conducted throughout this work. It enables quantification of NF-κB activation by a reporter system measuring NF-κB-dependent d2EGFP expression (Hellweg *et al.*, 2003). It was shown by several research groups that the NF-κB pathway, including the classical and the genotoxin-induced sub-pathway, is functional in HEK cells (Matsuda *et al.*, 2003; Hellweg *et al.*, 2006; Muscat *et al.*, 2007; Simon and Samuel, 2007). HEK cells have a high NF-κB activating response to TNF-α (Aoudjit *et al.*, 1997) which induces NF-κB-dependent gene expression in these cells (Li *et al.*, 1998). Additionally, HEK cells express neuronal markers similar to that of neuronal stem cells (Shaw *et al.*, 2002; Arnhold *et al.*, 2008).

Few studies on high LET radiation with HEK cells exist (Ueda *et al.*, 2001; Irarrazabal *et al.*, 2006; Tang *et al.*, 2011, Sridharan *et al.*, 2012). As HEK cells are quickly dividing embryonic cells, they are rather radiosensitive.

4.1 Activation of NF-κB depends on LET

In order to compare activation of the NF-κB pathway via the classical and the genotoxin-induced sub-pathway, TNF-α was used in the irradiation experiments as activator of the classical pathway. TNF-α is known to be a strong activator of NF-κB-dependent gene expression. In HEK-pNF-κB-d2EGFP/Neo L2 cells, an increased binding of the NF-κB subunit RelA to the κB binding site 15 minutes after incubation with TNF-α was demonstrated, using an oligonucleotide-based NF-κB-ELISA (Hellweg *et al.*, 2003). Here, it was shown by immunofluorescence with the same cell line that translocation of RelA into the nucleus occurs 15 to 30 minutes after treatment with TNF-α.

HEK-pNF-κB-d2EGFP/Neo L2 cells showed NF-κB-dependent d2EGFP expression after incubation with TNF-α starting from 3 hours, and reaching its maximum after 6 to 24 hours (Hellweg *et al.*, 2003, 2005; Baumstark-Khan *et al.*, 2005). Here, TNF-α and ionizing radiation were used to activate NF-κB, resulting in a maximum d2EGFP expression 16 to 18 hours after induction for both agents (Fig. 20). This time point was determined to measure NF-κB activation by many different radiation qualities and doses when maximal response can be expected. The kinetics of NF-κB activation in response to X-rays and carbon ions additionally show that heavy ions induce a stronger NF-κB activation than X-rays. NF-κB activation is activated by lower doses of carbon ions compared to X-rays, and the maximal response is higher and observed at a lower dose (10.9 Gy carbon ions versus 16 Gy X-rays). More data supporting these findings have recently been published by the Cellular Biodiagnostics group (Hellweg *et al.*, 2011). Further, NF-κB activation is dose-dependent, due to the increasing DNA damage potential of increasing fluences.

Subsequently, the potential to activate NF-κB of several energetic heavy ions of different LET was studied (Fig. 21 A). A first hint that heavy ions are stronger NF-κB activators than low-LET radiation was published in 2005: high LET ^{36}Ar ions (272 keV/μm) had a higher potency to activate NF-κB-dependent d2EGFP expression in HEK cells than X-rays (Hellweg *et al.*, 2005; Baumstark-Khan *et al.*, 2005). A rapid and persistent NF-κB activation after exposure to ^{56}Fe ions was shown in human monocytes already at low doses of 0.35-1.4 Gy (Natarajan *et al.*, 2002), indicating a high RBE of ^{56}Fe ions for this biological endpoint (Groesser *et al.*, 2007). Further, exposure to accelerated ^{12}C and ^{16}O ions influences expression of NF-κB itself in Chinese Hamster V79 cells (Mitra *et al.*, 2004, 2005), while it remains unclear which NF-κB subunit was analyzed in those studies.

A maximum in biological efficiency in cell killing was determined in a LET range of 90-200 keV/μm (Thacker *et al.*, 1979; Ainsworth *et al.*, 1983; Kraft *et al.*, 1989). Concerning NF-κB activation, the maximal activation was observed for heavy ions with an LET of 90-300 keV/μm, with a maximal RBE of ∼ 9 for argon ions with an LET of 272 keV/μm (Hellweg *et al.*, 2011). Results in this work complement these data by showing that NF-κB dependent d2EGFP expression rises quickly with increasing doses after irradiation with heavy ions within an LET range of 34 to 92 keV/μm. For high doses of 16 to 20 Gy, up to 60 % of the irradiated cell population express the reporter d2EGFP[(+)], indicating NF-κB activation in the majority of the population. On the contrary, ^{58}Ni ions with a very high LET of 906 keV/μm activate NF-κB in only up to 25 % of the irradiated cells, and much higher doses are required to induce a significant increase of d2EGFP[(+)] cells

to the double of the background (ca. 8 Gy). This might be explained by the 'overkill' effect (Mehnati *et al.*, 2005) that was observed also for other biological endpoints. This overkill effect observed with ions with an LET above 500-1000 keV/µm is explained by wasted energy which does not contribute to biologically significant damages. Such a high LET increases the degree of ionization and DNA damage clustering without further increasing e.g. cell death or mutations induction. According to the formula to convert fluence to energy dose (equation 19), LET contributes to the energy dose, and a very high LET results in higher energy doses, which energy is partly 'wasted' in terms of biological effectiveness. At an LET resulting in maximal RBE, it is proposed that the probability is highest that one single charged particle causes a DSB, which is the basis for most biological effects. The degree of DNA lesion complexity correlates with increasing LET (Tilly *et al.*, 2002). This overkill effect is also present for NF-κB activation, as shown for nickel ions in this work. For lead ions with very high LET ($\sim$ 9700 keV/µm) (Hellweg *et al.*, 2011), the RBE even drops below 1.

NF-κB can be anti-apoptotic and is involved in regulation of cellular survival and proliferation. Inhibition of NF-κB activation is associated with a tendency towards apoptosis (Gao *et al.*, 2004). In this work, NF-κB dependent d2EGFP expression was correlated with survival (Fig. 21 B). NF-κB activation and the cell killing effect decrease with very high LET (^{58}Ni ions, 75 MeV/n), resulting in better survival compared to heavy ions with an LET below 100 keV/µm. It is assumed that this effect is due to the decrease in the lethal damage per unit dose, resulting in decreased RBE for cell killing (Mehnati *et al.*, 2005). Presence of non-hit cells among hit cells is one of the significant features for exposure to very high-LET heavy ions. The relationship of NF-κB activation and survival seems therefore quite complex in the very high LET range that results in overkill effects, with the moderate extent of NF-κB activation giving no complete explanation for the better survival of ^{58}Ni ion exposed HEK cells compared to exposure with ions of a lower LET. The extremely inhomogeneous dose distribution on the microscopic level, resulting in very high doses at the sub-micrometer range with areas without any exposure might explain the apparently better survival after ^{58}Ni ions exposure.

The survival curves resulting from heavy ion exposure do not show the typical shoulder formation, which is usually observed in response to exposure to low LET ionizing radiation (Bird and Burki, 1975; Yang *et al.*, 1977; Stoll *et al.*, 1995; Durante *et al.*, 1995). In the experiments described here, the LET was high enough to abolish shoulder formation, which means that cells are not capable to repair potentially lethal DNA damages adequately. This purely exponential course of the survival curves obtained after heavy

ion exposure is in line with the results from other research groups (Barendsen *et al.*, 1963; Stoll *et al.*, 1995; 1996).

4.2   Chemical inhibition of the NF-κB pathway

Several chemical inhibitors were tested for their cytotoxicity and ability to suppress NF-κB activation by several agents in HEK-pNF-κB-d2EGFP/Neo L2 cells in order to investigate the effect of an impaired NF-κB pathway on several biological endpoints. The effects of the ATM inhibitor KU-55933 and the proteasome inhibitor MG-132 are shown and discussed in this work. Inhibition with Parthenolide, Capsaicin, Isohelenin and caffeic acid phenethyl ester (CAPE), all targeting different elements of the NF-κB pathway, was either insufficient or cytotoxic and results are not shown.

Cytotoxicity of the inhibitors was tested by means of the MTT test to determine the appropriate, non-cytotoxic concentration for further studies. The MTT test indirectly measures cell viability by quantification of mitochondrial enzymatic activity.

4.2.1   NF-κB activation by ionizing radiation is ATM dependent

TNF-α was used as a positive control to activate NF-κB and to determine the inhibitor concentration needed to suppress NF-κB signaling. As the ATM inhibitor KU-55933 was not able to suppress NF-κB activation induced by TNF-α within its non-cytotoxic range, a suitable concentration from literature (Hickson *et al.*, 2004) was used in irradiation experiments. KU-55933 is specific for ATM with respect to inhibition of other related kinases such as DNA-dependent protein kinase (DNA-PK) or phosphatidylinositol 3'-kinase (PI3K) which required a ∼ 200 times higher concentration for their inhibition (Hickson *et al.*, 2004). Results showed that while it was not possible to suppress TNF-α induced NF-κB activation, KU-55933 was able to suppress ionizing radiation induced NF-κB activity completely. Increasing doses of X-rays and ^{36}Ar ions were used to induce NF-κB, showing its dose and LET dependency, as the percentage of d2EGFP$^{(+)}$ cells increased with increasing doses and ^{36}Ar ions had a higher impact on NF-κB dependent d2EGFP expression than X-rays.

Involvement of ATM in the induction of NF-κB-dependent gene expression after exposure of human cells to X-rays (Ruscher, 2008) and to heavy ions had been shown in previous projects of the Cellular Biodiagnostics working group. These results support the assumption that ionizing radiation, including high-LET heavy ions, activates the genotoxic stress induced NF-κB pathway and proofs that NF-κB activation induced by

ionizing radiation is strictly ATM dependent. ATM foci form quickly in the nuclei of human cells after exposure to carbon or iron ions and are believed to facilitate or initiate DNA DSB repair by NHEJ and HR (Xue *et al.*, 2009; Takahashi *et al.*, 2008). ATM was recently shown to be activated in human cells to a higher extent by carbon ions (LET 290 keV/μm) than by low-LET γ-rays (Ghosh *et al.*, 2011). This stronger ATM phosphorylation after heavy ion exposure might be important for the strong NF-κB activation that was observed in the LET range of 90-300 keV/μm.

In contrast, TNF-α induced NF-κB activation was not impaired by KU-55933, as ATM is not involved in the classical pathway, which is activated by TNF-α.

4.2.2 IκB degradation by the proteasome is essential for TNF-α and ionizing radiation induced NF-κB activity

Incubation of HEK cells with the proteasome inhibitor MG-132 revealed that already at low concentrations cells reduced the viability to 80-90 %. This viability level was still well suitable for the irradiation experiments, but shows the involvement of the proteasome not only in IκB degradation but in numerous processes, which are essential for viability of the cell.

Within non-cytotoxic concentrations (viability above 80%), MG-132 was able to suppress TNF-α and ionizing radiation induced NF-κB activity, showing that IκB degradation by the proteasome is an essential step in both, the genotoxic stress and the TNF-α induced pathway.

However, it has to be considered, that disturbing proteasome functions with MG-132 leads to the loss of regulation of essential functions within the cell. MG-132 is effective in inhibiting the NF-κB pathway and can thus be used for heavy ion experiments. Nevertheless, as MG-132 not only inhibits IκB degradation but degradation of numerous proteins, the observed biological outcomes cannot be ascribed to NF-κB inhibition alone.

In conclusion, MG-132 and KU-55933 are useful to study the involvement of different elements in the NF-κB pathway as it is activated in the cellular response to heavy ion exposure. The results presented here show the relevance of ATM kinase and the proteasome in the NF-κB activation that is induced during the cellular response to ionizing radiation, including high-LET heavy ions. However, these chemical inhibitors are not NF-κB specific.

4.3 Knockdown of RelA by RNA interference (RNAi)

To inhibit the NF-κB pathway more specifically, RNAi was used to knockdown the RelA subunit for subsequent studies with space-relevant radiation.

In this work, transfection with a shRNA vector was chosen to develop a stable knockdown cell line. This allows studying the effect of silencing gene expression without transfecting cells prior to every experiment, which is of special importance when experiments are conducted at heavy particle accelerators, where the procedure of experiments is often unpredictable and experiments have to be adapted to the prevailing circumstances. A stably transfected cell line provides a long-term knockdown, permanently silencing the gene of interest, which cannot be achieved in repeated transient transfection assays. It eliminates experimental variation, especially when it is used not only for one unique experiment but repetitively, due to investigations under varying conditions. Additionally, transient transfection with siRNA does not allow transfected cells to be identified due to a lack of selection markers. Therefore, siRNA transfected cells cannot be enriched and transfection efficiency cannot be determined. In such experiments, the knockdown level has to be verified for every transfection by RT-qPCR.

Stable transfection was performed with HEK-pNF-κB-d2EGFP/Neo L2 cells which were developed by the Cellular Biodiagnostics working group several years ago and evaluated extensively using different agents for activation of NF-κB (Hellweg *et al.*, 2006), including ionizing radiation (Hellweg *et al.*, 2005; Baumstark-Khan *et al.*, 2005). In this cell line, NF-κB can be induced and the resulting reporter gene expression can be quantified by flow cytometry. These cells allowed easy pre-screening of knockdown efficiency by means of the NF-κB-dependent d2EGFP expression. The d2EGFP fluorescence in response to TNF-α was expected to be reduced or completely abolished in case of successful knockdown.

HEK-pNF-κB-d2EGFP/Neo L2 cells already contain a Neomycin-resistance marker, therefore a SureSilencing™ shRNA Plasmid containing a Hygromycin-resistance marker for selection of stably transfected cells was chosen.

The NF-κB dimer that is activated by TNF-α and by ionizing radiation as X-rays and accelerated carbon ions was previously shown to contain RelA, therefore, it was decided to knockdown this NF-κB subunit (Hellweg and Baumstark-Khan, 2007a; Hellweg *et al.*, 2009; 2011b).

Four individual shRNA plasmids were tested for their ability to suppress RelA expression. The knockdown level of each transfected cell population was measured respectively. As each the initially transfected cell populations were polyclonal, including cells with both, high and low knockdown levels depending on the integration site, the

overall knockdown efficiency for each population only reached average knockdown levels of ∼ 40 to 50 %. This amount is defined as 'mediocre' in the SABiosciences evaluation sheet. A knockdown level of ≥ 70 % has to be achieved for gene suppression to be defined as 'successful'.

Cells were sub-cloned to select for single integration events. This allows to achieve a more consistent and higher knockdown level, as cells grown from a single clone are assumed to have the same integration site of the plasmid. The greatest knockdown (83.1 %) was reached for the cell line growing from clone 4-9, which was later named 'HEK shRNA RelA'.

The cell line 'HEK shRNA control', which had been stably transfected with a negative control shRNA vector, allows to create a baseline for measuring mRNA knockdown efficiency. Further, it is needed to control for nonspecific side effects caused by stable transfection.

The knockdown was verified on several levels. Measurement of steady state mRNA levels by real-time RT-qPCR is very sensitive and the most direct way to proof the decreasing amount of the RelA gene transcript. Still, it does not predict expected protein levels, as mRNA can be translated several times and additionally modified post-transcriptionally to enhance or reduce its stability. Residual mRNA might be sufficient to compensate for the loss of the high percentage of mRNA, which has been degraded. To show that RNAi also has an impact on translation rate, the knockdown has to be shown on protein level and in the case of a transcription factor as NF-κB, on the level of gene induction via the κB site.

Knockdown verification on the protein level was performed by immunofluorescence. This allowed visualization of RelA within the cell, confirming the substantial decrease in RelA protein by the much lower fluorescence signal in HEK shRNA RelA cells compared to the original cell line. Also, the cytoplasmic localization of RelA in unstimulated cells was confirmed.

The loss of transcriptional activation by NF-κB in RelA knockdown cells was demonstrated on reporter protein level by measuring d2EGFP expression in response to TNF-α and ionizing radiation. Results show a minor residual ability of activating NF-κB, which can be ascribed to the remaining ∼ 17 % of RelA mRNA, which is not degraded.

HEK shRNA control cells show that induction of d2EGFP dependent NF-κB expression is still measurable and stable transfection does not affect the reporter system.

In HEK shRNA control cells the amount of d2EGFP$^{(+)}$ cells reaches ∼ 70 % after TNF-α treatment and thereby slightly exceeds the expression of green fluorescence compared to the original HEK-pNF-κB-d2EGFP/Neo L2 cell line. This might be due to

further selection of cells during incubation with hygromycin, which by chance are slightly more responsive to NF-κB activating agents.

4.4   Characterization of HEK shRNA RelA cells

4.4.1   Changes in growth and cell cycle progression in absence of RelA

NF-κB is considered to be an important regulator of cellular proliferation (Li and Verma, 2002; Hayden and Ghosh, 2004). Therefore, to reveal possible differences in growth behavior between the original and the cell line HEK shRNA RelA, growth curves of both cell lines were compared. Both curves showed the typical division into lag phase, exponential growth (log) phase and stationary phase. Though, the cell number of HEK shRNA RelA cells initially decreases in lag phase, and cells enter the log phase only after 48 to 72 hours. There is no initial decrease in cell number in HEK-pNF-κB-d2EGFP/Neo L2 cells, which enter log phase already after 24 to 48 hours. Further, knockdown cells seem to grow less dense in the stationary phase compared to the original cell line. This supports the findings about the essential role of NF-κB in cell proliferation.

As it was shown in literature, defects in the NF-κB pathway are related to changes in proliferation and growth behavior (Baichwal and Baeuerle, 1997; Sonenshein, 1997). NF-κB inhibition by BAY11-7082 leads to decreased lymphocyte proliferation (Zhu *et al.*, 2008) and in a skeletal differentiation model, lack of NF-κB was related to accelerated differentiation, assuming that NF-κB plays a role in proliferation while inhibiting differentiation (Guttridge *et al.*, 1999) which normally results in reduced or stopped cell division. In line with this, it was shown that sustained myoblast proliferation and inhibition of myogenic differentiation is NF-κB-dependent and that inhibition of myogenesis is specific to RelA (Langen *et al.*, 2004; Dahlman *et al.*, 2009).

In contrast, additional findings indicate that epidermal RelA deficiency leads to increased proliferation in the epidermis of mice (Zhang *et al.*, 2003) and that NF-κB subunits, including RelA, inhibit keratinocyte growth (Seitz *et al.*, 1998; 2000). Though, it was demonstrated, that RelA induces growth inhibitory genes in epidermal cells but not in other cell types (Hinata *et al.*, 2003).

Results in this work show that cell proliferation is delayed in absence of NF-κB. As it will be discussed later, loss of NF-κB might lead to impaired cell-cell communication. A prerequisite for this so-called bystander effect has been shown to be close proximity between cells (Gerashchenko and Howell, 2003). Cells were seeded in low density at the beginning of the growth curve experiments, which might explain the delay in proliferation in the RelA knockdown-cell line.

According to literature, NF-κB transmits growth signals directly to key regulators of the cell cycle (Hinz *et al.*, 1999). Primary fibroblasts lacking NF-κB activity exhibit reduced proliferation rates in conjunction with lower cyclin D1 levels, revealing the role of cyclin D1, a key regulator of G1 checkpoint control and progression from G1 to S-phase, for proper cell growth control. Loss of NF-κB affects cell cycle progression as NF-κB regulates expression of cyclin D1 (Guttridge *et al.*, 1999; Hinz *et al.*, 1999). It was shown that suppression of NF-κB leads to slowed cell cycle progression and that this reduction can be recovered via transfection and expression of a cyclin D1 containing plasmid (Guttridge *et al.*, 1999; Hinz *et al.*, 1999). From all NF-κB subunits, RelA has specifically been associated to be a transcriptional activator of cyclin D1 gene expression (Dahlman *et al.*, 2009).

In this work, a comparison of the distribution of cells within the cell cycle phases for both cell lines revealed no differences in the untreated state (without activation of the NF-κB pathway), suggesting a comparable regulation of cell cycle progression with and without RelA. As it was shown that the NF-κB subunit p52 (NF-κB2) can also regulate cyclin D1 (Westerheide *et al.*, 2001; Rocha *et al.*, 2003; Schumm *et al.*, 2006), it might substitute for the lack of RelA.

4.4.2 Changes in NF-κB target gene expression in RelA knockdown cells

To reveal changes in gene expression between HEK shRNA RelA and HEK-pNF-κB-d2EGFP/Neo L2 cells, gene expression under different conditions was investigated with the help of two different RT^2 Profiler™ PCR Arrays. Overall, 162 genes, involved in cell cycle control, apoptosis, DNA damage, stress and toxicity and NF-κB signaling were investigated. In the course of these studies, a down- or upregulation specifically of NF-κB target genes emerged, therefore, expression studies finally focused on this pathway. C_t values indicating the amount of a specific mRNA were compared for the RelA knockdown cells and the HEK-pNF-κB-d2EGFP/Neo L2 cells. In a cautious data interpretation, the threshold for significant up- or downregulation was set to -3 or +3, respectively, to avoid misinterpretation of physiological fluctuation of mRNA levels. First, genes that are regulated more than threefold in the untreated knockdown cell line compared to the untreated original cell line are discussed here.

CCND1 (Cyclin D1) is downregulated (-3.7) in absence of RelA, confirming it being targeted by RelA, as discussed previously. Cyclins are positive regulators of cell cycle entry, regulating progression from G1 to S phase. Overexpression of cyclin shortens the duration of G1 phase, as a high level of cyclin D1 is needed for transition to S phase. Increased proliferation in fibroblasts, regulated by NF-κB mediated cyclin D1,

leads to delayed differentiation (Guttridge *et al.*, 1999). Downregulation of cyclin D1 accelerates exit from the cell cycle and inhibits proliferation. Decreased cyclin D1 levels are important for proper initiation of keratinocyte differentiation and cyclin D1 knock-down in SCC9 cells enhanced loss of colony-forming ability (Nishi *et al.*, 2009), which was also shown in this work by survival experiments. Downregulation of cyclin D1 by knocking down RelA therefore gives a possible explanation why proliferation of HEK shRNA RelA cells is delayed in growth experiments.

IL8 (Interleukin 8, CXCL8) is severely downregulated (-8.1) in HEK shRNA RelA cells. This cytokine is part of the CXC chemokine family and acts as proinflammatory medi-ator, further activating proinflammatory cytokines in a positive feedback loop. It attracts and activates neutrophils (Baggiolini *et al.*, 1989), causing them to migrate towards the site of infection. It was shown for several cell types, that the NF-κB binding site is essential for transcription of IL8 (Stein and Baldwin, 1993; Wu *et al.*, 1997; Elliot *et al.*, 2001). Kunsch *et al.* (1994) showed this especially for the subunit RelA. IL8 secretion is increased in response to oxidative stress, mediated by TNF-α, which further induces RelA-binding to the binding site of the IL8 promoter (Vlahopoulos *et al.*, 1999).

JUN (JUN oncogene; c-Jun) is the only gene that is more than threefold (4.3) upregu-lated in RelA knockdown cells. It is one of the main members of the AP-1 family, activating oncogenes. c-Jun affects cell proliferation, migration and invasion and, like NF-κB, actively participates in tumorigenesis (Galardi *et al.*, 2011). It was shown that both, NF-κB and c-JUN activity are required for activating macrophage inflammatory protein (MIP-2, CXCL2), a CXC chemokine in mice (Kim *et al.*, 2003). It directly inter-acts with RelA, which results in synergistic transcriptional activity via the κB binding sites (Yang *et al.*, 1999). Upregulation of the JUN oncogene might be a regulatory mechanism to compensate for the loss of RelA.

RELA (V-rel reticuloendotheliosis viral oncogene homolog A, nuclear factor of kappa light polypeptide gene enhancer in B-cells 3, p65) was expected to be downregulated, as it was chosen as the target gene for RNAi. Its downregulation was shown to be -6.2, meaning that there was six times less RelA mRNA in the HEK shRNA RelA cells com-pared to the HEK-pNF-κB-d2EGFP/Neo L2 cells, resulting in a reduction of the expression level of 100 % to 17 % with a downregulation of 83%. This knockdown level is in line with the 83.1 % observed using the RelA primer assays before.

TNF (Tumor necrosis factor; TNF-α) is a cytokine and key mediator of inflammation that can contribute to carcinogenesis through the activation of NF-κB (Pikarsky *et al.*, 2004; Balkwill, 2009). It binds to the receptors TNF-R1 and TNF-R2. TNF-R1 is expressed in most tissues, while TNF-R2 is found only in cells of the immune system. In addition to NF-κB, TNF-α can activate the MAPK pathway, which involves activation of the pro-apoptotic transcription factor c-Jun. A third, death signaling, pathway is induced by binding of TNF-α to TNF-R1 (Gaur and Aggarwal, 2003). Though TNF-α can induce apoptosis, its major role is its involvement in inflammatory processes. Its apoptotic effect is often masked by the anti-apoptotic effects of NF-κB. In many cell types, TNF has no apoptotic effect due to its parallel triggering of a signaling pathway that activates NF-κB (Chen and Goeddel, 2002). TNF-α activates inflammation by inducing a proin-flammatory cytokine cascade, mediated through expression of IL8 (Vlahopoulos *et al.*, 1999). It induces a delayed ROS-dependent signaling pathway that is required for NF-κB transcriptional activation.

In general, cytokines are downregulated in HEK shRNA RelA cells, indicating their restriction to transcriptional control by NF-κB (RelA).

After treating both cell lines with TNF-α, a clear upregulation of CXC chemokine genes, including CXCL1, CXCL10, CXCL2 (MIP-2) and CXCL8 (IL8) was observed in HEK-pNF-κB-d2EGFP/Neo L2 cells, but not in HEK shRNA RelA cells. CXC chemokines are one out of four groups within the chemokine family of small cytokines. Chemokines are secreted by infected cells and induce chemotaxis or migration of cells, especially of neutrophils, by acting as chemoattractants. Neutrophils act as first responders of inflam-matory cells to migrate towards site of inflammation. In wound healing, damaged cells cause an increase of chemokine concentration, leading to movement of cells to site of damage. In contrast, loss of chemokine induction leads to dysfunctional cell migration and therefore impaired wound healing. Models of mycobacterial infection have shown the essential role of TNF in the early induction of chemokines and subsequent recruit-ment of leukocytes (Roach *et al.*, 2002). Here, in TNF-/- cells induction of chemokines and cellular recruitment was delayed. CXCL2 (MIP-2), which is upregulated after TNF-α treatment, was also shown to be activated *in vitro* by *M. tuberculosis* (Rhoades *et al.*, 1995). It was recently published, that NF-κB inhibitor Curcumin inhibits prostate cancer metastasis by targeting the inflammatory cytokines CXCL1 and CXCL2 (Killian *et al.*, 2012). Cells lacking RelA might thus be susceptible to infections, but less prone to evolve metastatic potential after neoplastic transformation.

As expected, TNF-α treatment induced high upregulation (13.9) of TNF, as TNF-α, after being released as a response to immunological stimuli, acts as a positive autocrine feedback signal to augment NF-κB activation (Coward *et al.*, 2002). In the knockdown cell line, no upregulation of TNF was observed, as NF-κB is a key transcription factor involved in the synthesis of TNF-α (May and Ghosh, 1998).

Upregulation of NFKBIA (encoding IκBα) in the original cell line was expected as well, as in addition to increasing the transcription of cytokines and adhesion proteins, NF-κB also increases the transcription of the inhibitor IκB, thus leading to its own inactivation and subsequent termination of the response (Baldwin, 1996).

None of the genes upregulated in HEK-pNF-κB-d2EGFP/Neo L2 cells was induced in the knockdown cell line. Instead, downregulation of a few NF-κB target genes only slightly exceeding the threshold of -3 was observed, including CCR5, EXO1, IL10, MT3 and SOD3. CCR5 is a chemokine receptor targeted by NF-κB (Liu *et al.*, 1998). Exonuclease 1 (EXO1) is involved in DNA damage signaling (Souto-Carneiro *et al.*, 2008). The NF-κB target gene interleukin 10 (IL10) is known as immunsuppressive cytokine and controls the overproduction of inflammatory cytokines (Cao *et al.*, 2006). Its downregulation might therefore balance the loss of RelA in HEK shRNA RelA cells, which would induce proinflammatory genes in case of appropriate stimuli. Methallothionein (MT3) might function as a negative regulator of NF-κB (Sakurai *et al.*, 1999). Its downregulation probably antagonizes the RelA knockdown in HEK shRNA RelA cells. For superoxide dismutases (e.g. SOD3) it was shown, that RelA controls its transcription mediated by TNF-α (Maehara *et al.*, 2000).

4.5 The role of RelA in response to radiation of different LET

While the NF-κB pathway has been studied intensively in regard to different aspects throughout more than two decades, not much is known about its role in response to different radiation qualities, especially to high LET particles. In this project, the HEK shRNA RelA cell line had been established to conduct irradiation experiments with cells lacking the NF-κB subunit RelA.

Due to the limited number of beam time available at particle accelerators, only few, in maximum four heavy ion experiments were run per year. Most experiments were therefore previously established and tested using the X-ray facility at DLR in Cologne. This additionally provides the opportunity to finally compare biological outcomes after exposure to different LET, and in this context, X-rays serve as a low-LET reference radiation.

4.5.1 Cell cycle progression after irradiation

Ionizing radiation is known to perturb cell-cycle progression in a dose-dependent manner, thereby causing delay in proliferation (Park *et al.*, 2002; Gerashchenko *et al.*, 2004). Distribution of cell cycle phases was analyzed at several time points after irradiation with X-rays and ^{48}Ti ions (Fig. 38 and Fig. 39). Both cell lines, HEK-pNF-κB-d2EGFP/Neo L2 and HEK shRNA RelA, exhibit a significant G2 arrest after ~ 16 to 24 hours, independent of the radiation type, indicating a block in G2 phase, allowing more time for DNA repair. This was expected for HEK-pNF-κB-d2EGFP/Neo L2 cells, as they have been characterized by a significant G2 phase arrest in response to irradiation (Hellweg, 2012). X-ray experiments show that cell cycle arrest depends on dose, as G2 arrest is more severe after irradiation with 4 Gy compared to 2 Gy. Also, the time of recovery to the original state of cell cycle distribution was delayed with increasing doses of X-rays. While cell cycle distribution has come back to the uninduced state ~ 32 to 40 hours after irradiation with 2 Gy of X-rays, a reduced number of cells in G1 phase was still observed 48 hours after X-irradiation with 4 Gy.

The response to higher LET radiation is shown after ^{48}Ti ion irradiation. Comparing cell cycle distribution after irradiation with different radiation qualities, 2 Gy of ^{48}Ti ions cause a more severe cell cycle arrest as well as a prolonged recovery time than 2 Gy of X-rays, with ~ 40 % of the cell population remaining in G2 compared to 10-15% of the mock-irradiated cells.

Cell cycle arrest is induced only after several hours, as transcription of cyclin kinase inhibitors is necessary. The duration of G2 arrest depends on the amount and severity of DNA damage. During G2 phase, the DNA repair machinery can use the intact sister chromatid as a template and induce HR (Shrivastav *et al.*, 2008). With increasing dose and LET, DNA damage becomes more severe and complex, which explains its influence on G2 arrest.

Absence of NF-κB was associated with a delay in cell cycle progression in G1 (Bargou *et al.*, 1997; Grumont *et al.*, 1998). However, as it was already observed in unirradiated cells, none of the cell cycle experiments performed in this work showed a difference between both cell lines. This indicates that cell cycle progression in the G1 phase does not exclusively depend on RelA controlled expression of cyclin D1 in HEK cells. Instead, other transcription factors such as AP-1 or other NF-κB subunits could compensate the missing RelA. Another possible explanation is that cyclin E and cyclin-dependent kinase 2 (CDK2) alone without the CDK4-cyclin D complex could initiate the transition from the G1 to the S-phase of the cell cycle (Wilson *et al.*, 2004).

Furthermore, induction of a G2 arrest after radiation exposure is not affected by the absence of RelA and the resulting downregulation of cyclin D1 expression. This is in

line with the general view that the complex of CDK1 and cyclin B is responsible for the transition of cells from the G2 phase to mitosis, and that cyclin D1 is not involved in radiation-induced G2 arrest (Wilson *et al.*, 2004; Metting and Little, 1995).

4.5.2 Survival ability after irradiation

Cellular survival after exposure of HEK-pNF-κB-d2EGFP/Neo L2 and HEK shRNA RelA cells to ionizing radiation was measured by colony forming ability test. Both cell lines were irradiated with X-rays (Fig. 36), a low LET reference radiation, and high LET ^{64}Ni ions (LET 175 keV/μm; Fig. 37), which is within the range of maximum biological efficiency (Thacker *et al.*, 1979; Ainsworth *et al.*, 1983; Kraft *et al.*, 1989).

Comparing survival curves of X-ray experiments with HEK-pNF-κB-d2EGFP/Neo L2 cells to those using heavy ions, data in this work confirms the findings, that doses needed to achieve a clonogenic killing effect decrease with increasing LET. Here, high-LET radiation exposure of HEK-pNF-κB-d2EGFP/Neo L2 cells results in purely exponential survival curves. Survival curves of different cell types show no shoulder formation after heavy ion exposure, depending on LET (Bird and Burki, 1975; Durante *et al.*, 1995; Hellweg *et al.*, 2011). Absence of the shoulder means that also at low doses, cells are not able to repair DNA damage adequately. The same was shown for HEK shRNA RelA cells. Exposure to ^{64}Ni ions results in a much steeper curve than X-irradiation lacking shoulder formation. After exposure to X-rays, the survival curve of HEK shRNA RelA cells shows a smaller shoulder compared to HEK-pNF-κB-d2EGFP/Neo L2 cells.

Inhibition of NF-κB activation is associated with a tendency towards apoptosis (Gao *et al.*, 2004) and therefore, as expected, RelA knockdown cells showed a significantly increased radiosensitivity after X-ray exposure compared to HEK-pNF-κB-d2EGFP/Neo L2 cells. Several studies have shown the impact of NF-κB inhibition on sensitivity towards low-LET radiation (Pajonk *et al.*, 2000; Raju *et al.*, 1999; Raju *et al.*, 1997; Yang *et al.*, 2000). It was published that NF-κB activation promoted survival in mice and primates being irradiated with lethal doses and that radiosensitive tissues can be protected against radiation damage through Toll-like receptor 5 (TLR5)-dependent activation of NF-κB using derivatives of bacterial flagellin (Burdelya *et al.*, 2008).

Upon irradiation, DNA DSB are induced, resulting in ATM activation that then triggers amongst others NF-κB signaling. At the same time, ATM activates the pro-apoptotic transcription factor p53, which competes with NF-κB for interaction with transcriptional co-activators (Ravi *et al.*, 1998; Wadgaonkar *et al.*, 1999). In absence of NF-κB, pro-apoptotic signaling therefore dominates, as seen here. However, in other cellular

settings, NF-κB is required for p53 pro-apoptotic signaling (Ryan *et al.*, 2000). A sustained NF-κB activation could permit cells that have accumulated radiation-induced DNA damage, to escape elimination by apoptosis (Jung and Dritschilo, 2001).

Surprisingly, the effect of an increased radiosensitivity in absence of RelA was not observed after exposure to ^{64}Ni ions. Here, survival curves of both cell lines showed the same progression. Several possible reasons might explain this effect. In contrast to the X-ray experiment, where cells have been seeded immediately, due to technical reasons, cells were seeded only 4 hours after irradiation in the heavy ion experiment. This time frame might have given knockdown cells the possibility to repair DNA damage. It was shown that HeLa cells repair most strand breaks caused by oxidative DNA damage within 1 h (Collins *et al.*, 1995). Phosphorylated histone H2AX (γ-H2AX) foci, indicating sites of DSBs, continue to grow in size for about 1 hour after exposure to X-rays and then disappear slowly over time. γ-H2AX is proposed to recruit repair factors to sites of DNA damage (Celeste *et al.*, 2003).
Faster recruitment kinetics of repair proteins after high LET irradiation was attributed not only to a higher number of DSBs, but also to a higher spatial density of the DSB clusters (Hable *et al.*, 2012). Another group reports in a recent study that foci are formed twice as fast after irradiation with 2 Gy of X-rays compared to 0.1 Gy (Neumeier *et al.*, 2012). According to this data, repair mechanisms are accelerated depending on the complexity and amount of DNA damage. Alternatively, the given time frame might have activated repair mechanisms to compensate for the loss of RelA.

Additionally, the type of DNA damage differs between high and low LET radiation and therefore, repair mechanisms might differ after X-irradiation and heavy ion exposure. As it is known, densely ionizing HZE particles cause a higher proportion of direct than indirect DNA damage, due to direct ionization, with complex clusters of DNA damages with distinct protein signaling kinetics compared with low LET radiation like X-rays. Ionizing radiation can also induce DNA damage by generating ROS. It has been suggested that the radiolytic formation of an oxygenated microenvironment around the tracks of high-LET heavy ions is an important factor in their enhanced biological efficiency (Meesungnoen and Jay-Gerin, 2009). Probably these different kinds of damage induce distinct repair mechanisms.
Little is known about the involvement of NF-κB in DSB repair. Recently, it was shown that NF-κB strongly stimulates the removal of DSB by enhancement of homologous recombination (HR; Volcic *et al.*, 2012). Further data suggest a link between inhibition of NF-κB and inhibition of DSB repair that leads to enhancement of X-ray-induced cell

killing *in vitro* in non-small-cell lung cancer cells (Estabrook *et al.*, 2011). It is known that ATM responds to DSBs via the activation of NF-κB. Additionally, ATM can protect cells from ROS accumulation by promoting NADPH production and the synthesis of nucleotides required for the repair of DSB. ATM promotes the anti-oxidant response and DNA repair through regulating the pentose phosphate pathway (PPP; Cosentino *et al.*, 2011). It might be possible, that repair of complex DNA damage caused by heavy ions is not dependent on NF-κB, and therefore no differences are seen after exposure to ^{64}Ni ions.

Another explanation for the missing effect of RelA knockdown might be the high LET which is in the range of the highest observed biological efficiency. The cell killing effect in the LET range of 100-200 keV/μm is already very high, so that disturbed cellular signaling pathways might not be able to further increase cell killing. This was observed for the pro-apoptotic p53 in some cell systems: apoptosis was independent of the p53 status (Mori *et al.*, 2009; Takahashi *et al.*, 2004).

Furthermore, the gene expression profile described below will give more insight in the differences in the role of NF-κB in cellular survival after exposure to X-rays and heavy ions, even though these experiments had to be performed with another heavy ion (^{48}Ti instead of ^{64}Ni ions).

4.5.3 Target gene expression after irradiation

NF-κB was shown to translocate into the nucleus 15 to 30 minutes after induction. To find the appropriate time point for investigation of its target gene expression, the expression kinetics of the NF-κB target genes GADD45β and NFKBIA was measured after exposure to ^{48}Ti ions (1000 MeV/n, LET 108 keV/μm). Six hours after irradiation, gene expression showed its maximum, with the expression level increasing with augmenting doses. GADD45β, which is regulated by NF-κB, is a cell cycle regulating gene which is upregulated upon environmental stress like ionizing radiation and regulates cell growth (Liebermann and Hoffmann, 2008). NFKBIA codes for the NF-κB inhibitor IκBα. Its upregulation indicates its function of negatively regulating NF-κB in order to prevent its overexpression. In HEK shRNA RelA cells, none of these genes was upregulated.

4.5.3.1 Target gene expression depending on radiation quality and quantity

The target gene array, investigating 162 genes after X- and ^{48}Ti ion irradiation, showed that NF-κB-dependent gene expression does not only depend on dose, but also on

LET. Radiation induced gene expression depending on LET was shown in literature (Nelson *et al.*, 2002). The extent of gene expression increases with increasing doses. Further, the degree of regulation is significantly stronger after 4 Gy of ^{48}Ti ion exposure than after X-irradiation of the same dose. Genes that are regulated more than threefold and at the same time are controlled by RelA are discussed here.

In HEK-pNF-κB-d2EGFP/Neo L2 cells, the set of genes, that has already been shown to be upregulated after TNF-α treatment, was likewise upregulated after exposure to X-rays and heavy ions. It includes **CXC chemokines**, **TNF** and the NF-κB inhibitor **IκBα**. This shows that expression of these genes is activated not only by the classical NF-κB pathway, but also the genotoxic stress induced pathway, independent of the radiation quality.

Especially the CXC chemokines are strongly upregulated, in case of CXCL10 up to 21.9 fold after irradiation with 8 Gy X-rays. None of the genes that are upregulated at higher doses in the original cell line exceeds the threshold of 3 after irradiation with 0.5 Gy of both, X-rays and ^{48}Ti ions. Though, after 4 Gy of X-rays, CXC chemokines reach expression values of 3.3 to 5.5 fold. For the same dose, these genes are expressed up to 9.8 fold after ^{48}Ti ion irradiation. Additionally, exposure to 4 Gy of ^{48}Ti ions results in the expression of genes that are only expressed after irradiation with 8 Gy of X-rays.

Apart from the genes expressed after both, TNF-α treatment and irradiation, additional genes are upregulated only upon X-irradiation, not after heavy ion exposure, proving the relation between radiation quality or LET and gene expression. These genes include BIRC3, LTA, NFKB2 and RELB:

BIRC3 (c-IAP2) encodes a member of the IAP family of proteins that inhibit apoptosis by binding to the tumor necrosis factor receptor-associated factors TRAF1 and TRAF2. It modulates inflammatory signaling and immunity, mitogenic kinase signaling and cell proliferation, as well as cell invasion and metastasis (Bertrand *et al.*, 2011). BIRC3 binds to TNF-R2, which is involved in apoptosis, and is activated by NF-κB to inhibit apoptosis. c-IAP2 expression is upregulated by ionizing radiation through NF-κB binding sites (Ueda *et al.*, 2001). Unlike what was expected, only one gene involved in apoptosis was regulated after X-ray exposure.

LTA (TNF-β, TNFSF1) is a member of the TNF superfamily of proteins, having overlapping functions with TNF-α. It signals through TNF-R1 and TNF-R2 activating the classical NF-κB pathway (Wolf *et al.*, 2010).

RELB and **NFKB2** code for NF-κB subunits, which are both involved in the non-canonical NF-κB pathway. NFKB2 codes for p100 which is processed to p52. These elements of the non-canonical pathway seem to be upregulated only by X-rays and not by heavy

ions. The RelB : p52 dimer was shown to confer radioresistance to prostate cancer cells by upregulating the expression of the antioxidant enzyme manganese superoxide dismutase (MnSOD) (Josson *et al.*, 2006; Xu *et al.*, 2007; 2008; Holley *et al.*, 2010).

The different gene expression profile after [48]Ti ion irradiation indicates distinct responses, depending on radiation quality, eventually including different repair mechanisms, as indicated in the survival curves in this work. These genes are expressed after X-irradiation, but not after [48]Ti ion exposure. The missing expression of the antiapoptotic BIRC3 and the protecting RelB genes after heavy ion exposure might be another explanation why RelA knockdown results in higher X-ray sensitivity, but not in higher heavy ion exposure sensitivity. Their protecting effect ceases to exist in HEK shRNA RelA cells after X-irradiation, but it is not induced after heavy exposure even in case of normal RelA levels.

Surprisingly, all genes that are expressed after TNF-α treatment, are also induced after irradiation with both radiation qualities. Genes that are additionally upregulated upon X-irradiation are not influenced by TNF-α or [48]Ti ions.

The only gene upregulated after both radiation species, but not TNF-α, is **CD83**. CD83 is one of the central regulatory molecules in immune functions with anti-tumor effects (Fujimoto and Tedder, 2006). It acts as a co-stimulator during activation of T-cells by antigen-presenting cells and is therefore essential for the induction of the adaptive immune response. NF-κB regulates inducible CD83 gene expression in activated T lymphocytes during an adaptive immune response (McKinsey *et al.*, 2000). Increased expression of this co-stimulatory molecule indicates that exposure to ionizing radiation does not only induce inflammation as a prominent innate immune response via pro-inflammatory cytokines such as TNF-α and via chemokines, but also induces selected steps towards activation of adaptive immunity.

Expression of JUN was investigated for [48]Ti ions only, as for X-rays, only the RT[2] Profiler™ PCR Array for NF-κB signaling targets, which does not involve JUN, was used. For comparison, increased JUN expression was also observed in human breast epithelial cells after exposure to α-particles (LET 150 keV/µm; Calaf and Hei, 2001).

Differences in gene expression depending on the radiation type are also observed in absence of RelA, as discussed in the next chapter.

4.5.3.2 Target gene expression depending on RelA

In absence of RelA, none of the genes regulated in HEK-pNF-κB-d2EGFP/Neo L2 cells are induced. However, as already seen in HEK-pNF-κB-d2EGFP/Neo L2 cells, gene expression differs between X-ray and heavy ion exposure. Again, different gene expres-

sion profiles after [48]Ti ion irradiation indicate distinct responses depending on radiation quality, providing an explanation for the differences in survival response of both cell lines.

Genes expressed after X- but not heavy ion-irradiation in the knockdown cell line are CCL11, CD80, EGR2 and LTB.

CCL11 encodes a cytokine called eotaxin, recruiting eosinophils by inducing their chemotaxis. It seems to play a role in the pathogenesis of asthma and inflammatory bowel disease (Park *et al.*, 2006; Bischoff and Ulmer, 2008; Waddell *et al.*, 2011). CCL11 was shown to be slightly upregulated in the spleen of mice irradiated with simulated solar particle event (SPE) protons, but downregulated after low-dose (0.05 Gy) and low-dose rate (0.24 mGy/h) γ-irradiation (Rizvi *et al.*, 2011).

The protein encoded by **CD80** (also known as B7.1) is a costimulatory molecule that is expressed normally on dendritic cells and induces T-cell proliferation and cytokine production during adaptive immune responses. It is an important signal during antigen-presentation by dendritic cells to T-cells. CD80 was shown to be upregulated in the spleen of mice irradiated with low-dose (0.05 Gy) and low-dose rate (0.24 mGy/h) γ-rays alone or incombination with simulated SPE protons (Rizvi *et al.*, 2011). Increased expression of CD80 in antigen-presenting cells might result in a more efficient T helper response.

EGR2 is a transcription factor involved in the early growth response. Besides its role in control of inflammation and of antigen-induced B cell proliferation (Li *et al.*, 2012), it was recently found that it plays a role as transcriptional regulator in T cell anergy (Zheng *et al.*, 2012). T cells go in this hyporesponsive state when antigen binds to their T cell receptor in absence of costimulation by CD80 or CD83 for example. Upregulation of this factor might therefore counteract the effects of increased CD80 expression.

LTB is a membrane protein of the TNF family which anchors lymphotoxin-α to the cell surface.

Overall, these genes are only slightly exceeding the threshold of 3. While upregulation of genes upon irradiation in the original cell line seems to be explainable, gene expression in HEK shRNA RelA cells appears to be rather random. Regulation of these genes does not seem to have a compensating effect, except maybe CD80 for CD83, for the loss of RelA and appears to be a consequence of the misregulation of several pathways which is due to the RelA knockdown.

Genes regulated after both, X- and heavy ion-irradiation, are TNFRSF1B and TNFSF10. They are of special interest, not only because they are clearly exceeding the threshold of 3/-3, but also because they are the only genes up-regulated after X-irradiation and downregulated after exposure to [48]Ti ions.

TNFRSF1B encodes for the TNF receptor TNF-R2. It was shown that TNFRSF1B receptor signaling resulted in the activation of anti-apoptotic survival proteins (Yang *et al.*, 2012). At the same time, TNFRSF1B promotes TNF-α induced apoptosis (Onizawa *et al.*, 2009). Baseline plasma TNFRSF1B, a marker of inflammation and a soluble TNF antagonist, was significantly associated with an increased risk of human colorectal cancer (Chan *et al.*, 2011). TNF-α bound to TNFRSF1B recruits intracellular adaptor proteins to activate multiple signal transduction pathways including NF-κB (Thommesen and Laegreid, 2005). The activation of NF-κB in intestinal epithelial cells by TNF-α through TNFRSF1B receptor signaling has been previously linked to carcinogenesis. Silencing TNFRSF1B increased apoptosis (Yang *et al.*, 2012). However, NF-κB interferes with apoptotic signals at various levels. The best example is found in the TNF-R1 pathway (Chen and Goeddel, 2002). It is therefore not sure, whether increased apoptosis results from pro-apoptotic TNFRSF1A signaling.

BIRC3 and **LTA**, which have been shown to be upregulated in HEK-pNF-κB-d2EGFP/Neo L2 cells after X-irradiation, bind to TNFRSF1B. As these genes are not expressed in the knockdown cell line, upregulation of TNFRSF1B in response to X-rays might have a compensating effect. Noticeably, TNFRSF1B is expressed inversely proportional to BIRC3 and LTA expression. After 4 Gy of X-rays, BIRC3 and LTA are not expressed more than threefold. However, in knockdown cells, 4 Gy of X-rays result in a TNFRSF1B upregulation of 9.7. With increasing X-ray dose (8 Gy), BIRC3 and LTA expression increases in the original cell line, while TNFRSF1B expression decreases. After exposure to ⁴⁸Ti ions, BIRC3 and LTA are not expressed in HEK-pNF-κB-d2EGFP/Neo L2 cells. Therefore, no balancing regulatory upregulation of TNFRSF1B is observed for ⁴⁸Ti ions in HEK shRNA RelA cells. Instead, expression of this gene is downregulated, indicating a different molecular mechanism as response to heavy ion exposure.

The cytokine **TNFSF10** is linked to apoptosis in transformed and tumor cells, but not in normal cells (RefSeq AC007919.18 and AC016938.24, www.ncbi.nlm.nih.gov). It is upregulated after X-irradiation, but downregulated after exposure to ⁴⁸Ti ions. This downregulation possibly indicates the onset of a rescue mechanism in absence of RelA that prevents increased radiosensitivity after heavy ion exposure in comparison with the original cell line, but not after X-ray exposure, as observed in survival experiments. The overlapping gene expression after TNF-α and radiation treatment in HEK-pNF-κB-d2EGFP/Neo L2 cells cannot be observed in RelA knockdown cells.

Overall, results revealed the outstanding role of NF-κB in cytokine expression. Surprisingly, anti-apoptotic genes were not noticeably influenced by knocking down RelA, and only one antiapoptotic NF-κB dependent gene, BIRC3, was upregulated after X-ray exposure.

4.5.3.3 NF-κB and the bystander effect

Target gene array experiments have revealed a strong correlation between an intact NF-κB pathway and cytokine and chemokine expression. After treatment of cells with TNF-α and different radiation qualities, a strong upregulation of genes coding for chemokines is observed in HEK-pNF-κB-d2EGFP/Neo L2 cells. In RelA knockdown cells, this expression profile is completely abolished, indicating the dependence of expression of these cytokines on NF-κB.

Cytokines are responsible for cell-cell communication and many aspects of the bystander effect. Chemokines in particular regulate chemotaxis of cells. Impaired cytokine expression results in the loss of intercellular communication. There is little known about how inflammatory cytokines mediate the bystander effect. Still, it was shown that the central inflammatory cytokine TNF-α acts as a diffuse mediator of the bystander effect (Yang *et al.*, 2012). A radiation induced bystander effect has already been observed earlier (Gerashchenko and Howell, 2003). Another group has shown a strong upregulation of chemokines in the rat liver after X-irradiation (Moriconi *et al.*, 2008).

There is direct evidence for the participation of gap junction intercellular communication (GJIC), allowing the transmission of damage signals resulting from irradiation with from α-particles to bystander effect (Azzam *et al.*, 2001). It is known that GJIC contributes to the maintenance of normal cell growth. Further, the rate of cell growth is inversely correlated with the extent of GJIC and growth inhibition correlates with intercellular communication (Mehta *et al.*, 1986; Loewenstein and Rose, 1992). Loss of NF-κB leads to impaired GJIC and bystander effects. The correlation between NF-κB, cytokines and GJIC has been shown (Chanson *et al.*, 2001). According to the results shown in this work, NF-κB is directly involved in cell-cell communication by inducing cytokines, and insofar the aspects of the bystander effect that represent an inflammatory and immune response are impaired in absence of NF-κB.

4.6   Conclusion and Outlook

The overall aim of this work was to improve the understanding of the role of NF-κB in the cellular response to space relevant radiation, as the NF-κB pathway might be a potential pharmacological target during space flights.

In cancer therapy, NF-κB has been shown to be a potential pharmacological target, as its inhibition would be an approach to potentiate radiation effects in radiotherapy, mainly by supporting the killing effect (Lee *et al.*, 2007; Baud and Karin, 2009; Madonna *et al.*, 2012). During space missions, a constant exposure to low doses of radiation, especially energetic heavy ions, is associated with an increased cancer risk. The absence of

increased killing by heavy ion exposure in RelA knockdown has to be clarified in experiments with and without repair time and with heavy ions of lower LET than the ^{64}Ni ions (175 keV/µm) used in this work. If increased cell killing is observed for such heavy ions for cells with downregulated RelA, this pathway could be an appropriate target to eliminate cells with DNA damage. To decrease the long-term risk of late effects like cancer, inhibition of NF-κB would then be a potential pharmacological target.

Though, inhibition of NF-κB will not only result in increased apoptosis, but also lower TNF production and inflammation (Linard *et al.*, 2004). It has to be considered, that immunosuppression is one of the major risks to the astronauts' health during long-term spaceflights. In space, microgravity (µg) leads to impaired T cell activation and an ineffective proinflammatory host defenses by downregulating immediate early genes, involving TNF and the Rel/NF-κB pathway (Chang *et al.*, 2012). Astronauts are prone to infections and show impaired wound healing which might be, among other factors, due to downregulation of NF-κB in µg. Considering knowledge about the role of NF-κB in the immune system and results in this work, additional suppression of NF-κB for radioprotection would probably potentiate the immunosuppressive effect. Therefore, inhibition of one of the NF-κB target genes that were identified in this work to be upregulated by high-LET radiation might be a better choice to avoid side effects on the immune system.
However, when astronauts are exposed to high radiation doses during solar particle events, an increased NF-κB level will be necessary to tolerate or prevent acute effects such as cell death.

Future work should focus on the role of the NF-κB target genes identified here in the cellular response to heavy ions. To analyze their function, they could be downregulated by RNAi as described in this work, or knock-out cell lines could be used. Furthermore, as these target genes where predominantly involved in cell-cell communication, their role in the bystander effect which is of eminent importance for single particle effects should be investigated. Microbeam experiments enable irradiation of single cells and subcellular compartments by using single particle beams.

5 Abstract

Radiation is currently one of the most important limiting factors for manned space flight. During such missions, there is a constant exposure to low doses of galactic cosmic radiation and in particular high-energy heavy ions. Together this is associated with an increased cancer risk which currently cannot be sufficiently reduced by shielding. As such, cellular radiation response needs to be further studied in order to improve risk estimation and develop appropriate countermeasures.

It has been shown that exposure of human cells to accelerated heavy ions, in fluences that can be reached during long-term missions, leads to activation of the Nuclear Factor κB (NF-κB) pathway. Heavy ions with a linear energy transfer (LET) of 90 to 300 keV/μm were most effective in activating NF-κB. NF-κB as an important modulating factor in the cellular radiation response could improve cellular survival after heavy ion exposure, thereby influencing the cancer risk of astronauts. The NF-κB pathway may be a potential pharmacological target in the mitigation of radiation response during space missions; such as the prevention of massive cell death after high dose irradiation (acute effects), in addition to neoplastic cell transformation during chronic low-dose exposure (late effects).

The aim of this work was to examine the role of NF-κB in the cellular response to space-relevant radiation. Firstly, NF-κB activation in human embryonic kidney cells (HEK) after exposure to different radiation qualities and quantities was investigated. Key elements of different NF-κB sub-pathways were chemically inhibited to analyze their role in NF-κB activation induced by low and high LET ionizing radiation. Finally a cell line, stably transfected with a plasmid coding for a short-hairpin RNA (shRNA) for a knockdown of the NF-κB subunit RelA, was established to assess the role of RelA in the cellular response to space-relevant radiation. The knockdown was verified on several levels and the cell line was characterized concerning proliferation, cell cycle progression and gene expression. Additionally, the effects of the RelA knockdown on cell cycle progression, cellular survival and gene expression after exposure to low and high LET radiation were investigated.

It was shown that activation of NF-κB depends on radiation quality and quantity. Experiments with chemical inhibitors revealed that NF-κB activation by ionizing radiation is strictly ATM dependent and degradation of the NF-κB inhibitor IκB by the proteasome is essential for both the classical and genotoxic stress-induced NF-κB pathway.

Absence of NF-κB dimers containing RelA resulted in a prolonged lag-phase but did not affect cell cycle progression significantly in untreated cells. After irradiation, a dose and radiation quality dependent arrest in the G2 phase of the cell cycle occurred and

also upon downregulation of RelA expression. RelA knockdown resulted in higher sensitivity of HEK cells to the killing effect of X-irradiation. In contrast, RelA knockdown did not further reduce the cellular survival after heavy ion exposure.

Further, NF-κB target genes were not inducible in the RelA knockdown cell line. NF-κB-dependent gene expression rely on radiation dose and LET. Chemokine expression (e.g. CXCL1, 2, 8 and 10) was induced in a proportional manner to radiation quality and quantity, emphasizing the role of NF-κB in the bystander effect. These NF-κB regulated genes are interesting targets for countermeasure development against the effects of space radiation.

6   Zusammenfassung

Die Weltraumstrahlung gilt derzeit als einer der wichtigsten limitierenden Faktoren für die bemannte Raumfahrt. Während solcher Missionen herrscht eine konstante Exposition mit geringen Dosen galaktischer kosmischer Strahlung, insbesondere hochenergetischen Schwerionen. Dies wird mit einem erhöhten Krebsrisiko assoziiert, welches durch Abschirmung nicht ausreichend reduziert werden kann. Deshalb muss die zelluläre Strahlenantwort untersucht werden, um die Risikoabschätzung zu verbessern und angemessene Gegenmassnahmen zu entwickeln.

Es wurde gezeigt, dass die Exposition von menschlichen Zellen mit beschleunigten Schwerionen in Fluenzen, die während Langzeitmissionen erreicht werden können, zur Aktivierung des Nuclear Factor κB (NF-κB) Signalweges führen. Schwerionen mit einem linearen Energietransfer (LET) von 90 bis 300 keV/µm hatten den stärksten Effekt auf die NF-κB Aktivierung. NF-κB als ein wichtiger regulierender Faktor in der zellulären Strahlenantwort könnte das zelluläre Überleben nach Schwerionenbestrahlung erhöhen und demnach das Krebsrisiko von Astronauten beeinflussen. Der NF-κB Signalweg könnte ein potentieller pharmakologischer Angriffspunkt für die Abschwächung der Strahlenantwort während Weltraummissionen sein, um den massiven Zelltod nach Bestrahlung mit hohen Dosen (akute Effekte) oder neoplastische Zelltransformation nach chronischer Bestrahlung mit niedrigen Dosen (Spätfolgen) zu verhindern.

Das Ziel dieser Arbeit war der Kenntnisgewinn über die Rolle von NF-κB in der zellulären Antwort auf weltraumrelevante Strahlung. Zuerst wurde die NF-κB Aktivierung in menschlichen embryonalen Nierenzellen (human embryonic kidney cells, HEK) nach Exposition mit verschiedenen Strahlenqualitäten und -quantitäten untersucht. Zentrale Elemente verschiedener NF-κB Signalwege wurden durch Chemikalien inhibiert, um deren Rolle in der NF-κB Aktivierung, induziert durch ionisierende Strahlung mit niedrigem und hohem LET, zu analysieren. Zuletzt wurde eine Zellinie mit einem short-hairpin RNA (shRNA) Plasmid für den Knockdown der NF-κB Untereinheit RelA stabil transfiziert, um die Rolle von RelA in der zellulären Antwort auf weltraumrelevante Strahlung abzuschätzen. Der Knockdown wurde auf verschiedenen Ebenen verifiziert und die Zellinie wurde hinsichtlich Proliferation, Zellzyklus-Progression und Genexpression untersucht. Zusätzlich wurden die Effekte des RelA Knockdowns auf Zellzyklus-Progression, zelluläres Überleben und Genexpression nach Exposition mit Strahlung mit niedrigem und hohem LET untersucht.

Es wurde gezeigt, dass die Aktivierung von NF-κB von Strahlenqualität und -quantität abhängig ist. Experimente mit chemischen Inhibitoren zeigten, dass NF-κB Aktivierung durch ionisierende Strahlung strikt ATM abhängig ist und der Abbau des NF-κB In-

hibitors IκB durch das Proteasom essentiell ist für beide, den klassischen und den durch genotoxischen Stress induzierten NF-κB Signalweg.

Abwesenheit von RelA-enthaltenden NF-κB-Dimeren resultierte in einer verlängerten lag-Phase, hatte aber keinen signifikanten Einfluss auf die Zellzyklus-Progression in unbehandelten Zellen. Nach Bestrahlung wurde auch in der RelA Knockdown Zellinie ein von Dosis und Strahlenqualität abhängiger Arrest in der G2 Phase des Zellzyklus beobachtet. Der RelA Knockdown resultierte in erhöhter Sensitivität von HEK Zellen für den abtötenden Effekt von Röntgenstrahlung. Im Gegensatz dazu reduziert der RelA Knockdown das zelluläre Überleben nach Schwerionenbestrahlung nicht stärker.

Des Weiteren waren Zielgene von NF-κB in der RelA Knockdown-Zellinie nicht induzierbar. Die NF-κB-abhängige Genexpression ist abhängig von Strahlendosis und LET. Die Expression von Chemokinen (z. B. CXCL1, 2, 8 und 10) wurde proportional zu Strahlenqualität und -quantität induziert, und unterstreicht somit die Rolle von NF-κB im Bystander-Effekt. Diese NF-κB regulierten Gene sind interessante Angriffspunkte für die Entwicklung von Massnahmen gegen die Effekte von Weltraumstrahlung.

7 Appendix

7.1 Gene expression profiles

Table 17: *List of all genes included in either the customized RT² Profiler™ PCR Array or the RT² Profiler™ PCR Array focussing on Human NF-κB Signaling Targets (SABiosciences).* The column 'ARRAY' indicates, in which of both arrays the respective gene occurs.

Gene symbol	Description	Gene bank	Array
ACTB	Actin, beta	NM_001101	Both
ADM	Adrenomedullin	NM_001124	NF-κB
AGT	Angiotensinogen (serpin peptidase inhibitor, clade A, member 8)	NM_000029	NF-κB
AKT1	V-akt murine thymoma viral oncogene homolog 1	NM_005163	NF-κB
ALDH3A2	Aldehyde dehydrogenase 3 family, member A2	NM_000382	NF-κB
ATM	Ataxia telangiectasia mutated	NM_000051	Customized
ATR	Ataxia telangiectasia and Rad3 related	NM_001184	Customized
B2M	Beta-2-microglobulin	NM_004048	Both
BCL2A1	BCL2-related protein A1	NM_004049	NF-κB
BCL2L1	BCL2-like 1	NM_138578	NF-κB
BCL3	B-cell CLL/lymphoma 3	NM_005178	Customized
BIRC2	Baculoviral IAP repeat containing 2	NM_001166	NF-κB
BIRC3	Baculoviral IAP repeat containing 3	NM_001165	NF-κB
BIRC5	Baculoviral IAP repeat-containing 5 (survivin)	NM_001168	Customized
BRCA2	Breast cancer 2, early onset	NM_000059	Customized
BRCA5	Breast cancer 1, early onset	NM_007294	Customized
C3	Complement component 3	NM_000064	NF-κB
CASP3	Caspase 3, apoptosis-related cysteine peptidase	NM_004346	Customized
CASP8	Caspase 8, apoptosis-related cysteine peptidase	NM_001228	Customized
CASP9	Caspase 9, apoptosis-related cysteine peptidase	NM_001229	Customized
CAT	Catalase	NM_001752	Customized
CCL11	Chemokine (C-C motif) ligand 11	NM_002986	NF-κB
CCL2	Chemokine (C-C motif) ligand 2	NM_002982	NF-κB
CCL22	Chemokine (C-C motif) ligand 22	NM_002990	NF-κB
CCL5	Chemokine (C-C motif) ligand 5	NM_002985	NF-κB
CCND1	Cyclin D1	NM_053056	NF-κB
CCNE1	Cyclin E1	NM_001238	Customized
CCNE2	Cyclin E2	NM_057749	Customized
CCR5	Chemokine (C-C motif) receptor 5	NM_000579	NF-κB
CD40	CD40 molecule, TNF receptor superfamily member 5	NM_001250	NF-κB
CD69	CD69 molecule	NM_001781	NF-κB
CD80	CD80 molecule	NM_005191	NF-κB
CD83	CD83 molecule	NM_004233	NF-κB
CDC2	Cell division cycle 2, G1 to S and G2 to M	NM_001786	Customized
CDC25A	Cell division cycle 25 homolog A (S. pombe)	NM_001789	Customized
CDKN1A	Cyclin-dependent kinase inhibitor 1A (p21, Cip1)	NM_000389	Both
CDKN2A	Cyclin-dependent kinase inhibitor 2A (melanoma, p16, inhibits CDk4)	NM_000077	Customized
CFB	Complement factor B	NM_001710	NF-κB
CHEK1	CHK1 checkpoint homolog (S. pombe)	NM_001274	Customized
CHEK2	CHK2 checkpoint homolog (S. pombe)	NM_007194	Customized
CSF1	Colony stimulating factor 1 (macrophage)	NM_000757	NF-κB
CSF2	Colony stimulating factor 2 (granulocyte-macrophage)	NM_000758	NF-κB

CSF2RB	Colony stimulating factor 2 receptor, beta, low-affinity (granulocyte-macrophage)	NM_000395	NF-κB
CSF3	Colony stimulating factor 3 (granulocyte)	NM_000759	NF-κB
CUL1	Cullin 1	NM_003592	Customized
CXCL1	Chemokine (C-X-C motif) ligand 1 (melanoma growth stimulating activity, alpha)	NM_001511	NF-κB
CXCL10	Chemokine (C-X-C motif) ligand 10	NM_001565	NF-κB
CXCL2	Chemokine (C-X-C motif) ligand 2	NM_002089	NF-κB
CXCL9	Chemokine (C-X-C motif) ligand 9	NM_002416	NF-κB
DDB1	Damage-specific DNA binding protein 1, 127kDa	NM_001923	Customized
DDIT3	DNA-damage-inducible transcript 3	NM_004083	Customized
DNAJA1	DnaJ (Hsp40) homolog, subfamily A, member 1	NM_001539	Customized
E2F1	E2F transcription factor 1	NM_005225	Customized
EGFR	Epidermal growth factor receptor	NM_005228	NF-κB
EGR1	Early growth response 1	NM_001964	Customized
EGR2	Early growth response 2	NM_000399	NF-κB
EIF2AK2	Eukaryotic translation initiation factor 2-alpha kinase 2	NM_002759	Customized
ERCC3	Excision repair cross-complementing rodent repair deficiency, complementation group 3 (xeroderma pigmentosum group B complementing)	NM_000122	Customized
EXO1	Exonuclease 1	NM_130398	Customized
F3	Coagulation factor III (thromboplastin, tissue factor)	NM_001993	NF-κB
F8	Coagulation factor VIII, procoagulant component	NM_000132	NF-κB
FANCG	Fanconi anemia, complementation group G	NM_004629	Customized
FAS	Fas (TNF receptor superfamily, member 6)	NM_000043	NF-κB
FASLG	Fas ligand (TNF superfamily, member 6)	NM_000639	NF-κB
GADD45A	Growth arrest and DNA-damage-inducible, alpha	NM_001924	Customized
GADD45B	Growth arrest and DNA-damage-inducible, beta	NM_015675	NF-κB
GADD45G	Growth arrest and DNA-damage-inducible, gamma	NM_006705	Customized
GAPDH	Glyceraldehyde-3-phosphate dehydrogenase	NM_002046	Both
GJA1	Gap junction protein, alpha 1, 43kDa	NM_000165	Customized
GPX1	Glutathione peroxidase 1	NM_000581	Customized
GTF2H2	General transcription factor IIH, polypeptide 2, 44kDa	NM_001515	Customized
HPRT1	Hypoxanthine phosphoribosyltransferase 1	NM_000194	Both
HRK	Harakiri, BCL2 interacting protein (contains only BH3 domain)	NM_003806	Customized
HSF1	Heat shock transcription factor 1	NM_005526	Customized
HSP90AA2	Heat shock protein 90kDa alpha (cytosolic), class A member 2	NM_001040141	Customized
HSPA1A	Heat shock 70kDa protein 1A	NM_005345	Customized
ICAM1	Intercellular adhesion molecule 1	NM_000201	NF-κB
IFNB1	Interferon, beta 1, fibroblast	NM_002176	NF-κB
IFNG	Interferon, gamma	NM_000619	NF-κB
IKBKB	Inhibitor of kappa light polypeptide gene enhancer in B-cells, kinase beta	NM_001556	Customized
IKBKE	Inhibitor of kappa light polypeptide gene enhancer in B-cells, kinase epsilon	NM_014002	Customized
IKBKG	Inhibitor of kappa light polypeptide gene enhancer in B-cells, kinase gamma	NM_003639	Customized
IL10	Interleukin 10	NM_000572	Customized
IL12B	Interleukin 12B (natural killer cell stimulatory factor 2, cytotoxic lymphocyte maturation factor 2, p40)	NM_002187	NF-κB
IL15	Interleukin 15	NM_000585	NF-κB
IL1A	Interleukin 1, alpha	NM_000575	Both
IL1B	Interleukin 1, beta	NM_000576	NF-κB
IL1R2	Interleukin 1 receptor, type II	NM_004633	NF-κB
IL1RN	Interleukin 1 receptor antagonist	NM_000577	NF-κB
IL2	Interleukin 2	NM_000586	NF-κB
IL2RA	Interleukin 2 receptor, alpha	NM_000417	NF-κB
IL4	Interleukin 4	NM_000589	NF-κB
IL6	Interleukin 6 (interferon, beta 2)	NM_000600	Both

IL8	Interleukin 8	NM_000584	Both
INS	Insulin	NM_000207	NF-κB
IRF1	Interferon regulatory factor 1	NM_002198	NF-κB
JUN	Jun oncogene	NM_002228	Customized
KRAS	V-ki-ras2 kirsten rat sarcoma viral oncogene homolog	NM_004985	Customized
LIG1	Ligase I, DNA, ATP-dependent	NM_000234	Customized
LTA	Lymphotoxin alpha (TNF superfamily, member 1)	NM_000595	NF-κB
LTB	Lymphotoxin beta (TNF superfamily, member 3)	NM_002341	NF-κB
MAP2K6	Mitogen-activated protein kinase kinase 6	NM_002758	NF-κB
MAPK1	Mitogen-activated protein kinase 1	NM_002745	Customized
MDM2	Mdm2, transformed 3T3 cell double minute 2,p53 binding protein (mouse)	NM_002392	Customized
MMP9	Matrix metallopeptidase 9 (gelatinase B, 92kDa gelatinase, 92kDa type IV collagenase)	NM_004994	NF-κB
MT2A	Metallothionein 2A	NM_005953	Customized
MT3	Metallothionein 3	NM_005954	Customized
MYC	V-myc myelocytomatosis viral oncogene homolog (avian)	NM_002467	NF-κB
MYD88	Myeloid differentiation primary response gene (88)	NM_002468	NF-κB
NBN	Nibrin	NM_002485	Customized
NCOA3	Nuclear receptor coactivator 3	NM_181659	NF-κB
NFKB1	Nuclear factor of kappa light polypeptide gene enhancer in B-cells 1 (p105)	NM_003998	Both
NFKB2	Nuclear factor of kappa light polypeptide gene enhancer in B-cells 2 (p49/p100)	NM_002502	Both
NFKBIA	Nuclear factor of kappa light polypeptide gene enhancer in B-cells inhibitor, alpha	NM_020529	Both
NOS2	Nitric oxide synthase 2A (inducible, hepatocytes)	NM_000625	Customized
NQO1	NAD(P)H dehydrogenase, quinone 1	NM_000903	NF-κB
NR4A2	Nuclear receptor subfamily 4, group A, member 2	NM_006186	NF-κB
OGG1	8-oxoguanine DNA glycosylase	NM_002542	Customized
P53AIP1	P53-regulated apoptosis-inducing protein 1	NM_022112	Customized
PCNA	Proliferating cell nuclear antigen	NM_182649	Customized
PDGFB	Platelet-derived growth factor beta polypeptide	NM_002608	NF-κB
PIK3Ca	Phosphoinositide-3-kinase, catalytic, alpha polypeptide	NM_006218	Customized
PLAU	Plasminogen activator, urokinase	NM_002658	NF-κB
PRKCA	Protein kinase C, alpha	NM_002737	Customized
PTGS2	Prostaglandin-endoperoxide synthase 2 (prostaglandin G/H synthase and cyclooxygenase)	NM_000963	NF-κB
RAD51	RAD51 homolog (RecA homolog, E. coli) (S. cerevisiae)	NM_002875	Customized
RAD9A	RAD9 homolog A (S. pombe)	NM_004584	Customized
RASA1	RAS p21 protein activator (GTPase activating protein) 1	NM_002890	Customized
RB1	Retinoblastoma 1 (including osteosarcoma)	NM_000321	Customized
REL	V-rel reticuloendotheliosis viral oncogene homolog (avian)	NM_002908	Both
RELA	V-rel reticuloendotheliosis viral oncogene homolog A, nuclear factor of kappa light polypeptide gene enhancer in B-cells 3, p65 (avian)	NM_021975	Both
RELB	V-rel reticuloendotheliosis viral oncogene homolog B	NM_006509	NF-κB
RPL13A	Ribosomal protein L13a	NM_012423	Customized
RPLP0	Ribosomal protein, large, P0	NM_001002	NF-κB
SELE	Selectin E	NM_000450	NF-κB
SELP	Selectin P (granule membrane protein 140kDa, antigen CD62)	NM_003005	NF-κB
SNAP25	Synaptosomal-associated protein, 25kDa	NM_003081	NF-κB
SOD1	Superoxide dismutase 1, soluble (amyotrophic lateral sclerosis 1 (adult))	NM_000454	Customized
SOD2	Superoxide dismutase 2, mitochondrial	NM_000636	Both
SOD3	Superoxide dismutase 3, extracellular	NM_003102	Customized
SOS1	Son of sevenless homolog 1 (Drosophila)	NM_005633	Customized
STAT1	Signal transducer and activator of transcription 1, 91kDa	NM_007315	NF-κB
STAT3	Signal transducer and activator of transcription 3 (acute-phase response factor)	NM_003150	NF-κB

STAT5B	Signal transducer and activator of transcription 5B	NM_012448	NF-κB
TLR1	Toll-like receptor 1	NM_003263	Customized
TNF	Tumor necrosis factor (TNF superfamily, member 2)	NM_000594	Both
TNFRSF1B	Tumor necrosis factor receptor superfamily, member 1B	NM_001066	NF-κB
TNFSF10	Tumor necrosis factor (ligand) superfamily, member 10	NM_003810	NF-κB
TP53	Tumor protein p53	NM_000546	Both
TP53BP2	Tumor protein p53 binding protein, 2	NM_005426	Customized
TP73	Tumor protein p73	NM_005427	Customized
TRADD	TNFRSF1A-associated via death domain	NM_003789	Customized
TRAF2	TNF receptor-associated factor 2	NM_021138	NF-κB
UNG	Uracil-DNA glycosylase	NM_003362	Customized
VCAM1	Vascular cell adhesion molecule 1	NM_001078	NF-κB
WT1	Wilms tumor 1	NM_000378	Customized
XIAP	X-linked inhibitor of apoptosis	NM_001167	NF-κB
XRCC1	X-ray repair complementing defective repair in Chinese hamster cells 1	NM_006297	Customized
XRCC2	X-ray repair complementing defective repair in Chinese hamster cells 2	NM_005431	Customized
XRCC3	X-ray repair complementing defective repair in Chinese hamster cells 3	NM_005432	Customized
XRCC5	X-ray repair complementing defective repair in Chinese hamster cells 5 (double-strand-break rejoining; ku autoantigen, 80kDa)	NM_021141	Customized
XRCC6BP1	XRCC6 binding protein 1	NM_033276	Customized

Table 18: *Analysis of gene expression in HEK shRNA RelA cells compared to the original cell line using the RT² Profiler™ PCR array (SABiosciences).* Listed are all genes from both, the customized and the NF-κB signaling array. Mean of fold up- or downregulation and SE are calculated from up to five independent experiments. Genes that are more that threefold up- or downregulated are highlighted.

Gene	μ	SE	Gene	μ	SE	Gene	μ	SE
ACTB	0.19	0.53	EGR1	2.17	0.67	MYD88	-1.32	1.40
ADM	0.19	1.37	EGR2	0.38	0.78	NBN	-2.76	0.89
AGT	0.17	0.90	EIF2AK2	-1.25	0.03	NCOA3	1.32	0.10
AKT1	-0.57	0.97	ERCC3	-0.23	1.26	NFKB1	0.14	0.58
ALDH3A2	-1.15	0.00	EXO1	-0.48	1.56	NFKB2	-0.08	0.70
ATM	-1.79	0.06	F3	1.12	0.07	NFKBIA	-1.92	0.22
ATR	1.41	0.19	F8	0.49	0.79	NOS2	1.29	0.24
B2M	-0.30	0.59	FANCG	-1.49	0.05	NQO1	-0.10	0.99
BCL2A1	-0.32	0.75	FAS	-1.48	0.14	NR4A2	2.33	0.30
BCL2L1	-0.30	0.81	FASLG	2.27	0.59	OGG1	-0.06	1.18
BCL3	-1.31	0.20	GADD45A	-1.31	0.21	P53AIP1	0.47	1.74
BIRC2	-0.41	0.72	GADD45B	2.67	0.53	PCNA	1.24	0.08
BIRC3	0.20	0.95	GADD45G	-0.48	1.92	PDGFB	0.32	0.72
BIRC5	0.05	1.22	GAPDH	0.34	0.59	PIK3Ca	1.12	0.02
BRCA2	0.06	1.15	GJA1	-1.35	0.27	PLAU	-1.86	0.12
BRCA5	-1.25	0.21	GPX1	1.50	0.25	PRKCA	-0.08	1.19
C3	-0.29	0.83	GTF2H2	-1.27	0.16	PTGS2	1.66	0.14
CASP3	1.27	0.22	HPRT1	0.39	0.60	RAD51	0.02	1.06
CASP8	-1.62	0.20	HRK	-1.34	0.22	RAD9A	1.04	0.04
CASP9	-1.07	0.03	HSF1	-0.04	1.37	RASA1	-1.25	0.01
CAT	-0.08	1.23	HSP90AA2	1.78	0.51	RB1	0.00	1.12
CCL11	-0.42	0.86	HSPA1A	1.94	0.84	REL	-1.30	0.07
CCL2	1.34	0.18	ICAM1	0.27	1.31	**RELA**	**-6.18**	**1.47**
CCL22	0.32	0.72	IFNB1	0.32	0.72	RELB	0.31	0.77
CCL5	2.82	1.49	IFNG	0.32	0.72	RPL13A	-1.17	0.10
CCND1	**-3.69**	**1.15**	IKBKB	-1.41	0.22	RPLP0	-0.56	0.82
CCNE1	0.02	1.09	IKBKE	-2.42	0.07	SELE	0.73	0.94
CCNE2	0.10	1.16	IKBKG	-0.05	1.42	SELP	0.32	0.72
CCR5	0.78	1.13	IL10	1.48	0.26	SNAP25	1.48	0.15
CD40	-1.15	0.06	IL12B	-1.20	0.14	SOD1	0.22	1.41
CD69	0.32	0.72	IL15	-1.00	1.09	SOD2	-0.71	0.44
CD80	-0.40	0.73	IL1A	0.17	0.62	SOD3	1.54	0.21
CD83	-1.92	0.72	IL1B	0.40	0.77	SOS1	-1.15	0.04
CDC2	0.05	1.14	IL1R2	-1.34	1.52	STAT1	1.24	0.02
CDC25A	1.22	0.17	IL1RN	0.32	0.72	STAT3	-0.45	0.78
CDKN1A	-0.20	0.53	IL2	0.32	0.72	STAT5B	-1.13	0.04
CDKN2A	0.12	1.17	IL2RA	0.32	0.72	TLR1	1.14	0.03
CFB	-0.59	0.80	IL4	1.81	0.36	**TNF**	**-3.37**	**1.54**
CHEK1	-0.05	1.09	IL6	0.32	0.61	TNFRSF1B	-1.12	1.39
CHEK2	-1.12	0.05	**IL8**	**-8.12**	**5.20**	TNFSF10	-0.69	0.92
CSF1	-1.30	0.19	INS	0.32	0.72	TP53	-1.22	0.07
CSF2	-0.44	1.23	IRF1	-0.50	0.81	TP53BP2	-0.20	1.38
CSF2RB	0.32	0.72	**JUN**	**4.25**	**2.48**	TP73	0.00	1.05
CSF3	1.23	0.09	KRAS	-1.08	0.02	TRADD	-1.47	0.00
CUL1	0.01	1.12	LIG1	-0.49	1.51	TRAF2	-1.13	0.06
CXCL1	-2.95	1.66	LTA	1.30	0.15	UNG	1.69	0.48
CXCL10	-1.90	1.96	LTB	-0.51	0.84	VCAM1	0.32	0.72
CXCL2	-0.57	0.93	MAP2K6	-1.41	0.17	WT1	0.24	1.37
CXCL9	0.63	0.89	MAPK1	-1.15	0.04	XIAP	-1.20	0.10
DDB1	0.10	1.29	MDM2	-1.29	0.00	XRCC1	0.00	1.15
DDIT3	1.33	0.17	MMP9	-0.87	1.05	XRCC2	-1.55	0.09
DNAJA1	-0.31	1.33	MT2A	0.00	1.19	XRCC3	-0.18	1.26
E2F1	0.04	1.26	MT3	0.32	1.42	XRCC5	0.09	1.25
EGFR	-0.45	0.74	MYC	0.33	0.95	XRCC6BP1	-1.26	0.26

Table 19: *Analysis of gene expression in HEK-pNF-κB-d2EGFP/Neo L2 cells 6 hours after treatment with TNF-α using the RT² Profiler™ PCR array (SABiosciences).* Fold up- or downregulation is shown for all genes from both, the customized and the NF-κB signaling array. SE is shown for those genes that occur in both arrays. Genes that are more that threefold up- or downregulated are highlighted.

Gene	µ	SE	Gene	µ	SE	Gene	µ	SE
ACTB	-0.05	1.07	EGR1	1.20		MYD88	-1.03	
ADM	-1.20		EGR2	1.52		NBN	-1.08	
AGT	1.13		EIF2AK2	-1.02		NCOA3	1.00	
AKT1	1.06		ERCC3	1.27		NFKB1	2.63	0.31
ALDH3A2	-1.15		EXO1	1.02		NFKB2	1.60	0.26
ATM	1.03		F3	1.93		**NFKBIA**	**6.31**	**0.52**
ATR	-1.36		F8	1.09		NOS2	1.17	
B2M	1.12	0.01	FANCG	1.14		NQO1	-1.01	
BCL2A1	1.72		FAS	-1.06		NR4A2	-1.09	
BCL2L1	1.16		FASLG	1.19		OGG1	-1.02	
BCL3	1.76		GADD45A	1.59		P53AIP1	1.77	
BIRC2	1.13		GADD45B	1.39		PCNA	1.17	
BIRC3	1.50		GADD45G	1.34		PDGFB	-1.05	
BIRC5	-1.15		GAPDH	0.03	1.05	PIK3Ca	1.08	
BRCA2	1.11		GJA1	1.13		PLAU	2.06	
BRCA5	1.10		GPX1	1.04		PRKCA	1.24	
C3	1.26		GTF2H2	1.46		PTGS2	1.65	
CASP3	1.10		HPRT1	-1.03	0.01	RAD51	-1.04	
CASP8	-1.08		HRK	1.04		RAD9A	1.13	
CASP9	-1.03		HSF1	-1.02		RASA1	1.02	
CAT	-1.05		HSP90AA2	1.40		RB1	1.12	
CCL11	1.39		HSPA1A	-1.14		REL	1.83	0.08
CCL2	2.75		ICAM1	1.23		RELA	0.02	1.12
CCL22	-1.05		IFNB1	-1.03		RELB	1.51	
CCL5	-1.17		IFNG	-1.02		RPL13A	-1.11	
CCND1	-1.14		IKBKB	1.00		RPLP0	-1.01	
CCNE1	1.01		IKBKE	1.34		SELE	1.48	
CCNE2	-1.07		IKBKG	1.48		SELP	-1.05	
CCR5	1.58		IL10	1.04		SNAP25	1.19	
CD40	1.40		IL12B	1.64		SOD1	-1.03	
CD69	2.99		IL15	1.29		SOD2	1.17	0.09
CD80	1.46		IL1A	1.19	0.12	SOD3	1.04	
CD83	2.09		IL1B	-1.05		SOS1	-1.01	
CDC2	-1.07		IL1R2	-1.04		STAT1	-1.01	
CDC25A	1.28		IL1RN	-1.05		STAT3	1.10	
CDKN1A	1.14	0.04	IL2	-1.05		STAT5B	1.07	
CDKN2A	-1.25		IL2RA	-1.05		TLR1	-1.43	
CFB	-1.01		IL4	1.28		**TNF**	**13.91**	**0.53**
CHEK1	-1.01		IL6	0.00	1.04	TNFRSF1B	1.50	
CHEK2	1.10		**IL8**	**5.35**	**0.31**	TNFSF10	1.48	
CSF1	1.82		INS	-1.05		TP53	1.20	0.05
CSF2	1.27		IRF1	2.04		TP53BP2	1.07	
CSF2RB	-1.05		JUN	2.37		TP73	1.29	
CSF3	-1.01		KRAS	1.07		TRADD	1.17	
CUL1	-1.16		LIG1	1.22		TRAF2	1.15	
CXCL1	**11.73**		LTA	1.44		UNG	-1.02	
CXCL10	**5.14**		LTB	1.88		VCAM1	-1.05	
CXCL2	**6.51**		MAP2K6	-1.08		WT1	1.22	
CXCL9	1.84		MAPK1	1.07		XIAP	-1.12	
DDB1	1.29		MDM2	1.17		XRCC1	1.22	
DDIT3	-1.01		MMP9	-1.31		XRCC2	-1.03	
DNAJA1	1.14		MT2A	-1.17		XRCC3	1.16	
E2F1	1.16		MT3	1.04		XRCC5	1.02	
EGFR	1.23		MYC	-1.12		XRCC6BP1	-1.05	

Table 20: *Analysis of gene expression in HEK shRNA RelA cells 6 hours after treatment with TNF-α using the RT² Profiler™ PCR array (SABiosciences).* Fold up- or downregulation is shown for all genes from both, the customized and the NF-κB signaling array. SE is shown for those genes that occur in both arrays. Genes that are more that threefold up- or downregulated are highlighted.

Gene	μ	SE	Gene	μ	SE	Gene	μ	SE
ACTB	-0.04	1.12	EGR1	1.18		MYD88	1.01	
ADM	-1.34		EGR2	1.01		NBN	1.43	
AGT	-1.32		EIF2AK2	1.04		NCOA3	-1.07	
AKT1	-1.11		ERCC3	1.36		NFKB1	1.22	0.08
ALDH3A2	-1.14		**EXO1**	**-4.92**		NFKB2	0.14	1.32
ATM	1.29		F3	1.28		NFKBIA	1.84	0.11
ATR	1.31		F8	1.24		NOS2	1.04	
B2M	1.17	0.10	FANCG	1.11		NQO1	-1.01	
BCL2A1	1.00		FAS	1.10		NR4A2	-1.17	
BCL2L1	1.03		FASLG	-1.79		OGG1	1.10	
BCL3	1.00		GADD45A	1.86		P53AIP1	-1.20	
BIRC2	1.09		GADD45B	-1.03		PCNA	1.00	
BIRC3	1.14		GADD45G	-1.19		PDGFB	-1.27	
BIRC5	-1.11		GAPDH	-1.32	0.18	PIK3Ca	1.10	
BRCA2	1.17		GJA1	-1.08		PLAU	1.22	
BRCA5	1.00		GPX1	-1.28		PRKCA	-1.12	
C3	-1.75		GTF2H2	1.43		PTGS2	1.22	
CASP3	1.41		HPRT1	0.10	1.14	RAD51	-1.10	
CASP8	1.02		HRK	-1.08		RAD9A	-1.22	
CASP9	-1.10		HSF1	-1.11		RASA1	1.17	
CAT	1.01		HSP90AA2	-1.05		RB1	1.01	
CCL11	-1.29		HSPA1A	-1.19		REL	1.24	0.05
CCL2	-1.06		ICAM1	-1.98		RELA	0.03	1.08
CCL22	-1.27		IFNB1	-1.27		RELB	-1.45	
CCL5	-1.16		IFNG	-1.27		RPL13A	1.10	
CCND1	-1.96		IKBKB	1.05		RPLP0	1.03	
CCNE1	-1.03		IKBKE	-1.71		SELE	-1.60	
CCNE2	1.25		IKBKG	-1.52		SELP	-1.27	
CCR5	**-4.59**		**IL10**	**-3.11**		SNAP25	1.13	
CD40	-1.06		IL12B	1.28		SOD1	-1.26	
CD69	-1.27		IL15	1.43		SOD2	0.04	1.13
CD80	1.17		IL1A	-1.16	0.16	**SOD3**	**-3.11**	
CD83	1.60		IL1B	-1.02		SOS1	-1.13	
CDC2	-1.06		IL1R2	1.18		STAT1	-1.01	
CDC25A	1.12		IL1RN	-1.27		STAT3	-1.15	
CDKN1A	1.19	0.08	IL2	-1.27		STAT5B	-1.08	
CDKN2A	-1.22		IL2RA	-1.27		TLR1	-2.20	
CFB	-1.05		IL4	-1.76		TNF	2.49	0.21
CHEK1	-1.06		IL6	-2.10	1.01	TNFRSF1B	1.10	
CHEK2	1.02		IL8	2.77	1.65	TNFSF10	-1.17	
CSF1	-1.13		INS	-1.27		TP53	1.21	0.07
CSF2	-1.60		IRF1	1.17		TP53BP2	1.12	
CSF2RB	-1.27		JUN	1.02		TP73	-1.84	
CSF3	-1.45		KRAS	1.13		TRADD	-1.32	
CUL1	-1.20		LIG1	-1.19		TRAF2	1.01	
CXCL1	-1.28		LTA	-1.14		UNG	-1.19	
CXCL10	-1.42		LTB	1.07		VCAM1	-1.27	
CXCL2	-1.01		MAP2K6	-1.16		WT1	-1.26	
CXCL9	-1.31		MAPK1	1.09		XIAP	-1.02	
DDB1	-1.12		MDM2	1.21		XRCC1	-1.13	
DDIT3	1.20		MMP9	1.10		XRCC2	1.26	
DNAJA1	1.10		MT2A	-1.35		XRCC3	-1.27	
E2F1	1.04		**MT3**	**-3.11**		XRCC5	1.04	
EGFR	-1.01		MYC	1.06		XRCC6BP1	1.13	

Table 21: *Analysis of gene expression in HEK-pNF-κB-d2EGFP/Neo L2 cells after treatment with X-rays (200 kV).* RNA was isolated 6 hours after cells have been irradiated with 0.5, 4 and 8 Gy. Fold up- or downregulation was investigated with the RT^2 Profiler™ PCR Array focussing on Human NF-κB Signaling Targets (SABiosciences). Listed are all genes from the array. Genes more than threefold up- or downregulated are highlighted.

Gene	0.5 Gy	4 Gy	8 Gy	Gene	0.5 Gy	4 Gy	8 Gy
ADM	1.23	1.16	1.08	IL6	1.03	1.12	-1.06
ACTB	1.02	-1.06	-1.09	**IL8**	1.21	**3.27**	**7.26**
AGT	1.03	1.12	1.07	INS	1.03	1.12	-1.06
AKT1	1.07	1.10	1.20	IRF1	1.23	1.66	2.58
ALDH3A2	1.04	1.06	-1.04	**LTA**	1.99	2.26	**3.23**
B2M	1.04	1.04	1.22	LTB	1.22	1.80	2.55
BCL2A1	1.03	1.12	-1.06	MAP2K6	-1.04	-1.30	-2.10
BCL2L1	1.32	1.31	1.57	MMP9	-1.21	-1.25	-1.31
BIRC2	1.04	1.08	1.40	MYC	1.10	-1.10	-1.24
BIRC3	1.10	1.58	**3.16**	MYD88	-1.04	-1.06	1.23
C3	2.79	1.90	1.78	NCOA3	1.17	1.06	-1.13
CCL11	1.27	2.14	2.58	NFKB1	1.11	1.83	2.87
CCL2	-1.14	1.70	2.79	**NFKB2**	1.22	2.80	**3.94**
CCL22	1.03	1.12	-1.06	**NFKBIA**	1.16	2.25	**4.23**
CCL5	1.03	1.12	-1.06	NQO1	-1.09	-1.02	-1.14
CCND1	1.34	1.17	1.30	NR4A2	1.13	1.05	1.23
CCR5	1.67	2.03	2.38	PDGFB	1.03	1.12	-1.06
CD40	1.10	1.40	1.44	PLAU	1.20	1.28	1.77
CD69	1.03	1.12	-1.06	PTGS2	-1.04	1.43	1.85
CD80	1.16	1.74	2.39	REL	1.07	1.27	1.62
CD83	-1.11	2.39	**3.81**	RELA	1.22	1.23	1.40
CDKN1A	-1.09	1.32	1.39	**RELB**	1.22	1.47	**3.05**
CFB	1.24	-1.01	1.04	RPLP0	-1.11	1.03	-1.07
CSF1	1.10	1.49	1.77	SELE	1.39	2.01	2.91
CSF2	1.58	1.51	1.69	SELP	1.03	1.12	-1.06
CSF2RB	1.03	1.12	-1.06	SNAP25	-1.30	-1.02	-1.21
CSF3	1.05	1.03	1.34	SOD2	1.09	1.03	-1.01
CXCL1	1.56	**4.22**	**8.94**	STAT1	1.14	-1.03	1.06
CXCL10	1.03	**5.53**	**21.86**	STAT3	1.07	1.03	1.05
CXCL2	1.02	2.55	**4.72**	STAT5B	1.00	-1.09	-1.05
CXCL9	1.03	1.47	2.91	**TNF**	1.03	2.69	**9.32**
EGFR	1.27	1.32	1.39	TNFRSF1B	1.07	1.56	2.22
EGR2	1.21	2.05	2.75	TNFSF10	1.26	1.70	1.72
F3	-1.24	1.16	1.33	TP53	1.17	1.35	1.49
F8	-1.04	-1.11	1.04	TRAF2	1.05	1.16	1.26
FAS	1.13	1.10	1.29	VCAM1	1.03	1.12	1.60
FASLG	1.39	1.81	2.85	XIAP	1.15	1.21	1.01
GADD45B	1.12	1.76	2.27				
GAPDH	1.02	1.03	-1.08				
HPRT1	1.02	-1.04	1.03				
ICAM1	1.60	1.67	1.43				
IFNB1	1.03	1.12	-1.06				
IFNG	1.03	1.12	-1.06				
IL12B	1.03	1.12	1.61				
IL15	1.47	1.26	1.78				
IL1A	-1.03	-1.20	1.27				
IL1B	1.03	1.12	-1.06				
IL1R2	1.08	1.30	1.12				
IL1RN	1.03	1.12	-1.06				
IL2	1.03	1.12	-1.06				
IL2RA	1.03	1.12	-1.06				
IL4	1.41	1.40	1.36				

Table 22: *Analysis of gene expression in HEK shRNA RelA cells after treatment with X-rays (200 kV).* RNA was isolated 6 hours after cells have been irradiated with 0.5, 4 and 8 Gy. Fold up- or downregulation was investigated with the RT^2 Profiler™ PCR Array focussing on Human NF-κB Signaling Targets (SABiosciences). Listed are all genes from the array. Genes more than threefold up- or downregulated are highlighted.

Gene	0.5 Gy	4 Gy	8 Gy	Gene	0.5 Gy	4 Gy	8 Gy
ADM	1.36	1.58	1.53	IL6	1.26	1.16	1.14
ACTB	1.03	-1.09	-1.22	IL8	1.21	1.39	1.02
AGT	-1.01	1.08	-1.09	INS	1.08	1.16	1.14
AKT1	-1.07	-1.00	-1.02	IRF1	-1.03	1.26	1.40
ALDH3A2	-1.04	-1.14	-1.11	LTA	1.20	2.90	1.56
B2M	-1.07	-1.04	1.10	**LTB**	1.16	**4.78**	2.33
BCL2A1	1.08	1.60	1.14	MAP2K6	-1.29	-1.22	-1.14
BCL2L1	-1.21	1.41	-1.06	MMP9	-1.19	-1.07	1.01
BIRC2	-1.13	1.19	1.13	MYC	1.06	1.02	1.02
BIRC3	-1.22	1.50	1.26	MYD88	1.12	1.14	-1.00
C3	-1.21	2.04	1.70	NCOA3	-1.02	1.00	-1.19
CCL11	**3.22**	**3.26**	2.11	NFKB1	1.25	1.29	1.39
CCL2	1.33	1.16	1.10	NFKB2	1.35	1.85	2.01
CCL22	1.08	1.16	1.14	NFKBIA	1.07	1.79	2.05
CCL5	1.70	2.28	-1.34	NQO1	1.04	1.06	1.31
CCND1	1.26	1.87	1.85	NR4A2	-1.15	-1.05	1.53
CCR5	1.53	1.51	-1.02	PDGFB	1.08	1.16	1.14
CD40	1.42	2.06	1.28	PLAU	1.47	1.52	-1.07
CD69	1.08	1.16	1.14	PTGS2	-1.37	-1.02	-1.14
CD80	1.35	**4.37**	1.34	REL	-1.18	1.04	1.04
CD83	1.03	1.53	2.08	RELA	-1.08	1.05	-1.04
CDKN1A	1.05	1.41	1.83	RELB	1.20	1.48	1.38
CFB	-1.10	-1.16	1.04	RPLP0	1.12	1.11	1.10
CSF1	1.08	1.22	1.24	SELE	1.81	1.76	-1.06
CSF2	1.22	1.20	-1.24	SELP	1.08	1.16	1.14
CSF2RB	1.08	1.16	1.14	SNAP25	1.12	1.31	1.37
CSF3	1.26	1.03	-1.30	SOD2	-1.10	-1.05	1.08
CXCL1	1.08	1.54	2.05	STAT1	1.02	-1.04	-1.14
CXCL10	1.08	2.29	2.10	STAT3	-1.01	-1.03	-1.04
CXCL2	1.34	2.15	1.80	STAT5B	-1.02	-1.10	-1.19
CXCL9	1.09	2.15	1.25	TNF	1.08	1.16	1.14
EGFR	-1.03	1.11	1.01	**TNFRSF1B**	1.10	**9.69**	**5.65**
EGR2	-1.02	**3.17**	1.59	**TNFSF10**	1.19	**5.37**	**3.13**
F3	1.04	1.21	1.55	TP53	-1.12	1.00	-1.02
F8	-1.31	-1.50	-1.44	TRAF2	1.02	-1.19	-1.11
FAS	-1.07	1.03	1.03	VCAM1	1.08	1.16	1.14
FASLG	1.47	1.62	-1.40	XIAP	1.08	1.04	-1.04
GADD45B	1.40	1.27	1.14				
GAPDH	1.07	-1.02	-1.12				
HPRT1	-1.15	1.03	1.13				
ICAM1	-1.29	-1.27	-1.14				
IFNB1	1.08	1.16	1.14				
IFNG	1.08	1.16	1.14				
IL12B	1.08	2.21	1.25				
IL15	1.11	1.50	1.59				
IL1A	-1.42	1.51	-1.03				
IL1B	1.08	1.16	1.14				
IL1R2	1.12	1.99	1.26				
IL1RN	1.08	1.16	1.14				
IL2	1.08	1.16	1.14				
IL2RA	1.08	1.16	1.14				
IL4	1.16	-1.10	-1.51				

Table 23: *Gene expression in HEK-pNF-κB-d2EGFP/Neo L2 cells 6 hours after irradiation with 0.5 Gy of ^{48}Ti ions (1000 MeV/n, LET 108 keV/μm) using the RT^2 Profiler™ PCR array (SABiosciences).* Fold up- or downregulation is shown for all genes from both, the customized and the NF-κB signaling array. Genes more than threefold up- or downregulated are highlighted. SE is shown for genes occuring in both arrays.

Gene	μ	SE	Gene	μ	SE	Gene	μ	SE
ACTB	1.09	0.01	EGR1	1.30		MYD88	-1.00	
ADM	-1.33		EGR2	-1.08		NBN	-1.11	
AGT	-1.05		EIF2AK2	-1.17		NCOA3	-1.16	
AKT1	-1.01		ERCC3	-1.10		NFKB1	1.15	0.05
ALDH3A2	-1.05		EXO1	1.30		NFKB2	-1.02	0.01
ATM	1.07		F3	1.21		NFKBIA	0.08	1.15
ATR	-1.28		F8	-1.24		NOS2	-1.12	
B2M	0.00	1.05	FANCG	1.19		NQO1	-1.28	
BCL2A1	-1.11		FAS	-1.20		NR4A2	1.04	
BCL2L1	-1.17		FASLG	-1.39		OGG1	1.12	
BCL3	-1.19		GADD45A	-1.29		P53AIP1	-2.80	
BIRC2	-1.09		GADD45B	-1.47		PCNA	1.29	
BIRC3	1.09		GADD45G	-1.12		PDGFB	-1.05	
BIRC5	-1.20		GAPDH	-0.03	1.05	PIK3Ca	1.02	
BRCA2	-1.46		GJA1	-1.03		PLAU	-1.27	
BRCA5	1.09		GPX1	1.16		PRKCA	1.02	
C3	1.40		GTF2H2	-1.17		PTGS2	1.47	
CASP3	-1.16		HPRT1	-0.02	1.05	RAD51	1.02	
CASP8	-1.43		HRK	-1.06		RAD9A	1.08	
CASP9	1.20		HSF1	1.18		RASA1	-1.01	
CAT	1.14		HSP90AA2	1.08		RB1	-1.14	
CCL11	-1.42		HSPA1A	1.24		REL	0.11	1.22
CCL2	1.01		ICAM1	-1.05		RELA	1.13	0.13
CCL22	-1.05		IFNB1	-1.05		RELB	-1.18	
CCL5	-1.08		IFNG	-1.05		RPL13A	-1.08	
CCND1	-1.28		IKBKB	1.00		RPLP0	-1.00	
CCNE1	1.22		IKBKE	1.03		SELE	-1.19	
CCNE2	1.39		IKBKG	1.02		SELP	-1.05	
CCR5	-1.06		IL10	1.39		SNAP25	1.05	
CD40	1.18		IL12B	1.05		SOD1	-1.20	
CD69	-1.05		IL15	-1.46		SOD2	0.07	1.12
CD80	-1.05		IL1A	-1.22	0.03	SOD3	1.68	
CD83	1.22		IL1B	-1.05		SOS1	1.04	
CDC2	1.08		IL1R2	-1.35		STAT1	-1.05	
CDC25A	1.33		IL1RN	-1.05		STAT3	-1.05	
CDKN1A	1.14	0.12	IL2	-1.05		STAT5B	1.05	
CDKN2A	1.04		IL2RA	-1.05		TLR1	-1.21	
CFB	-1.36		IL4	1.08		TNF	1.53	0.15
CHEK1	-1.02		IL6	0.32	1.37	TNFRSF1B	-1.05	
CHEK2	-1.16		IL8	1.24	0.10	TNFSF10	-1.07	
CSF1	-1.04		INS	-1.05		TP53	1.06	0.04
CSF2	-2.09		IRF1	1.10		TP53BP2	-1.13	
CSF2RB	-1.05		JUN	1.28		TP73	1.15	
CSF3	1.23		KRAS	-1.16		TRADD	-1.35	
CUL1	1.09		LIG1	1.01		TRAF2	-1.12	
CXCL1	1.23		LTA	1.04		UNG	-1.01	
CXCL10	1.15		LTB	-1.11		VCAM1	-1.05	
CXCL2	1.65		MAP2K6	-1.31		WT1	1.33	
CXCL9	1.00		MAPK1	1.17		XIAP	-1.11	
DDB1	1.15		MDM2	1.10		XRCC1	1.17	
DDIT3	1.05		MMP9	1.01		XRCC2	1.04	
DNAJA1	-1.03		MT2A	1.05		XRCC3	1.23	
E2F1	1.17		MT3	1.68		XRCC5	1.07	
EGFR	-1.02		MYC	-1.15		XRCC6BP1	1.04	

Table 24: *Gene expression in HEK-pNF-κB-d2EGFP/Neo L2 cells 6 hours after irradiation with 4 Gy of ^{48}Ti ions (1000 MeV/n, LET 108 keV/μm) using the RT^2 Profiler™ PCR array (SABiosciences).* Fold up- or downregulation is shown for all genes from both, the customized and the NF-κB signaling array. Genes more than threefold up- or downregulated are highlighted. SE is shown for genes occuring in both arrays.

Gene	μ	SE	Gene	μ	SE	Gene	μ	SE
ACTB	0.00	1.01	EGR1	1.84		MYD88	-1.20	
ADM	1.23		EGR2	-2.11		NBN	-1.06	
AGT	1.21		EIF2AK2	-1.04		NCOA3	1.07	
AKT1	1.11		ERCC3	1.37		NFKB1	2.72	0.14
ALDH3A2	-1.16		EXO1	1.88		NFKB2	2.16	0.90
ATM	1.19		F3	2.04		**NFKBIA**	**3.57**	**0.12**
ATR	1.12		F8	-1.07		NOS2	-1.32	
B2M	1.10	0.07	FANCG	1.38		NQO1	-1.35	
BCL2A1	1.14		FAS	1.09		NR4A2	1.05	
BCL2L1	-1.58		FASLG	-1.50		OGG1	1.34	
BCL3	1.27		GADD45A	1.64		P53AIP1	-1.41	
BIRC2	-1.11		GADD45B	1.57		PCNA	1.67	
BIRC3	1.35		GADD45G	1.62		PDGFB	1.21	
BIRC5	-1.71		GAPDH	-1.12	0.06	PIK3Ca	1.04	
BRCA2	1.44		GJA1	-1.45		PLAU	1.39	
BRCA5	1.04		GPX1	1.15		PRKCA	1.03	
C3	-1.10		GTF2H2	1.01		PTGS2	2.24	
CASP3	1.30		HPRT1	1.08	0.01	RAD51	1.20	
CASP8	-1.10		HRK	1.08		RAD9A	1.25	
CASP9	1.06		HSF1	1.13		RASA1	1.04	
CAT	1.09		HSP90AA2	1.20		RB1	1.03	
CCL11	-2.55		HSPA1A	1.19		REL	1.81	0.32
CCL2	2.52		ICAM1	-1.10		RELA	1.42	0.16
CCL22	1.21		IFNB1	1.21		RELB	1.09	
CCL5	1.17		IFNG	1.21		RPL13A	-1.19	
CCND1	1.43		IKBKB	1.07		RPLP0	1.09	
CCNE1	1.85		IKBKE	1.06		SELE	-1.46	
CCNE2	2.29		IKBKG	1.08		SELP	1.21	
CCR5	-2.22		IL10	1.37		SNAP25	-1.30	
CD40	-1.57		IL12B	-1.05		SOD1	-1.25	
CD69	1.21		IL15	-1.03		SOD2	1.16	0.11
CD80	-1.60		IL1A	-1.42	0.24	SOD3	2.19	
CD83	**4.26**		IL1B	1.21		SOS1	1.01	
CDC2	-1.05		IL1R2	-2.08		STAT1	1.13	
CDC25A	1.92		IL1RN	1.21		STAT3	-1.07	
CDKN1A	1.71	0.00	IL2	1.21		STAT5B	1.02	
CDKN2A	-1.10		IL2RA	1.21		TLR1	-1.49	
CFB	-1.20		IL4	1.04		**TNF**	**8.40**	**0.19**
CHEK1	1.17		IL6	1.35	0.14	TNFRSF1B	-2.28	
CHEK2	-1.01		**IL8**	**5.71**	**0.64**	TNFSF10	-1.88	
CSF1	1.88		INS	1.21		TP53	1.48	0.07
CSF2	-1.49		IRF1	2.95		TP53BP2	-1.02	
CSF2RB	1.21		**JUN**	**7.93**		TP73	1.62	
CSF3	1.22		KRAS	1.03		TRADD	-1.09	
CUL1	-1.06		LIG1	1.18		TRAF2	1.33	
CXCL1	**9.27**		LTA	-2.10		UNG	1.26	
CXCL10	**9.79**		LTB	-2.80		VCAM1	1.53	
CXCL2	**4.41**		MAP2K6	-1.83		WT1	1.66	
CXCL9	-2.20		MAPK1	1.26		XIAP	1.09	
DDB1	1.21		MDM2	1.20		XRCC1	1.03	
DDIT3	1.96		MMP9	-1.27		XRCC2	1.28	
DNAJA1	1.06		MT2A	-1.02		XRCC3	1.38	
E2F1	2.01		MT3	1.49		XRCC5	1.09	
EGFR	1.17		MYC	1.21		XRCC6BP1	-1.02	

Table 25: *Gene expression in HEK shRNA RelA cells 6 hours after irradiation with 0.5 Gy of ⁴⁸Ti ions (1000 MeV/n, LET 108 keV/µm) using the RT² Profiler™ PCR array (SABiosciences).* Fold up- or downregulation is shown for all genes from both, the customized and the NF-κB signaling array. Genes more than threefold up- or downregulated are highlighted. SE is shown for genes occuring in both arrays.

Gene	µ	SE	Gene	µ	SE	Gene	µ	SE
ACTB	-1.07	0.01	EGR1	1.08		MYD88	1.34	
ADM	1.37		EGR2	1.29		NBN	1.15	
AGT	-1.07		EIF2AK2	1.01		NCOA3	1.24	
AKT1	1.23		ERCC3	1.03		NFKB1	1.05	0.02
ALDH3A2	1.10		EXO1	1.08		NFKB2	1.09	0.03
ATM	1.52		F3	1.30		NFKBIA	1.13	0.04
ATR	1.32		F8	1.17		NOS2	-1.16	
B2M	1.07	0.05	FANCG	1.33		NQO1	1.17	
BCL2A1	1.37		FAS	1.37		NR4A2	1.18	
BCL2L1	1.30		FASLG	1.17		OGG1	1.20	
BCL3	1.24		GADD45A	1.48		P53AIP1	1.12	
BIRC2	1.17		GADD45B	1.37		PCNA	1.03	
BIRC3	1.17		GADD45G	1.51		PDGFB	-1.14	
BIRC5	-1.06		GAPDH	1.03	0.03	PIK3Ca	-1.01	
BRCA2	1.71		GJA1	-1.18		PLAU	1.22	
BRCA5	1.15		GPX1	-1.10		PRKCA	-1.14	
C3	-1.13		GTF2H2	1.21		PTGS2	1.34	
CASP3	1.04		HPRT1	1.16	0.08	RAD51	1.14	
CASP8	1.36		HRK	1.15		RAD9A	-1.02	
CASP9	1.05		HSF1	-1.06		RASA1	1.11	
CAT	1.04		HSP90AA2	1.05		RB1	1.16	
CCL11	1.26		HSPA1A	1.15		REL	0.05	1.05
CCL2	1.14		ICAM1	1.05		RELA	1.09	0.03
CCL22	-1.14		IFNB1	-1.14		RELB	1.08	
CCL5	-1.01		IFNG	-1.14		RPL13A	-1.35	
CCND1	1.09		IKBKB	1.25		RPLP0	-1.05	
CCNE1	1.02		IKBKE	1.48		SELE	1.07	
CCNE2	1.24		IKBKG	1.25		SELP	-1.14	
CCR5	1.44		IL10	-1.23		SNAP25	1.33	
CD40	1.05		IL12B	1.25		SOD1	-1.09	
CD69	-1.14		IL15	-1.12		SOD2	0.00	1.04
CD80	1.41		IL1A	1.81	0.25	SOD3	-1.02	
CD83	1.22		IL1B	1.15		SOS1	1.11	
CDC2	1.05		IL1R2	-1.11		STAT1	-1.09	
CDC25A	1.03		IL1RN	-1.14		STAT3	1.14	
CDKN1A	1.14	0.07	IL2	-1.14		STAT5B	1.14	
CDKN2A	-1.14		IL2RA	-1.14		TLR1	-1.15	
CFB	1.72		IL4	1.04		TNF	0.26	1.40
CHEK1	1.00		IL6	0.33	1.41	TNFRSF1B	1.07	
CHEK2	1.05		IL8	-0.10	1.16	TNFSF10	1.06	
CSF1	-1.03		INS	-1.14		TP53	-1.05	0.04
CSF2	-2.61		IRF1	1.10		TP53BP2	-1.01	
CSF2RB	-1.14		JUN	1.11		TP73	-1.14	
CSF3	1.41		KRAS	1.05		TRADD	1.13	
CUL1	-1.15		LIG1	1.36		TRAF2	1.10	
CXCL1	-1.27		LTA	1.14		UNG	-1.00	
CXCL10	-1.14		LTB	1.31		VCAM1	-1.14	
CXCL2	1.14		MAP2K6	1.09		WT1	-1.16	
CXCL9	1.14		MAPK1	-1.06		XIAP	1.04	
DDB1	-1.05		MDM2	1.01		XRCC1	-1.13	
DDIT3	1.11		MMP9	1.37		XRCC2	1.55	
DNAJA1	1.03		MT2A	-1.07		XRCC3	1.37	
E2F1	1.24		MT3	-1.29		XRCC5	1.06	
EGFR	1.12		MYC	-1.05		XRCC6BP1	1.05	

Table 26: *Gene expression in HEK shRNA RelA cells 6 hours after irradiation with 4 Gy of ^{48}Ti ions (1000 MeV/n, LET 108 keV/µm) using the RT^2 Profiler™ PCR array (SABiosciences).* Fold up- or downregulation is shown for all genes from both, the customized and the NF-κB signaling array. Genes more than threefold up- or downregulated are highlighted. SE is shown for genes occuring in both arrays.

Gene	µ	SE	Gene	µ	SE	Gene	µ	SE
ACTB	-1.09	0.07	EGR1	1.07		MYD88	1.64	
ADM	1.39		EGR2	-1.86		NBN	-1.04	
AGT	1.41		EIF2AK2	1.15		NCOA3	-1.11	
AKT1	1.18		ERCC3	1.18		NFKB1	1.21	0.16
ALDH3A2	-1.13		EXO1	1.49		NFKB2	1.15	0.05
ATM	1.24		F3	1.30		NFKBIA	1.63	0.09
ATR	1.40		F8	-1.03		NOS2	1.19	
B2M	1.11	0.10	FANCG	1.64		NQO1	-1.11	
BCL2A1	-1.01		FAS	1.38		NR4A2	1.01	
BCL2L1	-1.77		FASLG	1.48		OGG1	1.47	
BCL3	1.46		GADD45A	1.92		P53AIP1	1.23	
BIRC2	-1.26		GADD45B	1.66		PCNA	1.57	
BIRC3	-1.28		GADD45G	1.56		PDGFB	-1.01	
BIRC5	-1.37		GAPDH	-1.11	0.08	PIK3Ca	1.07	
BRCA2	1.20		GJA1	-1.09		PLAU	-1.11	
BRCA5	1.32		GPX1	-1.01		PRKCA	-1.03	
C3	-1.54		GTF2H2	1.25		PTGS2	1.27	
CASP3	1.28		HPRT1	1.11	0.02	RAD51	1.48	
CASP8	-1.21		HRK	1.29		RAD9A	1.41	
CASP9	1.12		HSF1	-1.03		RASA1	1.07	
CAT	1.15		HSP90AA2	1.28		RB1	1.02	
CCL11	1.45		HSPA1A	1.25		REL	-0.07	1.14
CCL2	1.91		ICAM1	1.25		RELA	1.23	0.17
CCL22	-1.01		IFNB1	-1.01		RELB	-1.12	
CCL5	2.29		IFNG	-1.01		RPL13A	1.01	
CCND1	1.08		IKBKB	1.19		RPLP0	-1.05	
CCNE1	1.79		IKBKE	1.33		SELE	1.14	
CCNE2	2.18		IKBKG	1.68		SELP	-1.01	
CCR5	1.87		IL10	1.23		SNAP25	1.04	
CD40	-1.42		IL12B	1.30		SOD1	1.12	
CD69	-1.01		IL15	-1.31		SOD2	1.11	0.03
CD80	-2.21		IL1A	0.20	1.27	SOD3	-1.10	
CD83	1.60		IL1B	-1.01		SOS1	1.17	
CDC2	-1.12		IL1R2	-2.01		STAT1	-1.11	
CDC25A	1.50		IL1RN	-1.01		STAT3	-1.05	
CDKN1A	1.53	0.01	IL2	-1.01		STAT5B	-1.08	
CDKN2A	-1.19		IL2RA	-1.01		TLR1	-1.25	
CFB	1.09		IL4	1.33		TNF	0.84	1.86
CHEK1	1.06		IL6	1.41	0.13	**TNFRSF1B**	**-7.09**	
CHEK2	-1.06		IL8	1.72	0.20	**TNFSF10**	**-3.26**	
CSF1	1.02		INS	-1.01		TP53	0.17	1.17
CSF2	1.96		IRF1	1.69		TP53BP2	1.10	
CSF2RB	-1.01		**JUN**	**3.30**		TP73	1.08	
CSF3	2.02		KRAS	1.18		TRADD	1.06	
CUL1	-1.06		LIG1	1.57		TRAF2	1.28	
CXCL1	1.41		LTA	-1.56		UNG	1.01	
CXCL10	-1.01		LTB	-2.17		VCAM1	-1.01	
CXCL2	1.04		MAP2K6	-1.26		WT1	1.21	
CXCL9	-1.67		MAPK1	1.26		XIAP	-1.24	
DDB1	1.24		MDM2	1.27		XRCC1	1.13	
DDIT3	1.70		MMP9	1.34		XRCC2	1.54	
DNAJA1	1.28		MT2A	1.01		XRCC3	1.77	
E2F1	1.88		MT3	1.33		XRCC5	1.23	
EGFR	1.09		MYC	1.13		XRCC6BP1	1.23	

7.2 Abbreviations

aa	amino acid
ATM	*Ataxia telangiectasia-mutated*
bp	base pairs
BSA	bovine serum albumin
C_t	threshold cycle
CAPE	caffeic acid phenethyl ester
CDK	cyclin-dependent kinase
C.I.	confidence interval
CKI	cyclin-dependent kinase inhibitor
CPT	camptothecin
cDNA	complementary DNA
CFA	colony forming ability
COX2	cyclooxygenase 2
D	energy dose
d2EGFP	destabilized enhanced green fluorescent protein
DAPI	4',6-diamidino-2-phenylindole
ddH_2O	double-distilled water
DDR	DNA damage response
dH_2O	distilled water
DLR	*Deutsches Zentrum für Luft- und Raumfahrt*
DMSO	dimethyl sulfoxide
DNA	deoxyribonucleic acid
DSB	double strand break
DSMZ	*Deutsche Sammlung von Mikroorganismen und Zellkulturen GmbH*
dsRNA	double-stranded RNA
E. coli	*Escherichia coli*
EDTA	ethylenediaminetetraacetic acid
EGFP	enhanced green fluorescent protein
ELAM-1	endothelial-leukocyte adhesion molecule-1
ELISA	enzyme-linked immunosorbent assay
ELKS	glutamine/leucine/lysine/serine
EVA	extravehicular activity
FACScan	fluorescence-activated cell scanner
FA	formaldehyde
FBS	fetal bovine serum
FSC	forward scatter
F	fluence
Fig.	figure
g	gram
G1	G1 cell cycle phase
G2/M	G2/M cell cycle phase
GADD45	growth arrest and DNA damage-inducible gene 45
GANIL	*Grand Accélérateur National d'Ions Lourds*
GCR	galactic cosmic rays
GJIC	gap junction intercellular communication

GOI	gene of interest
GSI	*Gesellschaft für Schwerionenforschung*
Gy	gray
µg	microgravity
µg	microgram
H	equivalent dose
HEK cells	human embryonic kidney cells
HKG	housekeeping gene
HR	homologous recombination
h	hours
HZE	high atomic number and high-energy
IF	immunofluorescence
IKK	IκB kinase
IκB	inhibitor of Nuclear factor-κB
iNOS	inducible nitric oxide synthase
ISS	*International Space Station*
J	joule
kb	kilobases
KD	knockdown
keV	kiloelectronvolt
kg	kilogram
l	liter
µl	microliter
LB	Luria Bertani
LEO	low Earth orbit
LET	linear energy transfer
m	slope of the growth curve
MeV	megaelectronvolt
mg	milligram
min	minute(s)
ml	milliliter
mRNA	messenger RNA
MTT	3-(4,5-dimethylthiazole-2-yl)-2,5-diphenyltetrazolium bromide
µm	mircometre
n	nucleon
NC	negative control
NCL	nuclear-localization sequences
NEMO	NF-κB essential modulator
NF-κB	Nuclear factor κB
ng	nanogram
NHEJ	non-homologous end-joining
NIK	NF-κB inducing kinase
NRE	NF-κB-responsive element
nm	nanometer
o/n	over night
OD	optical density
P	particles
PBS	phosphate buffered saline

PCR	polymerase chain reaction
PE	plating efficiency
PI	propidium iodide
PIDD	p53-inducible death domain-containing protein
PPP	pentose phosphate pathway
Q	radiation quality factor
QC	quality control
RBE	relative biological effectiveness
REST©	*Relative Expression Software Tool*
RHD	Rel homology domain
RIN	RNA Integrity Number
RIP	receptor-interacting protein
RISC	RNAi induced silencing complex
RNA	ribonucleic acid
RNAi	RNA interference
RNase	ribonuclease
ROS	reactive oxygen species
rpm	rotations per minute
rRNA	ribosomal RNA
RT	reverse transcription
S	S cell cycle phase
SCR	solar cosmic radiation
SD	standard deviation
SDS	sodium dodecyl sulfate
SE	standard error
shRNA	short hairpin RNA
siRNA	small interfering RNA
SSA	single-strand annealing
SSB	single strand break
SSC	side scatter
s	second(s)
SF	surviving fraction
SIS	heavy ion synchotron *(Schwerionen-Synchotron)*
S-medium	selection medium
Sv	sievert
TAE	tris base/acetic acid/EDTA
TLR	Toll-like receptor
TNF-α	tumor necrosis factor α
TNF-R	tumor necrosis factor receptor
uPA	urokinase plasminogen activator
VEGF	vascular endothelial growth factor
WinMDI	Windows multiple document interface
λ_{max}	emission maximum

All gene abbreviations occuring in gene expression analysis are listed and described in Table 17.

7.3   List of figures

7.4 List of tables

7.5 Screen for *Mycoplasma* contamination

Leibniz-Institut DSMZ-Deutsche Sammlung von Mikroorganismen und Zellkulturen GmbH

DSMZ

Leibniz-Institut DSMZ GmbH · Inhoffenstraße 7 B · 38124 Braunschweig · GERMANY

DLR – Deutsches Zentrum für
Luft- und Raumfahrt e.V.
Institut für Luft- und Raumfahrtmedizin
Dr. Patrick Lau

51170 Köln

Inhoffenstraße 7 B
38124 Braunschweig
GERMANY

Tel.:   +49(0)531 26 16-0
Fax: +49(0)531 26 16-418
E-mail: contact@dsmz.de
Internet: www.dsmz.de

Ihr Zeichen/Your ref.	Unser Zeichen/Our ref. CUP - 330	+49 (0)531-2616- 156	Datum/Date 02.03.2012

Untersuchung von Zellkulturüberständen auf Mycoplasma-Kontaminationen

Sehr geehrter Herr Dr. Lau,

vielen Dank für Ihren Auftrag vom 27.02.2012 zur Untersuchung von fünf Zellkulturüberständen auf Kontaminationen mit Mycoplasmen mittels Polymerase-Kettenreaktion (PCR).

Am 28.02.2012 erhielten wir von Ihnen jeweils zwei Kryoröhrchen mit Zellkulturüberstand der Zellkulturen SaOs-2 P39, OCT-1 P17, ATSCs (LW 29) P7, HEK-NF-κB-DDtd Tomato C-8 P3 und HEK-shRNA 4 #9 P9. Wir isolierten die DNA aus jeweils 0,2 ml der Proben und reinigten sie mittels Säulenaufarbeitung auf (RTP DNA/RNA Virus Mini Kit, Invitek). Aliquote der Eluate wurden in PCR-Reaktionen mit einem Primermix zur Amplifikation einer konservierten Region der 16S rDNA von in Zellkulturen vorkommenden Mycoplasmaspezies eingesetzt. Bei Kontaminationen zeigen sich - je nach Mycoplasmaspezies - 504-519 bp große DNA-Fragmente im ethidiumbromidgefärbten Agarosegel. Als interne Kontrolle wurde in Parallelreaktionen ein Plasmid in einer Grenzverdünnung zum Reaktionsansatz dazugegeben, um einen fehlerfreien Verlauf der PCR nachzuweisen. Bei den Ansätzen mit der internen Kontrolle werden mit derselben Primermischung 975 bp große DNA-Fragmente mit amplifiziert (siehe Abbildung).

Die PCR-Analyse ergab keine Amplifizierung mycoplasmaspezifischer Sequenzen in den oben genannten Kulturüberständen. Die überprüften Kulturen sind somit als mycoplasmenfrei einzustufen.

Für weitere Fragen stehe ich Ihnen gern zur Verfügung und verbleibe

mit freundlichen Grüßen
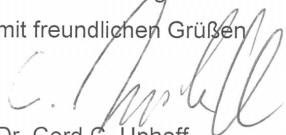
Dr. Cord C. Uphoff
Bereich Menschliche und
Tierische Zellkulturen

I:\Cord\AUFTR\DLR_Lau.doc
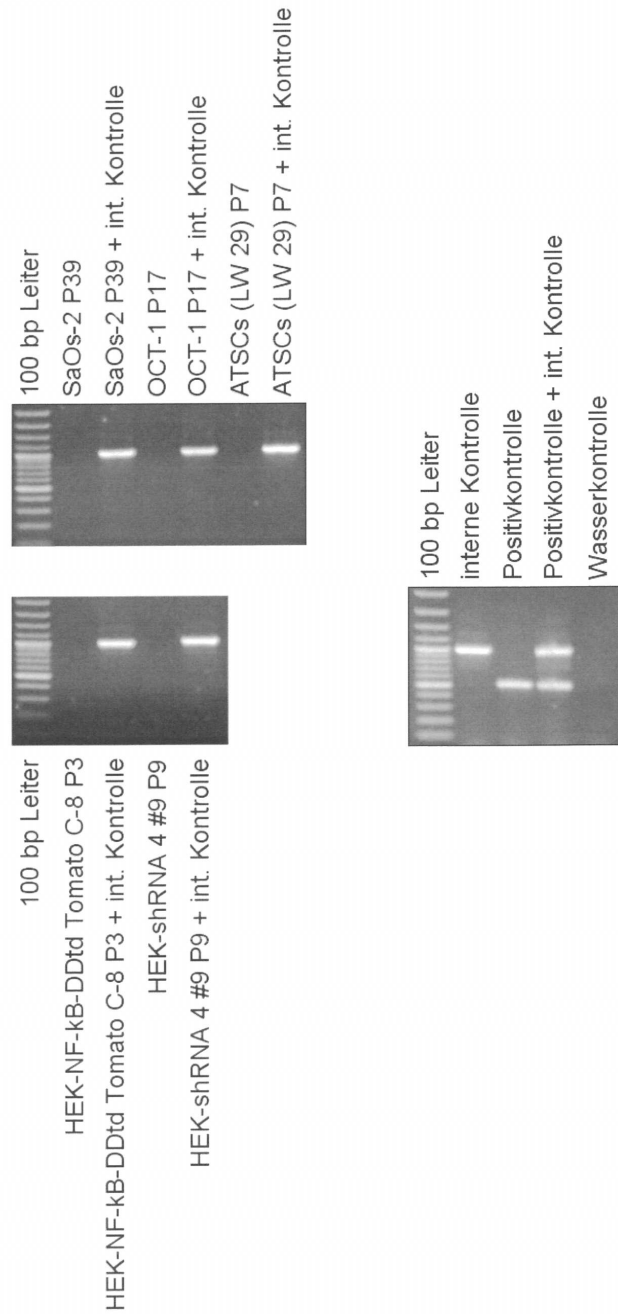
Fig. 41: *Certificate of* Mycoplasma *test.* Cell culture samples were sent to the *Leibnitz-Institut DSMZ-Deutsche Sammlung von Mikroorganismen und Zellkulturen GmbH* to ensure that cells are free from *Mycoplasma* contamination. Here, the knockdown cell line HEK shRNA RelA is named HEK-shRNA 4 #9 P9.

8 References

Ahn, K.S., Sethi, G., and Aggarwal, B.B. (2007). Nuclear factor-kappa B: from clone to clinic. Curr. Mol. Med. 7, 619-637.

Ainsworth, E.J., Kelly, L.S., Mahlmann, L.J., Schooley, J.C., Thomas, R.H., Howard, J., and Alpen, E.L. (1983). Response of colony-forming units-spleen to heavy charged particles. Radiat. Res. 96, 180-197.

Aoudjit, F., Brochu, N., Bélanger, B., Stratowa, C., Hiscott, J., and Audette, M. (1997). Regulation of intercellular adhesion molecule-1 gene by tumor necrosis factor-alpha is mediated by the nuclear factor-kappaB heterodimers p65/p65 and p65/c-Rel in the absence of p50. Cell Growth Differ. 8, 335-342.

Arnhold, S., Post, C., Glüer, S., Hoopmann, M., Wenisch, S., Volpers, C., and Addicks, K. (2008). Neuronal characteristics of amniotic fluid derived cells after adenoviral transformation. Cell Biol. Int. 32, 1559-1566.

Azzam, E.I., Toledo, S.M. de, and Little, J.B. (2001). Direct evidence for the participation of gap junction-mediated intercellular communication in the transmission of damage signals from alpha -particle irradiated to nonirradiated cells. Proc. Natl. Acad. Sci. U.S.A. 98, 473-478.

Badhwar, G.D. (1997). Deep space radiation sources, models, and environmental uncertainty. In: Wilson, J.W., Miller, J., Konradi, A., Cucinotta, F.A. (eds). Shielding strategies for human space exploration. NASA Conference Publication 3360, NASA Langley Research Center, Hampton, VA, USA, pp 17–28.

Baggiolini, M., Walz, A., and Kunkel, S.L. (1989). Neutrophil-activating peptide-1/interleukin 8, a novel cytokine that activates neutrophils. J. Clin. Invest. 84, 1045-1049.

Baichwal, V.R., and Baeuerle, P.A. (1997). Activate NF-kappa B or die? Curr. Biol. 7, R94-6.

Baker, R.G., Hayden, M.S., and Ghosh, S. (2011). NF-κB, inflammation, and metabolic disease. Cell Metab. 13, 11-22.

Bakkenist, C.J., and Kastan, M.B. (2003). DNA damage activates ATM through intermolecular autophosphorylation and dimer dissociation. Nature 421, 499-506.

Baldwin, A.S. (1996). The NF-kappa B and I kappa B proteins: new discoveries and insights. Annu. Rev. Immunol. 14, 649-683.

Baldwin, A.S. (2001). Control of oncogenesis and cancer therapy resistance by the transcription factor NF-kappaB. J. Clin. Invest. 107, 241-246.

Balkwill, F. (2009). Tumour necrosis factor and cancer. Nat. Rev. Cancer 9, 361-371.

Banerjee, D., and Liefshitz, A. (2001). Potential of the proteasomal inhibitor MG-132 as an anti-cancer agent, alone and in combination. Anticancer Res. 21, 3941-3947.

Barendsen, G.W., Beusker, T.L., Vergroesen, A.J., and Budke, L. (1960). Effects of different radiations on human cells in tissue culture. II. Biological experiments. Radiat. Res. 13, 841-849.

Barendsen, G.W., Walter, H.M., Fowler, J.F., and Bewley, D.K. (1963). Effect of different ionizing radiations on human cells in tissue culture. III. Experiments with cyclotron-accelerated alpha-particles and deuterons. Radiat. Res. 18, 106-119.

Baud, V., and Karin, M. (2009). Is NF-kappaB a good target for cancer therapy? Hopes and pit-falls. Nat. Rev. Drug Discov. 8, 33-40.

Baumstark-Khan, C. (1993). X-ray-induced DNA double-strand breaks as lethal lesions in diploid human fibroblasts compared to Chinese hamster ovary cells. Int. J. Radiat. Biol. 63, 305-311.

Baumstark-Khan, C., Hellweg, C.E., Arenz, A., and Meier, M.M. (2005). Cellular monitoring of the nuclear factor kappaB pathway for assessment of space environmental radiation. Radiat. Res. 164, 527-530.

Beaujean, R., Kopp, J., Burmeister, S., Petersen, F., and Reitz, G. (2002). Dosimetry inside MIR station using a silicon detector telescope (DOSTEL). Radiat. Meas. 35, 433-438.

Beg, A.A., Sha, W.C., Bronson, R.T., Ghosh, S., and Baltimore, D. (1995). Embryonic lethality and liver degeneration in mice lacking the RelA component of NF-kappa B. Nature 376, 167-170.

Bennardo, N., Cheng, A., Huang, N., and Stark, J.M. (2008). Alternative-NHEJ is a mechanistically distinct pathway of mammalian chromosome break repair. PLoS Genet. 4, e1000110.

Berger, T., and Reitz, G. (2006). Weltraumspaziergang eines Phantoms. DLR Nachrichten 113

Bergonié, J., and Tribondeau, L. (1906). De Quelques Résultats de la Radiothérapie et Essai de Fixation d'une Technique Rationnelle. Comptes-Rendus des Séances de l'Académie des Sciences 143, 983–985.

Bertrand, M.J.M., Lippens, S., an Staes, Gilbert, B., Roelandt, R., Medts, J. de, Gevaert, K., Declercq, W., and Vandenabeele, P. (2011). cIAP1/2 are direct E3 ligases conjugating diverse types of ubiquitin chains to receptor interacting proteins kinases 1 to 4 (RIP1-4). PLoS ONE 6, e22356.

Bird, R.P., and Burki, H.J. (1975). Survival of synchronized Chinese hamster cells exposed to radiation of different linear-energy transfer. Int. J. Radiat. Biol. Relat. Stud. Phys. Chem. Med. 27, 105-120.

Bischoff, S.C., and Ulmer, F.A. (2008). Eosinophils and allergic diseases of the gastrointestinal tract. Best Pract. Res. Cl. Ga. 22, 455-479.

Bonizzi, G., and Karin, M. (2004). The two NF-kappaB activation pathways and their role in innate and adaptive immunity. Trends Immunol. 25, 280-288.

Bottero, V., Busuttil, V., Loubat, A., Magné, N., Fischel, J.L., Milano, G., and Peyron, J.F. (2001). Activation of nuclear factor kappaB through the IKK complex by the topoisomerase poisons SN38 and doxorubicin: a brake to apoptosis in HeLa human carcinoma cells. Cancer Res. 61, 7785-7791.

Brach, M.A., Hass, R., Sherman, M.L., Gunji, H., Weichselbaum, R., and Kufe, D. (1991). Ionizing radiation induces expression and binding activity of the nuclear factor kappa B. J. Clin. Invest. 88, 691-695.

Burdelya, L.G., Krivokrysenko, V.I., Tallant, T.C., Strom, E., Gleiberman, A.S., Gupta, D., Kurnasov, O.V., Fort, F.L., Osterman, A.L., and Didonato, J.A., et al. (2008). An agonist of toll-like receptor 5 has radioprotective activity in mouse and primate models. Science 320, 226-230.

Busuttil, V., Bottero, V., Frelin, C., Imbert, V., Ricci, J.-E., Auberger, P., and Peyron, J.-F. (2002). Blocking NF-kappaB activation in Jurkat leukemic T cells converts the survival agent and tumor promoter PMA into an apoptotic effector. Oncogene 21, 3213-3224.

Calaf, G., and Hei, T.K. (2001). Oncoprotein expression in human breast epithelial cells transformed by high-LET radiation. Int. J. Radiat. Biol. 77, 31-40.

Cann, K.L., and Hicks, G.G (2006). Absence of an immediate G1/S checkpoint in primary MEFs following gamma-irradiation identifies a novel checkpoint switch. Cell Cycle 5, 1823–1830.

Cao, S., Zhang, X., Edwards, J.P., and Mosser, D.M. (2006). NF-kappaB1 (p50) homodimers differentially regulate pro- and anti-inflammatory cytokines in macrophages. J. Biol. Chem. 281, 26041-26050.

Celeste, A., Fernandez-Capetillo, O., Kruhlak, M.J., Pilch, D.R., Staudt, D.W., Lee, A., Bonner, R.F., Bonner, W.M., and Nussenzweig, A. (2003). Histone H2AX phosphorylation is dispensable for the initial recognition of DNA breaks. Nat. Cell Biol. 5, 675-679.

Chan, A.T., Ogino, S., Giovannucci, E.L., and Fuchs, C.S. (2011). Inflammatory markers are associated with risk of colorectal cancer and chemopreventive response to anti-inflammatory drugs. Gastroenterology 140, 799-808, quiz e11.

Chang, T.T., Walther, I., Li, C.-F., Boonyaratanakornkit, J., Galleri, G., Meloni, M.A., Pippia, P., Cogoli, A., and Hughes-Fulford, M. (2012). The Rel/NF-κB pathway and transcription of immediate early genes in T cell activation are inhibited by microgravity. J. Leukoc. Biol. 92, 1133-1145.

Chanson, M., Berclaz, P.Y., Scerri, I., Dudez, T., Wernke-Dollries, K., Pizurki, L., Pavirani, A., Fiedler, M.A., and Suter, S. (2001). Regulation of gap junctional communication by a pro-inflammatory cytokine in cystic fibrosis transmembrane conductance regulator-expressing but not cystic fibrosis airway cells. Am. J. Pathol. 158, 1775-1784.

Chastel, C., Jiricny, J., and Jaussi, R. (2004). Activation of stress-responsive promoters by ionizing radiation for deployment in targeted gene therapy. DNA Repair (Amst.) 3, 201-215.

Chen, G., and Goeddel, D.V. (2002). TNF-R1 signaling: a beautiful pathway. Science 296, 1634-1635.

Chen, L.-F., and Greene, W.C. (2003). Regulation of distinct biological activities of the NF-kappaB transcription factor complex by acetylation. J. Mol. Med. 81, 549-557.

Chen, L.-F., and Greene, W.C. (2004). Shaping the nuclear action of NF-kappaB. Nat. Rev. Mol. Cell Biol. 5, 392-401.

Collins, A.R., Ma, A.G., and Duthie, S.J. (1995). The kinetics of repair of oxidative DNA damage (strand breaks and oxidised pyrimidines) in human cells. Mutat. Res. 336, 69-77.

Cosentino, C., Grieco, D., and Costanzo, V. (2011). ATM activates the pentose phosphate pathway promoting anti-oxidant defence and DNA repair. EMBO J. 30, 546-555.

Costes, S.V., Boissière, A., Ravani, S., Romano, R., Parvin, B., and Barcellos-Hoff, M.H. (2006). Imaging features that discriminate between foci induced by high- and low-LET radiation in human fibroblasts. Radiat. Res. 165, 505-515.

Coward, W.R., Okayama, Y., Sagara, H., Wilson, S.J., Holgate, S.T., and Church, M.K. (2002). NF-kappa B and TNF-alpha: a positive autocrine loop in human lung mast cells? J. Immunol. 169, 5287-5293.

Dahlman, J.M., Wang, J., Bakkar, N., and Guttridge, D.C. (2009). The RelA/p65 subunit of NF-kappaB specifically regulates cyclin D1 protein stability: implications for cell cycle withdrawal and skeletal myogenesis. J. Cell. Biochem. 106, 42-51.

Dalinka, M.K., and Mazzeo, V.P. (1985). Complications of radiation therapy. Crit. Rev. Diagn. Imaging 23, 235-67.

Deckbar, D., Stiff, X., Koch, B., Reis, C., Lobrich, M., and Jeggo, P.A. (2010). The limitations of the G1-S checkpoint. Cancer Res. 70, 4412-4421.

Dejardin, E. (2006). The alternative NF-kappaB pathway from biochemistry to biology: pitfalls and promises for future drug development. Biochem. Pharmacol. 72, 1161-1179.

Desai, N., Davis, E., O'Neill, P., Durante, M., Cucinotta, F.A., and Wu, H. (2005). Immunofluorescence detection of clustered gamma-H2AX foci induced by HZE-particle radiation. Radiat. Res. 164, 518-522.

Deveraux, Q.L., and Reed, J.C. (1999). IAP family proteins--suppressors of apoptosis. Genes Dev. 13, 239-252.

Durante, M., and Cucinotta, F.A. (2008). Heavy ion carcinogenesis and human space exploration. Nat. Rev. Cancer 8, 465-472.

Durante, M., Grossi, G.F., Gialanella, G., Pugliese, M., Nappo, M., and Yang, T.C. (1995). Effects of alpha-particles on survival and chromosomal aberrations in human mammary epithelial cells. Radiat. Environ. Biophys. 34, 195-204.

Elliott, C.L., Allport, V.C., Loudon, J.A., Wu, G.D., and Bennett, P.R. (2001). Nuclear factor-kappa B is essential for up-regulation of interleukin-8 expression in human amnion and cervical epithelial cells. Mol. Hum. Reprod. 7, 787-790.

Estabrook, N.C., Chin-Sinex, H., Borgmann, A.J., Dhaemers, R.M., Shapiro, R.H., Gilley, D., Huda, N., Crooks, P., Sweeney, C., and Mendonca, M.S. (2011). Inhibition of NF-κB and DNA double-strand break repair by DMAPT sensitizes non-small-cell lung cancers to X-rays. Free Radic. Biol. Med. 51, 2249-2258.

Fakir, H., Sachs, R.K., Stenerlöw, B., and Hofmann, W. (2006). Clusters of DNA double-strand breaks induced by different doses of nitrogen ions for various LETs: experimental measurements and theoretical analyses. Radiat. Res. 166, 917-927.

Falck, J., Coates, J., and Jackson, S.P. (2005). Conserved modes of recruitment of ATM, ATR and DNA-PKcs to sites of DNA damage. Nature 434, 605-611.

Fernandez-Capetillo, O., Mahadevaiah, S.K., Celeste, A., Romanienko, P.J., Camerini-Otero, R.D., Bonner, W.M., Manova, K., Burgoyne, P., and Nussenzweig, A. (2003). H2AX is required for chromatin remodeling and inactivation of sex chromosomes in male mouse meiosis. Dev. Cell 4, 497-508.

Fire, A., Xu, S., Montgomery, M.K., Kostas, S.A., Driver, S.E., and Mello, C.C. (1998). Potent and specific genetic interference by double-stranded RNA in Caenorhabditis elegans. Nature 391, 806-811.

Friedland, W. (2006). Modellrechnungen zu DNA-Wechselwirkungen mit ionisierender Strahlung. Mensch + Umwelt, 18, 25, Gerber, Kirchheim, Germany.

Fujimoto, Y., and Tedder, T.F. (2006). CD83: a regulatory molecule of the immune system with great potential for therapeutic application. J. Med. Dent. Sci. 53, 85-91.

Furuta, T., Takemura, H., Liao, Z.-Y., Aune, G.J., Redon, C., Sedelnikova, O.A., Pilch, D.R., Rogakou, E.P., Celeste, A., and Chen, H.T., et al. (2003). Phosphorylation of histone H2AX and activation of Mre11, Rad50, and Nbs1 in response to replication-dependent DNA double-strand breaks induced by mammalian DNA topoisomerase I cleavage complexes. J. Biol. Chem. 278, 20303-20312.

Galardi, S., Mercatelli, N., Farace, M.G., and Ciafrè, S.A. (2011). NF-kB and c-Jun induce the expression of the oncogenic miR-221 and miR-222 in prostate carcinoma and glioblastoma cells. Nucleic Acids Res. 39, 3892-3902.

Gao, N., Dai, Y., Rahmani, M., Dent, P., and Grant, S. (2004). Contribution of disruption of the nuclear factor-kappaB pathway to induction of apoptosis in human leukemia cells by histone deacetylase inhibitors and flavopiridol. Mol. Pharmacol. 66, 956-963.

Gaur, U., and Aggarwal, B.B. (2003). Regulation of proliferation, survival and apoptosis by members of the TNF superfamily. Biochem. Pharmacol. 66, 1403-1408.

George, J.S., Lave, K.A., Wiedenbeck, M.E., Binns, W.R., Cummings, A.C., Davis, A.J., de Nolfo, G.A., Hink, P.L., Israel, M.H., Leske, R.A., Mewaldt, R.A., Scott, L.M., Stone, E.C., von Rosenvinge, T.T., and Yanasak, N.E. (2009). Elemental composition and energy spectra of Gaactic Cosmic Rays during Solar Cycle 23. Astrophys. J. 698, 1666-1681.

Gerashchenko, B.I., and Howell, R.W. (2003a). Cell proximity is a prerequisite for the proliferative response of bystander cells co-cultured with cells irradiated with gamma-rays. Cytometry A 56, 71-80.

Gerashchenko, B.I., and Howell, R.W. (2003b). Flow cytometry as a strategy to study radiation-induced bystander effects in co-culture systems. Cytometry A 54, 1-7.

Gerashchenko, B.I., Azzam, E.I., and Howell, R.W. (2004). Characterization of cell-cycle progression and growth of WB-F344 normal rat liver epithelial cells following gamma-ray exposure. Cytometry A 61, 134-141.

Ghosh, S., May, M.J., and Kopp, E.B. (1998). NF-kappa B and Rel proteins: evolutionarily conserved mediators of immune responses. Annu. Rev. Immunol. 16, 225-260.

Ghosh, S., Narang, H., Sarma, A., Krishna, M. (2011). DNA damage response signaling in lung adenocarcinoma A549 cells following gamma and carbon beam irradiation. Mutat. Res. 716, 10-19.

Gómez, J., García-Domingo, D., Martínez-A, C., and Rebollo, A. (1997). Role of NF-kappaB in the control of apoptotic and proliferative responses in IL-2-responsive T cells. Front. Biosci. 2, 49-60.

Graham, F.L., Smiley, J., Russell, W.C., and Nairn, R. (1977). Characteristics of a human cell line transformed by DNA from human adenovirus type 5. J. Gen. Virol. 36, 59-74.

Grigoriev, A.I., Svetaylo, E.N., and Egorov, A.D. (1998). Manned interplanetary missions: prospective medical problems. Environ Med 42, 83-94.

Groesser, T., Chun, E., and Rydberg, B. (2007). Relative biological effectiveness of high-energy iron ions for micronucleus formation at low doses. Radiat. Res. 168, 675-682.

Guttridge, D.C., Albanese, C., Reuther, J.Y., Pestell, R.G., and Baldwin, A.S. (1999). NF-kappaB controls cell growth and differentiation through transcriptional regulation of cyclin D1. Mol. Cell. Biol. 19, 5785-5799.

Hable, V., Drexler, G.A., Brüning, T., Burgdorf, C., Greubel, C., Derer, A., Seel, J., Strickfaden, H., Cremer, T., and Friedl, A.A., et al. (2012). Recruitment kinetics of DNA repair proteins Mdc1 and Rad52 but not 53BP1 depend on damage complexity. PLoS ONE 7, e41943.

Habraken, Y., and Piette, J. (2006). NF-kappaB activation by double-strand breaks. Biochem. Pharmacol. 72, 1132-1141.

Hada, M., and Sutherland, B.M. (2006). Spectrum of complex DNA damages depends on the incident radiation. Radiat. Res. 165, 223-230.

Hall, E.J., and Giaccia, A.J. (2012a). Radiobiology for the radiologist, Chapter 7: Linear energy transfer and relative biological effectiveness (Philadelphia: Wolters Kluwer Health/Lippincott Williams & Wilkins).

Hall, E.J., and Giaccia, A.J. (2012b). Radiobiology for the radiologist, Chapter 22: Cell, tissue and tumor kinetics (Philadelphia: Wolters Kluwer Health/Lippincott Williams & Wilkins).

Hall, E.J., and Giaccia, A.J. (2012c). Radiobiology for the radiologist, Chapter 3: Cell survival curves (Philadelphia: Wolters Kluwer Health/Lippincott Williams & Wilkins).

Hannon, G.J. (2002). RNA interference. Nature 418, 244-251.

Hayden, M.S., and Ghosh, S. (2004). Signaling to NF-kappaB. Genes Dev. 18, 2195-2224.

He, L., Kim, B.Y., Kim, K.A., Kwon, O., Kim, S.O., Bae, E.Y., Lee, M.S., Kim, M.S., Jung, M., and Moon, A., et al. (2007). NF-kappaB inhibition enhances caspase-3 degradation of Akt1 and apoptosis in response to camptothecin. Cell. Signal. 19, 1713-1721.

Hellweg, C.E. (2012). Cellular response to exposure with different radiation qualities with a focus on Nuclear factor κB. Habilitationsschrift, Fachbereich Veterinärmedizin der Freien Universität Berlin.

Hellweg, C.E., and Baumstark-Khan, C. (2007a). Detection of UV-induced activation of NF-kappaB in a recombinant human cell line by means of Enhanced Green Fluorescent Protein (EGFP). Radiat Environ Biophys 46, 269-279.

Hellweg, C.E., and Baumstark-Khan, C. (2007b). Getting ready for the manned mission to Mars: the astronauts' risk from space radiation. Naturwissenschaften 94, 517-526.

Hellweg, C.E., Arenz, A., and Baumstark-Khan, C. (2007). Assessment of space environmental factors by cytotoxicity bioassays. Acta Astronaut, 60 (4-7), 525-533.

Hellweg, C.E., Langen, B., Klimow, G., Ruscher, R., Schmitz, C., Baumstark-Khan, C., and Reitz, G. (2009). Upstream events in the nuclear factor κB activation cascade in response to sparsely ionizing radiation. Adv. Space Res. 44, 907-916.

Hellweg, C.E., Arenz, A., Bogner, S., Schmitz, C., and Baumstark-Khan, C. (2006). Activation of nuclear factor kappa B by different agents: influence of culture conditions in a cell-based assay. Ann. N. Y. Acad. Sci. 1091, 191-204.

Hellweg, C.E., Baumstark-Khan, C., and Horneck, G. (2003). Generation of stably transfected Mammalian cell lines as fluorescent screening assay for NF-kappaB activation-dependent gene expression. J. Biomol. Screen 8, 511-521.

Hellweg, C.E., Baumstark-Khan, C., Schmitz, C., Lau, P., Meier, M.M., Testard, I., Berger, T., and Reitz, G. (2011a). Activation of the nuclear factor κB pathway by heavy ion beams of different linear energy transfer. Int. J. Radiat. Biol. 87, 954-963.

Hellweg, C.E., Baumstark-Khan, C., Schmitz, C., Lau, P., Meier, M.M., Testard, I., Berger, T., and Reitz, G. (2011b). Carbon-ion-induced activation of the NF-κB pathway. Radiat. Res. 175, 424-431.

Hickson, I., Zhao, Y., Richardson, C.J., Green, S.J., Martin, N.M., Orr, A.I., Reaper, P.M., Jackson, S.P., Curtin, N.J., and Smith, G.C. (2004). Identification and characterization of a novel and specific inhibitor of the ataxia-telangiectasia mutated kinase ATM. Cancer Res. 64, 9152-9159.

Hinata, K., Gervin, A.M., Jennifer Zhang, Y., and Khavari, P.A. (2003). Divergent gene regulation and growth effects by NF-kappa B in epithelial and mesenchymal cells of human skin. Oncogene 22, 1955-1964.

Hinz, M., Krappmann, D., Eichten, A., Heder, A., Scheidereit, C., and Strauss, M. (1999). NF-kappaB function in growth control: regulation of cyclin D1 expression and G0/G1-to-S-phase transition. Mol. Cell. Biol. 19, 2690-2698.

Hoffmann, A., Natoli, G., and Ghosh, G. (2006). Transcriptional regulation via the NF-kappaB signaling module. Oncogene 25, 6706-6716.

Holley, A.K., Xu, Y., St Clair, D.K., and St Clair, W.H. (2010). RelB regulates manganese super-oxide dismutase gene and resistance to ionizing radiation of prostate cancer cells. Ann. N. Y. Acad. Sci. 1201, 129-136.

Horneck, G., Facius, R., Reichert, M., Rettberg, P., Seboldt, W., Manzey, D., Comet, B., Maillet, A., Preiss, H., Schauer, L., Dussap, C.G., Poughon, L., Belyavin, A., Reitz, G., Baumstark-Khan, C., and Gerzer, R. (2006). HUMEX, a study on the survivability and adaptation of humans to long-duration exploratory missions, part II: Missions to Mars. Adv. Space Res. 38, 752–759.

Irarrazabal, C.E., Burg, M.B., Ward, S.G., and Ferraris, J.D. (2006). Phosphatidylinositol 3-kinase mediates activation of ATM by high NaCl and by ionizing radiation: Role in osmoprotective transcriptional regulation. Proc. Natl. Acad. Sci. USA. 103, 8882-8887.

Jackson S.P., and Bartek J. (2009). The DNA-damage response in human biology and disease. Nature 461, 1071-1078.

Janssens, S., Tinel, A., Lippens, S., and Tschopp, J. (2005). PIDD mediates NF-kappaB activation in response to DNA damage. Cell 123, 1079-1092.

Josson, S., Xu, Y., Fang, F., Dhar, S.K., St Clair, D.K., St Clair, W.H. (2006). RelB regulates manganese superoxide dismutase gene and resistance to ionizing radiation of prostate cancer cells. Oncogene 25, 1554-1559.

Joyce, D., Albanese, C., Steer, J., Fu, M., Bouzahzah, B., and Pestell, R.G. (2001). NF-kappaB and cell-cycle regulation: the cyclin connection. Cytokine Growth Factor Rev. 12, 73-90.

Jung, M., and Dritschilo, A. (2001). NF-kappa B signaling pathway as a target for human tumor radiosensitization. Semin. Radiat. Oncol. 11, 346-351.

Kao, J., Lavaf, A., Lan, C., Fu, S. (2010). Inhibition of Gamma-H2AX after Ionizing Radiation as a Biological Surrogate of Impaired Upstream DNA Damage Signaling and Radiosensitivity. J. Cancer Mol. 5, 49-54.

Karagiannis, T.C., and El-Osta, A. (2004). Double-strand breaks: signaling pathways and repair mechanisms. Cell. Mol. Life Sci. 61, 2137-2147.

Karin, M., and Ben-Neriah, Y. (2000). Phosphorylation meets ubiquitination: the control of NF-[kappa]B activity. Annu. Rev. Immunol. 18, 621-663.

Karin, M., and Delhase, M. (2000). The I kappa B kinase (IKK) and NF-kappa B: key elements of proinflammatory signalling. Semin. Immunol. 12, 85-98.

Karin, M., and Lin, A. (2002). NF-kappaB at the crossroads of life and death. Nat. Immunol. 3, 221-227.

Kellerer, A.M., and Hug, O. (1968). Random factors in the survival curve. Adv. Biol. Med. Phys. 12, 353-366.

Khanna, K.K., Lavin, M.F., Jackson, S.P., and Mulhern, T.D. (2001). ATM, a central controller of cellular responses to DNA damage. Cell Death Differ. 8, 1052-65.

Killian, P.H., Kronski, E., Michalik, K.M., Barbieri, O., Astigiano, S., Sommerhoff, C.P., Pfeffer, U., Nerlich, A.G., and Bachmeier, B.E. (2012). Curcumin inhibits prostate cancer metastasis in vivo by targeting the inflammatory cytokines CXCL1 and -2. Carcinogenesis 33, 2507-2519.

Kim, D.-S., Han, J.H., and Kwon, H.-J. (2003). NF-kappaB and c-Jun-dependent regulation of macrophage inflammatory protein-2 gene expression in response to lipopolysaccharide in RAW 264.7 cells. Mol. Immunol. 40, 633-643.

Kraft, G. (1987). Radiobiological Effects of Very Heavy Ions: Inactivation, Induction of Chromosome Aberrations and Strand Breaks. Band 87, Ausgabe 22 von Preprint. Gesellschaft für Schwerionenforschung mbH, GSI

Kraft, G., Kraft-Weyrather, W., Ritter, S., Scholz, M., and Stanton, J. (1989). Cellular and subcellular effect of heavy ions: a comparison of the induction of strand breaks and chromosomal aberration with the incidence of inactivation and mutation. Adv. Space Res. 9, 59-72.

Krempler, A., Deckbar, D., Jeggo, P.A., Löbrich, M. (2007). An imperfect G2M checkpoint contributes to chromosome instability following irradiation of S and G2 phase cells. Cell Cycle 6, 1682-1686.

Kreuz, S., Siegmund, D., Scheurich, P., and Wajant, H. (2001). NF-kappaB inducers upregulate cFLIP, a cycloheximide-sensitive inhibitor of death receptor signaling. Mol. Cell. Biol. 21, 3964-3973.

Kucharczak, J., Simmons, M.J., Fan, Y., and Gélinas, C. (2003). To be, or not to be: NF-kappaB is the answer--role of Rel/NF-kappaB in the regulation of apoptosis. Oncogene 22, 8961-8982.

Kunsch, C., Lang, R.K., Rosen, C.A., and Shannon, M.F. (1994). Synergistic transcriptional activation of the IL-8 gene by NF-kappa B p65 (RelA) and NF-IL-6. J. Immunol. 153, 153-164.

Kuroda, S., Urata, Y., and Fujiwara, T. (2012). Ataxia-telangiectasia mutated and the Mre11-Rad50-NBS1 complex: promising targets for radiosensitization. Acta Med. Okayama 66, 83-92.

Landsverk, K.S., Patzke, S., Rein, I.D., Stokke, C., Lyng, H., Angelis, P.M. de, and Stokke, T. (2011). Three independent mechanisms for arrest in G2 after ionizing radiation. Cell Cycle 10, 819-829.

Langen, R.C.J., van der Velden, J.L.J., Schols, A.M.W.J., Kelders, M.C.J.M., Wouters, E.F.M., and Janssen-Heininger, Y.M.W. (2004). Tumor necrosis factor-alpha inhibits myogenic differentiation through MyoD protein destabilization. FASEB J. 18, 227-237.

Lavin, M.F., and Shiloh, Y. (1996). Ataxia-telangiectasia: a multifaceted genetic disorder associated with defective signal transduction. Curr. Opin. Immunol. 8, 459-464.

Lee, C.H., Jeon, Y.-T., Kim, S.-H., and Song, Y.-S. (2007). NF-kappaB as a potential molecular target for cancer therapy. Biofactors 29, 19-35.

Lee, S.J., Dimtchev, A., Lavin, M.F., Dritschilo, A., and Jung, M. (1998). A novel ionizing radiation-induced signaling pathway that activates the transcription factor NF-kappaB. Oncogene 17, 1821-1826.

Li, C.C., Dai, R.M., Chen, E., and Longo, D.L. (1994). Phosphorylation of NF-KB1-p50 is involved in NF-kappa B activation and stable DNA binding. J. Biol. Chem. 269, 30089-30092.

Li, F., and Sethi, G. (2010). Targeting transcription factor NF-kappaB to overcome chemoresistance and radioresistance in cancer therapy. Biochim. Biophys. Acta 1805, 167-180.

Li, L., Story, M., and Legerski, R.J. (2001). Cellular responses to ionizing radiation damage. Int. J. Radiat. Oncol. Biol. Phys. 49, 1157-1162.

Li, Q., and Verma, I.M. (2002). NF-kappaB regulation in the immune system. Nat. Rev. Immunol. 2, 725-734.

Li, S., Miao, T., Sebastian, M., Bhullar, P., Ghaffari, E., Liu, M., Symonds, A.L., and Wang, P. (2012). The Transcription Factors Egr2 and Egr3 Are Essential for the Control of Inflammation and Antigen-Induced Proliferation of B and T Cells. Immunity 37, 685-696.

Li, X., Zhao, X., Fang, Y., Jiang, X., Duong, T., Fan, C., Huang, C.C., and Kain, S.R. (1998). Generation of destabilized green fluorescent protein as a transcription reporter. J. Biol. Chem. 273, 34970-34975.

Liebermann, D.A., and Hoffman, B. (2008). Gadd45 in stress signaling. J. Mol. Signal. 3, 15.

Lin, Y., Ma, W., and Benchimol, S. (2000). Pidd, a new death-domain-containing protein, is induced by p53 and promotes apoptosis. Nat. Genet. 26, 122-127.

Linard, C., Marquette, C., Mathieu, J., Pennequin, A., Clarençon, D., and Mathé, D. (2004). Acute induction of inflammatory cytokine expression after gamma-irradiation in the rat: effect of an NF-kappaB inhibitor. Int. J. Radiat. Oncol. Biol. Phys. 58, 427-434.

Linke, S.P., Harris, M.P., Neugebauer, S.E., Clarkin, K.C., Shepard, H.M., Maneval, D.C., and Wahl, G.M. (1997). p53-mediated accumulation of hypophosphorylated pRb after the G1 restriction point fails to halt cell cycle progression. Oncogene 15, 337–345.

Liu, R., Zhao, X., Gurney, T.A., and Landau, N.R. (1998). Functional analysis of the proximal CCR5 promoter. AIDS Res. Hum. Retroviruses 14, 1509-1519.

Loewenstein, W.R., and Rose, B. (1992). The cell-cell channel in the control of growth. Semin. Cell Biol. 3, 59-79.

Luce, A., Courtin, A., Levalois, C., Altmeyer-Morel, S., Romeo, P.H., Chevillard, S., and Lebeau, J. (2009). Death receptor pathways mediate targeted and non-targeted effects of ionizing radiations in breast cancer cells. Carcinogenesis 30, 432-9.

Maciszewski, W., and Scharf, W. (2004). Particle accelerators for radiotherapy. Present status and future. Phys. Medica XX, 137-145.

Madonna, G., Ullman, C.D., Gentilcore, G., Palmieri, G., and Ascierto, P.A. (2012). NF-κB as potential target in the treatment of melanoma. J. Transl. Med. 10, 53.

Maehara, K., Hasegawa, T., and Isobe, K.I. (2000). A NF-kappaB p65 subunit is indispensable for activating manganese superoxide: dismutase gene transcription mediated by tumor necrosis factor-alpha. J. Cell. Biochem. 77, 474-486.

Matsuda, A., Suzuki, Y., Honda, G., Muramatsu, S., Matsuzaki, O., Nagano, Y., Doi, T., Shimo-tohno, K., Harada, T., and Nishida, E., et al. (2003). Large-scale identification and characterization of human genes that activate NF-kappaB and MAPK signaling pathways. Oncogene 22, 3307-3318.

May, M.J., and Ghosh, S. (1997). Rel/NF-kappa B and I kappa B proteins: an overview. Semin. Cancer Biol. 8, 63-73.

May, M.J., and Ghosh, S. (1998). Signal transduction through NF-kappa B. Immunol. Today 19, 80-88.

McKinsey, T.A., Chu, Z., Tedder, T.F., and Ballard, D.W. (2000). Transcription factor NF-kappaB regulates inducible CD83 gene expression in activated T lymphocytes. Mol. Immunol. 37, 783-788.

Meesungnoen, J., and Jay-Gerin, J.-P. (2009). High-LET ion radiolysis of water: oxygen production in tracks. Radiat. Res. 171, 379-386.

Mehnati, P., Morimoto, S., Yatagai, F., Furusawa, Y., Kobayashi, Y., Wada, S., Kanai, T., Hanaoka, F., and Sasaki, H. (2005). Exploration of "over kill effect" of high-LET Ar- and Fe-ions by evaluating the fraction of non-hit cell and interphase death. J. Radiat. Res. 46, 343-350.

Mehta, P.P., Bertram, J.S., and Loewenstein, W.R. (1986). Growth inhibition of transformed cells correlates with their junctional communication with normal cells. Cell 44, 187-196.

Metting, N.F., and Little, J.B. (1995). Transient Failure to Dephosphorylate the Cdc2-Cyclin B1 Complex Accompanies Radiation-Induced G(2)-Phase Arrest in Hela-Cells. Radiat. Res. 143, 286-292.

Mitra, A.K., Bhat, N., Sarma, A., and Krishna, M. (2005). Alteration in the expression of signaling parameters following carbon ion irradiation. Mol. Cell. Biochem. 276, 169-173.

Mitra, A.K., Sarma, A., Krishna, M., Verma, N.C. (2004). Expression of NF-kappaB and ERK following heavy ion irradiation. J Environ Pathol Toxicol Oncol. 23(1), 53-9.

Mori, E., Takahashi, A., Yamakawa, N., Kirita, T., and Ohnishi, T. (2009). High LET heavy ion radiation induces p53-independent apoptosis. J. Radiat. Res. 50, 37-42.

Moriconi, F., Christiansen, H., Raddatz, D., Dudas, J., Hermann, R.M., Rave-Fränk, M., Sheikh, N., Saile, B., Hess, C.F., and Ramadori, G. (2008). Effect of radiation on gene expression of rat liver chemokines: in vivo and in vitro studies. Radiat. Res. 169, 162-169.

Moynagh, P.N. (2005). The NF-kappaB pathway. J. Cell. Sci. 118, 4589-4592.

Muscat, S., Pelka, J., Hegele, J., Weigle, B., Münch, G., and Pischetsrieder, M. (2007). Coffee and Maillard products activate NF-kappaB in macrophages via H2O2 production. Mol. Nutr. Food Res. 51, 525-535.

Narici, L., Belli, F., Bidoli, V., Casolino, M., Pascale, M.P. de, Di Fino, L., Furano, G., Modena, I., Morselli, A., and Picozza, P., et al. (2004). The ALTEA/ALTEINO projects: studying functional effects of microgravity and cosmic radiation. Adv. Space Res. 33, 1352-1357.

Natarajan, M., Aravindan, N., Meltz, M.L., and Herman, T.S. (2002a). Post-translational modification of I-kappa B alpha activates NF-kappa B in human monocytes exposed to 56Fe ions. Radiat. Environ. Biophys. 41, 139-144.

Natarajan, M., Aravindan, N., Meltz, M.L., and Herman, T.S. (2002b). Post-translational modification of I-kappa B alpha activates NF-kappa B in human monocytes exposed to 56Fe ions. Radiat. Environ. Biophys. 41, 139-144.

National Council on Radiation Protection and Measurements [NCRP] (2006). Information needed to make radiation protection recommendations for space missions beyond low-earth orbit. NCPR report No. 153.

Nelson, G.A., Jones, T.A., Chesnut, A., and Smith, A.L. (2002). Radiation-induced gene expression in the nematode Caenorhabditis elegans. J. Radiat. Res. 43, S199-203.

Neumaier, T., Swenson, J., Pham, C., Polyzos, A., Lo, A.T., Yang, P., Dyball, J., Asaithamby, A., Chen, D.J., and Bissell, M.J., et al. (2012). Evidence for formation of DNA repair centers and dose-response nonlinearity in human cells. Proc. Natl. Acad. Sci. U.S.A. 109, 443-448.

Nimon, J. (2013). How space station can help humans follow curiosity to Mars and beyond. taken from www.nasa.gov web page: http://www.nasa.gov/mission-pages/station/research/news/ curiosity.html; last uptated: January 24th, 2013.

Nishi, K., Inoue, H., Schnier, J.B., and Rice, R.H. (2009). Cyclin D1 downregulation is important for permanent cell cycle exit and initiation of differentiation induced by anchorage-deprivation in human keratinocytes. J. Cell. Biochem. 106, 63-72.

Nishikori, M. (2005). Classical and alternative NF-kappaB activation pathways and their roles in lymphoid malignancies. J. Clin. Exp. Hematopathol. 45, 15–24.

Norbury, J.W., and Maung, K. (2007). Electromagnetic Dissociation and space radiation. Acta Astronaut. 60, 770-774.

Ohnishi, T., Takahashi, A., and Ohnishi K. (2002). Studies about space radiation promote new fields in radiation biology. J. Radiat. Res. 43, Suppl:S7-12.

Okayasu, R. (2012). Repair of DNA damage induced by accelerated heavy ions--a mini review. Int. J. Cancer 130, 991-1000.

Onizawa, M., Nagaishi, T., Kanai, T., Nagano, K.-i., Oshima, S., Nemoto, Y., Yoshioka, A., Totsuka, T., Okamoto, R., and Nakamura, T., et al. (2009). Signaling pathway via TNF-alpha/NF-kappaB in intestinal epithelial cells may be directly involved in colitis-associated carcinogenesis. Am. J. Physiol. Gastrointest. Liver Physiol. 296, G850-9.

Pajonk, F., Pajonk, K., and McBride, W.H. (2000). Apoptosis and radiosensitization of hodgkin cells by proteasome inhibition. Int. J. Radiat. Oncol. Biol. Phys. 47, 1025-1032.

Park, H.S., Kim, S.H., and Park, C.S. (2006). The role of novel genes in modifying airway responses in asthma. Curr. Allergy Asthm. R. 6, 112-116.

Park, W.-Y., Hwang, C.-I., Im, C.-N., Kang, M.-J., Woo, J.-H., Kim, J.-H., Kim, Y.S., Kim, J.-H., Kim, H., and Kim, K.-A., et al. (2002). Identification of radiation-specific responses from gene expression profile. Oncogene 21, 8521-8528.

Pawlik, T.M., and Keyomarsi K. (2004). Role of cell cycle in mediating sensitivity to radiotherapy. Int. J. Radiat. Oncol. Biol. Phys. 59, 928-942.

Pazolli, E., and Stewart, S.A. (2008). Senescence: the good the bad and the dysfunctional. Curr. Opin. Genet. Dev. 18, 42-47.

Pierce, D.A., and Preston, D.L. (2000). Radiation-related cancer risks at low doses among atomic bomb survivors. Radiat. Res. 154, 178-86.

Pierce, D.A., Shimizu, Y., Preston, D.L., Vaeth, M., and Mabuchi, K. (2012). Studies of the mortality of atomic bomb survivors. Report 12, part I. Cancer: 1950-1990. Radiat. Res. 178, AV61-87.

Pikarsky, E., Porat, R.M., Stein, I., Abramovitch, R., Amit, S., Kasem, S., Gutkovich-Pyest, E., Urieli-Shoval, S., Galun, E., and Ben-Neriah, Y. (2004). NF-kappaB functions as a tumour promoter in inflammation-associated cancer. Nature 431, 461-466.

Pouget, J.P., and Mather, S.J. (2001). General aspects of the cellular response to low- and high-LET radiation. Eur. J. Nucl. Med. 28, 541-561.

Pouget, J.P., Navarro-Teulon, I., Bardiès, M., Chouin, N., Cartron, G., Pèlegrin, A., and Azria, D. (2011). Clinical radioimmunotherapy--the role of radiobiology. Nat. Rev. Clin. Oncol. 8, 720-734.

Puck, T.T., and Marcus, P.I. (1956). Action of x-rays on mammalian cells. J. Exp. Med. 103, 653-666.

Raju, U., Gumin, G.J., and Tofilon, P.J. (1999). NF kappa B activity and target gene expression in the rat brain after one and two exposures to ionizing radiation. Radiat. Oncol. Investig. 7, 145-152.

Raju, U., Lu, R., Noel, F., Gumin, G.J., and Tofilon, P.J. (1997). Failure of a second X-ray dose to activate nuclear factor kappaB in normal rat astrocytes. J. Biol. Chem. 272, 24624-24630.

Rashi-Elkeles, S., Elkon, R., Weizman, N., Linhart, C., Amariglio, N., Sternberg, G., Rechavi, G., Barzilai, A., Shamir, R., and Shiloh, Y. (2006). Parallel induction of ATM-dependent pro- and antiapoptotic signals in response to ionizing radiation in murine lymphoid tissue. Oncogene 25, 1584-1592.

Ravi, R., Bedi, A., Fuchs, E.J., and Bedi, A. (1998a). CD95 (Fas)-induced caspase-mediated proteolysis of NF-kappaB. Cancer Res. 58, 882-886.

Ravi, R., Mookerjee, B., van Hensbergen, Y., Bedi, G.C., Giordano, A., El-Deiry, W.S., Fuchs, E.J., and Bedi, A. (1998b). p53-mediated repression of nuclear factor-kappaB RelA via the transcriptional integrator p300. Cancer Res. 58, 4531-4536.

Reddy, M.C., and Vasquez, K.M. (2005). Repair of genome destabilizing lesions. Radiat. Res. 164, 345-356.

Reitz, G., Beaujean, R., Benton, E., Burmeister, S., Dachev, T., Deme, S., Luszik-Bhadra, M., and Olko, P. (2005). Space radiation measurements on-board ISS-the DOSMAP experiment. Radiat. Prot. Dosimetry 116, 374-379.

Rhoades, E.R., Cooper, A.M., and Orme, I.M. (1995). Chemokine response in mice infected with Mycobacterium tuberculosis. Infect. Immun. 63, 3871-3877.

Rizvi, A., Pecaut, M.J., and Gridley, D.S. (2011). Low-dose Gamma-rays and Simulated Solar Particle Event Protons Modify Splenocyte Gene and Cytokine Expression Patterns. J. Radiat. Res. 52, 701-711.

Roach, D.R., Bean, A.G.D., Demangel, C., France, M.P., Briscoe, H., and Britton, W.J. (2002). TNF regulates chemokine induction essential for cell recruitment, granuloma formation, and clearance of mycobacterial infection. J. Immunol. 168, 4620-4627.

Rocha, S., Martin, A.M., Meek, D.W., and Perkins, N.D. (2003). p53 represses cyclin D1 transcription through down regulation of Bcl-3 and inducing increased association of the p52 NF-kappaB subunit with histone deacetylase 1. Mol. Cell. Biol. 23, 4713-4727.

Ruscher, R. (2008). NF-kappaB in the Mammalian Cellular Response to Exposure with Ionising Radiation. Diplomarbeit, Fachbereich Biologie der Mathematisch-Naturwissenschaftlichen Fakultät der Universität zu Köln.

Russell, J.S., Raju, U., Gumin, G.J., Lang, F.F., Wilson, D.R., Huet, T., and Tofilon, P.J. (2002). Inhibition of radiation-induced nuclear factor-kappaB activation by an anti-Ras single-chain antibody fragment: lack of involvement in radiosensitization. Cancer Res. 62, 2318-2326.

Ryan, K.M., Ernst, M.K., Rice, N.R., and Vousden, K.H. (2000). Role of NF-kappaB in p53-mediated programmed cell death. Nature 404, 892-897.

Sahijdak, W.M., Yang, C.R., Zuckerman, J.S., Meyers, M., and Boothman, D.A. (1994). Alterations in transcription factor binding in radioresistant human melanoma cells after ionizing radiation. Radiat. Res. 138, S47-51.

Sakurai, A., Hara, S., Okano, N., Kondo, Y., Inoue, J., and Imura, N. (1999). Regulatory role of metallothionein in NF-kappaB activation. FEBS Lett. 455, 55-58.

Schumm, K., Rocha, S., Caamano, J., and Perkins, N.D. (2006). Regulation of p53 tumour suppressor target gene expression by the p52 NF-kappaB subunit. EMBO J. 25, 4820-4832.

Seitz, C.S., Deng, H., Hinata, K., Lin, Q., and Khavari, P.A. (2000). Nuclear factor kappaB subunits induce epithelial cell growth arrest. Cancer Res. 60, 4085-4092.

Seitz, C.S., Lin, Q., Deng, H., and Khavari, P.A. (1998). Alterations in NF-kappaB function in transgenic epithelial tissue demonstrate a growth inhibitory role for NF-kappaB. Proc. Natl. Acad. Sci. USA. 95, 2307-2312.

Sen, R., and Baltimore, D. (1986). Multiple nuclear factors interact with the immunoglobulin enhancer sequences. Cell 46, 705-716.

Senftleben, U., Cao, Y., Xiao, G., Greten, F.R., Krähn, G., Bonizzi, G., Chen, Y., Hu, Y., Fong, A., and Sun, S.C., et al. (2001). Activation by IKKalpha of a second, evolutionary conserved, NF-kappa B signaling pathway. Science 293, 1495-1499.

Shaw, G., Morse, S., Ararat, M., and Graham, F.L. (2002). Preferential transformation of human neuronal cells by human adenoviruses and the origin of HEK 293 cells. FASEB J. 16, 869-871.

Sheikh, M.S., and Huang, Y. (2003). Death receptor activation complexes: it takes two to activate TNF receptor 1. Cell Cycle 2, 550-552.

Shih, V.F.-S., Tsui, R., Caldwell, A., and Hoffmann, A. (2011). A single NFκB system for both canonical and non-canonical signaling. Cell Res. 21, 86-102.

Shrivastav, M., Haro, L.P. de, and Nickoloff, J.A. (2008). Regulation of DNA double-strand break repair pathway choice. Cell Res. 18, 134-147.

Simon, R., and Samuel, C.E. (2007). Activation of NF-kappaB-dependent gene expression by Salmonella flagellins FliC and FljB. Biochem. Biophys. Res. Commun. 355, 280-285.

Skarsgard, L.D. (1998). Radiobiology with heavy charged particles: a historical review. Phys. Med. 14, Suppl. 1: 1-19.

Sonenshein, G.E. (1997). Rel/NF-kappa B transcription factors and the control of apoptosis. Semin. Cancer Biol. 8, 113-119.

Souto-Carneiro, M.M., Fritsch, R., Sepúlveda, N., Lagareiro, M.J., Morgado, N., Longo, N.S., and Lipsky, P.E. (2008). The NF-kappaB canonical pathway is involved in the control of the exonucleolytic processing of coding ends during V(D)J recombination. J. Immunol. 180, 1040-1049.

Sridharan, D.M., Whalen, M.K., Almendrala, D., Cucinotta, F.A., Kawahara, M., Yannone, S.M., and Pluth, J.M. (2012). Increased Artemis levels confer radioresistance to both high and low LET radiation exposures. Radiat. Oncol. 7, 96.

Stein, B., and Baldwin, A.S. (1993). Distinct mechanisms for regulation of the interleukin-8 gene involve synergism and cooperativity between C/EBP and NF-kappa B. Mol. Cell. Biol. 13, 7191-7198.

Stoll, U., Schmidt, A., Schneider, E., and Kiefer, J. (1995). Killing and mutation of Chinese hamster V79 cells exposed to accelerated oxygen and neon ions. Radiat. Res. 142, 288-294.

Takahashi, A., Matsumoto, H., Yuki, K., Yasumoto, J., Kajiwara, A., Aoki, M., Furusawa, Y., Ohnishi, K., and Ohnishi, T. (2004). High-LET radiation enhanced apoptosis but not necrosis regardless of p53 status. Int. J. Radiat. Oncol. Biol. Phys. 60, 591-597.

Tang, C. (2011). Zerumbone protects HEK 293 cells from irradiation-induced DNA damage via activating Keap1/Nrf2/ARE pathway. Afr. J. Pharm. Pharmacol. 5.

Thacker, J., Stretch, A., and Stephens, M.A. (1979). Mutation and inactivation of cultured mammalian cells exposed to beams of accelerated heavy ions. II. Chinese hamster V79 cells. Int. J. Radiat. Biol. Relat. Stud. Phys. Chem. Med. 36, 137-148.

Thirsk, R., Kuipers, A., Mukai, C., and Williams, D. (2009). The space-flight environment: the International Space Station and beyond. CMAJ 180 (12), 1216-1220.

Thommesen, L., and Laegreid, A. (2005). Distinct differences between TNF receptor 1- and TNF receptor 2-mediated activation of NFkappaB. J. Biochem. Mol. Biol. 38, 281-289.

Tilly, N., Fernández-Varea, J.M., Grusell, E., and Brahme, A. (2002). Comparison of Monte Carlo calculated electron slowing-down spectra generated by 60Co gamma-rays, electrons, protons and light ions. Phys. Med. Biol. 47, 1303-1319.

Trikalinos, T.A., Terasawa, T., Ip, S., Raman, G., Lau, J. (2009). Particle Beam Radiation Therapies for Cancer [Internet]. Rockville (MD): Agency for Healthcare Research and Quality (US), Nov. Report No.: 09-EHC019-EF.

Ueda, T., Akiyama, N., Sai, H., Oya, N., Noda, M., Hiraoka, M., and Kizaka-Kondoh, S. (2001). c-IAP2 is induced by ionizing radiation through NF-kappaB binding sites. FEBS Lett. 491, 40-44.

Uziel, T., Lerenthal, Y., Moyal, L., Andegeko, Y., Mittelman, L., and Shiloh, Y. (2003). Requirement of the MRN complex for ATM activation by DNA damage. EMBO J. 22, 5612-5621.

Valko, M., Izakovic, M., Mazur, M., Rhodes, C.J., and Telser, J. (2004). Role of oxygen radicals in DNA damage and cancer incidence. Mol. Cell. Biochem. 266, 37-56.

van Antwerp, D.J., Martin, S.J., Kafri, T., Green, D.R., and Verma, I.M. (1996). Suppression of TNF-alpha-induced apoptosis by NF-kappaB. Science 274, 787-789.

van Gent, D.C., Hoeijmakers, J.H., and Kanaar, R. (2001). Chromosomal stability and the DNA double-stranded break connection. Nat. Rev. Genet. 2, 196-206.

Vlahopoulos, S., Boldogh, I., Casola, A., and Brasier, A.R. (1999). Nuclear factor-kappaB-dependent induction of interleukin-8 gene expression by tumor necrosis factor alpha: evidence for an antioxidant sensitive activating pathway distinct from nuclear translocation. Blood 94, 1878-1889.

Volcic, M., Karl, S., Baumann, B., Salles, D., Daniel, P., Fulda, S., and Wiesmüller, L. (2012). NF-κB regulates DNA double-strand break repair in conjunction with BRCA1-CtIP complexes. Nucleic Acids Res. 40, 181-195.

Waddell, A., Ahrens, R., Steinbrecher, K., Donovan, B., Rothenberg, M.E., Munitz, A., and Hogan, S.P. (2011). Colonic Eosinophilic Inflammation in Experimental Colitis Is Mediated by Ly6C(high) CCR2(+) Inflammatory Monocyte/Macrophage-Derived CCL11. J. Immunol. 186, 5993-6003.

Wadgaonkar, R., Phelps, K.M., Haque, Z., Williams, A.J., Silverman, E.S., and Collins, T. (1999). CREB-binding protein is a nuclear integrator of nuclear factor-kappaB and p53 signaling. J. Biol. Chem. 274, 1879-1882.

Walker, J.T., Todd, P., and Walker, O.A. (2002). Heritable non-lethal damage to cultured human cells irradiated with heavy ions. J. Radiat. Res. 43, S187-91.

Wang, C.Y., Mayo, M.W., and Baldwin, A.S. (1996). TNF- and cancer therapy-induced apoptosis: potentiation by inhibition of NF-kappaB. Science 274, 784-787.

Wang, X., and Huycke, M.M. (2007). Extracellular superoxide production by Enterococcus faecalis promotes chromosomal instability in mammalian cells. Gastroenterology 132, 551-561.

Westerheide, S.D., Mayo, M.W., Anest, V., Hanson, J.L., and Baldwin, A.S. (2001). The putative oncoprotein Bcl-3 induces cyclin D1 to stimulate G(1) transition. Mol. Cell. Biol. 21, 8428-8436.

Whiteside, S.T., and Israël, A. (1997). I kappa B proteins: structure, function and regulation. Semin. Cancer Biol. 8, 75-82.

Wilson, G.D. (2004). Radiation and the cell cycle, revisited. Cancer Metast. Rev. 23, 209–225.

Wilson, J.W., Townsend, L.W., Nealy, J.E., Chun, S.Y., Hong, B.S., Buck, W.W., Lamkin, S.L., Ganapol, B.D., Khan, F., and Cucinotta, F.A. (1989). BRYNTRN: A baryon transport model. NASA technical paper 2887.

Wolf, M.J., Seleznik, G.M., Zeller, N., and Heikenwalder, M. (2010). The unexpected role of lymphotoxin beta receptor signaling in carcinogenesis: from lymphoid tissue formation to liver and prostate cancer development. Oncogene 29, 5006-5018.

Wood, R.D. (1996). DNA repair in eukaryotes. Annu. Rev. Biochem. 65, 135-167.

Wu, G.D., Lai, E.J., Huang, N., and Wen, X. (1997). Oct-1 and CCAAT/enhancer-binding protein (C/EBP) bind to overlapping elements within the interleukin-8 promoter. The role of Oct-1 as a transcriptional repressor. J. Biol. Chem. 272, 2396-2403.

Wuerzberger-Davis, S.M., Chang, P.-Y., Berchtold, C., and Miyamoto, S. (2005). Enhanced G2-M arrest by nuclear factor-{kappa}B-dependent p21waf1/cip1 induction. Mol. Cancer Res. 3, 345-353.

Wulf, H., Kraft-Weyrather, W., Miltenburger, H.G., Blakely, E.A., Tobias, C.A., and Kraft, G. (1985). Heavy-ion effects on mammalian cells: inactivation measurements with different cell lines. Radiat. Res. Suppl. 8, S122-34.

Xu, Y., Fang, F., St Clair, D.K., Sompol, P., Josson, S., and Clair, W.H. (2008). SN52, a novel nuclear factor-kappa B inhibitor, blocks nuclear import of RelB:p52 dimer and sensitizes prostate cancer cells to ionizing radiation. Mol. Cancer Ther. 7, 2367-2376.

Xu, Y., Fang, F., St Clair, D.K., Josson, S., Sompol, P., Spasojevic, I., and St Clair, W.H. (2007). Suppression of RelB-mediated manganese superoxide dismutase expression reveals a primary mechanism for radiosensitization effect of 1 alpha,25-dihydroxyvitamin D-3 in prostate cancer cells. Mol. Cancer Ther. 6, 2048-2056.

Yang, C.R., Wilson-Van Patten, C., Planchon, S.M., Wuerzberger-Davis, S.M., Davis, T.W., Cuthill, S., Miyamoto, S., and Boothman, D.A. (2000). Coordinate modulation of Sp1, NF-kappa B, and p53 in confluent human malignant melanoma cells after ionizing radiation. FASEB J. 14, 379-390.

Yang, T.C., Blakely, E., Chatterjee, A., Welch, G., and Tobias, C.A. (1977). Response of cultured mammalian cells to accelerated krypton particles. Life Sci. Space Res. 15, 169-174.

Yang, X., Chen, Y., and Gabuzda, D. (1999). ERK MAP kinase links cytokine signals to activation of latent HIV-1 infection by stimulating a cooperative interaction of AP-1 and NF-kappaB. J. Biol. Chem. 274, 27981-27988.

Yang, Y., Wang, X., Moore, D.R., Lightfoot, S.A., and Huycke, M.M. (2012). TNF-α mediates macrophage-induced bystander effects through Netrin-1. Cancer Res. 72, 5219-5229.

Yatagai, F. (2004). Mutations induced by heavy charged particles. Biol. Sci. Space 18, 224-234.

Zanotto-Filho, A., Delgado-Cañedo, A., Schröder, R., Becker, M., Klamt, F., and Moreira, J.C.F. (2010). The pharmacological NFkappaB inhibitors BAY117082 and MG132 induce cell arrest and apoptosis in leukemia cells through ROS-mitochondria pathway activation. Cancer Lett. 288, 192-203.

Zhang, J.Y., Green, C.L., Tao, S., and Khavari, P.A. (2004). NF-kappaB RelA opposes epidermal proliferation driven by TNFR1 and JNK. Genes Dev. 18, 17-22.

Zheng, Y., Zha, Y., Driessens, G., Locke, F., and Gajewski, T.F. (2012). Transcriptional regulator early growth response gene 2 (Egr2) is required for T cell anergy in vitro and in vivo. J. Exp. Med. 209, 2157-2163.

Zhou, D., Brown, S.A., Yu, T., Chen, G., Barve, S., Kang, B.C., and Thompson, J.S. (1999). A high dose of ionizing radiation induces tissue-specific activation of nuclear factor-kappaB in vivo. Radiat. Res. 151, 703-709.

Zhou, H. (2005). Mechanism of radiation-induced bystander effect: Role of the cyclooxygenase-2 signaling pathway. Proc. Natl. Acad. Sci. USA. 102, 14641-14646.

Zhou, H., Ivanov, V.N., Gillespie, J., Geard, C.R., Amundson, S.A., Brenner, D.J., Yu, Z., Lieberman, H.B., and Hei T.K. (2005). Mechanism of radiation-induced bystander effect: role of the cyclooxygenase-2 signaling pathway. Proc. Natl. Acad. Sci. USA. 102(41), 14641-6.

Zhu, B., Liu, Z., Wang, P., Wu, C., and Xu, H. (2008). A nuclear factor-kappaB inhibitor BAY11-7082 inhibits interactions between human endothelial cells, T cells, and monocytes. Transplant. Proc. 40, 2724-2728.

9   Acknowledgments

First of all, I would like to thank Prof. Dr. Jürgen Dohmen for the supervision of my thesis, as well as my second referee Prof. Dr. Carien Niessen and Prof. Dr. Ulrich Baumann for being my thesis committee on the part of the University of Cologne.

I would like to thank the Helmholtz Space Life Sciences Research School (SpaceLife) and the director of the Institute of Aerospace Medicine Prof. Dr. Rupert Gerzer for letting me be part of the SpaceLife program, for the scholarship and for opening up such a fascinating field of research to me. SpaceLife is funded in equal parts by the Helmholtz Association and the German Aerospace Centre (DLR).
I also want to thank Dr. Günther Reitz and the whole Radiation Biology department for a great working atmosphere.

I want to express my gratitude to Dr. Christa Baumstark-Khan for giving me the opportunity to work on a great project within her group, for always having an open door and supporting me whenever I needed help.
Thanks to Dr. Christine E. Hellweg, for directly supervising my project, being third referee and answering tons of questions over and over again. At the same time thanks go to her for excellently coordinating and organising SpaceLife.

Thanks to everyone who is (or was) part of the Cellular Biodiagnostics group, for being great colleagues and making endless night shifts during beam times fun. Patrick, for always letting me drive rental cars, despite points in Flensburg, Luis, the biggest mystery is and always will be the egg mystery, Sebastian and Claudia for the final survival curve and all of the support, without you there would most probably be chaos. All SpaceLife students, Arif for his sixth sense and teaching me how not to stress, and, together with Luna, going through thick and thin. Åsa for parcour walks and dancing 'Vortragstänze' with me, Petra for morning coffee or [Kafä:]. Tobi for giving wise advice, Birgit and Alankrita for emergency breaks, Charlie for proof-reading in 0.314619 seconds, wiki-Bernd, and everyone else. To all second generation students: loads of success, fun, don't give up. Thank you to helping hands at GANIL and GSI and thanks to Team Europe for the summer of 2011.

A huge thank you to my friends, especially Ute, Sandra and the whole gang, for always great times, for showing so much interest in the weird things I do at work, for understanding and always finding the right words to say, you are the best.

My greatest thanks goes to my family, Stefanie, and last but not least my parents for their guidance and support, for having faith and always being there, I love you.

I see Earth! It is so beautiful. *(Yuri Gagarin)*

10 Erklärung

Ich versichere, dass ich die von mir vorgelegte Dissertation selbstständig angefertigt, die benutzten Quellen und Hilfsmittel vollständig angegeben und die Stellen der Arbeit - einschließlich Tabellen, Karten und Abbildungen - , die anderen Werken im Wortlaut oder dem Sinn nach entnommen sind, in jedem Einzelfall als Entlehnung kenntlich gemacht habe; dass diese Dissertation noch keiner anderen Fakultät oder Universität zur Prüfung vorgelegt hat; dass sie noch nicht veröffentlich worden ist, sowie, dass ich eine solche Veröffentlichung vor Abschluss des Promotionsverfahrens nicht vornehmen werde. Die Bestimmungen der Promotionsordnung sind mir bekannt. Die von mir vorgelegte Dissertation ist von Herrn Prof. Dr. Jürgen Dohmen betreut worden.

Köln, April 2013

Kristina Koch

11   Lebenslauf

Kristina Koch
* 29. Mai 1981 in Ostfildern-Ruit, Deutschland

Promotion

seit Okt 2009   Doktorandin im Helmholtz Kolleg für Weltraum-Lebenswissen-schaften (SpaceLife), AG „Zelluläre Biodiagnostik" von Dr. Christa Baumstark-Khan, Strahlenbiologie, Institut für Luft- und Raumfahrtmedizin des DLR, Köln

Berufserfahrung

Sept 2008-Aug 2009   Diplomandin am Zentrum für Molekulare Medizin Köln (ZMMK), AG Prof. Dr. Carien Niessen
Titel der Diplomarbeit: *„The role of Rap2 GTPases regulating epidermal adhesion and differentiation"*

SoSe 2007   Praktikum am Institut für Pharmakologie, Universität zu Köln, AG Prof. Dr. Herzig

Jun-Aug 2006   Redaktionelles Praktikum:
GEOkompakt, Gruner + Jahr & Co KG, Hamburg

Hochschulausbildung

Feb 2004-Aug 2009   Studium der Biologie, Universität zu Köln
Abschluss: Diplom-Biologin (Hauptfach: Genetik)

Berufs- und Schulausbildung

Sept 2001-Feb 2004   Ausbildung zur Mediengestalterin für Digital- und Printmedien koelnermedienfabrik kmf AG & LUP AG, Köln

Aug 2000-Jul 2001   Praktikum: O/R/T/ Medienverbund, Krefeld

1997-2000   Albertus-Magnus-Gymnasium, Bensberg
1994-1997   Deutsche Schule Bombay, Mumbai, Indien
1991-1994   Albertus-Magnus-Gymnasium, Bensberg
1987-1991   Grundschule Immekeppel, Overath

Konferenzbeiträge

Kristina Koch, Christine E. Hellweg, Christa Baumstark-Khan, Isabelle Testard und Günther Reitz. Inhibition des NF-κB-Signalweges zur Untersuchung seiner Funktion in der zellulären Strahlenantwort. *50. Jahrestagung der DGLRM, Bonn, 27.-29. September 2012*

Kristina Koch, Christine E. Hellweg, Christa Baumstark-Khan, Claudia Schmitz, Isabelle Testard and Günther Reitz. Inhibition of the classical and the genotoxic stress induced NF-κB Pathway. *34. Jahrestagung der Deutschen Gesellschaft für Zellbiologie (DGZ), Bonn, 30. März-2. April 2011*

Kristina Koch, Christine E. Hellweg, Christa Baumstark-Khan, Claudia Schmitz, Patrick Lau, Isabelle Testard and Günther Reitz. Evaluation of NF-κB Pathway Inhibition for Space Radiation Biology Research. *Committee on Space Research (COSPAR), Bremen, 18.-25. Juli 2010*

Kristina Koch, Christine E. Hellweg, Christa Baumstark-Khan, Isabelle Testard and Günther Reitz. Inhibiting the NF-κB pathway to Assess its Function in the Cellular Response to Space Radiation. *Committee on Space Research (COSPAR), Mysore, Indien, 14.-22. Juli 2012*

Kristina Koch, Christine E. Hellweg, Christa Baumstark-Khan, Claudia Schmitz, Isabelle Testard and Günther Reitz. Evaluating the functionality of chemical inhibitors to suppress the NF-κB pathway. *14. Jahrestagung der Gesellschaft für biologische Strahlenforschung (GBS), Köln, 13.-16. September 2011*

Fortbildungen

Juni 2011	„NASA Space Radiation Summer School", Brookhaven National Laboratory (BNL), Upton, New York, USA
2009-2011	Soft Skills Courses I-III des Imperial College London: „Research Skills Development" „Communication and Presentation Skills" „Career and Leadership"
April 2010	„Radiation Biology Basics", Hochschule Bonn-Rhein-Sieg, Rheinbach
Jan 2010	„Grundlagen der medizinischen Statistik", Universität zu Köln